Geosynthetics '99

"Specifying Geosynthetics and Developing Design Details"

GEOSYNTHETICS 99 CONFERENCE
Boston, Massachusetts USA

Conference Proceedings

April 28-30, 1999

Organized by:

IFAI
Industrial Fabrics Association International

NAGS
North American Geosynthetics Society

GMA
Geosynthetic Materials Association

under the auspices of
IGS
International Geosynthetics Society

SPONSORED BY

Table of Contents

Time Dependent Behavior of Reinforcements

Filtration and Drainage I

Performance of Geosynthetics in Roads and Railroads

THE LONG-TERM STRENGTH OF GEOGRID REINFORCEMENT

N E WRIGLEY, R A AUSTIN & P E HARRISON
THE NETLON GROUP LIMITED / TENSAR INTERNATIONAL
UK

ABSTRACT

Geosynthetic reinforcement is commonly used in structures with design lives of up to 120 years. The critical nature of reinforced soil retaining walls, bridge abutments and embankments therefore requires the determination of long-term reinforcement strength at working temperature to be accurately established. Creep testing of reinforcement at a range of temperatures and time-temperature superposition of results are therefore essential for the safe determination of long-term strength with high confidence levels.

When geogrid reinforcement was first developed a performance limit strain of 10% was typically used as the basis for the calculation of long-term design strength and prediction techniques were devised to suit this approach. The development of design codes based on limit state principles, has changed the industry to defining long-term strength for ultimate limit state conditions based on creep rupture.

The paper details the testing and calculation of long-term strength for a geogrid reinforcement for both the 10% strain and rupture conditions to define the 120 year strength to a 95% lower confidence limit.

KEYWORDS

Geogrids, Creep, Rupture, Temperature, Extrapolation.

INTRODUCTION

Polymeric soil reinforcing materials are required to withstand high tensile loads for long durations. The calculation of long-term strength requires extensive creep testing on the finished product and detailed analysis of the resulting data, to enable the prediction of strength properties beyond the extent of available test data. Due to the visco-elastic nature of polymers such as High Density polyethylene (HDPE) and polypropylene (PP), the results of relatively short duration creep tests, at temperatures above the in-service temperature, but not bracketing the glass transition temperature of the polymer, can be used to calculate the long-term strength of the reinforcing material.

While creep testing of reinforcing materials has been carried out for many years, only recently with the development of national and international standards (British Standards Institution 1990, ISO 1995), have common test procedures for generating the required data been available. There remains, however, little guidance on the way creep data should be interpreted and how calculations to extrapolate long-term strength at high confidence levels beyond the term of the test data, should be undertaken. One approach to this problem is outlined below.

CREEP TESTING

The method of calculation of long-term strength developed uses data generated in-house in the creep test facility at Netlon, Figure 1, where creep tests are carried out on samples 5 ribs wide with the centre 3 ribs loaded using the procedure outlined in prEN 13431 (ISO 1995).

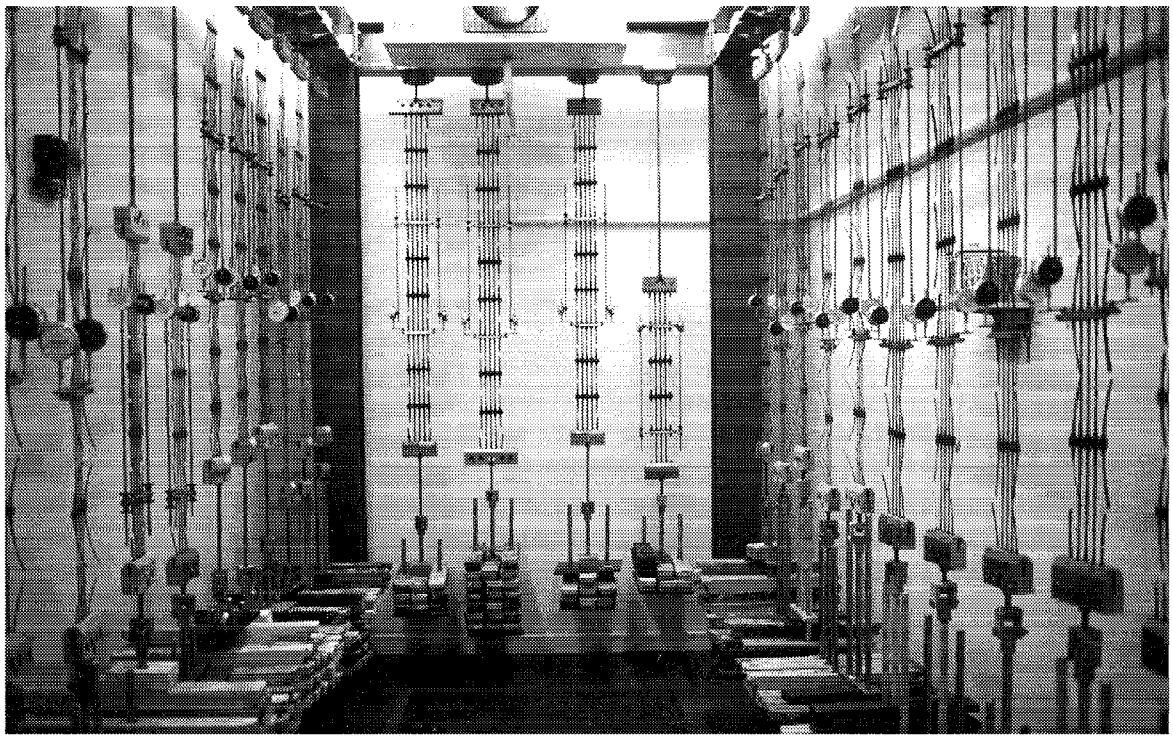

Figure 1. A Creep Testing Laboratory

Table 1. Manufacturer's Product Data

Geogrid Reference	Manufacturer's Name	Short-Term Strength (ISO 10319) kN/m	Mass Per Unit Area kg/m^2	Polymer
A	Tensar 40RE	52.5	0.29	HDPE
B	Tensar 55RE	64.5	0.40	HDPE
C	Tensar 80RE	88.0	0.60	HDPE
D	Tensar 120RE	136.0	0.94	HDPE
E	Tensar 160RE	173.0	1.24	HDPE

The family of geogrids tested and reported herein are detailed in Table 1.

At the start of the tests, instrumentation is fixed to the test specimen to monitor strain over a gauge length of at least 2 longitudinal ribs. Strain monitoring continues throughout the test unless the instrumentation is removed to prevent damage, when rupture is imminent. For tests left to rupture, the time to rupture is also recorded. Using this approach, depending on the test load, temperature and duration, the same tests can be used to determine the creep strain and creep rupture performance of the reinforcement.

Tests are carried out in temperature controlled laboratories at temperatures of 10, 20, 30, 40 and 50 °C, to enable time-shifting of results and ensure that test data is available above the in-soil temperature for all countries. From the creep testing undertaken, a load-strain-time curve is generated for each test load and product in the product range at a range of temperatures, Figure 2.

From Figure 2 and similar curves developed from tests carried out at the other test temperatures, it should be noted that for the tests left to rupture, rupture has occurred at a strain greater than 10%, a limit previously adopted as the failure strain for the design of structures reinforced with polymeric grids (McGown, Andrawes & Yeo, 1984).

The results of creep tests at different temperatures on one reinforcing product are summarised in Table 2 which shows the times to 10% strain and to rupture at the specified test load for the different test temperatures.

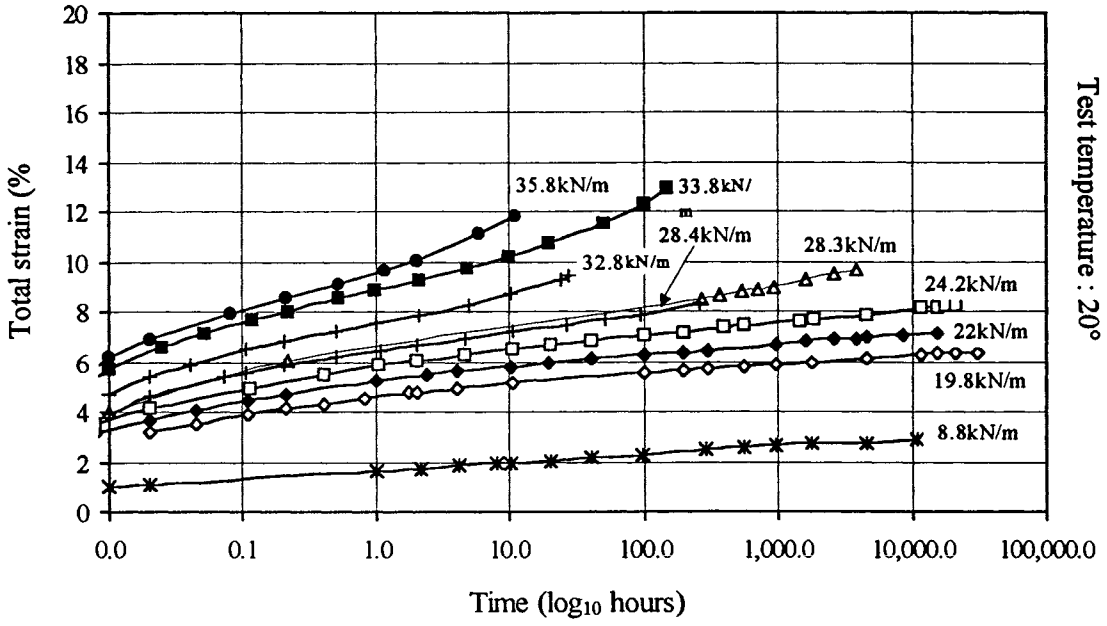

Figure 2. Load-strain-time curves for Geogrid B

Table 2. Creep Test Data for Geogrid B

Test Temperature (°C)	Test Load (kN/m)	Time to 10% Strain (hours)	Time to Rupture (hours)	Time Shift Factor
50	22.00	5000	9166.50	32000
50	25.18	14	621.68	32000
40	28.70	1.8	114.20	1600
40	24.20	800	19656	1600
30	31.60	2.35	52.70	40
20	35.80	1.8	94.25	1
20	33.30	7.5	145.97	1
10	35.80	41	2159.54	0.02
10	38.80	2.3	144.84	0.02
10	45.00	0.34	0.83	0.02

EXTRAPOLATION OF 10% STRAIN AND RUPTURE LIMITED STRENGTHS

Figure 3 shows a rupture strength curve fitted through the time shifted rupture data from Table 2. This curve is based on a linear fit through the test data points when shifted to a common temperature of 20°C. The time shifts used in the time temperature superposition are given in Table 2, i.e. to change the rupture time for a test at 10°C to 20°C for extrapolation, the rupture time is multiplied by 0.02. These time factors which are presented graphically in Figure 4, have been determined by minimising the error for a least-squares curve fit through all rupture data points using regression analysis.

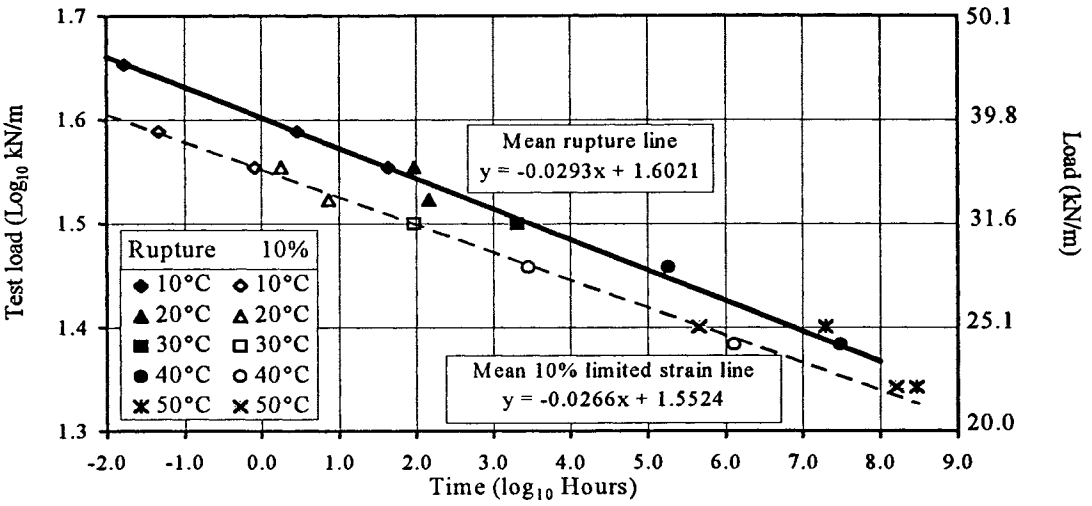

Figure 3. Creep data for Geogrid B shifted to 20°C

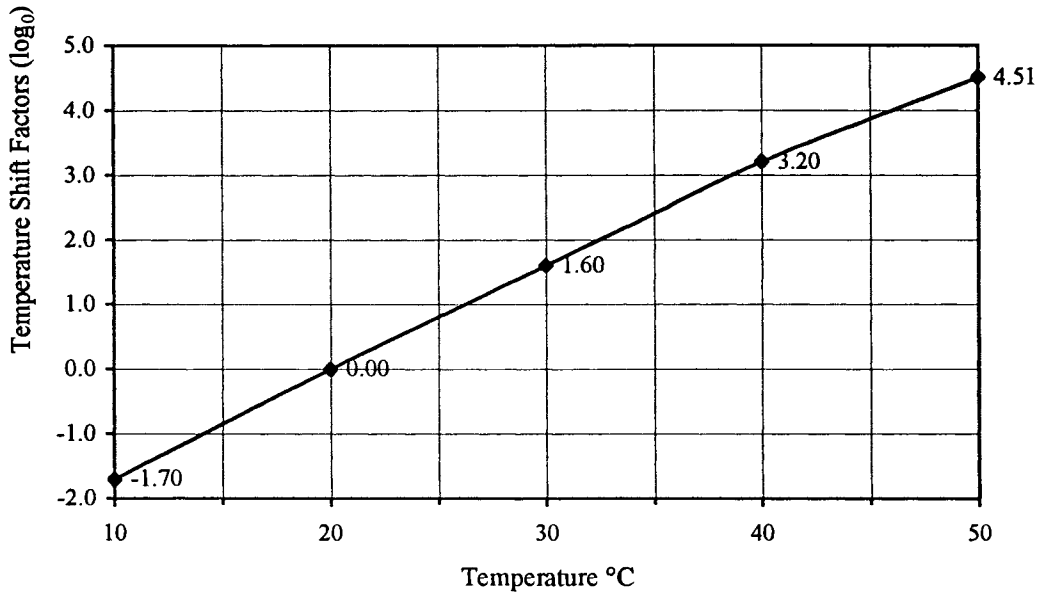

Figure 4. Temperature shift factors

A similar curve may be fitted through the 10% strain data points when shifted using the same shift factors to give the strain limited line on Figure 3. Undertaking this procedure for each product gives 10% strain and rupture limited strength curves at 20°C for each product in the range.

Care should be taken with the regression analysis to ensure that the correct formulae are used as for creep test data, the dependent variable is the time to 10% strain or rupture (*x*-axis) and the independent variable is the test load (*y*-axis). This form of presentation is contra to the format programmed into standard curve fitting packages.

NORMALISED DATA

The product family tested for this report are stiff integral uniaxial geogrids manufactured by drawing a punched sheet at elevated temperature which orients the long-chain polymer molecules to provide high tensile strength. Within this product range, the only difference in production between different products is the thickness of the original punched sheet. Due to this similarity and the geometry of the finished product, creep test results from each product in the range can be normalised on a common basis to increase confidence in the extrapolation of long-term strength.

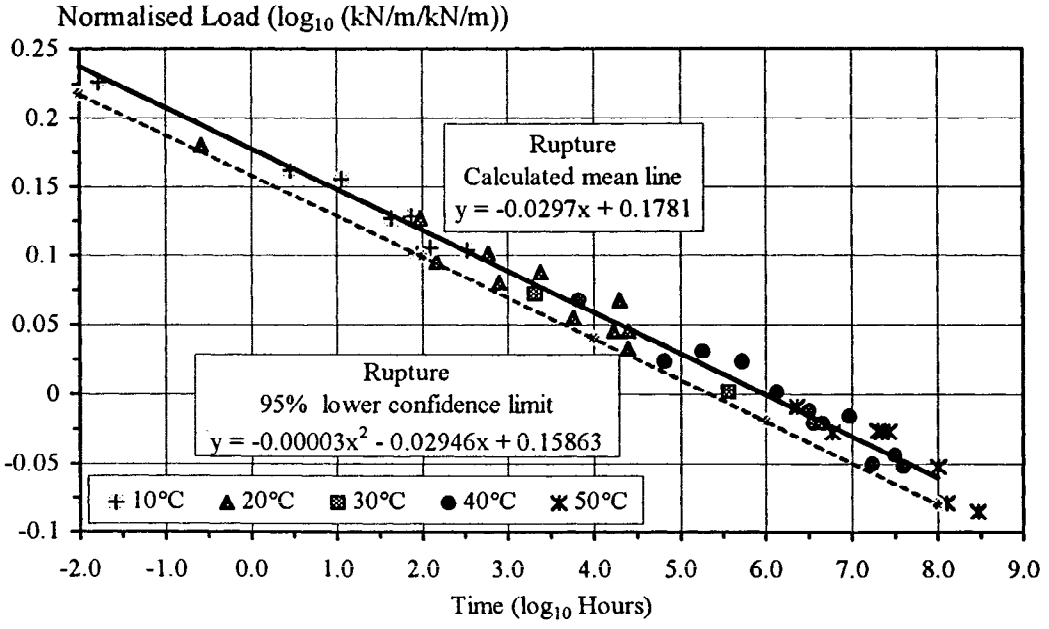

Figure 5. Normalised Rupture Curve for data shifted to 20°C

To include the behaviour of grids spanning the complete range from 52.5-173kN/m short-term strength, a method involving the normalisation of the creep test data was developed which for each product involves:

a) dividing the 10% strain test load used in each test by the calculated 10% strain limited load for a 10^6 hour (120 year) duration at 20°C.

b) dividing the creep rupture test load used in each test by the calculated rupture load for a 10^6 hour duration at 20°C

c) curve fitting through the normalised 10% strain and rupture points as shown in Figures 5 and 6.

The mean 10% strain limited loads and rupture loads at 10^6 hours used for this normalisation are calculated from the curve fit equations given in Figure 3 and similar curves for the other products in the range.

The curve fit equations on Figures 5 and 6 show good correlation between the test data for both design criteria and numerous shifted data points can be seen to lie at durations in excess of the 120 year maximum design life normally used. This normalising method allows data for all products in a product range to be plotted on a common axis, using a mechanism based on actual long-term performance of the products and enables all the test data for a family of products to be used in the calculation of long-term strength for design purposes.

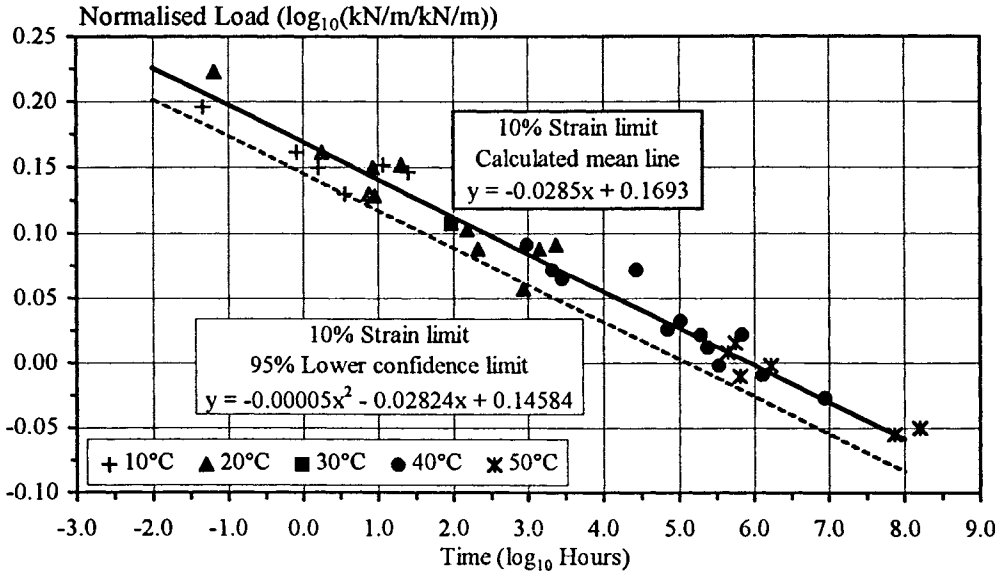

Figure 6. Normalised 10% Strain for data shifted to 20°C

Using this procedure, the long-term strengths of the family of grids based on a 10% strain limit and creep rupture, for a 120 year design life are as given in Table 3.

Whilst following the test procedures detailed in ISO 13431, the testing undertaken by Netlon on this family of geogrids, does not comply with the Standards requirement to use 4 separate test loads on 3 test specimens for each product and test temperature. For a product family of 5 grids, with testing undertaken at 5 temperatures, compliance with this requirement would require 300 creep tests to be undertaken, which is uneconomic. The application of the normalisation procedures described above demonstrate that by the use of time-temperature-superposition, a reduced number of test specimens can be used, whilst maintaining the ability to accurately extrapolate long-term product strength.

Table 3. Calculated 120 year grid strengths - mean values

Grid Type	10% Strain limited strength at 10^6 hours (kN/m)		Rupture strength at 10^6 hours (kN/m)	
	$10°C_{[1]}$	$20°C_{[1]}$	$10°C_{[1]}$	$20°C_{[1]}$
A	21.6	19.5	24.3	21.7
B	27.4	24.7	29.9	26.7
C	36.0	32.4	39.9	35.6
D	53.2	47.9	57.1	51.0
E	68.0	61.3	72.4	64.6

[1] in-soil temperature

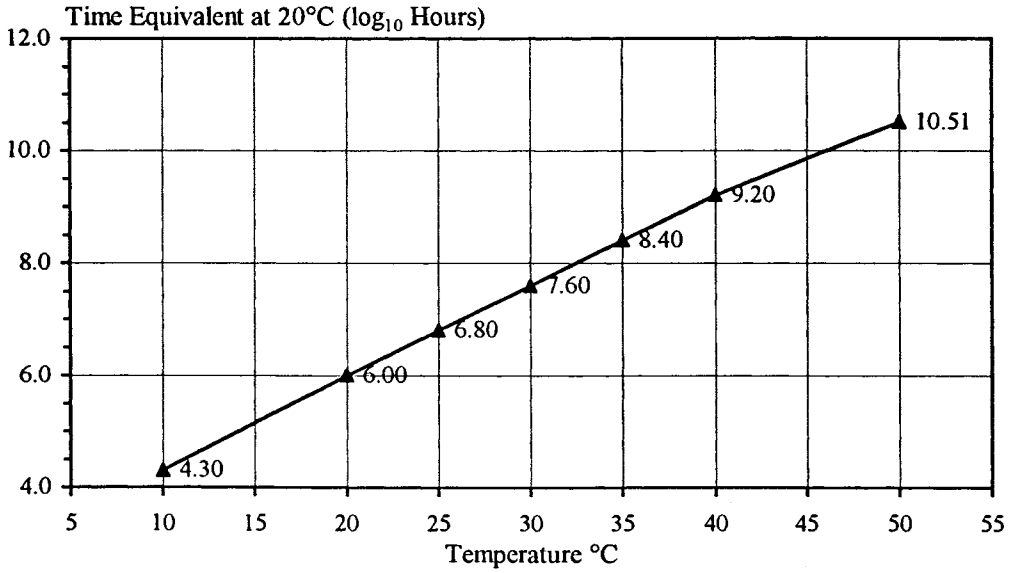

Figure 7. Time equivalent at 20°C vs Temperature

CALCULATION OF 10% STRAIN AND RUPTURE LIMITED STRENGTHS AT OTHER DESIGN TEMPERATURES

Having normalised the available test data for a family of products and curve fitted to this data, the long-term strength of any product in the range, at other design temperatures or design lives can be calculated. A plot of time equivalence corresponding to 10^6 hours at 20°C versus temperature using the shift factors determined previously, highlights the relationship between design life and design temperature, is obtained, Figure 7.

From Figure 7, the time equivalence at 20°C, corresponding to 10^6 hours at 10°C is $10^{4.3}$ hours. Substitution of this value of x = 4.3 into the equations of the curves given in Figures 5 and 6, allows the calculation of load factors which can be applied as multiplication factors to the calculated loads at 20°C for the 120 year design life. This approach enables the product 10% strain limited load and the rupture load at 10°C, or other design temperatures, to be determined taking account of all test data for the product range.

LOWER CONFIDENCE LIMIT ANALYSIS

Consideration needs to be given to the degree of scatter of data points about the regression curves used for the extrapolation of long-term strength, in particular the maximum lower bound deviation from the mean curve. Due to manufacturing variation, different products will have different degrees of scatter from this mean curve.

An Annex titled "Presentation of Stress Rupture Results", which specifies a method for calculating reinforcement strength to 95% lower confidence limits has been drafted and presented at a recent ERA seminar (Greenwood, 1997). The approach being developed re-writes the statistical formula for least square curve fitting in a suitable format to accept data where the dependent variable (the time to 10% strain or rupture), is plotted on the *x*-axis and the independent variable (the test load), is plotted on the *y*-axis. Adopting this approach, with the normalised creep data, a 95% lower confidence value for long-term strength can easily be determined, which correctly accounts for the value of creep test data obtained at temperatures above the in-soil temperature used for design.

The 95% lower confidence limit is obtained by combining the variance of the mean with the variance of the slope of the regression line and from symmetrical branches of a hyperbola which are closest at the mean and widen about the regression line with increasing extrapolation. The normalising technique presented above contains a large number of shifted data points at and beyond the 120 year design life used for critical structures. Consideration of these points results in a lower bound 95% confidence curve which closely approximates to a straight line parallel to the mean curve. The absence of any divergence of the 95% confidence limit curve from the mean curve further increases the confidence in the use of this analytical technique.

Using the techniques described above the calculated 120 year strengths for one product from the family of geogrids studied are as given in Table 4. To fully account for any variability in the product and creep test data, it is the 95% lower confidence limit strengths which should be used for design and specification purposes.

Table 4. Mean and 95% lower confidence limit 10% strain and rupture limited 120 year strengths for Geogrid B

Limiting Criteria	Mean grid strength kN/m		95% Lower confidence limit strength kN/m	
	10°C[1]	20°C[1]	10°C[1]	20°C[1]
10% Strain	27.4	24.7	26.2	23.3
Rupture	29.9	26.7	28.7	25.6

[1] in-soil temperature

CONCLUSIONS

1) For product families which have temperature-dependent visco-elastic creep properties as exhibited by the family reported here:-

   (i) The use of time-temperature-superposition techniques with test data obtained from tests at temperatures up to 50°C allows shifted data points, which lie beyond the 120 year design life to be generated within reasonable test durations.

   (ii) Use of the normalisation technique based on the calculated strength at 120 years for each product in a product family, permits the use of all test data from the family of products to be considered in the calculation long-term strength to 95% lower confidence limits.

   (iii) The method of calculating strengths to 95% lower confidence limits proposed in the draft Annex to ISO 13431 provides a reliable and practical way of accounting for the value of time shifted creep data in the calculation of long-term reinforcement strength for design.

   (iv) Use of elevated temperature testing and the calculation methods described above permits the long-term performance of a product to be calculated from an ecomomic numbers of tests, whilst retaining high confidence levels in the resulting long-term strength, as demonstated by the close correlation of the mean and lower 95% lower confidence curves on Figures 5 and 6.

2) From the testing and the calculations undertaken, the long-term strengths of a new range of uniaxial geogrids were accurately determined.

REFERENCES

1. BS 6906: Methods of test for geotextiles Part 5:1990, `Determination of creep', British Standards Institution, London, UK.

2. International Organisation for Standardisation, 1995, `prEN 13431:1998, Geotextiles and related products - determination of tensile creep and creep rupture behaviour', ISO, Geneva.

3. McGown, Andrawes & Yeo, 1984, `The load strain time behaviour of Tensar geogrids', Proceedings of polymer grid reinforcement conference.

4. Greenwood J H, `Derivation of design parameters and partial safety factors from laboratory data', Proceedings ERA Seminar on Creep and Assessment of Geosynthetics for Soil Reinforcement, December 1997, ERA, Leatherhead, UK.

TEMPERATURE EFFECTS ON TENSILE-CREEP BEHAVIOUR OF HIGH-STENGTH GEOSYNTHETICS

D. CAZZUFFI
ENEL SPA - ITALY
M. SACCHETTI
FLORENCE UNIVERSITY - ITALY

ABSTRACT

The creep behaviour of geosynthetics depends upon several factors, such as polymeric structure, manufacturing process, creep load and temperature. To investigate the effects of the above mentioned factors on tensile creep behaviour of high-strength geosynthetics a specific experimental research was developed.

The paper presents the final results of tensile creep tests performed on three gosynthetics: a HDPE extruded geogrid, a PET woven geogrid and a PP\PET woven\nonwoven geotextile. Each material was tested for duration up to 10^3 hours, with tensile load ranging between 20% and 50% of the wide-width tensile strength and with room temperature ranging between 10°C and 40°C.

The paper highlights the temperature effects on creep behaviour of three geosynthetics tested and verifies the use of time-temperature superposition principle to predict long-term creep strains from 10^3 hour tests.

INTRODUCTION

The growth of geosynthetic-reinforced soil applications in geotechnical engineering has highlighted the problems connected with the long-term stress-strain behaviour of the geosynthetics under the design load.

When a geosynthetic is used as reinforcement in a permanent soil structure it is necessary that both stresses and strains in the reinforcement do not exceed the allowable values during the entire life of the structure (in general 120 years). These allowable values are deduced from standard unconfined tensile creep laboratory tests, with a duration in general varying from a minimum of 10^3 hours to a maximum of 10^4 hours, and using an appropriate factor of safety for creep. This factor is used to reflect the difference of duration between the creep test and the life of structure. However, creep performance for a longer duration can be predicted carrying out accelerated creep tests and using time-temperature superposition principle.

It is well known that several factors influence the geosynthetic tensile creep behaviour, like physical properties of the polymer, fibre type, manufacturing process, temperature, intensity of tensile load and confining pressure.

To evaluate the effects of some of the above-mentioned factors on the tensile creep behaviour of three high strength geosynthetics, the experimental research program described herein was developed and carried out jointly by Research Group on Special Materials of ENEL Spa in Milano and the Civil Engineering Department of Florence University. The main purpose of this research, the full description of equipment and the procedures adopted to evaluate tensile creep of high strength geosynthetics are reported in Cazzuffi et al. (1997).

In this paper the final results of the research are presented; in particular the main effects produced by polymer type, manufacturing process, temperature and load level on the tensile creep behaviour of three above mentioned geosynthetics are highlighted.

In addition the procedure for extrapolating creep strains to longer time intervals based on time-temperature superposition principle is illustrated. The procedure was applied to predict long-term creep behaviour from 10^3 hour experimental creep results.

EXPERIMENTAL PROGRAM

In the experimental program undertaken by the by Research Group on Special Materials of ENEL Spa in Milano and the Civil Engineering Department of Florence University, three high strength geosynthetics are used: an HDPE extruded geogrid [M1], a PET woven geogrid [M2] and a PP\PET woven\nonwoven composite geotextile [M3].

The main characteristics of three geosynthetics employed are summarised in Table 1.

Table 1 - Main characteristics of geosynthetics tested

	Product name	Geosynthetic type	Polymer type	Specimen size		Wide-width tensile strength [kN/m]
				Width [mm]	Length [mm]	
[M1]	Tenax TT 201 SAMP	Extruded Geogrid	HDPE	3 rib	1000	52.71
[M2]	Fortrac 35/20-20	Woven Geogrid	PET	3 rib	1000	48.86
[M3]	Polyfelt PEC 50/25	Woven\nonwonen Geotextile	PP\PET	100	200	53.66

For each geosynthetic, three different tensile creep loads, 20% [C1], 30% [C2] and 50% [C3] of wide-width tensile strength and three different room temperatures, respectively of 10°C [T1], 20°C [T2] and 40°C [T3] were used. The tensile creep tests are conducted in isolation and in accordance with the new European standard CEN prEN ISO 13431 for a duration of 10^3 hours (Cazzuffi et. al., 1997).

TENSILE CREEP TEST RESULTS

All the tensile creep results are reported in plots of total strain vs. log time. To minimise the effects of loading procedure on the tensile creep behaviour the first hour experimental data has been excluded from the experimental creep results.

In Figures 1-3 are shown experimental results (dark dots) for the three geosynthetics, at room temperatures of 10°C [T1], 20°C [T2] and 40°C [T3], respectively, for a tensile load of 20% [C1] of the their wide-width tensile strength. Figures 4-6 show the corresponding experimental results for a tensile load level of 30% [C2]. Finally, Figures 7-9 show experimental data for a tensile load of 50% [C3].

Test results show a stable creep behaviour for the PET woven geogrid [M2] and the PP\PET woven\nonwoven [M3] between loads ranging from 20%[C1] to 50%[C3] and temperature ranging from 10°C[T1] to 40°C[T3]. For the HDPE extruded geogrid [M1], however the results show a stable tensile creep behaviour for tensile loads less than or equal to 30%[C3] and for temperature ranging from 10°C[T1] to 40°C[T3]. When a tensile load of 50%[C3] of wide-width tensile strength was applied, the creep behaviour of [M1] became unstable with increasing of creep strain rate. At a load level of 50%[C3] the HDPE extruded geogrid [M1] reached rupture after about 336 hours and 8 hours, for temperatures of 20°C [T2] and 40°C [T3] respectively.

In general the [M1] geosynthetic exhibits a lower value of initial strain (strain after one hour) than [M2] and [M3] geosynthetics. This fact is directly connected with the structure of these products: the integral structure of the [M1] geosynthetic produces a lower initial strain than the woven structure of the [M2] and [M3] geosynthetics because of immediate and unrecoverable strains caused by to the realignment of polymer fibres, necking and crimps.

The above mentioned plots (Figures 1-9) are also report the regression lines that best fit the creep results and the relative correlation coefficients obtained with regression analysis. With exception of the [M1] geosynthetic at the load level of 50% [C3] all the linear regressions (on the log plane) result in correlation coefficients near 1.

The effects of temperature on the tensile creep behaviour of the three geosynthetics are clearly shown in Figures 10-12 (Figures 10-12 provide the same data as Figure 4-6, except organised by material rather than temperature). These plots show that initial and final creep strains (dots) increase with an increase in temperature for all geosynthetics, and, in general, the slope of fitted curves (continuous lines) increase with an increase in temperature. The effects of temperature are quite pronounced for the HDPE extruded geogrid [M1], very small for the PET woven geogrid [M2] and intermediate for the PP\PET woven\nonwoven geotextile.

EXTRAPOLATION OF THE EXPERIMENTAL RESULTS

The possibility of forecasting the long-term creep behaviour of high strength geosynthetics from 10^3 hours tensile creep tests has been studied in the last years from several researchers (Ferrag, 1998; Ferrag, 1997; Müller-Rocholz et al.,1996; Rimoldi et al., 1993).

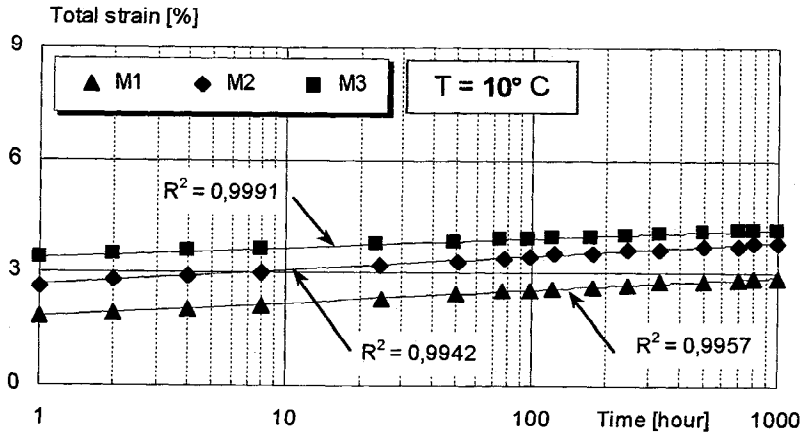

Figure 1 - Creep strains at load level of 20% [C1] and 10°C [T1]

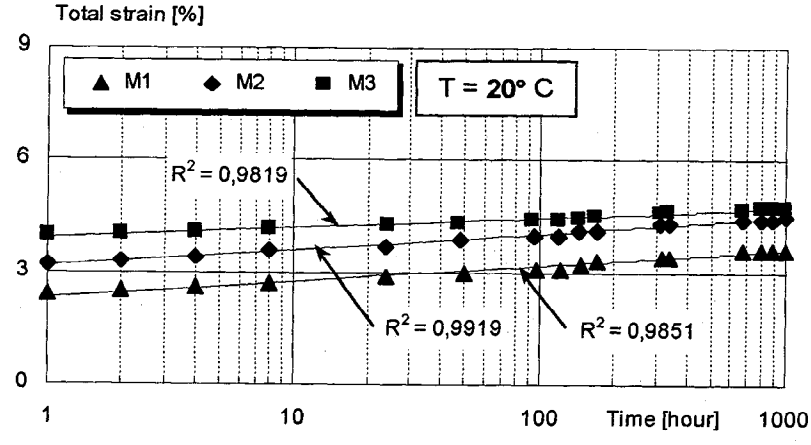

Figure 2 - Creep strains at load level of 20% [C1] and 20°C [T2]

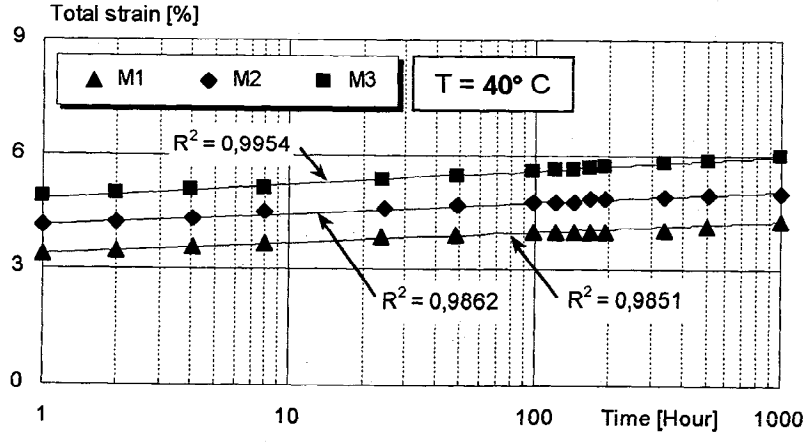

Figure 3 - Creep strains at load lev el of 20% [C1] and 40°C [T3]

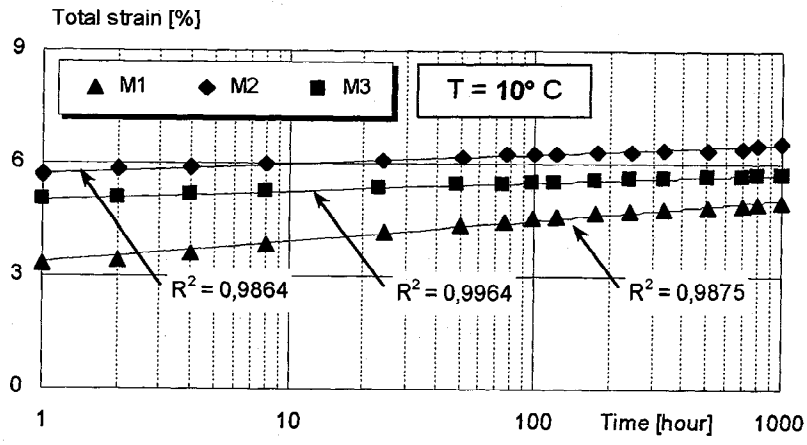

Figure 4 - Creep strains at load level of 30% [C2] and 10°C [T1]

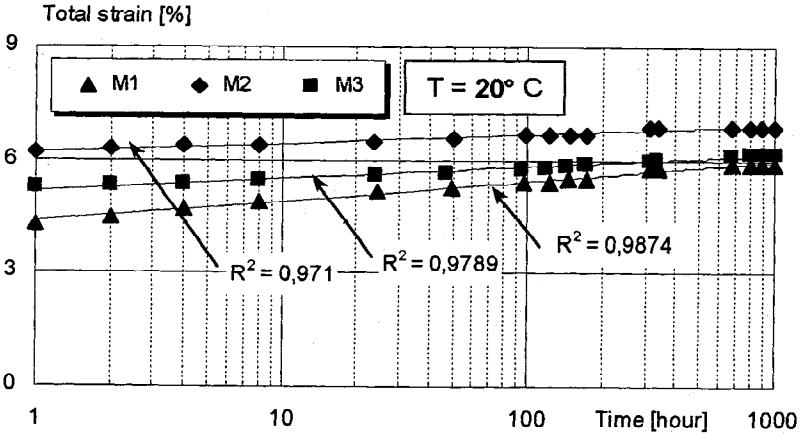

Figure 5 - Creep strains at load level of 30% [C2] and 20°C [T2]

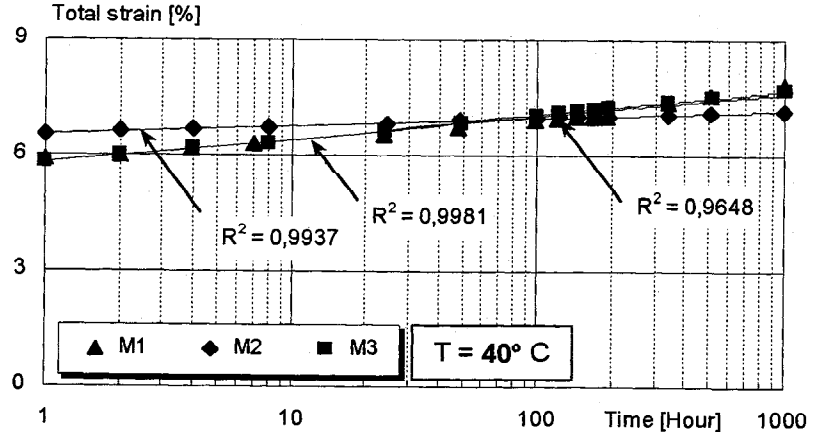

Figure 6 - Creep strains at load level of 30% [C2] and 40°C [T3]

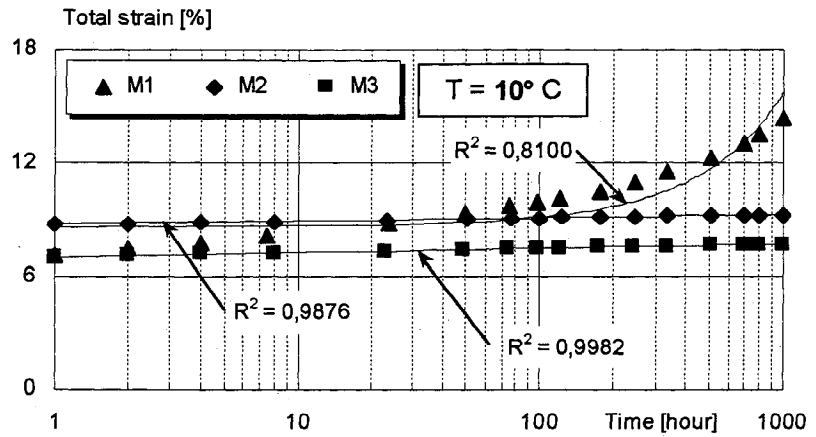

Figure 7 - Creep strains at load level of 50% [C3] and 10°C [T1]

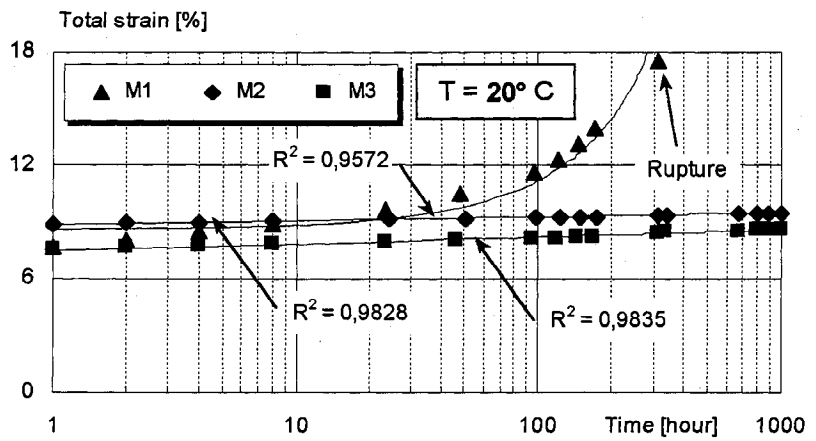

Figure 8 - Creep strains at load level of 50% [C3] and 20°C [T2]

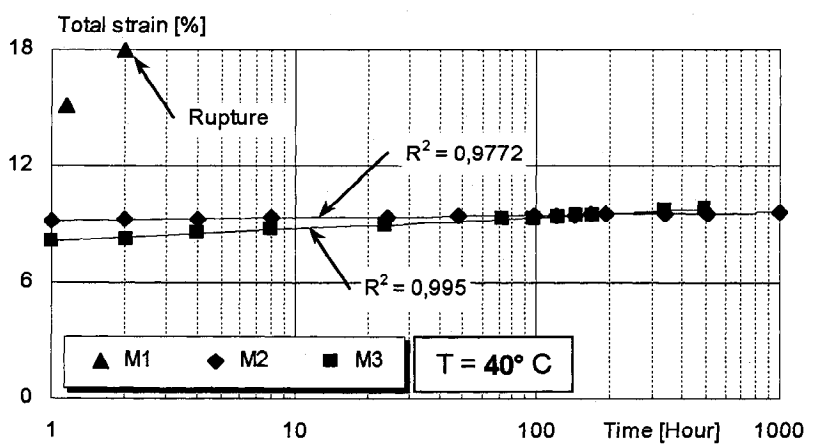

Figure 9 - Creep strains at load level of 50% [C3] and 40°C [T3]

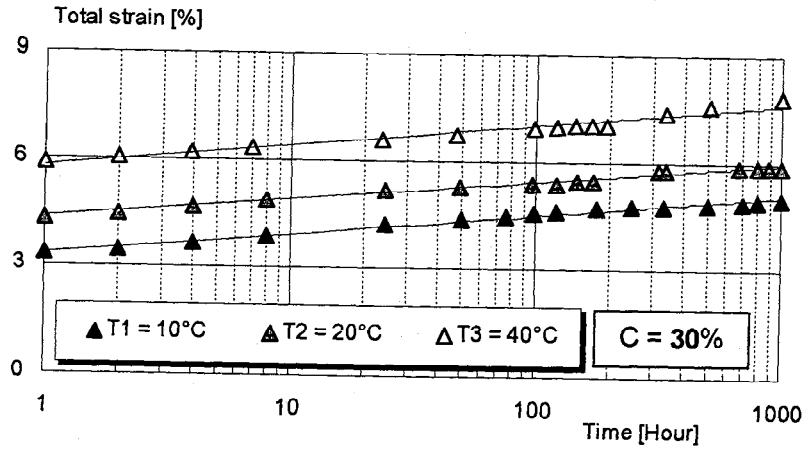

Figure 10 - Creep strains for [M1] at load level of 30%[C3]

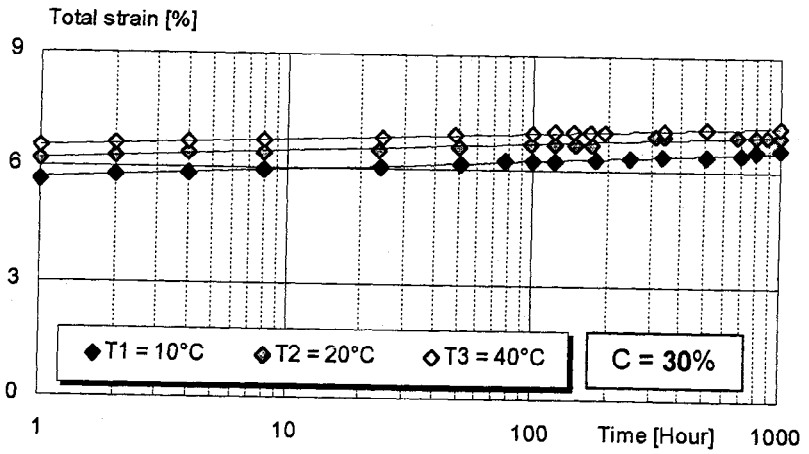

Figure 11 - Creep strains for [M2] at load level of 30%[C3]

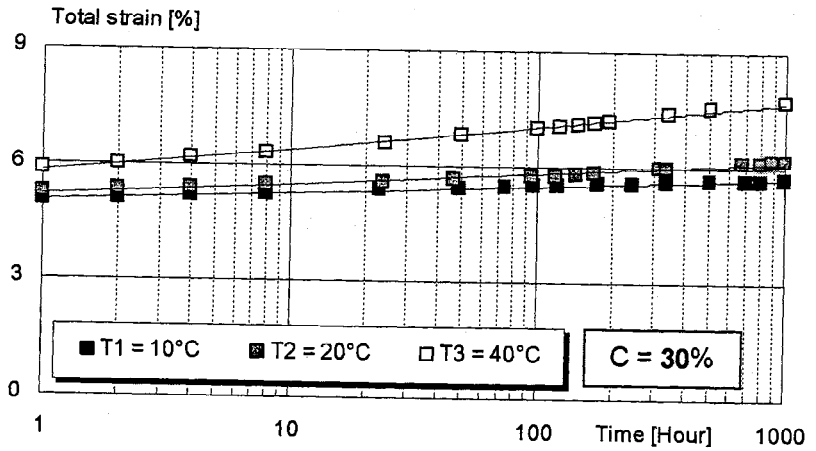

Figure 12 - Creep strains for [M3] at load level of 30%[C3]

In current design practice the possibility to extrapolate the creep strains until a 10^4 or 10^5 hours starting from 10^3 hours tensile creep results is well established. This is clearly applicable if the 10^3 hours tensile creep behaviour of the geosynthetic is stable with dominant primary creep.

A very useful procedure for extrapolating tensile creep strains to longer time intervals it is based on the time-temperature superposition principle, which consist in the application of time-shift factors for creep strain curves at elevated temperatures and the construction of a master strain curve for longer time intervals at reference (or design) temperature.

In general the master curve is simply constructed by shifting, along the log-time scale, the creep curves obtained at elevated temperatures by the time shift factor, a_T, defined by the following equation :

$$\varepsilon(T_O;t)=\varepsilon\left(T;\frac{t}{a_T}\right) \tag{1}$$

where ε is the creep strain, T_O is a reference temperature, T is a room temperature ($T > T_O$) and $a_T(T_O, T, C)$ is function of tensile load level C, reference temperature and room temperature. An analytical approach to the time shift factor is founded on the Williams-Landel-Ferry-equation, better known as WLF equation.

In the present paper the time shift factors are established graphically; in particular: starting from creep strain curves at 10°C [T1] (first reference temperature), obtained for each tensile load level, the creep strain curves at temperatures of 20°C [T2] are shifted to the right along the log-time scale. Finally, starting from creep strain curves at 20°C [T2] (second reference temperature) the creep strain curves at temperatures of 40°C [T3] are shifted to the right along the log-time scale, to obtain master curves extruding to 10^6 hours.

Figures 13-15 show, for example, master curves (established following the above mentioned procedure) for the three geosynthetics tested at tensile load levels of 20% [C1] and 30% [C2]. Table 2 shows the shift factors used in establishing mater curves.

Table 2 – Shift factors of the elevated-temperature creep tests

	Geosynthetic type	Polymer type	Load level	Shift factors		
				10°C	20°C	40°C
[M1]	Extruded Geogrid	HDPE	20%	1	30	300
			30%	1	40	400
[M2]	Woven Geogrid	PET	20%	1	25	100
			30%	1	80	25
[M3]	Woven\nonwonen Geotextile	PP\PET	20%	1	100	1000
			30%	1	10	200

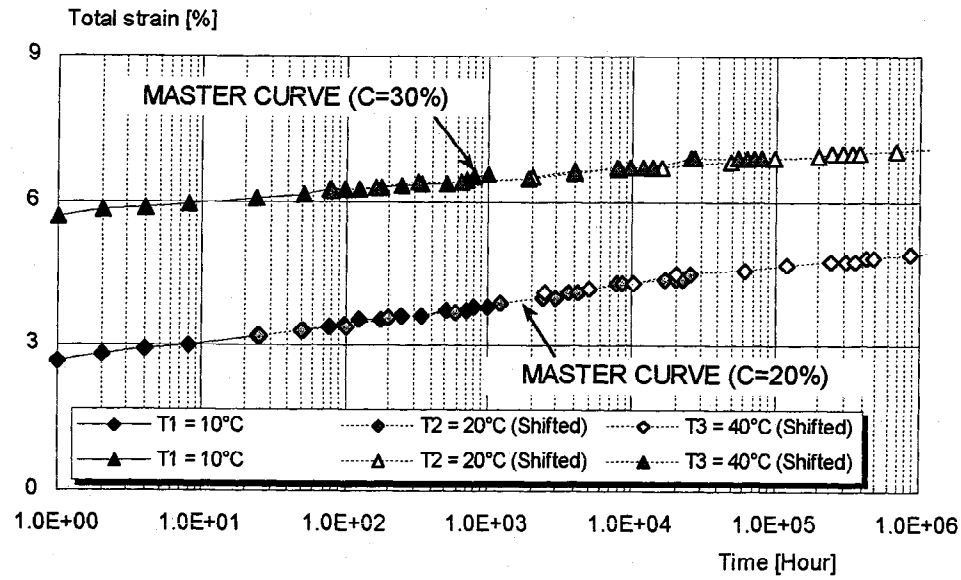

Figure 13 - Master curve for [M1] at load levels of 20%[C1] and 30%[C2]

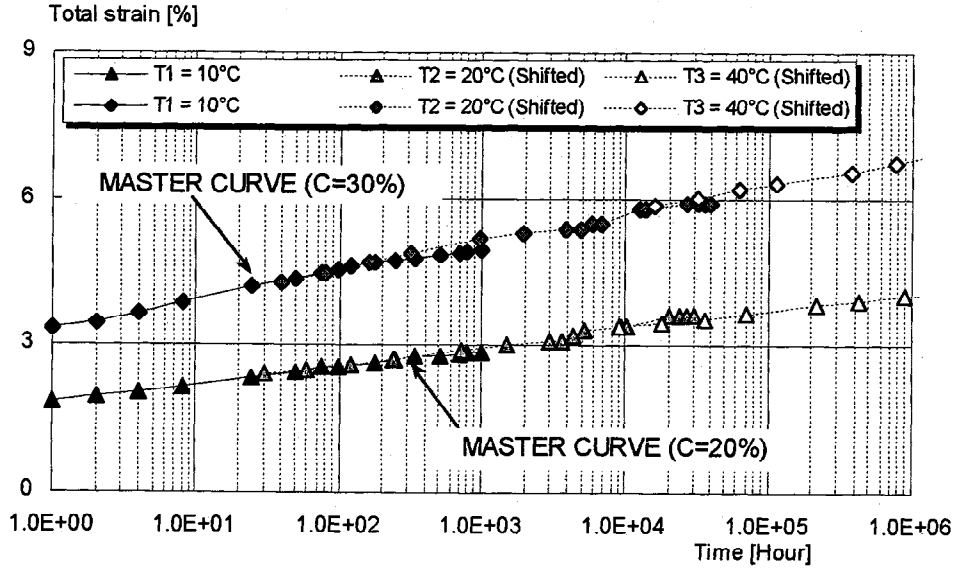

Figure 14 - Master curve for [M2] at load levels of 20%[C1] and 30%[C2]

CONCLUSION

To investigate the tensile creep behaviour of three high strength geosynthetics an experimental program has been undertaken by the Research Group on Special Materials of ENEL Spa in Milano and the Civil Engineering Department of Florence University.

The final results demonstrated that the choice of equipment was correct and suitable to test high strength geosynthetics.

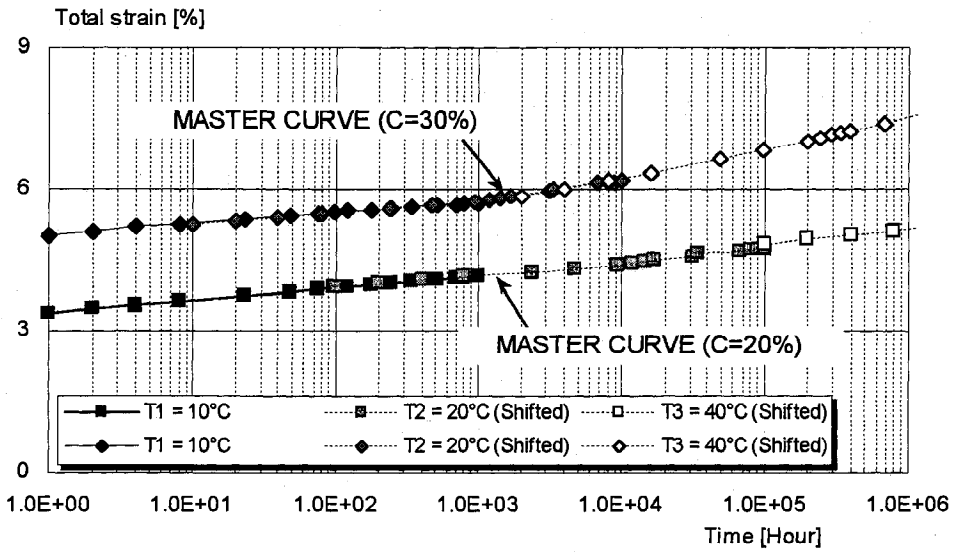

Figure 15 - Master curve for [M3] at load levels of 20%[C1] and 30%[C2]

The final results reported in this paper highlighted the main effect of polymer type, manufacturing process, temperature and tensile load level on the creep behaviour of the geosynthetics tested. In particular, the tensile creep behaviour of the HDPE extruded geogrid [M1] becomes unstable with dominant secondary creep when a load level of 50%[C3] of wide-width tensile strength was applied.

The creep behaviour of the PET woven geogrid [M2] and that of the PP\PET woven\nonwoven geotextile [M3] were both stable for all tensile load levels and room temperatures. The very good correlation coefficients obtained by linear regression (on the log plane) of creep results confirm that the semi-logarithmic creep behaviour persist over the full range of time.

The manufacturing process in contrast, influences the initial strain values; less for [M1] than for [M2] and [M3]. In general the creep strains (initial and final) increase with an increase in temperature for all geosynthetics, and, in general, also the slopes of regression lines that best fit the creep results increase with an increase in temperature. However the effects of exposure temperature are more pronounced for the HDPE extruded geogrid [M1] and very small for the PET woven geogrid [M2].

A procedure for extrapolating tensile creep strains to longer time intervals, based on the time-temperature superposition principle, has been applied to the experimental results. In particular, for each geosynthetic tested, it has been possible graphically construct build master curves capable of predicting the tensile creep response, at 10°C room temperature and for a duration until 10^6 hours, starting from 10^3 hours tensile creep results. The very good correlation coefficients obtained by linear regression of the master curves indicate that the same mechanism governs tensile creep over the range of loads and temperatures considered.

REFERENCES

ASTM D 5262 – 92 (1992) "Standard test method for evaluating the unconfined tension creep behaviour of geosynthetics", Annual Book of ASTM Standards, ASTM, Philadelphia, PA, USA.

CAZZUFFI, D. GHINELLI, A., SACCHETTI, M., VILLA, C., (1997) "European experimental approach to the tensile creep behaviour of high-strength geosynthetics", Geosynthetics '97, Long Beach, CA, USA, pp.253-266.

EN ISO 13431, (1998) "Geotextiles and Geotextiles related Products: determination of the Tensile Creep and Creep Rupture Properties".

FARRAG, K., (1997) "Prediction of long-term strains of geosynthetics from accelerated-creep tests", Geosynthetics '97, Long Beach, CA, USA, pp.267-276.

FARRAG, K., SHIRAZI, H., (1997) "Development of an Accelerated Creep Testing Procedure for Geosynthetics-Part I: Testing ", Geotechnical Testing Journal, GTJODJ, Vol.20, No.4, pp.414-422.

FARRAG, K., (1998) "Development of an Accelerated Creep Testing Procedure for Geosynthetics-Part II: Analysis ", Geotechnical Testing Journal, GTJODJ, Vol.21, No.1, pp.38-44.

MÜLLER-ROCHHOLZ, J., REINHARD, K., (1990) "Creep of geotextiles at different temperatures", Proc. IV Int. Conf. On Geotextiles, Geomembranes and Related Products, The Hauge, The Netherlands, pp.657-659.

MÜLLER-ROCHHOLZ, J., KOSLOWSKI, C., (1996) "Creep prediction", Proc. Of The First European Geosynthetics Conference EUROGEO 1, Maastricht, The Netherlands, pp.1027-1030.

RIMOLDI, P., MONTANELLI, F., (1993) "Creep and accelerated creep testing for Geogrids", Geosynthetics '93, Vancouver, Canada, pp.773-787.

THE RELATIONSHIP OF CREEP CURVES TO RAPID LOADING STRESS-STRAIN CURVES FOR POLYESTER GEOGRIDS

J. S. THORNTON
TEXAS RESEARCH INTERNATIONAL, INC.
C. J. SPRAGUE
TRI/ENVIRONMENTAL, INC.
J. KLOMPMAKER
LÜCKENHAUS TECHNISCHE TEXTILIEN GmbH
D. B. WEDDING
LÜCKENHAUS N.A, INC.

ABSTRACT

When generating a set of creep curves from a given lot of geosynthetic material, it is common to encounter a variation in the strain response levels at the same applied stress. The variation can be due to property differences in the material, or to differences in the testing details such as rate of load application. The uncertainty in the strain level can lead to interpretation problems including erroneous creep reduction factors for long term loading in strain limited applications. The purpose of this study was to further identify and quantify the problem for a family of geogrid products, and to propose and implement a solution.

Ramp and hold short term creep tests were performed on single ribs of three products of a geogrid family. The results of the ramp and hold tests were compared to rapid loading curves acquired on single rib and wide width specimens of the same products. These comparisons show similar results for the strains and times at the beginning of the constant stress portion of the creep curves.

To insure compatibility between the short term and the long term stress-strain relationships, we recommend that in the absence of an acceptable model for estimating the creep that occurs during the loading process, loading rates for generating rapid loading stress-strain curves and those for generating creep curves be the same. To facilitate and document this, we recommend that both load and extension during the loading ramp for creep tests be measured, recorded and included as part of the test report.

INTRODUCTION

Obtaining long term creep data on a geosynthetic manufacturer's soil reinforcement products is an expensive proposition. ASTM 5262 recommends that tests be conducted at 20, 30, 40 and 60% of the rapid loading ultimate tensile strength (UTS) of each product tested. With numerous products needed to fill a product line, it is easy enough to understand why performing replicate tests is not a popular concept from the producer's point of view. Yet, the specimen-to-specimen variation for creep strain results obtained at the same nominal stress level can be substantial. Coefficients of variation of 5% or greater are not unusual. This means that, as generated, the creep curves shown in Figure 1 may not represent adequately the central

tendency of product behavior at the stress levels tested. We refer to such creep strain curves that are disconnected from their ramp and initial rapid strain curves as singleton creep curves. Figure 1 displays creep strain data adapted from Figure 2 of Thornton, Paulson and Sandri (1998). In a related issue, it occasionally becomes desirable to modify construction details of a product to effect performance enhancements. Industry experience with polyester fiber based geosynthetics is that while small changes in structure may cause large changes in the rapid loading tensile characteristics, they have little measurable effect on the slopes of the creep strain vs. log time curves. For examples, see Koutsourias (1995). Therefore, the original creep curves may describe the creep rates of the modified products adequately, but are not appropriately placed at the strain levels that represent the overall creep performance of the modified products.

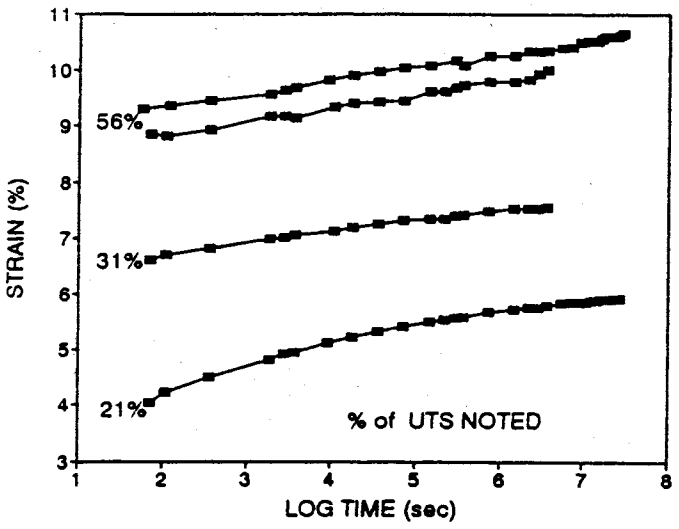

Figure 1. Creep curves for a polyester geogrid tested at 20C and 21, 31, and 56% of the ultimate tensile strength (UTS). The 21% curve and one of the 56% curves extend to 10,000 hours. (Adapted from Thornton et al., 1998.)

For both of these situations, it is convenient to have a rationale for adjusting the vertical locations of as generated creep curves to reflect the central and variational tendencies of the time dependent behavior of reinforcement products.

What has been done in the past is to look to the set of rapid loading tensile stress vs strain curves developed for the product to assign starting strains for the stress levels tested for creep response. This is an approach that will work, provided that the entire creep strain history from the time of the ramp-up peak has been preserved, and that the rapid loading tests and the ramp-up portion of the creep tests were performed under similar loading conditions. It is our experience that these conditions are rarely met. It is the industry conventional approach in the USA, as described in ASTM 5262, to perform creep tests in dead weight or lever action loading frames, taking creep strain data manually using dial indicators to measure strain. While it is recommended that a) the loading rate be 10% ± 3% per minute, that b) the total loading time be recorded, and that c) the initial extension readings be taken at 1, 2, 6, 10 and 30 minutes, there is no requirement that a) a zero time extension reading be taken and furthermore b) the practitioner is cautioned to disregard measurements within five times the loading time. Under these guidelines, it is unreasonable to expect that the information necessary to link the rapid loading data to the creep data will be retained. The amount of creep that takes place between the peak of the loading ramp and five times the duration of the loading ramp can be very significant. Figure 2 from Müller-Rochholz (1997) illustrates the effect of loading time on the shapes of creep strain vs log time curves for a polyester geogrid loaded to 50% of the UTS. Three loading times ranging over two orders of magnitude are shown. For the fastest ramp, over 3% strain occurs between the ramp peak at 5s and the 5x point at 25s. The two specimens at the middle rate show

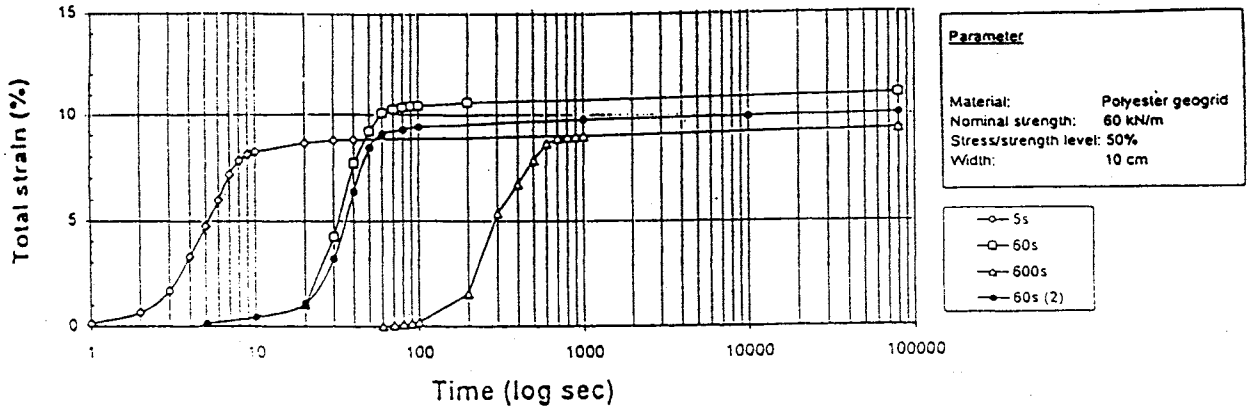

Figure 2. Creep response curves including the ramp for three loading rates to 50% of the ultimate tensile strength of a polyester geogrid (from Müller-Ruchhulz, 1997). The stress ramp peak for the left curve is 5s, those for the middle two curves are 60s each, and that for the right curve is 600s.

about 1.5% creep between 60 s and 300 s. The slowest ramp shows about 0.5% creep strain between 600 and 3000 s. Disregarding data from the ramp peak to 5 times the loading time is effective in eliminating the rapid initial creep from the record. What remains is the nearly linear semi-log creep curves. Setting the RLT ramp peak strain as the starting strain for the semi-log linear creep curves is clearly wrong as it would underestimate the long term creep results. Figure 2 also displays specimen- to-specimen variation of roughly ± 1% about the median at nearly 10^5 s.

The objective of this paper is to describe the use of very short term creep tests that we have labeled ramp and hold (R+H) tests to help determine the appropriate location of singleton creep curves. This is not a new solution but possibly a new application. For example, Greenwood (1990) used two or more contemporaneous R+H tests of 1 hour duration to reduce uncertainty in the vertical (strain axis) location of long term creep curves. As you will see shortly in the present applications, however, the opportunity to do significant contemporaneous replicate testing had not been taken. Thus, the R+H tests to be described post date the singleton creep curves by several years and at least one product improvement cycle.

MATERIALS AND METHODS

The materials investigated during this project were light, medium and heavy weight grades of PVC coated polyester geogrids. The nominal wide width strengths of these materials were 45 kN/m, 65 kN/m and 90 kN/m respectively. Tests performed on these materials included wide width tensile per ASTM 4595 and wide width creep per ASTM D5262. Numerous other tests were performed on single rib specimens and these consisted of rapid loading tensile (RLT) tests, ramp and hold (R+H) short term creep tests and stepped isothermal method (SIM) accelerated long term creep tests. The RLT tests were performed under crosshead rate control, and the ramp portions of the short term R+H and long term SIM tests were accomplished under load control. The strain rates achieved under these control conditions approximated 10% per minute for most of the tests to be reported upon herein.

For the wide-width creep, multi-station rigid lever action creep frames providing a 10:1 mechanical advantage in the loading train were employed. Temperature control to 21 ± 0.2C was achieved through the use of environmental chambers constructed to surround the specimens. Grips used in the wide width creep tests were a custom three roll design fabricated in-house. The wide-width tensile tests were conducted in the temperature controlled geosynthetics testing laboratory using a Model 5585 Instron testing machine equipped with capstan roll grips. Extension measurements for the creep tests were made using dial indicators attached to cross pieces that were clamped to the specimens to define their nominal 8" gage lengths. An Instron long travel extensometer was used to measure extension on the tensile test specimens.

A model 4505 Instron testing machine was used to perform the SIM creep tests on the single rib specimens. Temperature control of the creep tests was obtained by performing them in an Instron Model 3111 environmental chamber. The RLT tests and R+H tests were done using the Model 5583 Instron in the temperature controlled testing laboratory. Custom three-roll grips designed for narrower specimens were used for the single rib specimen tests. Extension measurements were made using two different instruments, an Epsilon extensometer, and the Instron long travel extensometer.

TEST INTEGRATION

Long term (16,000 hr) creep test results were acquired on wide width specimens of the light, medium and heavy geogrids at 20, 30, 40, and 60% of UTS for these products. This effort provided twelve creep curves. Linear extrapolations of the hard data trends were made to predict the strains at 10^6 hour (114 y). Several short term creep curves were generated along the way to confirm the general strain levels for the creep test results. However, at the completion of the long term tests, we did not have a statistical basis on which to judge whether the individual creep curves represented typical or extreme (high or low) responses to the stresses applied. Obviously, computed creep reduction factors based on atypical response curves would be misleading. The desire to have a rational method for normalizing the creep response curves was amplified by the idea that this could also offer a way to predict the effect of product improvements on long term performance. For reasons given earlier, the industry practice that disregards the initial rapid creep when assigning a "starting" strain for the long term creep curves was rejected.

Therefore, it was decided to perform a matrix of RLT and R+H tests to examine the specimen-to-specimen variability of the creep strain results including the initial rapid creep (within a factor of about 5 of the loading time) as well as the steady state rates. The full matrix is as follows:

Table 1. Test Matrix for RLT and R&H Study.

	No. of Conditions	Test Conditions
Test type	2	RLT, R&H
Ramp rate	2	10%/mm, 60%/min.
Specimen type	2	Wide-width, single rib
Stress level	4	20%, 30%, 40%, 60% of UTS
Materials	3	Light, Medium, Heavy weights

The total number of combinations tested is the product of the numbers of test conditions 2x2x2x4x3=

96. The plan calls for testing six specimens for each condition. The tests have not all been completed as of this writing, but we do have results for RLT and R+H at 10% per minute ramp rate for single rib specimens of all three materials at 40 and 60% of UTS. These will be discussed, along with the conventional creep results in the next section.

RESULTS AND DISCUSSION

Conventional Long Term (16,000 hr) Creep Results.

Long term conventional creep results are shown in Figure 3 for the three grid materials and the four stress levels. Of note is the fact that the medium weight product has the lowest strain response of the three materials at each stress level, although there is no a priori reason for this result. Also of interest are the variations in the spacings of the products at different stress levels. For example the response of the light and heavy products at 30% of UTS meld with that of medium product at 40% and the response of the medium product at 30% melds with those of the light and heavy products at 20%. These results all show consistent, generally linear creep rates in log time, but, as advertised, lack uniformity in vertical spacing. These results were obtained by the authors several years ago. Replicate creep tests of shorter duration were done for several of the conditions to verify general location, but these were not done for all conditions, nor used to adjust the vertical location of the long term tests.

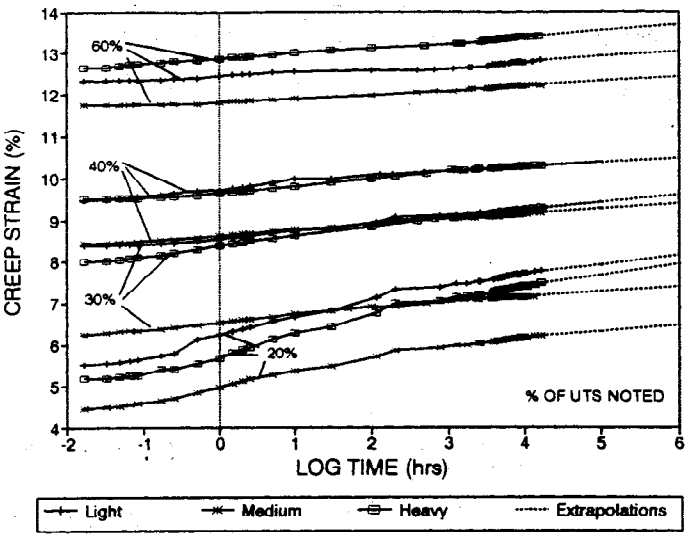

Figure 3. Conventional long term (16,000 hour) creep results per ASTM 5262 (wide-width) for the light, medium and heavy polyester geogrid materials of this study. Curves for stress levels of 20, 30, 40, and 60% of UTS are noted.

Preliminary RLT and R+H Results.

Figure 4 displays a set of RLT curves for single ribs of the medium strength polyester geogrid. The range of strains for a given stress is given by the width of the band of curves at that stress. At 120 lb/rib (40% of UTS) and at 180 lb/rib (60% of UTS) the range of strains in Figure 4 is 0.5% strain. Should the load ramp be interrupted and a constant load applied to the specimen at these points, then the range of starting strains for the resulting creep curves would be expected to span precisely the same 0.5% strain

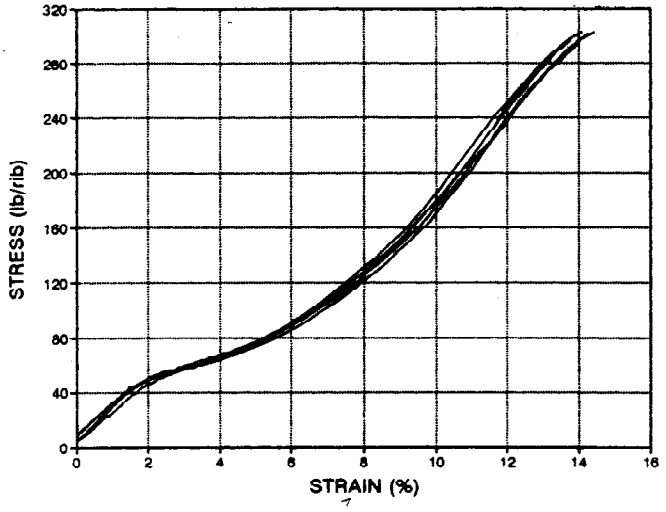

Figure 4. Rapid loading tensile (RLT) curves for single ribs of the medium weight polyester geogrid of this study obtained at a nominal strain rate of 10%/minute and at 20C.

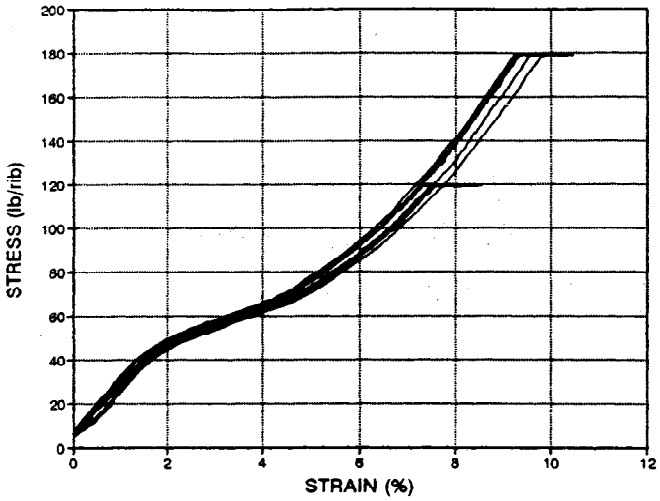

Figure 5. Ramp and hold (R+H) stress vs. strain curves for single ribs of the medium weight polyester geogrid of this study to 40% and 60% of UTS.

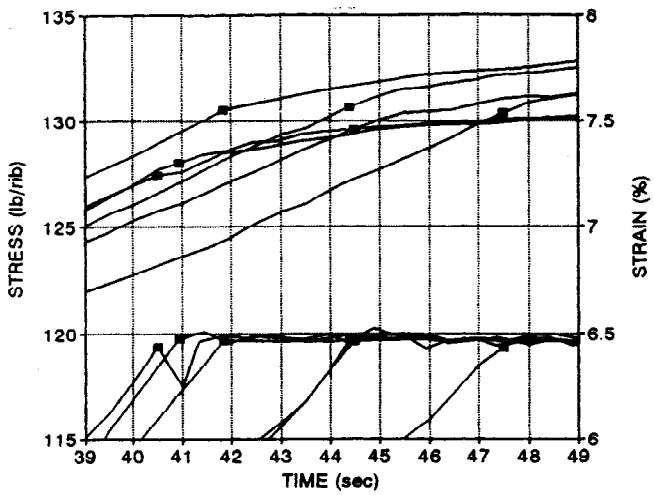

Figure 7. Stress and strain vs. linear time for the 40% R+H data of Figures 5 and 6. The stress data (with scale left) is below the strain data (with scale right). The ■ symbols indicate the stresses and strains at the ram peaks for each test.

for this group of specimens. This precision would require the stresses to be exactly the same. Figure 5 shows such example interrupted stress vs. strain curves that we call the R+H curves. The stress is held constant to obtain creep data for these specimens which are from the same lot of medium strength geogrid tested for RLT results for Figure 4. The strain ranges at 40% and 60% of UTS are about 0.25%* and 0.60% respectively. The creep curves shown in Figure 6 show the initial strains as + symbols on the cluster of strain ramp curves. The initial vertical strain ranges on the creep curves are almost exactly the same as the horizontal strain ranges on the stress vs. strain curves. Even out to log time 3 the creep strain curves, though noisy,

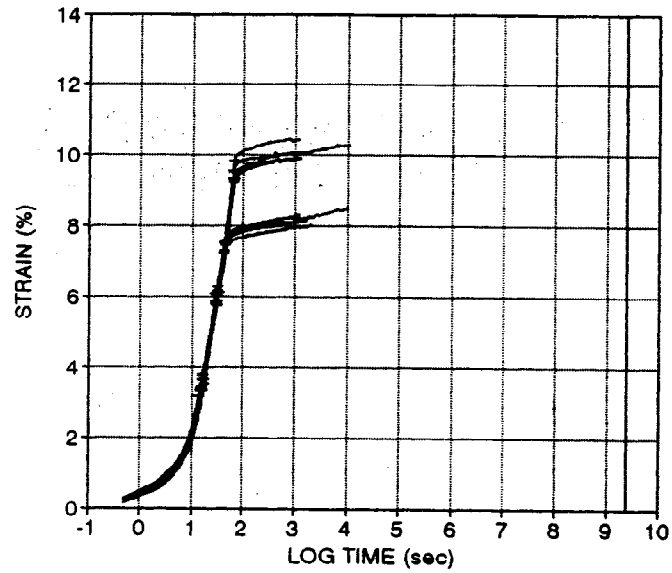

Figure 6. Strain vs. log time (creep) curves for the R+H data of Figure 5.

have not diverged appreciably. The rapid creep that has occurred between the ramp peak and log time 3 is about 0.6% strain at both stress levels. A closeup view of stress and strain vs. time curves at the 40% of UTS level is presented in Figure 7. This figure

*The 0.25% is the range for only the specimens ramped to and held at the 40% level. Obviously, the true uncertainty is larger than the range for the 40% specimens.

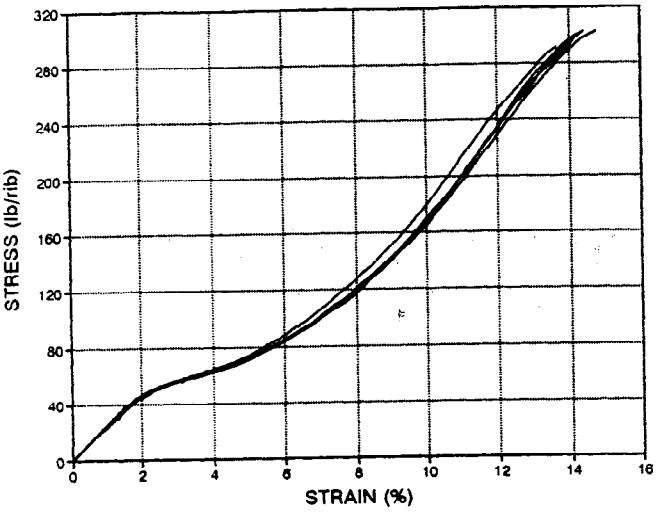

Figure 8. RLT Curves of Figure 4 after "pointing" (see text).

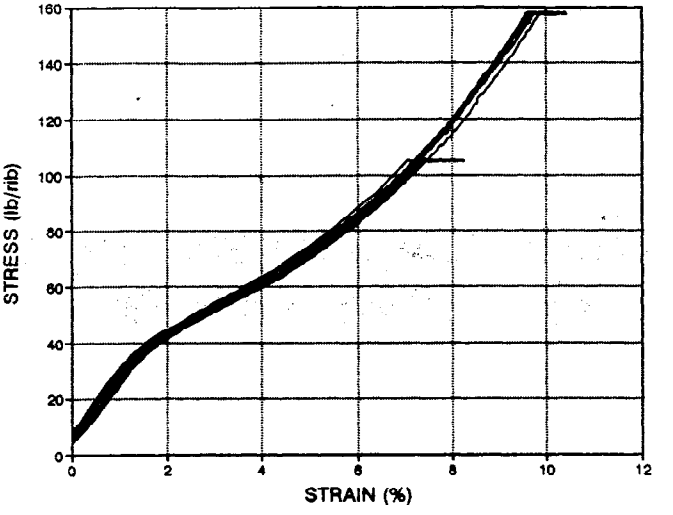

Figure 9. R+H stress vs. strain for single ribs of the lightweight polyester geogrid of this study to 40% and 60% of UTS.

indicates with the ■ symbols the stress and strains corresponding to the ramp peaks, and also shows that the peak strains would be difficult to detect just from the shapes of the strain vs. time curves. The breadth of the strain responses with stress caused some concern, which we address next.

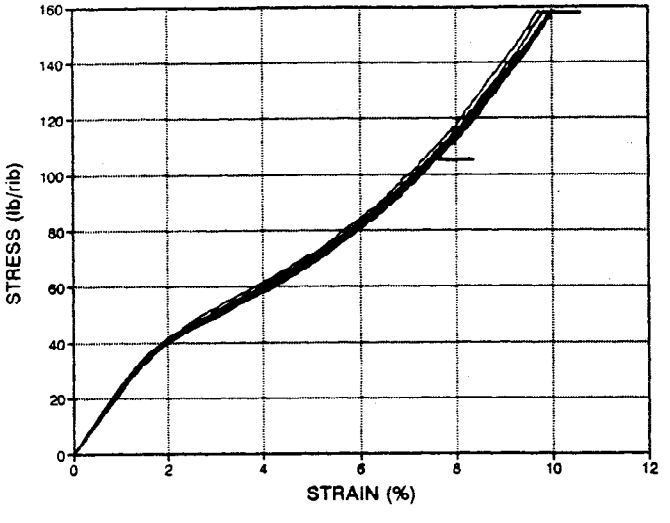

Figure 10. R+H curves of Figure 9 after "pointing" (see text).

Effects of Pointing.

RLT test data obtained on single rib specimens of the medium weight grid, shown in Figure 4 are presented again in Figure 8 after processing through a procedure we call pointing. The pointing procedure brings all the stress strain curves to a point at (0,0) by utilizing the offset tensile modulus generating protocol given in Appendix X.2 of ASTM 4595-86 *Standard Test Method for Tensile Properties of Geosynthetics by the Wide-Width Strip Method.* Essentially this method involves constructing a tangent to the maximum slope region of the initial part of the stress-strain curve and extending this line back to the zero stress axis. This tangent line replaces the initial loading positive curvature portion of the stress-strain relation. The intersection of the tangent line with the zero stress axis is the zero strain point from which the offset strain is measured. In pointing, the stress-strain

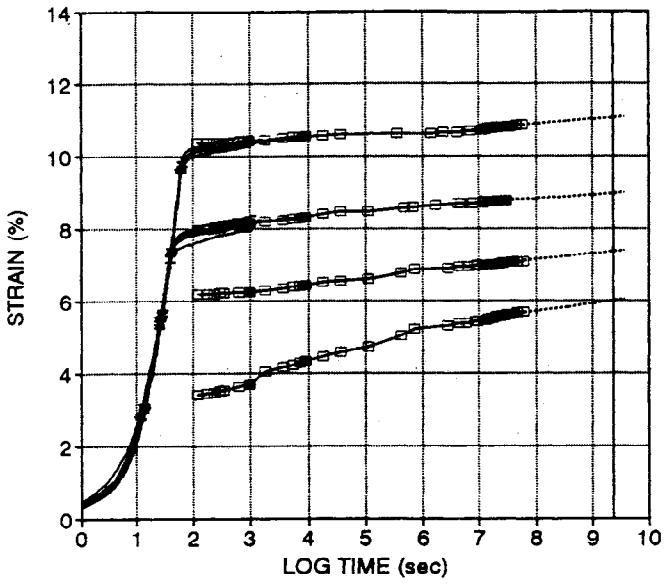

Figure 11. Creep strain vs. log time curves for the light polyester geogrid, showing the effect of lining up the long term curves at 40% and 60% with the mid range of the same stress level short term curves at log time 3. The long term 20% and 30% curves are placed to anticipate the forthcoming short term results.

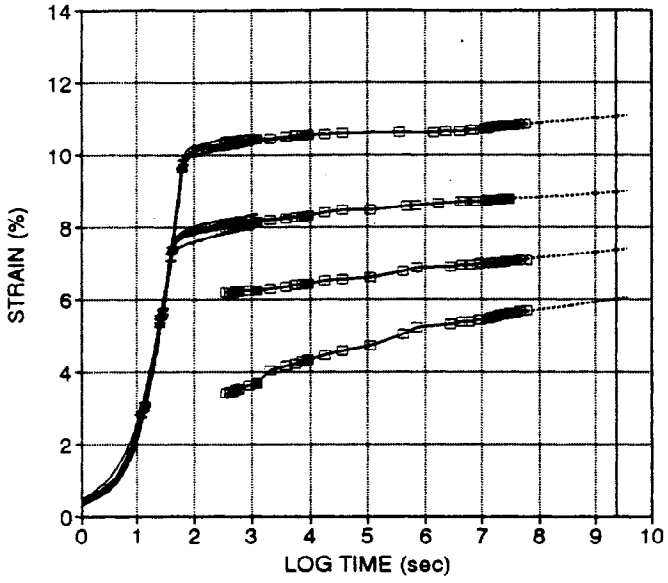

Figure 12. Creep strain vs. log time curves, merging the short term with the long term results after accounting for ramp time, for the light weight product of this study. The long term curves are extrapolated just past the vertical line at log time 9.374 (75 years).

curve which includes the tangent line is shifted to the left from the point of zero offset strain along the zero stress axis to the origin at (0,0). A comparison of Figures 8 and 4 shows that pointing reduces the total variation in strain for stresses below about 30% of the UTS, but in this example the curve for one specimen prevents the effect from continuing at higher stress levels. Before and after pointing, the R+H curves to 40 and 60% of UTS for the light grid single rib specimens appear in Figures 9 and 10. Pointing improves the strain range of the 40% curves from 0.391% strain to 0.281% strain but the range of the 60% curves increases slightly from 0.287% to 0.296% after pointing.

The examples given above were typical of the results obtained for all the RLT and R+H tests. Pointing was found to greatly improve strain variability at low stress levels and not greatly affect the range of strains at higher stress levels. In cases where the initial tensile modulus of the stress-strain curves is an important parameter, then pointing is essential.

Relating 16,000 hour Data to R+H Results

Figure 11 shows the effect of superimposing the long term creep results and the short term R+H results for the light weight polyester geogrid. The long term results are from Figure 3 and the short term results from the data of Figure 10. However, the long term results have been shifted vertically to be consistent with the short term results at log time 3. The apparent creep rates for the short term and the long term results do not agree well between log times 2 and 3. This is caused by the difference in the way time was recorded for the two sets of data. Short term results were clocked from the beginning of the ramp and long term results from the peak of the ramp. Figure 12 shows the improvement of

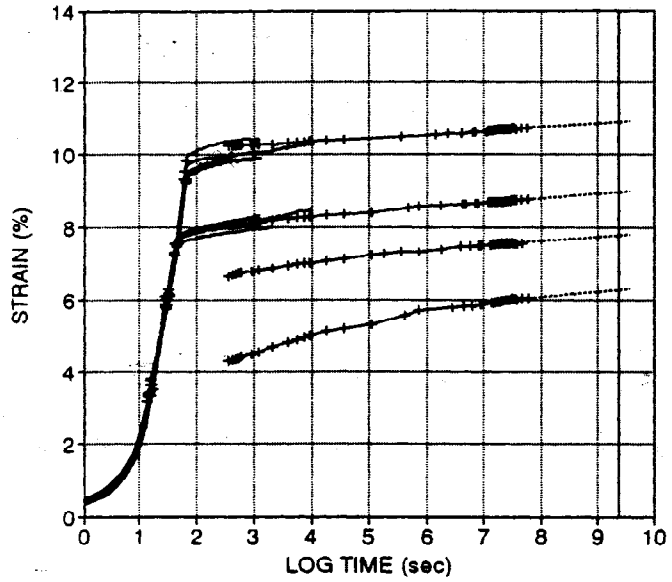

Figure 13. Creep strain vs. log time curves, merging the short term results after accounting for ramp time, for the medium weight product of this study.

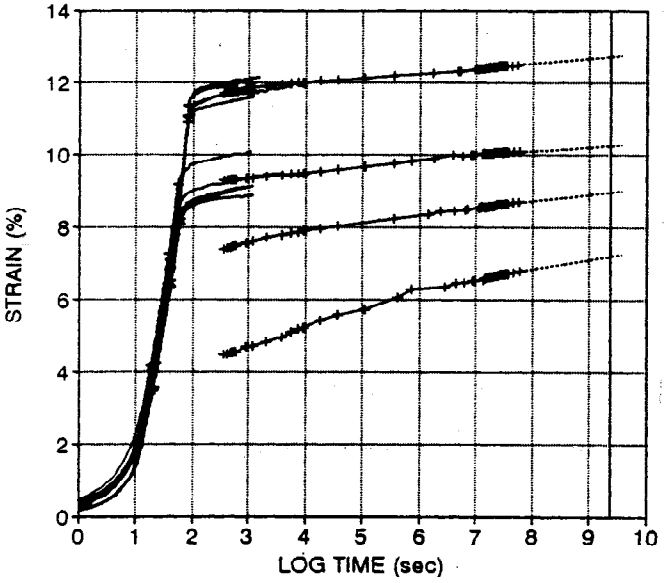

Figure 14. Creep strain vs. log time curves, merging the short term with the long term results after accounting for ramp time, for the heavy weight product of this study.

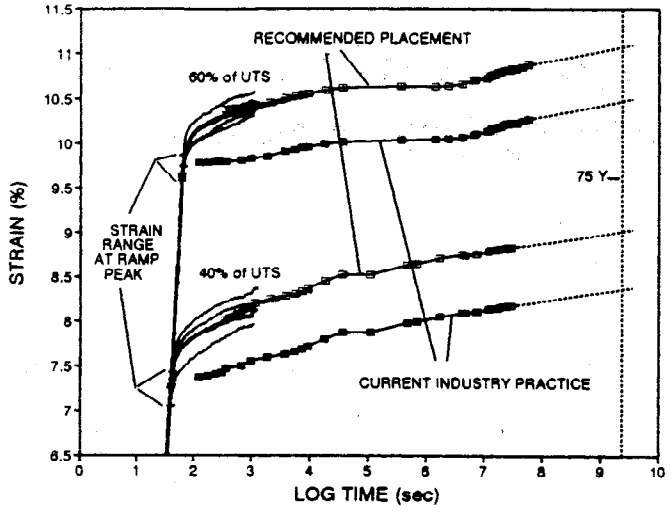

Figure 15. Creep strain vs. log time curves for the light weight product of this study showing recommended placement and current industry practice placement of the long term singleton creep curves.

rescaling -- adding time to each data point for the long term results. Note that the nearly 1/2 decade movement of the initial data points near log time 2 becomes a 1/10 decade movement of the filled rectangle at log time 3 and an imperceptible movement of the filled rectangle at log time 4.

Figures 12 through 14 show the rescaled 16,000 hour creep data for the three products at the 4 stress levels in conjunction with the R+H results at 40 and 60% of UTS for the three products. The long term creep data have been shifted vertically to align with the median of the strain range exhibited by the R+H branches and all creep curves rescaled to account for ramp time. The R+H data for 20% and 30% stress levels have not been completed as yet, but the strain ranges associated with them are indicated in the figures, and the long term creep curves are positioned to anticipate initial rapid creep from those ranges. Figure 15 presents enlargement of the results for 40% and 60% of UTS previously shown in Figure 12, showing the recommended placement position of the singleton creep curves. Also presented are the singleton creep curves of Figure 11 (i.e. before the adjustment for ramp time has been applied) which are placed in accordance with industry practice. The differences in the 75 year intercepts are 0.62% for the 60% curves and 0.665% for the 40% curves. These differences have a significant effect on the strain limit creep reduction factor. If 10% is chosen as the strain limit then the reduction factors for creep work out to 2.029 for the recommended placement and 1.808 for

the current practice placement.

CONCLUSIONS AND RECOMMENDATIONS

Our conclusions are as follows:

1. RLT data contain a lot of information on the variability short term strain response to tensile loads.
2. The causes of the variability were not a focus of the effort, but are surely as much due to testing details as material variability.
3. The initial creep strain variations for the same loads would be precisely the same as that exhibited in the RLT curves if the target loads were identical and there were no momentary over shoot of the target loads.
4. As a good approximation, the strain range exhibited by the RLT curves will be the strain range exhibited by the creep curves, even if the loads are not exactly the same and/or there is over shoot of the target loads.
5. The pointing process to obtain the offset tensile modulus (then shift the curve to the 0,0 point) is necessary to get accurate low stress strain information and modulus data, but is not imperative to obtain usable R+H data for the purpose intended.
6. Obtaining replicate short tem creep data of the R+H variety improves the confidence in locating conventional creep curves for which the initial rapid creep data has been discarded or otherwise.

Our recommendations are as follows:

1. Record the loading ramp for creep curves so that the relationship of the creep response to the applied load and the time are preserved.
2. Perform replicate short term creep tests (100-1000 sec) to establish the range of strains for a given applied stress and the extent of initial rapid creep.

REFERENCES

Greenwood, J.H. (1990), "The creep of geotextiles," *Fourth Int'l. Conf. On Geotextiles, Geomembranes, and Related Products*, The Hague, Balkema, Rotterdam, Netherlands, pp 645-650.

Koutsourias, M. (1995), "Correlating the creep strain component of the total strain as a function of load level for high tenacity polyester yarns, geogrids and geotextiles," *Geosynthetics '95,* Conference Proceedings, Nashville, TN, USA, pp 989-1000.

Thornton, J.S., Paulson, J.N., and Sandri, D. (1998), "Conventional and stepped isothermal methods for characterizing long term creep strength of polyester geogrids," *Sixth Int'l Conf. on Geosynthetics,* Atlanta, USA, pp691-698.

Müller-Rochhotz, J. (1997), "Practicalities of measurement of creep and stress-rupture," *Creep and Assessment of Geosynthetics for Soil Reinforcement*, Seminar Proceedings, ERA Report 9-0015, Leatherhead, UK, pp 1.1-1.12.

PREDICTION OF LONG-TERM PULLOUT BEHAVIOR OF RIGID GEOGRIDS USING ISOCHRONOUS CURVES

RAGUI F. WILSON-FAHMY
PARSONS BRINCKERHOFF-FG, USA
ROBERT M. KOERNER
GEOSYNTHETIC RESEARCH INSTITUTE, DREXEL UNIVERSITY, USA

ABSTRACT

In a previous paper by the authors, a simplified finite element method of analysis was presented which converts the two-dimensional structure of geogrids into an equivalent one dimensional structure. The method was applied in an incremental form to investigate the short-term pullout behavior of geogrids embedded in cohesionless soil. The same model is used in this paper to predict the long-term behavior of geogrids based on the isochronous load -extension curve concept. Isochronous curves corresponding to different loading times are treated as fictitious load-extension curves and used with the finite element method of analysis. The load is applied in increments up to the desired load level. By doing so, "isochronous" curves relating pullout load and displacement can be produced. Using these curves, the variation of pullout displacement with time can be predicted at any pullout load level. The variation with time of other parameters such as the distribution of tension along the geogrid can also be predicted. The method is applied in this paper using actual geogrid data on rigid homogeneous HDPE geogrids.

INTRODUCTION

A theoretical investigation is presented in this paper to study the long-term pullout behavior of rigid homogeneous HDPE geogrids. The analysis is based on the finite element model presented by Wilson-Fahmy and Koerner (1993) which was originally developed to investigate the short-term pullout behavior of geogrids. The method is combined with the isochronous load-extension curve concept to predict the long-term behavior. The analysis provides the variation of displacement, tension force, and frictional and bearing resistances along the geogrid with time.

METHOD OF ANALYSIS

The finite element model developed by Wilson-Fahmy and Koerner (1993) to simulate the soil-geogrid interaction in the pullout mode is used in this paper. The model converts the two-dimensional structure of the geogrid into an equivalent one-dimensional structure while maintaining its two dimensional properties. The technique is used in association with an incremental load transfer one-dimensional finite element type of analysis to study the pullout behavior of geogrids embedded in sand. The reader may refer to the cited paper for a detailed description of the finite element model and material characterization. However, for the reader's convenience, a brief description of the various parameters required to carry out the analysis is given below. This is followed by a description of the adaptation of the method to study long-term pullout behavior.

Ultimate Pullout Resistance

The ultimate pullout resistance for a geogrid embedded in cohesionless soil can be expressed as follows:

$$F = 2A_l\sigma_n' \tan\delta + 2A_t\sigma_n' \tan\delta + A_b\sigma_n' N_q \qquad (1)$$

The first term is the ultimate frictional resistance of the longitudinal ribs. The second term is the ultimate frictional resistance of the transverse ribs and the third term is the ultimate bearing resistance of the transverse ribs. The symbols used are defined as follows:

A_l = area covered by longitudinal ribs
A_t = net area covered by transverse ribs
A_b = bearing area of transverse ribs
σ_n' = effective normal stress at geogrid level
δ = interface angle of friction
and N_q = bearing capacity factor

Note that equation (1) represents the ultimate resistance at failure where all three components of resistance are fully mobilized along the geogrid. At lower load levels, the bearing and frictional resistances along the geogrid will depend on the geogrid deformation. If the tensile strength of the geogrid is less than the ultimate pullout resistance determined using equation (1), failure will be a tensile failure rather than a pullout failure.

Material Properties

The material properties required for the analysis include the load-extension behavior of the geogrid, the soil-geogrid frictional behavior and the transverse rib bearing resistance behavior.

- Geogrid Behavior

The load-extension relationship for a longitudinal rib can be expressed in a polynomial form as follows:

$$T = a_1\varepsilon + a_2\varepsilon^2 + a_3\varepsilon^3 + \ldots \quad (2)$$

where

T = tension force
ε = tensile strain
and a_1, a_2, a_3, ... = polynomial constants

The instantaneous tangent modulus can be obtained at any stress level by differentiating equation (1) with respect to the strain ε.

The transverse ribs are treated in two different manners depending on their stiffness. Short stiff ribs (as in rigid, homogeneous HDPE geogrids) are assumed to not deflect under load whereas transverse ribs with negligible flexural rigidity (as in textile-like PET geogrid) are assumed to take a parabolic shape when loaded. In this paper, only geogrids with stiff transverse ribs are analyzed. The reader may refer to the paper of Wilson-Fahmy and Koerner (1993) in which a transverse rib load-deflection relationship is derived to simulate the behavior of flexible transverse ribs.

- Soil-Geogrid Frictional Behavior

The soil-geogrid interface friction is represented using the hyperbolic formulation of Clough and Duncan (1971). The relationship between shear stress τ and relative displacement ρ is expressed as follows:

$$\tau = \rho \; / \; (a + b\rho) \quad (3)$$

and the tangent stiffness per unit area at any normal stress σ_n is obtained as follows:

$$s_f = [\, 1 - (R_f\, \tau)/(\sigma_n \tan\delta)\,]^2\, M_i \quad (4)$$

where

M_i = initial tangent stiffness per unit area at σ_n
R_f = correction factor
and a and b = constants

- Transverse Rib Bearing Resistance

The relationship between bearing stress q and displacement ρ is also approximated by a hyperbolic function which takes the following form:

$$q = \rho \; / \; (c + d\rho) \qquad (5)$$

and the tangent stiffness per unit area at any normal stress σ_n is determined as follows:

$$s_b = [\; 1 - (R_b \; q) / (\sigma_n \; N_q) \;]^2 \; N_i \qquad (6)$$

where

N_i = initial tangent stiffness per unit area at σ_n
R_b = correction factor
and c and d = constants

The above formulation is suited to the study of the short term-behavior of geogrids. For long-term behavior, the concept of isochronous curves is used as explained below.

APPROACH TO LONG-TERM BEHAVIOR

The procedure to investigate long-term behavior is based on the concept of load-extension isochronous curves. These curves are developed by conducting sustained load or creep tests. The load is applied rapidly up to the desired load level and then the variation of strain with time is monitored. The test is repeated at different load levels and a series of time-strain curves are developed. From these relationships, the variation of strain with the load causing it is determined at any desired time. The load-extension curve obtained in this manner at any particular time is called an isochronous curve and a series of these curves are plotted at different times. The concept is explained in detail by McGown et al (1985) and Andrawes and McGown (1986). The use of isochronous curves to determine the long-term design strength of geogrids is discussed by various researchers, e.g., McGown et al (1985) and Bush (1990). In this paper, isochronous curves are used to predict the long-term behavior of geogrids in the pullout mode.

Difference between Short-Term and Long-Term Conditions

The prediction of the short-term pullout behavior of geogrids using the method by Wilson-Fahmy and Koerner (1993) is based essentially on the three relationships previously discussed. The stress path is basically a simple one due to the following two reasons:

(a) The loading is assumed to be a rapid one and hence neither creep nor stress relaxation are considered in the analysis, and one load-extension curve characterizes the geogrid behavior.
(b) The pullout test and hence the pullout analysis is carried out under a constant normal stress at the geogrid level. Accordingly, the variation of the frictional and bearing resistances with relative displacement are represented by two single curves. Note that the analysis is carried out for an increasing pullout load and hence no unloading-reloading condition occurs.

Under sustained loading the above conditions vary respectively as follows:

(a) The pullout load is maintained at a certain level at the leading end of the geogrid. Thus, the strain in the geogrid becomes a time dependent one. Creep and stress relaxation are thus likely modes along the geogrid.
(b) Because of the strain variation with time, there is a possibility of a redistribution of friction and bearing resistances along the geogrid. Isochronous curves indicate that the geogrid becomes more extensible with time and this affects the frictional and bearing stresses along the geogrid. This can be visualized by considering an inextensible geogrid where the degree of mobilization of shear and bearing stresses will be almost the same along the geogrid length. On the other hand, an extensible geogrid will mobilize friction and bearing stresses in a progressive manner and more concentration of stresses would be expected toward the leading end of the geogrid. Thus, with time, because of the increased extensiblity, there is a possibility of a decrease in friction and bearing or "unloading" toward the trailing end of the geogrid. It is known that the unloading-reloading response for soils can be stiffer than the first loading response (Duncan and Chang, 1970). A rigorous analysis would allow for this phenomenon.

Despite the above differences between short-term and long-term analyses, the solution of long-term behavior can be pursued based on the assumptions and implications discussed below.

Assumptions

The following assumptions are made in order to carry out the long-term pullout analysis:

(a) The relationship between load and extension for the geogrid at any given time can be represented by an isochronous curve regardless of the load or extension paths. This assumption is implied in developing isochronous curves and substantiated by the references cited previously.

(b) The frictional and bearing resistance curves (equations 3 and 5) are unique curves at any given normal stress and the unloading-reloading path is the same as the first loading curve. Thus these curves represent purely nonlinear elastic reponses. It will be shown later in the paper that the effect of this assumption on the results is insignificant.

Based on the above assumptions, the solution for any given time becomes the search for the equilibrium and compatibility conditions that satisfy along the length of the geogrid, the load-extension isochronous curve at this particular time and the frictional and bearing resistance curves at the applied normal stress. Conceptually, this can be performed at any load level by conducting an iterative finite element analysis. Alternatively, an incremental nonlinear procedure can be used up to the desired load level. The latter technique is used in this paper with each isochronous curve treated as a fictitious load-extension curve.

EXAMPLE

In this section, a stiff, homogeneous uniaxial HDPE geogrid is analyzed using the proposed finite element analysis. The geogrid data are given below followed by the analysis of the finite element results.

Geogrid Analyzed

The uniaxial HDPE geogrid is described by McGown et al (1985). It should be noted, however, that various improvements were made to enhance the properties of this type of geogrid over the past few years and a geogrid with the properties given by McGown et al (1985) may not be available at the present time.

The geometry of the geogrid used in the finite element analysis is given below.

Longitudinal Ribs
- Length (C.L. to C.L. of Transverse Ribs = 103.4 mm
- Width = 9 mm
- Thickness = 1.34 mm

Transverse Ribs
- Length (between longitudinal Ribs) = 13.7 mm
- Width = 12.69 mm
- Thickness = 0.44 mm

Note that the above geometry was deduced from the data provided by McGown et al (1985). The thickness of the transverse rib is assigned a larger value than the actual thickness to reflect the

additional bearing area provided by the transverse ribs at the rib junctions where the thickness of the transverse ribs is larger than that of the longitudinal ribs. It should be mentioned that the width of the longitudinal ribs vary being maximum where they intersect the transverse ribs and minimum in the middle between the transverse ribs. The width given above is an average width.

In the paper by McGown et al (1985), four isochronous curves at 20° C temperature were presented at 1, 10, 100 and 1000 hours. Polynomial fitting to the fourth order was performed and the polynomial coefficients representing the four curves are given in Table 1 below. Figure 1 shows the isochronous curves per meter width of the geogrid.

Table 1 Polynomial coefficients for Isochronous curves

Polynomial Coefficient	Isochronous Curve Polynomial Coefficients (kN/Rib)			
	at 1 Hour	at 10 Hours	at 100 Hours	at 1000 Hours
a_1	14.75	11.88	10.56	8.54
a_2	-105.50	-47.00	-64.70	-26.70
a_3	932.40	115.60	462.50	118.50
a_4	-3142.90	54.00	-1392.60	-272.20

The frictional and bearing resistance behavior were obtained from Wilson-Fahmy et al (1994) who characterized these properties for a uniaxial HDPE geogrid embedded in dense sand and subjected to a normal stress of 69 kN/m^2. The parameters to be used in equations (4) and (6) are given below;

Frictional Resistance

M_i = 137298 kN/m^2/m

δ = 30.6 degrees

R_f = 0.87

Bearing Resistance

N_i = 588420 kN/m^2/m

N_q = 26.5

R_b = 0.77

Results and Analysis

Figure 2 shows the isochronous pullout load - displacement curves obtained from the finite element analysis at 1, 10, 100 and 1000 hours. These curves were deduced from load-strain isochronous curves at 20° C temperature. The displacements are those at the leading end of the geogrid. The maximum load level was taken as 35 kN/m in all cases. The reason for this choice is given later. As expected, the longer the time considered the flatter is the isochronous curve. It is interesting to note that the pullout load-displacement isochronous

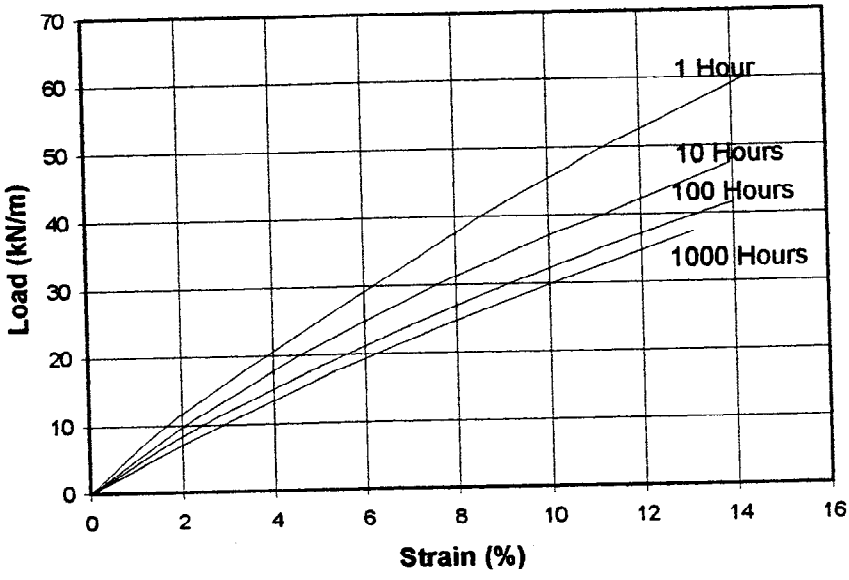

Fig. 1 Load-Extension Isochronous Curves (after McGown et al, 1985)

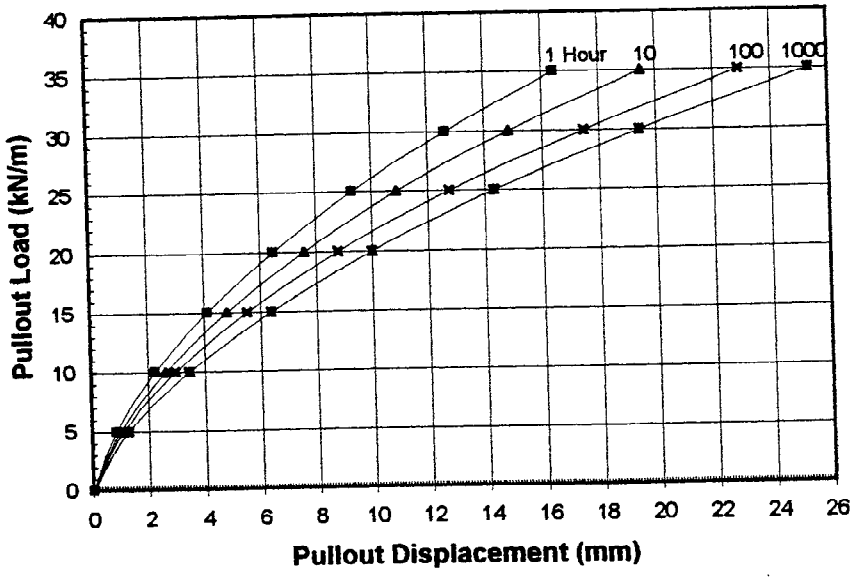

Fig. 2 Pullout Load-Displacement Isochronous Curves (Up to 35 kN/m Load Level)

curves up to the maximum load level considered take the same shape as the load-extension isochronous curves shown in Figure 1 up to the same load level.

From the isochronous curves, the time-displacement curves at different load levels are determined and plotted in Figure 3. Clearly, the curves reflect the fact that the higher the load level the steeper is the time-displacement curve. Note that at the low load level of 5 kN/m, the curve is almost horizontal.

Figure 4 reflects the variation of the tension force distribution with time along the geogrid. In the figure, the tension force at the middle of each of the first six longitudinal ribs is plotted against time at a pullout load level of 35 kN/m. Note that this load level was chosen as it represents approximately the maximum load level attained by McGown et al (1985) in determining the 1000 hours isochronous load-strain curve. A high load level would highlight the effect of time on the geogrid behavior better than a low load level. In general, the tension distribution does not appear to be significantly affected by time indicating that under the conditions analyzed, creep rather than stress relaxation is the dominant phenomenon. A slight reduction in tension with time is, however, noted as the distance increases away from the leading end of the geogrid. This reflects the fact that the geogrid becomes more extensible with time.

In Figure 5, the total resistance (friction + bearing) offered by the transverse ribs is plotted against time again at a pullout load level of 35 kN/m. The ribs are numbered starting from the first embedded transverse rib counting from the leading end towards the trailing end of the geogrid. In the analysis, the transverse rib at the leading end is assumed to be attached to the loading clamp and hence does not offer any resistance. Accordingly, it was not considered in Figure 5. The trend of results indicate some increase in the transverse rib resistance with time up to the third transverse rib. The following ribs indicate some slight reduction in resistance. Again, this reflects the fact that the geogrid tends to become more extensible with time resulting in more concentration of stresses toward the leading end. In general, the fact that the frictional and bearing resistances are assumed to follow a purely elastic nonlinear behavior in the analysis appears to be a reasonable assumption as previously mentioned.

Figure 6 shows the variation of displacement with time at the transverse ribs. As would be expected, the first transverse rib shows a sharper increase of displacement with time compared with the following transverse ribs. Note that there is almost no variation in displacement at the fourth and fifth transverse ribs. This trend of results is similar to the actual measurements recorded by Collin and Berg (1993) and Wilson-Fahmy et al (1995) which showed that the

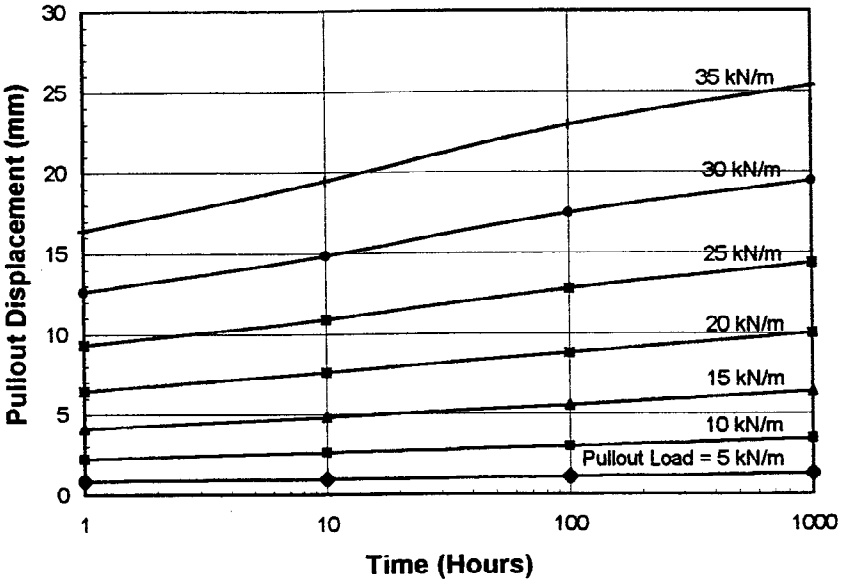

Fig. 3 Time – Displacement Relationships at Different Pullout Load Levels

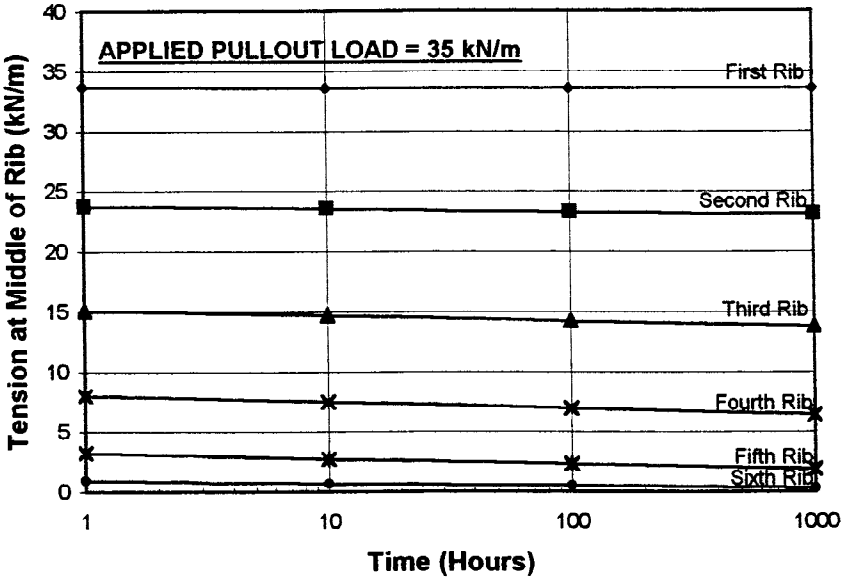

Fig. 4 Variation of Tension Force with Time at Middle of Longitudinal Rib

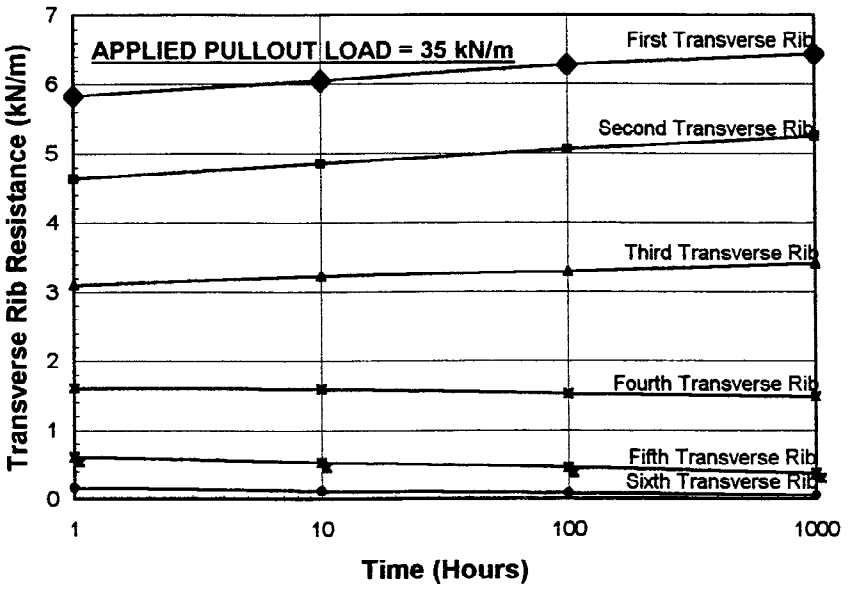

Fig. 5 Variation of Transverse Rib Resistance with Time

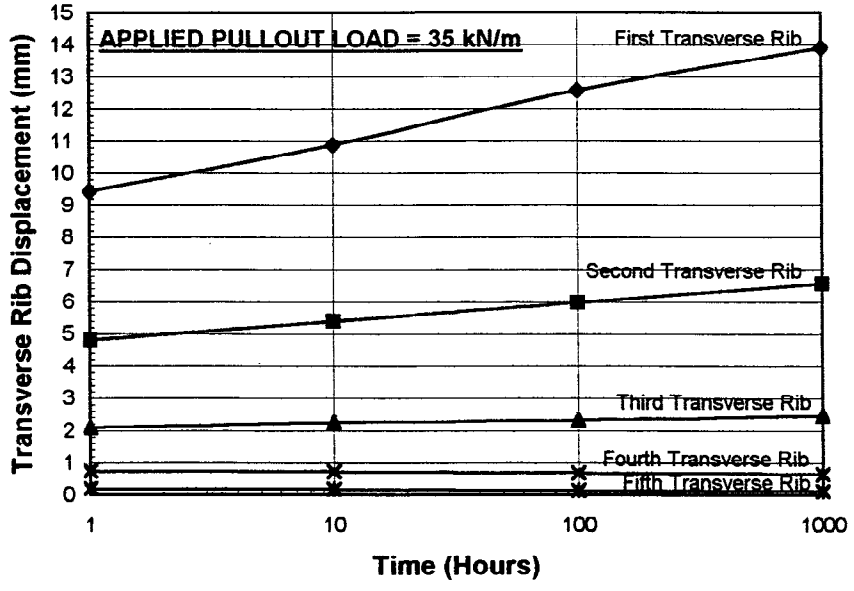

Fig. 6 Variation of Transverse Rib Displacement with Time

further the distance is from the leading of the geogrid, the lesser is the variation of displacement with time.

CONCLUSIONS

The finite element method of analysis of Wilson-Fahmy and Koerner (1993) was used in conjunction with the isochronous curve concept to study the long-term pullout behavior of geogrids embedded in sand. The method was applied to an actual stiff, homogeneous, uniaxial HDPE geogrid and the behavior of the geogrid up to 1000 hours of sustained pullout loading was predicted. The results indicate that creep (rather than stress relaxation) is the predominant behavior along the geogrid.

REFERENCES

Andrawes, K.Z., McGown, A., and Murray, R.T. (1986) "The load-strain-time-temperature behavior of geotextiles and geogrids" Proceedings of the Third International Conference on Geotextiles, Vol. 3, Vienna, Austria, pp. 702-712.

Bush, D.I. (1990) "Variation of long term design strength of geosynthetics in temperatures up to 40o C", Proceedings of the Fourth International Conference on Geotextiles, Geomembranes, and Related Products, Vol. 2, The Hague, The Netherlands, pp. 667-672.

Collin, J.G., and Berg, R.R. (1990) "Comparison of short-term and long-term pullout testing of geogrid reinforcements:, ASTM STP 1190, S.C.J. Cheng, ed., ASTM Philadelphia, USA, pp. 184-194.

Duncan, J.M. and Chang, C.Y. (1970) "Nonlinear Analysis of Stress and Strain in Soils", Journal of Soil Mechanics and Foundation Division, ASCE, Vol. 96, No. SM5.

McGown, A., Andrawes, K.Z., Yeo, K.C., and DuBois, D. (1985)"The load-strain-time behavior of Tensar geogrids", Polymer Grid Reinforcement, Thomas Telford Ltd, pp. 11-17.

Wilson-Fahmy, R.F., and Koerner, R.M. (1993) "Finite element modeling of soil-geogrid interaction with application to the behavior of geogrids in a pullout loading condition", Geotextiles and Geomembranes, Vol. 12, No. 5, pp. 479-501.

Wilson-Fahmy, R.F., Koerner, R.M., and Sansone, L.J. (1994) "Experimental behavior of polymeric geogrids in pullout", Journal of Geotechnical Engineering, ASCE, Vol. 120, No. 4, pp. 661-677.

Wilson-Fahmy, R.F., Koerner, R.M., and Andrew Harpur, W. (1995) "Long-term pullout behavior of polymeric geogrids", Journal of Geotechnical Engineering, ASCE, Vol. 121, No. 10, pp. 723-728

STRAIN EFFECTS ON THE FILTRATION PROPERTIES OF GEOTEXTILES

HORACE MOO-YOUNG
DEPARTMENT OF CIVIL AND ENVIRONMENTAL ENGINEERING, LEHIGH UNIVERSITY, USA

CHARLES OCHOLA
DEPARTMENT OF CIVIL AND ENVIRONMENTAL ENGINEERING, LEHIGH UNIVERSITY, USA

ABSTRACT

There exist various methods to determine the filtration properties of geotextiles, and most of these methods are based on the Apparent Opening Size (AOS) or O_{95} value as designated by ASTM D-4751 "Standard Test Method for Determining Apparent Opening Size of a Geotextile." The ability of a geotextile to function as an effective filter is dependent on the granularity of the medium being filtered, hydraulic conditions, and the configuration of the pore spaces within the geotextile.

This study investigates the changes in AOS with various strains, and how these changes affect the filtration properties of the geotextiles. Tests included dry sieve analysis and pressure filtration tests on various configurations of four non-woven geotextiles, and a woven geotextile under different strains. Contaminated sediment used in earlier studies was also utilized in these tests to enable a quantitative comparison on the amount of fines that were not trapped within the geotextiles.

INTRODUCTION

Due to recent changes in environmental regulations, restrictions have been imposed on the open water disposal of contaminated dredged sediment from the New York Harbor. These restrictions have reduced the amount of dredged sediment by 70%. As a result, the decreases in harbor depth will have a severe impact on the volume of trade conducted since larger cargo ships will be forced to dock at deeper ports.

The use of Geosynthetic Fabric Containers (GFCs) to reduce the movement of contaminated sediments outside the boundary of the disposal site is a method that has been investigated to deal with this problem. GFCs are constructed from synthetic fibers that are made into flexible porous fabric by weaving, knitting, or matting, and act to filter the dredged sediment. During the dredging operation, a split hull barge is lined with the appropriate GFC and the sediment is either mechanically or hydraulically placed into it. After placement of the sediment, the opening of the GFC is closed and the GFC is released from the barge after transport to an aquatic disposal site.

During the actual disposal process very high stresses are experienced by GFCs as they are exiting the barge (Figure 1) as well as hitting the ocean floor. Stresses on the GFCs induce various strains on the geotextile, and it is believed that these strains affect the apparent opening size (AOS) of the geotextiles. AOS is defined as a property which indicates the approximate largest particle that can pass through a geotextile, and is related to the fabrics ability to retain material of a given grain size. Two sets of tests were conducted on the various geotextiles. Fabric analysis strain tests were carried out to study the strain effects on AOS, and Filtration tests under varying strain were conducted to study the migration of fines. In this paper a brief description of GFCs and contaminated sediments along with Fabric analysis strain tests, Filtration tests with varying strain and conclusions are provided as follows.

Description of GFCs

The GFCs consist of an outer woven geotextile that acts as the strength layer, and an inner non-woven needle-punched geotextile that acts as the filter layer. In this

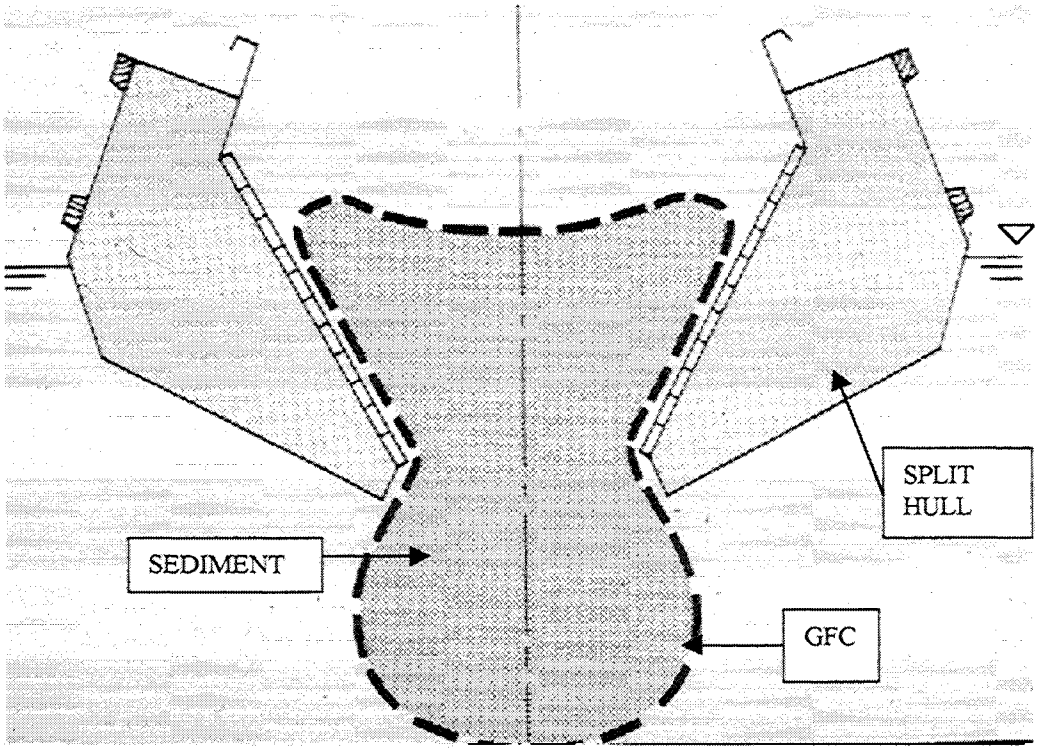

Figure 1. Schematic Illustration of GFC being squeezed during deployment

study, strains of 0, 3, 6, and 9 % respectively were induced on the various geotextiles prior to testing. Strains of up to 9 % were utilized since the outer geotextile, which acts as the strength layer, has a grab strength associated with 10 % strain. Any strain greater than 10% would cause the strength layer to rupture resulting in failure of the GFC.

Geotextiles tested in this study included a woven geotextile that is utilized as the strength and reinforcement layer of GFCs. The filter fabrics consisted of non-woven needle-punched geotextiles weighing 4, 8, 12, and 16 ounces. Table 1 summarizes the various properties of these geotextiles.

Fabric Properties	Test Method	Units	Woven Strength	4oz liner	Fabric 8oz liner	12oz liner	16oz liner
Weight	D-5261	G/m^2	NP	136	272	480	544
		(oz/yd^2)		4.0	8.0	12	16
Thickness	D-5199	mm	NP	1.8	2.7	3.7	4.7
		(mils)		70	105	145	185
Permittivity*	D-4491	Sec-1	NP	2.0	1.26	0.75	0.571
Grab Elongation	D-4632 D-4595[a]	%	10	50	50	50	60
Apparent Opening Size	D-4751	mm (US Sieve)	0.250 60	0.212 70	0.212 70	0.15 100	0.15 100

NP - Not provided by manufacturer
a - D-4595 test method for woven fabric
* - The volumetric flow rate of water per unit cross section per unit head under laminar flow conditions in the normal direction through a geotextile

Table 1. Geotextile Properties (from manufacturers literature)

Description of Contaminated Sediment

Contaminated sediment (Category III by U.S. Army Corps of Engineers, New York District (CENAN) classification) from New York Harbor was used in this study. The sediment was mixed in a 250-gallon tank for three hours. Samples of the mixed sediment were collected for geotechnical index analysis and according to ASTM designation D-2487, the sediment classifies as sandy clay (CH). Geotextiles in this study meet the recommended soil filter criterion which requires the AOS to be less than two to three times (Carroll, 1983) the soil particle size for which 85% of the total soil is finer AOS $<$(2 or 3) d_{85}. The initial water content (ASTM procedure D-2974) of the sediment was 207%, and the specific gravity (ASTM procedure D-854) of the sediment was 2.57.

FABRIC ANALYSIS STRAIN TESTS

The purpose of this series of experiments was to determine the variation in the apparent opening size of the geotextile containers when exposed to different strains. It is anticipated that the strain acting on the geotextile will result in a variation in the AOS, a criterion that determines the fabric's ability to retain a particular minimum grain size. The actual test is a modification of ASTM's D-4751 test. The major difference is that the geotextile being tested is under a predetermined strain.

Apparatus

A customized fabric-straining device. as shown in Figure 2. is utilized in this study. This device is marked with settings for 0, 3, 6 and 9% strains respectively. Geotextiles used were cut into rectangles of 24 cm by 20 cm along both the warp and weft directions. Spherical glass beads ranging in size from 0.053 mm to 0.600 mm were utilized. A heavy-duty triple beam weighing balance with a

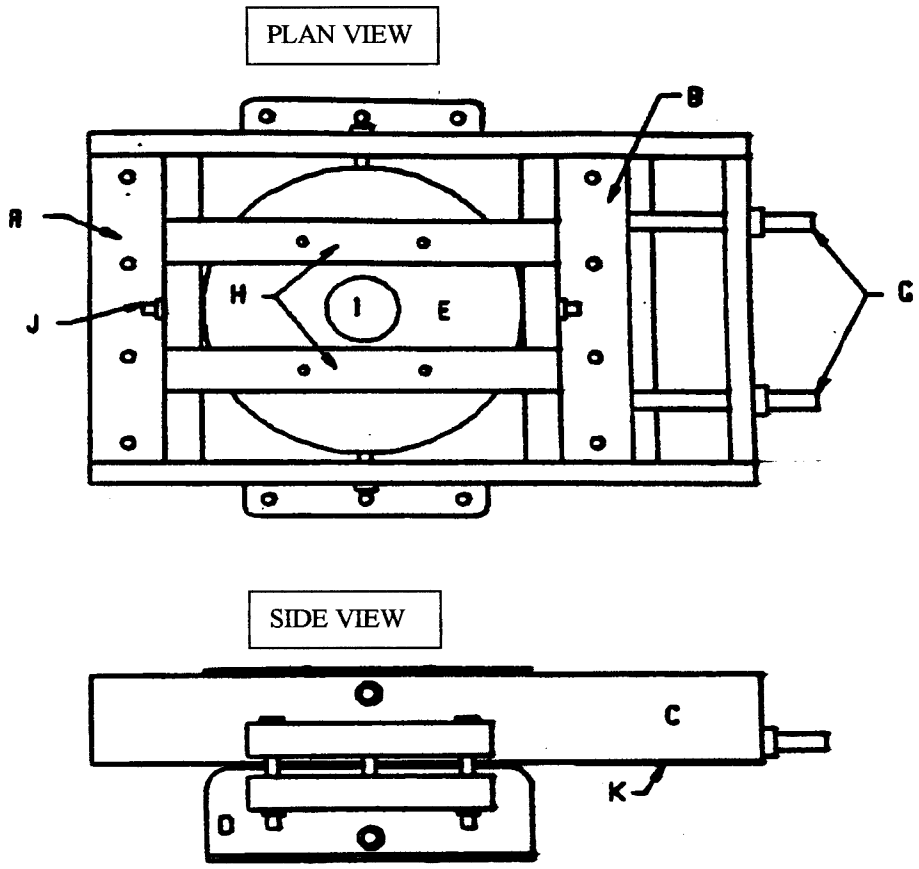

A: FIXED SAMPLE CLAMP (1st END OF GEOTEXTILE CLAMPED HERE)
B: ADJUSTABLE SAMPLE CLAMP (2nd END OF GEOTEXTILE CLAMPED HERE)
C: UPPER JIG FIXTURE
D: LOWER JIG FIXTURE AND SIEVE CUP
E: UPPER SIEVE CUP ON TOP OF CLAMPED GEOTEXTILE
G: ADJUSTING SCREWS FOR SAMPLE STRETCHING
H: SIEVE CUP REATINING PLATES
I: SIEVE CUP LOADING PLUG (BEADS LOADED HERE)
J: SIEVE CUP ALIGNMENT BOLTS
K: ADJUSTABLE SAMPLE CLAMP RETAINING BOLTS

Figure 2. Fabric Straining Apparatus

capacity of 20 Kg was used. A commercial anti-static spray (Static Guard) was utilized to eliminate static electricity. A mechanical sieve shaker was used to agitate the fabric straining device. A 1.5 hp Sears Craftsman air compressor with an air delivery rate of 7.0 ft^3/min at 40 psi, and 5.5 ft^3/min at 90 psi with a capacity of 12 gallons was used to blow out any glass beads trapped within the geotextile.

Procedures

1. The specimens tested were prepared according to ASTM's D-4751 specimen preparation section.

2. Each of the geotextiles was initially coated uniformly with a commercial anti static spray (Static Guard).
3. The geotextile was then secured firmly on the straining device, such that at 0% strain the fabric was taut with no wrinkles or bulges.
4. 50 grams of the glass beads starting with the smallest diameter (0.053-mm) were then placed on top of the geotextile through the upper sieve cup-loading plug as shown in Figure 2. A set of 4 marbles was also placed on top of the geotextile. The upper sieve cup was then plugged.
5. The receiving cup was then mounted onto the straining device.
6. The straining device, geotextile and bead configuration was then secured onto a mechanical sieve shaker. A 2.54-cm block had to be placed between the straining device, and a hammer on the sieve shaker to ensure adequate contact. This configuration was then shaken for 15 minutes.
7. The bottom-receiving cup was then removed from the straining device and its new weight was recorded.
8. The glass beads were then emptied out of both the receiving cup and the geotextile secured onto the straining device. To ensure that all the glass beads were removed, compressed air was blown through the apparatus especially the geotextile, until the original weights were attained.
9. Steps 4 through 8 were repeated using the next larger bead size. This trial was repeated using successively larger bead sizes until the weight of the fraction that passed through the geotextile was 5% or less
10. The geotextile was then strained to the next marking, and steps 4 through 9 repeated. This trial was repeated until a maximum strain of 9 % was achieved.

Marbles were used during testing to aid in the bouncing of the glass beads so as to ensure that all the various orientations were presented to the sieving surface of the geotextiles. The shaking was also increased from ten to fifteen minutes since we believed that the inclusion of the piece of wood between the shaker hammer and the straining device reduced the amount of force with which vertical motion was attained.

Results

Five specimens were tested from each of the five different geotextiles, and the average apparent opening sizes that were determined are summarized in the plot of Figure 3. The values reveal a much lower value for the AOS than those specified by the manufacturers at 0 % strain (Table 1). This difference in values may be attributed to test deviation.

An increase in the AOS with increase in strain is noticed for the woven fabric GT1000. This is most likely due to the fact that woven fabrics are produced by the interlacing of two or more elements, where one set of elements are parallel to the fabric axis (Koerner, 1994). A strain in one particular direction is therefore going to increase the spacing between adjacent parallel elements, which are perpendicular to the strain direction. However there is a negligible decrease in the spacing between adjacent parallel elements, which are parallel to the strain direction. The end result is an increase in the AOS. For the non-woven 4-oz fabric a slight decrease in the AOS is noticed after a 9 % strain. For the other non-woven fabrics, there is no noticeable change in the AOS at all levels of induced strain. Non-woven fabrics (such as 4, 8, 12, and 16 oz) consist of planar random textile structures interlocked together, which in this case is achieved by needle punching. This random orientation of the fibers could explain why in some instances there is a slight increase in the AOS, while in other

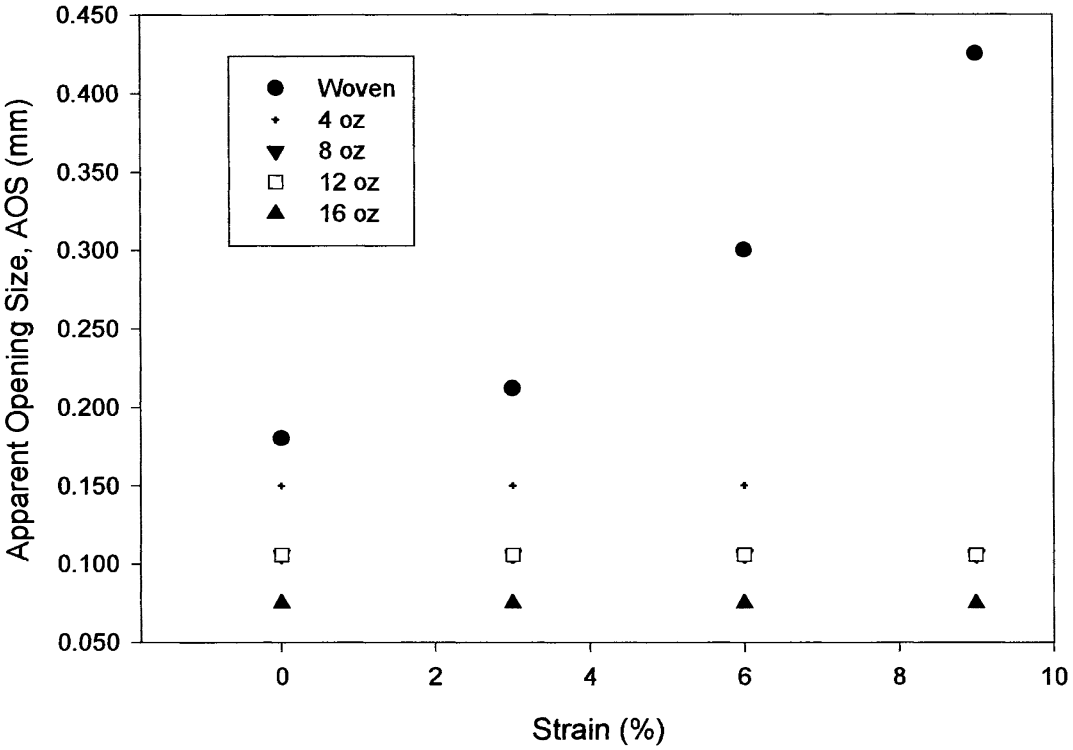

Figure 3. Apparent opening size vs. Strain.

instances there is a slight decrease. Also the grab elongation for the non-woven fabrics are on the order of 50-60 %. Therefore, within the strains experienced in these tests we do not expect drastic changes in the AOS.

FILTRATION TESTS WITH VARYING STRAIN

When sediment is placed into a split hull, the sediment consolidates under its self-weight. The primary purpose of a GFC is to retain the sediment. As consolidation occurs, the sediment forms a cake at the interface with the GFC. This cake enhances the filtration properties of the geotextiles. Cake formation also occurs after the placement of the GFC in the disposal facility. Moo-Young et al. (1997) conducted pressure filtration tests on geotextiles to determine the migration of fines. They showed that the GFCs would provide adequate retention of dredged sediment.

A GFC will undergo tensile stresses and tensile strains during transport to the disposal site, during the release/ or opening of the split hull, and during impact with the ocean floor. Tests were conducted to determine the effects of strain on geotextile performance as a filter regarding the migration of fines.

During these three situations, the apparent opening size of the fabric is altered which may result in a higher fine migration rate.

Apparatus

A Millipore Hazardous Waste Filtration System shown in Figure 4, (Millipore Corporation, Bedford Ma) was used to conduct the pressure filtration tests. This pressure filtration device is used for the Toxicity Characteristic Leaching Procedure (TCLP) in hazardous waste testing (U.S. Environmental Protection Agency (EPA), 1982). The filtration device is made of stainless steel and is coated with Teflon to eliminate heavy metal contamination.

A fabric-straining device as shown in figure 2 was used to stretch the geotextile prior to conducting the pressure filtration tests.

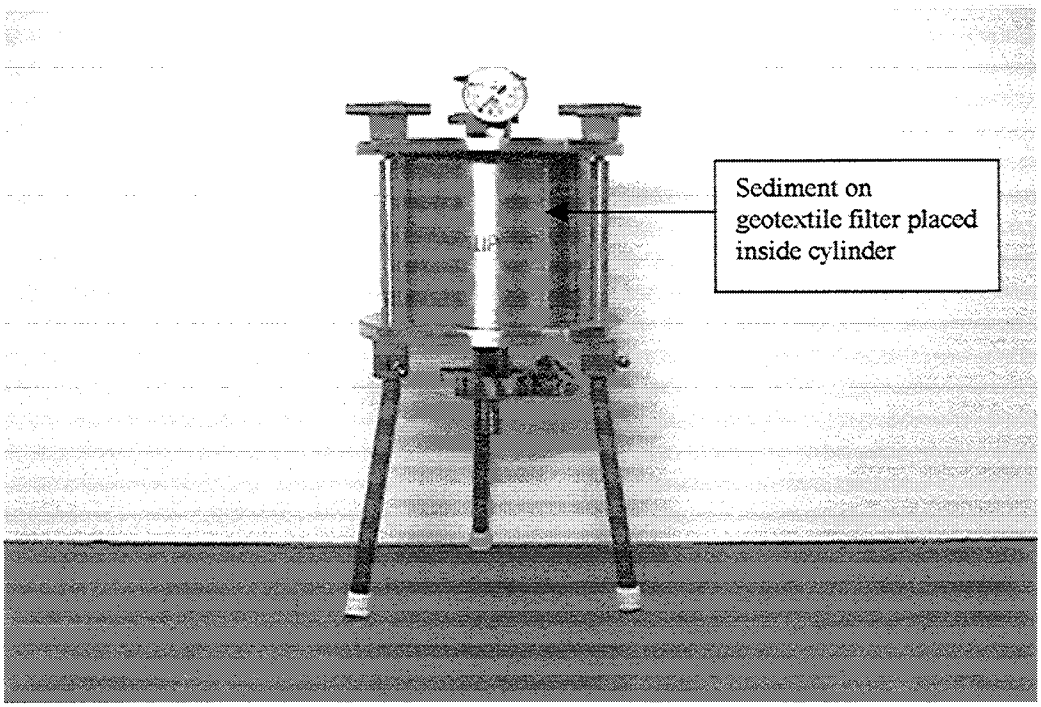

Figure 4. Pressure Filtration System

A Customized filter holder that is able to hold the geotextiles under strain was utilized in this study and is shown in Figure 5. This filter holder was designed such that once the geotextile configuration being tested was secured onto it, the holder could be placed within the filtration device The filter holder has a filtration area of approximately 43 cm^2.

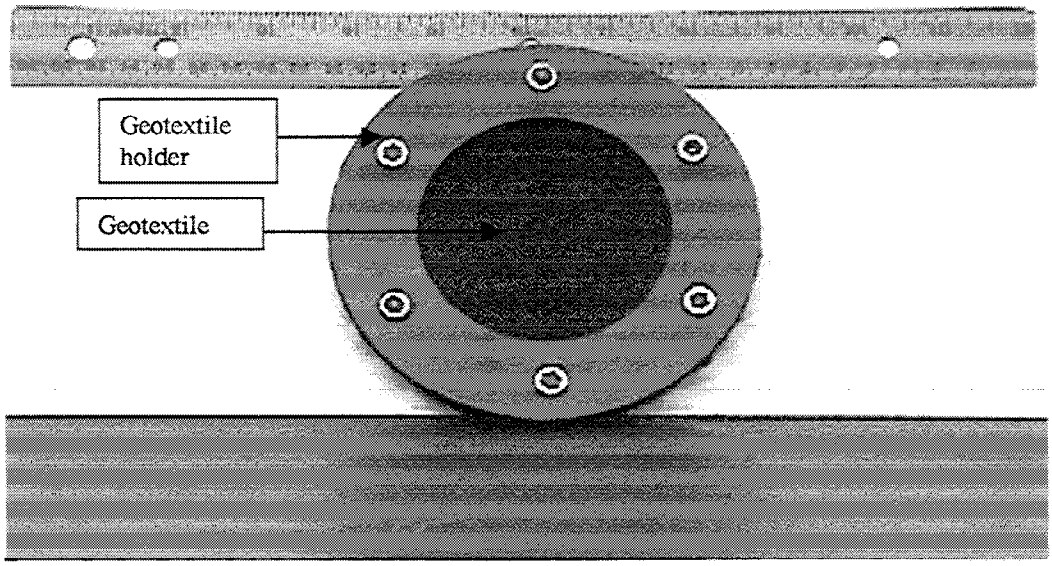

Figure 5. Strained geotextile holder.

Procedure

1. A similar procedure to the AOS test was utilized to set up the geotextile into the holder.
2. The customized filter holder was then secured onto the geotextile by sandwiching the geotextile between the two sides of the filter holder. The geotextile was then cut out of the straining device such that only the filter holder held the strained geotextile.
3. The lower portion of the filtration apparatus was assembled. The geotextile and the customized filter holder were weighed, and then placed into the filtration apparatus.
4. 200 grams of the sediment was weighed, placed into the filtration device, and allowed to settle before running the test.
5. Pressure from the nitrogen cylinder was gradually applied on top of the sample, until the desired pressure was achieved, and the filtrate was collected
6. Tests were conducted until the pressure began to decrease, and no more filtrate passed through the filter. When consolidation of the sediment at the applied pressure was completed, the filter cake was ruptured which caused a decrease in the applied pressure. The final water content of the filtered cake was obtained using ASTM procedure D-2216.
7. Total suspended solids (TSS) tests (Standard Methods for the Examination of Water and Wastewater method 2540 D) were conducted on the collected filtrate.

Results

Attempts to carry out filtration tests at 5 psi (34.5 kPa) proved fruitless since this pressure was too low to give any filtrate. The pressure was increased and filtration tests of the contaminated

sediment were conducted at pressures of 10 psi (69 kPa) and 20 psi (138 kPa). Three samples for each geotextile configuration, and at the four different strains, resulted in a total of 120 filtration tests. Five geotextile configurations were used: The woven strength fabric alone, the strength fabric and 4 oz liner, the strength fabric and 8 oz liner, the strength fabric and 12 oz liner, and the strength fabric and 16 oz liner.

The filtration efficiency in percent was determined by the following equation FE = ($TS_{initial}$ - TSS_{final})/$TS_{initial}$. x 100, where FE is the filtration efficiency, $TS_{initial}$ and TSS_{final} are the initial total solids concentration and the final total suspended solids concentration, respectively (Christopher and Holtz, 1985). At all configurations and under all strains the filtering efficiency was at least 99.9%. A minimum filtering efficiency for silt fence applications of 75 % is recommended. It was noticed that the filtrate although pretty clear, contained more suspended solids for the GT1000 unlined configuration, as opposed to the lined configurations. The general trend was that filtrate TSS seemed to decrease with the utilization of a heavier weight liner in the configuration.
An increase in the applied pressure also showed a slight increase in the filtrate total suspended solids. Figures 6 and 7 summarize the average TSS vs. strain for the five-geotextile configuration at 10psi and 20 psi respectively. In general, Figures 6 and 7 show that geotextile filtration properties are not affected by strains.

The rate of filtrate collection was very erratic and initially there seemed to be some resistance to its passage. When the filtrate eventually passed through the filter, it did not come out smoothly as one would expect, but rather seemed to burst through the geotextile configuration in a very short period of time. Even though consolidation is taken into account, it only explains the time lag before any filtrate is observed. Dierickx (1996) noted that some geotextiles require substantially high water heads before flow can be initiated.

CONCLUSIONS

This paper summarizes studies conducted on five geotextiles used in the construction of GFCs. Fabric analysis strain tests (FAST) to determine the AOS variation with strain, and pressure filtration tests under strain to determine the migration of fines were conducted. The following conclusions can be drawn from these studies:

1. Fabric analysis strain tests showed that with the exception of the outer strength layer, strain does not significantly affect the apparent opening size (AOS).
2. Filtration tests under strain showed little to no increase in suspended solids release with an increase in tensile strain with the exception of the woven fabric. However for the lined configurations this increase was very slight and in some instances there was a decrease especially with the heavier weight liners.

A comparison of the AOS at 0 % strain determined in this study with those given by the manufacturer (Table 1) show significant differences. This could be attributed to differences in testing conditions, but it is also important to note that sieving methods produce arbitrary results, because random chances govern whether a particle meets an opening of the size through which it can pass (Fischer et al, 1996).

This study showed that the heavier weight liners such as 16 oz liner had the best filtration properties under the strains considered here. There was very little difference between the 12-oz and 16-oz liner. Earlier studies by Moo-Young et al. (1997) indicated that the 12-oz liner was best suited as a filtration layer in GFCs filled with the contaminated New York sediment. Results from this study support the utilization of the 12-oz liner in these containers.

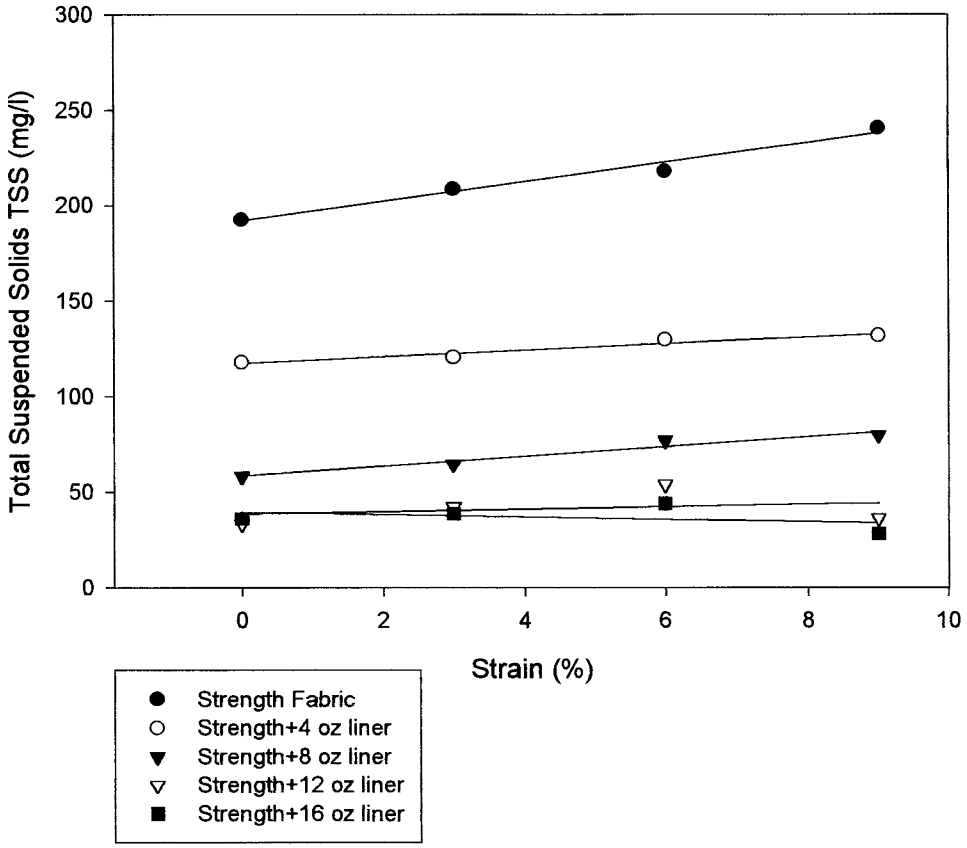

Figure 6. TSS vs. Strain at 10 psi

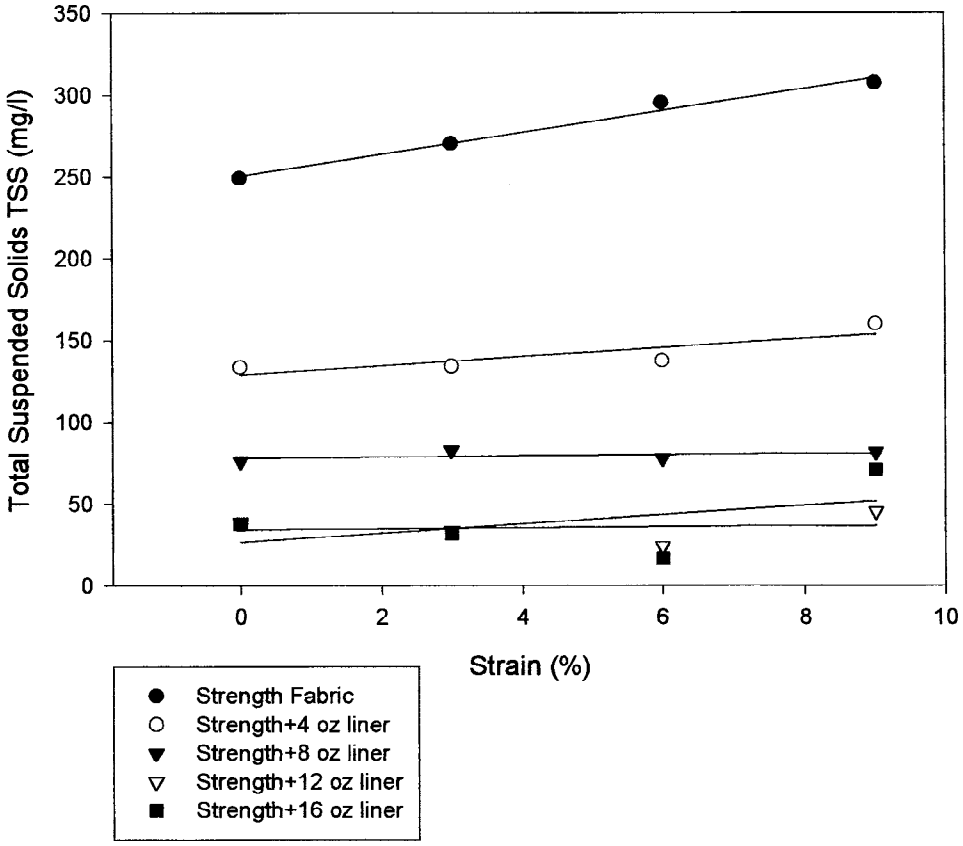

Figure 7. TSS vs. Strain at 20 psi

Acknowledgements

Support for this research was received from the following organizations: Army Research Office, Battelle, and Waterways Experiments station. We would like to thank Brian Tomlinson of BT Technology for his contribution to the research, and we would also like to thank T.C. Mirafi for providing samples for testing.

REFERENCES

Carroll, R. G. (1983). *Geotextile Filter Criteria*, TRR 916, Engineering Fabrics in Transportation Construction, Washington, DC, pp. 46-53.

Christopher, B.R. and Holtz, R.D. (1985). "Geotextile Engineering Manual," FHWA-TS-86-203. Washington, D.C. Federal Highway Administration.

Dierickx, W. (1996) " Determination of Water Penetration Resistance of Geotextiles," Recent Developments in Geotextile Filters and Prefabricated Drainage Geocomposites, ASTM STP 1281, Shobha K. Bhatia and L. David Suits, Eds., American Society for Testing and Materials.

Fischer, G.R., Holtz, R.D., and Christopher, B.R. (1996). "Characteristics of Geotextile Pore Structures," Recent Developments in Geotextile Filters and Prefabricated Drainage Geocomposites, ASTM STP 1281, Shobha K. Bhatia and L. David Suits, Eds., American Society for Testing and Materials.

Koerner, R.M. (1994). Designing with Geosynthetics. Prentice Hall, Englewood Cliffs

Moo-Young, H.K., Meyers, T., Townsend, D., Ochola, C. (1997). " Contaminant Migration Through Geo-Containers Used in Dredging Operations," Geoenvironmental Engineering-Contaminated Ground: Fate of Pollutants and Remediation, (Ed.) R. Yong and H.R. Thomas, Cardiff, Wales pp. 455-460.

U.S. Environmental Protection Agency (1982). "Test Methods for Evaluating Solid Waste," *SW-846*, 2nd ed., Office of Solid Waste and Emergency Response Washington, D.C.

TRANSMISSIVITY OF GEOSYNTHETICS UNDER HIGH NORMAL STRESSES

M.G.A. GARDONI
E.M. PALMEIRA
UNIVERSITY OF BRASÍLIA, BRAZIL

ABSTRACT

This paper presents the results of transmissivity tests on geotextiles and geocomposites under high normal stresses. An equipment for transmissivity tests capable of applying normal stresses up to 2000 kPa was built and used in this work. Five nonwoven and one woven geotextiles, three geonets and six geocomposites were tested. Results of geosynthetic transmissivity, permeability and discharge capacity were presented and discussed. Variations of in-plane (longitudinal) permeability coefficient with the geotextile specimen length were also obtained. A large scatter of test results was observed mainly due to differences in specimen mass per unit area as well as non-uniformities of geotextile in-plane permeability, particularly for the lighter geotextiles. Additionally, an expression was developed to estimate geotextile transmissivity as a function of its mass per unit area and the normal stress applied.

KEYWORDS: Transmissivity, Normal stresses, Geotextiles, Geocomposites, Geonets.

INTRODUCTION

Geosynthetics can be very useful as solutions for drainage and filtration problems in geotechnical and environmental engineering. A large number of products with different characteristics and properties is currently available that may cover most of the usual applications in those fields. In Brazil an increasing interest on the use of geosynthetics for drainage and filtration purposes in works dealing with environmental protection is being observed in the last decade. That has mainly been the case of projects involving waste disposal. In the case of regions of mining activities, the pile of mining wastes can reach heights of the order of 50 to 100 m. Because the unit weight of these wastes can be two or more times the unit weight of common soils, the geosynthetic layer may be subjected to very high normal stresses. Only a few works on the behaviour of geosynthetic hydraulic properties under pressure can be found in the literature

(Gourc et al., 1982, Ionescu and Kellner, 1982, for example). The lack of knowledge on the behaviour of geosynthetics under high normal stresses has limited their use in that type of work.

To investigate the behaviour of geosynthetics under high normal stresses a research programme is being conducted at the University of Brasilia, Brazil. An equipment for transmissivity capable of tests with normal stresses up to 2000 kPa tests was designed and built. Different types of geosynthetics, like geotextiles and geocomposites, were tested and factors such non uniformities along the geosynthetic layer were also investigated. This work presents the results and discussions on this series of tests.

MATERIALS AND EQUIPMENT USED

Test equipment

A testing equipment for transmissivity tests under pressure on geosynthetics was comissioned and built based on the general recommendations presented by ASTM D4716 (1991). Figure 1 presents a schematic view of the equipment. Geosynthetic specimens of 100 x 100 mm can be accomodated for the tests and the vertical stress is applied by a rigid metal plate covering the entire plan area of the specimen. The edges of the plate have rubber seals along its entire thickness. A hydraulic system maintains the vertical stress constant during the tests and a load cell measures the vertical load applied to the sample. For the tests described in this work the vertical stress applied to the geosynthetic specimen ranged from 10 to 2000 kPa. Destilled water reservoirs at the specimen ends allows the water flow under constant total hydraulic gradient whose values (ranging from 0.2 to 3) can be chosen by the user. Only tests with a hydraulic gradient equal to 1 are reported in the present work. Four piezometers equally spaced (20 mm) connected to the base of the specimen allow the measurement of water head variation along the geosynthetic length. The results from the piezometers proved to be very useful in detecting non uniformities of hydraulic properties along the geosynthetic length. All readings of the test were only taken after stabilization of plate settlements and discharge capacity.

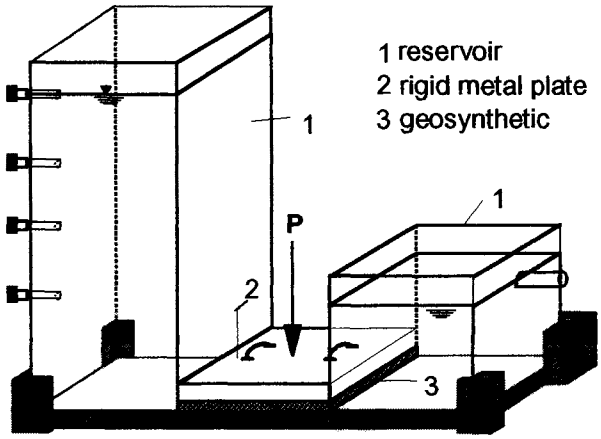

Figure 1. Schematic View of the Testing Equipment.

Geosynthetic materials used

Fifteen types of geosynthetics were used in the test programme and their main characteristics are summarized in Table 1. Figure 2 gives additional details on the geosynthetics tested. All the geosynthetics tested are well known products and commonly found in many parts of the world. Geotextiles G1 to G3 (Table 1) are nonwoven geotextiles, needle-punched, made of polyester continuous filaments of cylindrical shape. Geotextiles G4 and G5 are needle-punched nonwoven geotextiles made of polypropylene. Geotextile G6 is a light woven geotextile made of polypropylene and was only used for comparison purposes. From Table 1 it can be noted that the mass per unit area of the geotextiles varied between 130 and 600 g/m^2. These values of mass per unit area are nominal values presented in the manufacturers' catalogues. For the same product a significant scatter of mass per unit area can be observed and this affects the results obtained in the tests, as will be discussed later in this paper. The geosynthetic specimens were randomly chosen in each product by maping a layer of the product and chosing the specimens using a table of random numbers. A statistical technique associating number of specimens tested to an allowable error in the measure was employed to establish the number of specimens to be tested (Gardoni, 1998).

Table 1. Characteristics of the Geosynthetics Tested

Manufacturer	Geosynthetic Code	Mass per Unit Area (g/m^2)	Polymer Type	d_f (mm)	Fabric Type
1	G1	200	PET	0.027	NW, NP, CF
	G2	300	PET	0.027	NW, NP, CF
	G3	600	PET	0.027	NW, NP, CF
2	G4	150	PP	0.028	NW,NP
3	G5	130	PP	0.037	NW,NP
4	G6	150	PP	-------	Woven
5	GN1	250	PE	-------	Geonet
	GN2	450	PE	-------	Geonet
	GN3	550	PE	-------	Geonet
6	GC11	441	PE-PET	-------	GN1-G1
	GC13	873	PE-PET	-------	GN1-G3
	GC21	646	PE-PET	-------	GN2-G1
	GC23	1118	PE-PET	-------	GN2-G3
	GC31	615	PE-PET	-------	GN3-G1
	GC33	1011	PE-PET	-------	GN3-G3

Notes: PET = polyester, PP = polypropylene, PE = polyethylene, NW = nonwoven, NP = needle-punched, CF = continuous filaments, GN1-G1 = geonet GN1 between layers of geotextile G1, d_f = geotextile fiber diameter.

Three geonets (GN1 to GN3, in Table 1) made of polyethylene with varying masses per unit area were tested. Geocomposites (codes GC in Table 1) are combinations of geonets GN1 to GN3 with nonwoven geotextiles G1 and G3. In these cases the geocomposites consisted of the geonet with a layer of nonwoven geotextile on top. Therefore, as an example, the code GC11 in Table 1 means a product formed by geonet GN1 and the nonwoven geotextile G1.

Before testing the geosynthetic specimens were saturated by destilled water jetting followed by a period of 12 hours under vacuum.

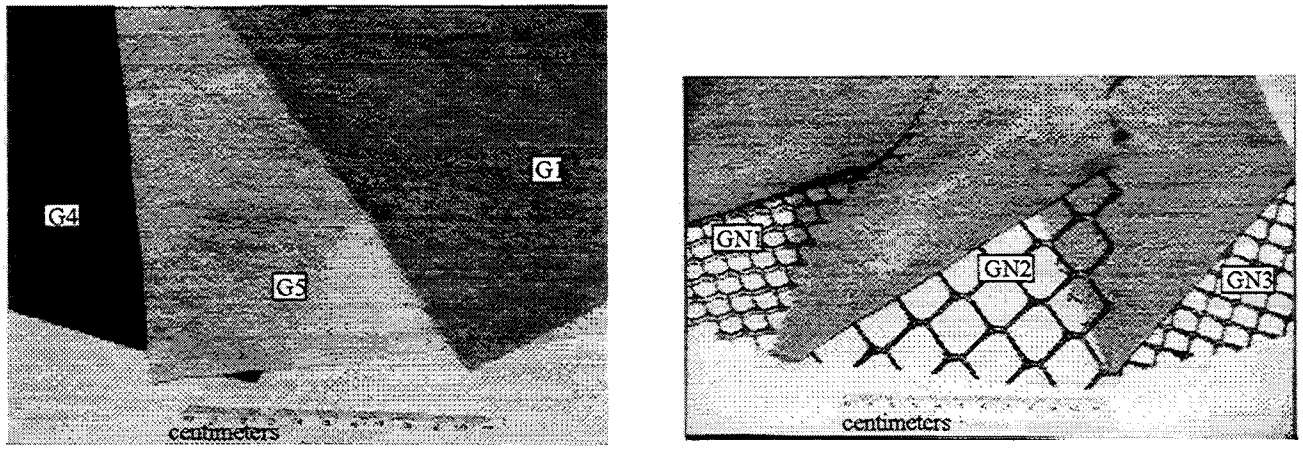

(a) Geotextiles G1, G4 and G5 (b) Geonets and geocomposites

Figure 2. General View of Some Geosynthetic Tested.

RESULTS OBTAINED

Geotextiles

The variation of geotextile thickness with normal stress for the lighter and heavier nonwoven geotextiles G1 and G3, respectively, is shown in Figure 3. A significant scatter of test results can be observed, particularly for the lighter geotextile (G1). This scatter is mainly caused by different values of mass per unit area of the specimens. The scatter of test results decreases with the increase of geotextile mass per unit area. The reduction in geotextile thickness was more significant for normal stresses up to 200 kPa. Figure 4 presents similar results for geotextiles G2, G4 and G5.

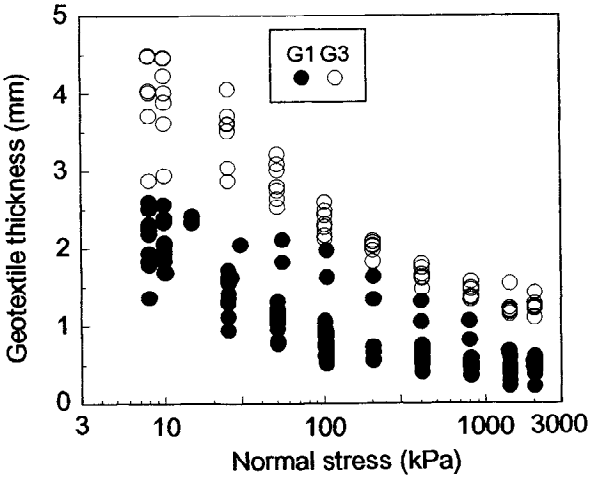

Figure 3. Variation of Thickness with Normal Stress for Geotextiles G1 and G3.

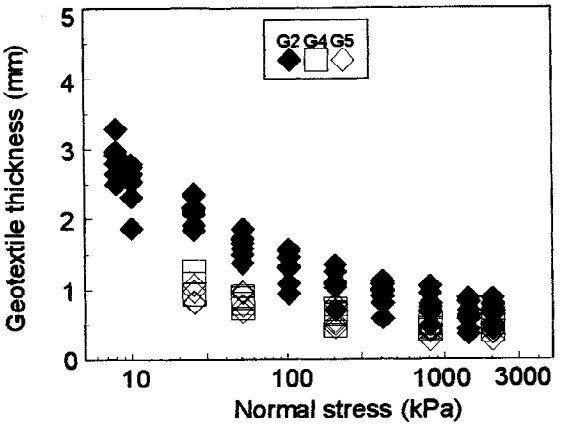

Figure 4. Variation of Thickness with Normal Stress for Geotextiles G2, G4 and G5.

Figures 5 to 9 show the results of apparent transmissivity versus normal stress for the nonwoven geotextiles tested. The term "apparent" is used here because the value of the geotextile transmissivity in this case was calculated as a function of the flow rate measured and the total head loss between the extremities of the specimen. In this case a linear variation of apparent transmissivity with normal stress (in log terms) can also observed in most cases (with the exception of geotextile G4) as well as a rather significant scatter between tests results. For geotextile G1, at a given normal stress, the ratio between upper and lower limits for the range of variation of test results in Figure 5 can vary between 5 and 8. For geotextile G3 this ratio drops to 2 to 3 depending on the normal stress considered. The results for geotextile G4 (Fig. 8) suggest a clear change of pattern of behaviour for stresses above 200 kPa, which is not noticeable for the other geotextiles.

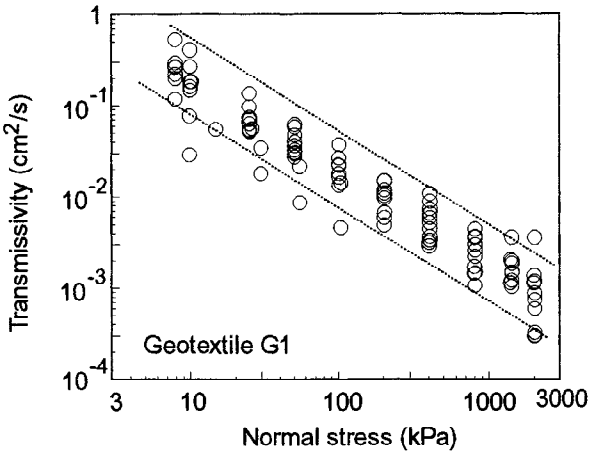

Figure 5. Results of Transmissivity Tests for Geotextile G1.

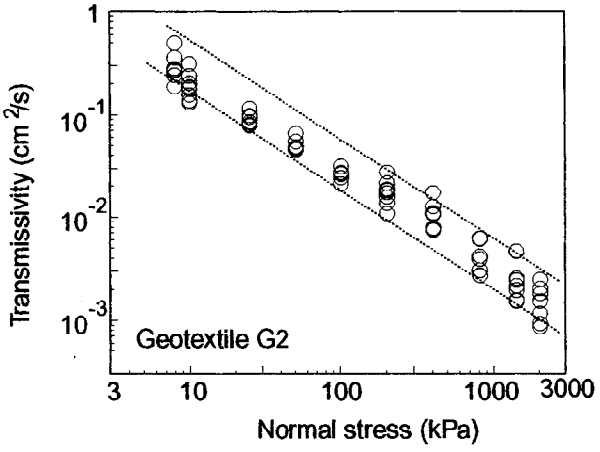

Figure 6. Results of Transmissivity Tests for Geotextile G2.

The results of all transmissivity tests with the geotextiles are presented in Figure 10. This figure gives a general idea of the magnitude of scatter of test results that can be expected in traditional transmissivity tests with different geotextile products. The result obtained for the light woven geotextile is also presented in this figure for comparison. In most of the cases the transmissivity of the nonwoven geotextiles tested were greater than the values observed for the woven geotextile. In spite of the scatter of test results for each product the results in Figure 10 suggest that the lighter the geotextile the lower its transmissivity, particularly for vertical stresses above 200 kPa. It can be observed that, for different products, close values of mass per unit area do not necessarily means close values of transmissivity, as shown by the results obtained for geotextiles G4 and G5 in Figure 10.

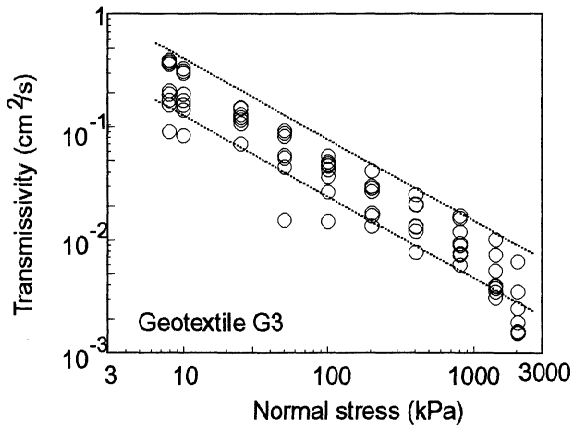

Figure 7. Results of Transmissivity Tests for Geotextile G3.

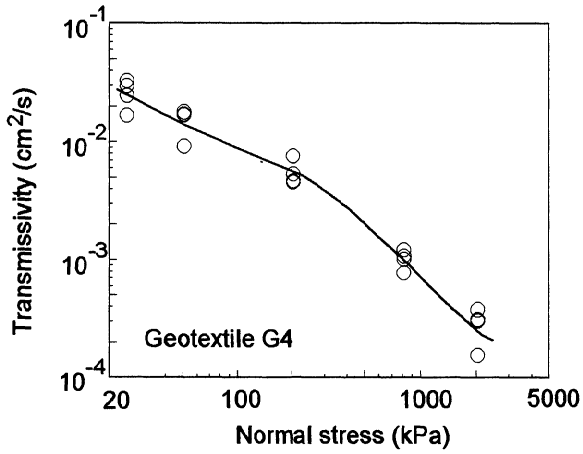

Figure 8. Results of Transmissivity Tests for Geotextile G4.

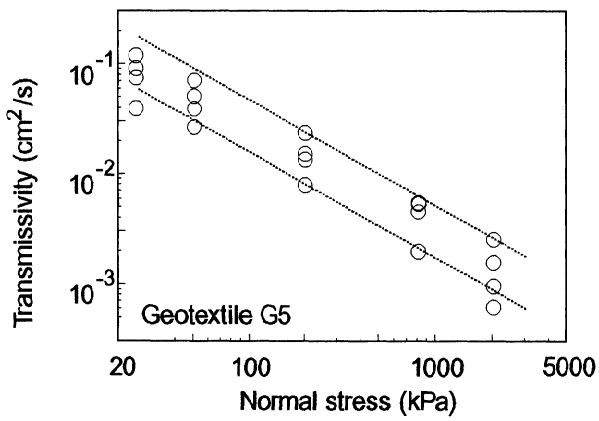

Figure 9. Results of Transmissivity Tests for Geotextile G5.

The variation of discharge capacity (per 10 cm sample width) versus normal stress for nonwoven geotextiles G1 and G3 is presented in Figures 11 and 12. A rather linear variation of the logarithm of the discharge capacity with the logarithm of the normal stress can be observed from these figures up to normal stresses of the order of 1000 kPa. Above this value the discharge capacity tends to drop at a greater rate.

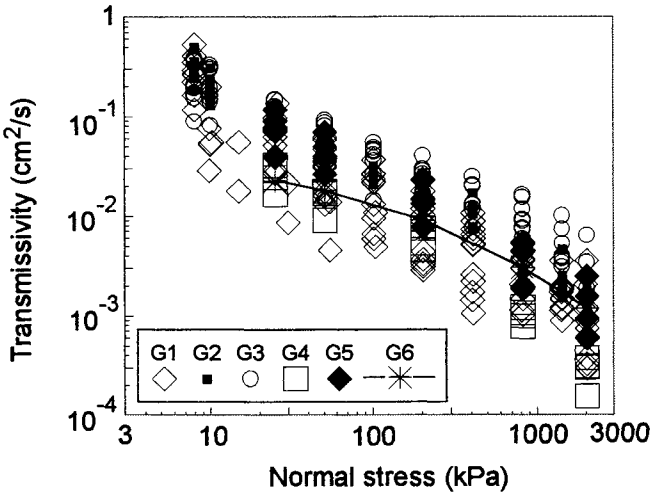

Figure 10. Results of Transmissivity Tests for All Geotextiles Tested.

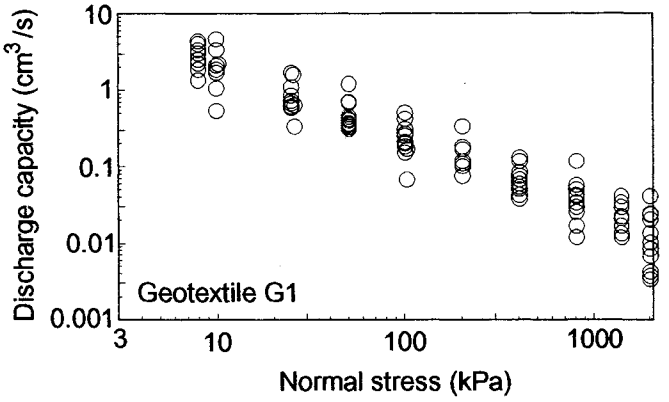

Figure 11. Discharge Capacity Versus Normal Stress for Geotextile G1.

Variations of head loss along the nonwoven geotextile length for a normal stress of 2040 kPa is shown in Figure 13. It can be clearly seen that the lighter the geotextile the less uniform is the variation of head loss along the reinforcement length. For the heavier nonwoven geotextile (G3) a rather linear variation of head loss with geotextile length can be observed.

As a consequence of the results presented in Figure 13 it would be expected a significant variation of geotextile in-plane permeability along the specimen length. That can be clearly seen in Figures 14 (a) and (b), where the variation of local in-plane permeability coefficient with the

specimen length for two values of normal stress is presented for geotextile G1 (hydraulic gradient equal to 1). The local coefficient of permeability was obtained from head losses between successive piezometric ports along the specimen length. The apparent geotextile permeability is also presented in these figures for comparison. This value was calculated as a function of the flow rate and total head loss between geotextile ends. In some parts of the specimen length the local coefficient of permeability can be significantly greater than the apparent permeability coefficient, particularly for high normal stresses (Fig. 14 b). These differences in permeability are likely to be mainly due to non-homogeneities of the geotextile, particularly with reference to mass per unit area. For the heavier nonwoven geotextile the variation of local in-plane permeability along the specimen length (specimen mass per unit area = 602 g/m^2) is less significant, as shown in Figures 15 (a) and (b), due to a more uniform distribution of mass per unit area in this case.

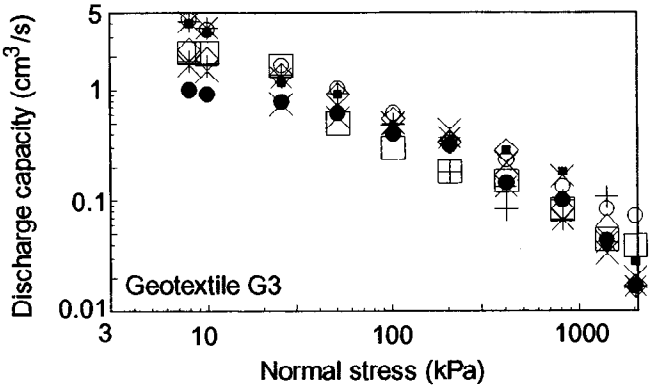

Figure 12. Discharge Capacity Versus Normal Stress for Geotextile G3

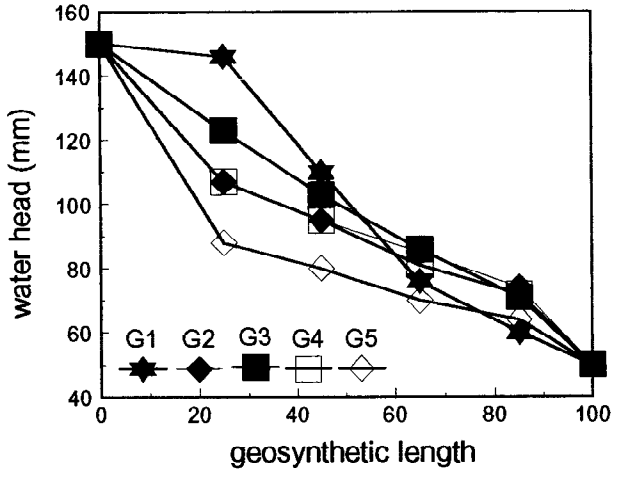

Figure 13. Water Head Variation Along the Geotextile Length (2040 kPa).

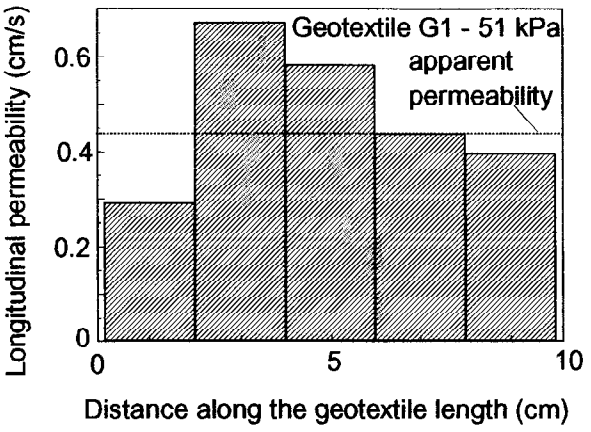

(a) Geotextile G1 at 51 kPa normal stress.

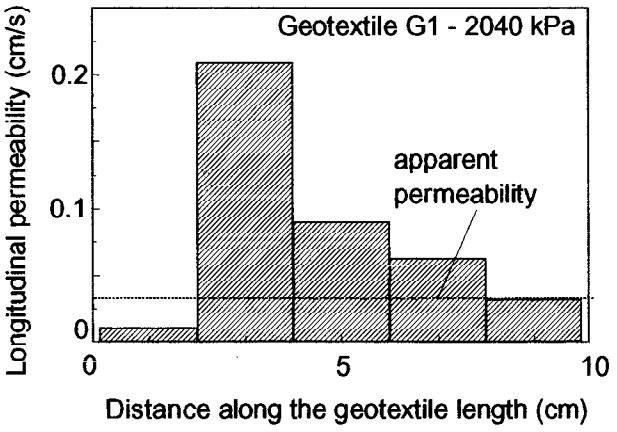

(b) Geotextile G1 at 2040 kPa normal stress.

Figure 14. In-plane Permeability Along the Specimen Length - Geotextile G1

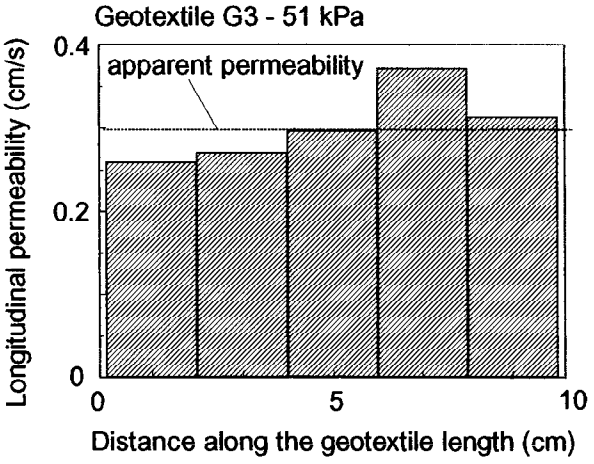

(a) Geotextile G3 at 51 kPa normal stress.

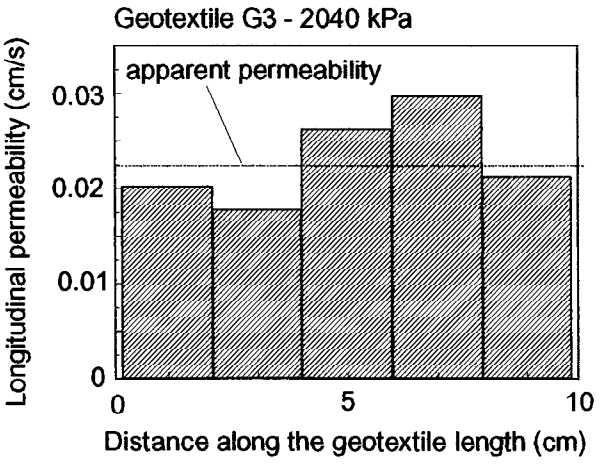

(b) Geotextile G3 at 2040 kPa normal stress.

Figure 15. In-plane Permeability Along the Specimen Length - Geotextile G3

Geonets and Geocomposites

Figure 16 shows the variation of geonet thickness with normal stresses. The results for geonets GN2 and GN3 are close and the rate of thickness reduction with normal stress is similar for the three geonets. As expected, the reduction of thickness for the geonets is substantialy lower than for the geotextiles. Figure 17 shows the variation of geonet transmissivity with

normal stresses where it can be observed that the three types of geonets behave similarly up to 200 kPa. Above this value the ligther geonet (GN1) exhibits a steeper loss of transmissivity with increasing normal stresses, while geonets GN2 and GN3 continue to present close results up to 2000 kPa normal stress. This behaviour of geonet GN1 must have been caused by some level of colapse of the geonet structure for larger stress levels.

Figure 18 shows the variation of geocomposite transmissivity with normal stresses. It can be observed that the nonwoven geotextile cover seems to have less influence on the geocomposite transmissivity for normal stresses up to 50 kPa. For larger normal stresses, the lighter the nonwoven geotextile used as cover for the geonet the greater the geocomposite transmissivity. Similar conclusions can be drawn from Figure 19 regarding the variation of discharge capacity with normal stress.

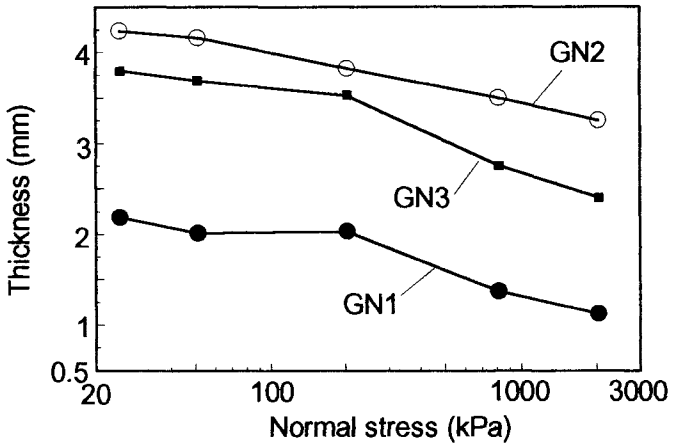

Figure 16. Variation of Geonet Thickness with Normal Stress.

ESTIMATE OF GEOTEXTILE TRANSMISSIVITY

The results presented so far show that for a given geotextile its transmissivity depends on the stress level and mass per unit area. From the results obtained in the tests with nonwoven geotextiles G1, G2 and G3 a non-linear multiple regression procedure (Anderson et al., 1991, Ryan, 1997) was used to develop an expression for the estimate of geotextile transmissivity. The expression obtained is presented below (for geotextiles G1 to G3):

$$\ln\theta = 0.524 - 1.112\ln\sigma_n - 0.00118\mu + 0.000575\mu\ln\sigma_n \quad (1)$$

Where: θ = geotextile transmissivity (cm^2/s), σ_n = normal stress (kPa) and μ = geotextile mass per unit area (g/m^2). The values of R^2 and C.V. obtained for this expression were 0.947 and -9.254, respectively.

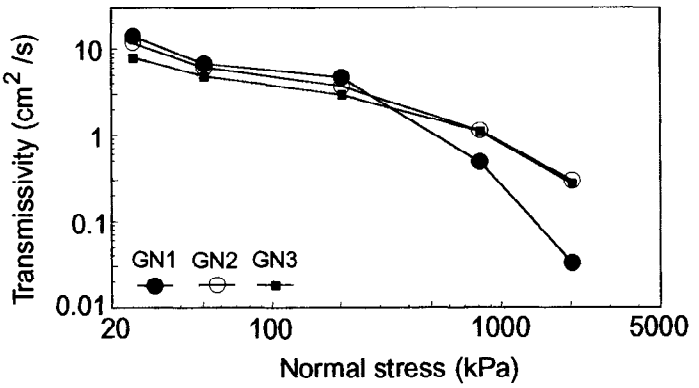

Figure 17. Geonet Transmissivity Versus Normal Stress.

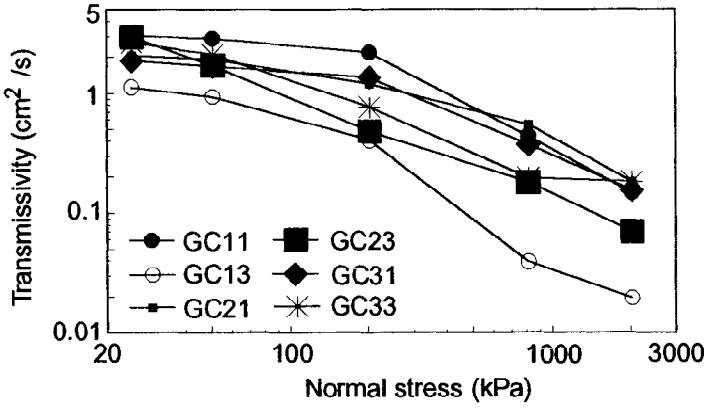

Figure 18. Geocomposite Transmissivity Versus Normal Stress.

Figures 20 (a) and (b) show comparisons between observed and predicted (expression 1) transmissivities versus normal stress for geotextile G1, the one which presented larger scatter of test results. Figure 20 (a) shows the best comparison obtained among all tests performed and Figure 20 (b) shows the worst. Even in the latter case the ratio between observed and predicted geotextile transmissivity was reduced to about 2.5, in comparison to the ratio of 5 to 8 between upper and lower limits for this geotextile, as reported before (Fig. 5). It should be pointed out that most of the comparisons between the test results and the predictions by expression 1 were as accurate as or close to the accuracy shown in Figure 20 (a).

Expression 1 can be a useful tool for the estimate of the transmissivity of geotextiles G1 to G3 for preliminary design purposes in geotechnical and environmental engineering works taking into account normal stresses (up to 2000 kPa) and mass per unit area. Note that geotextiles G1 to G3 are from the same manufacturer and have similar characteristics (manufacturing process, fiber diameter, polymer type, etc). However, it is likely to be possible to use expression 1 for transmissivity estimates for other very similar products (same type of geotextile, same

manufacturing process, same type and geometry of fiber, similar micro-structure, etc.) on a preliminary basis. Similar expressions can be also derived for other geotextile products.

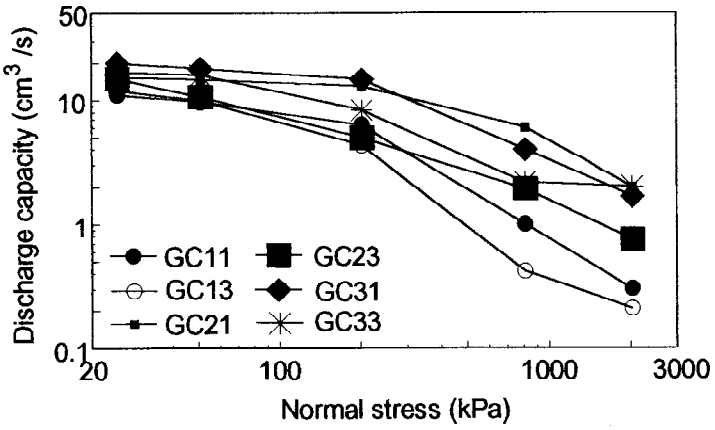

Figure 19. Geocomposite Discharge Capacity Versus Normal Stress.

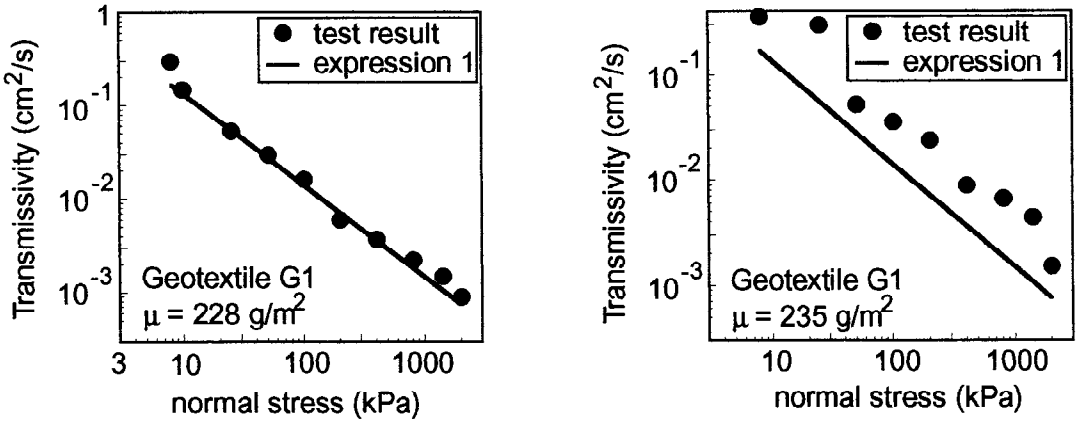

(a) Best comparison (b) Worst comparison

Figure 20. Comparison between predicted and observed transmissivities.

CONCLUSIONS

This paper described the behaviour of hydraulic properties of some geosynthetics when tested under high normal stresses. Large differences between results from different products that may look similar were observed. For a specific product, a considerable scatter of transmissivity results can also be obtained. These results suggest the need to carry out a reasonable number of tests (usually not less than 6 tests for each product) for a better determination of geosynthetic transmissivity values when using traditional transmissivity testing equipments, particularly for light geotextiles. The use of large equipments may reduce the need for many tests but brings some operational difficulties for tests under large normal stresses. Apropriate factors of safety

have to be applied to account for those uncertanties on the value of hydraulic properties of geosynthetics.

It was also observed a significant non-uniformity of geotextile in-plane permeability along the geotextile specimen length, particularly for the lighter geotextiles. For thicker and heavier geotextiles a more uniform distribution of permeability coefficient along the specimen length was obtained.

An expression obtained by the statistical treatment of the data for some geotextiles from the same manufacturer was obtained which provides an useful tool for the estimate of geotextile transmissivity under a rather wide range of normal stresses. Further research is being carried out to obtain a better understanding on the behaviour of geosynthetics under high stress levels.

REFERENCES

Anderson, D.R., Sweeney, D.J. and Williams, T.A. (1991) "Introduction to statistics - concepts and applications", West Publishing Company, New York, 2nd Edition, 714 pp.

Gardoni, M.G. (1998) "The behaviour of geosynthetics under pressure in drainage and filtration", PhD Thesis, Department of Civil Engineering, University of Brasilia, Brazil (in progress).

Gourc, J.P., Faure, Y., Rollin, A. and Lafleur, J. (1982) "Loi structurale de perméabilité pour les géotextiles", 2nd International Conference on Geosynthetics, Conference Proceedings, Las Vegas, USA, Vol. 1, pp. 149-154.

Ionescu, A. and Kellner, L. (1982) "About longitudinal permeability and draining capacity of nonwoven geotextiles", 2nd International Conference on Geosynthetics, Conference Proceedings, Las Vegas, USA, Vol. 1, pp. 127-131.

Ryan, T.P. (1997) "Modern regression methods", John Wiley and Sons Inc., New York, 520 pp.

BIOLOGICAL CLOGGING OF GEOTEXTILE FILTERS
A FIVE YEAR STUDY

ROBERT E. MACKEY, P.E., S2L, INCORPORATED
UNITED STATES OF AMERICA
GEORGE R. KOERNER, PH.D., P.E., & CQA, GEOSYNTHETIC INSTITUTE
UNITED STATES OF AMERICA

ABSTRACT

The leachate collection system at the base of a landfill must function over the operation period and post closure period of the landfill. Past work has led to concern with excessive clogging of the filter placed above the drainage layer or during this extensive period of service.

This paper addresses the findings of a five-year study at the Orange County Landfill in Florida. The study showed unexpected results in which permittivity of several different geotextile filters decreased, but never fully clogged, over the duration of the test. The test was conducted with actual onsite leachate and typical of municipal solid waste (MSW) leachate in Florida.

INTRODUCTION

The leachate collection and removal system (LCRS) of a solid waste landfill must properly function over its design lifetime, which includes both the operational and post closure periods. Located at the bottom of the landfill, a LCRS consists of drainage media (sand, gravel, geonet, or geocomposite) with a filter above it (usually) and a perforated pipe system within it. The pipe system drains to a sump, which is accessed by a manhole or sidewall pipe riser from which the leachate is removed.

Some clogging of the filter material placed above the drainage media is to be expected. Such clogging can occur without adversely affecting the drainage system, until it begins "starving" the underlying drainage media. At that point, leachate will begin to pool into the solid waste. The implication of such buildup, i.e., "perched leachate", is unknown, but certainly is not desirable. In the extreme case, a leachate level may rise to a point from which it can exit the sides of the facility via sidewall or cover seeps. Perched leachate may also result in waste instability.

The filter zone above the leachate collection system is an optimum location for clogging via several mechanisms. These mechanisms include particulate clogging, biological clogging and precipitate clogging. The range of leachate characteristics in municipal solid waste (MSW) landfills is great, making it difficult to speak generically. However, Koerner et al. (1994) have shown that particulates, microorganisms and precipitates are all common to MSW leachates.

ASTM D1987 "Standard Test Method for Biological Clogging of Geotextile or Soil/Geotextile Filters" was developed to allow interested parties to test specific geotextiles using site specific leachate(s). Several test sites were developed across the United States to test the applicability and precision of the test method. The paper addresses the findings of one test site near Orlando, Florida where four different geotextiles were tested over a five-year period. The geotextiles tested included the following:

- 271 g/m^2 polyester (PET) non-woven,
- 542 g/m^2 polyester (PET) non-woven,
- 7 percent open area polypropylene (PP) woven, and
- 32 percent open area polypropylene (PP) woven.

CLOGGING MECHANISMS

Leachate composition is a function of the landfill's specific waste composition, age of the waste, operations and climatic conditions. These factors influence the physical, chemical and biological processes that occur in sanitary landfills. High variability in leachate quality is common, seen not only among different landfill facilities, but also within the individual landfill facility (Andreottola and Cannas, 1992). To decrease this variability of leachate quality, leachate from the specific site should be used for filter studies.

The change in leachate characteristics over the life of the landfill may be viewed as a function of the phase of waste decomposition. The four phases of waste composition include aerobic phase, anaerobic acid phase, accelerated methane phase, and decelerated methane phase (Barlaz and Ham, 1993). Biological growth and chemical precipitation are dependent on waste decomposition and pH. Aerobic microorganisms predominate within the waste mound for a short period just after waste placement and until the oxygen is depleted. The pH of the waste and leachate quickly turns acidic during the aerobic phase. After oxygen within the waste pile is depleted, waste decomposition is performed by anaerobic microorganisms with methanogens as the most numerous organism within the waste. The pH gradually increases during anaerobic decomposition. Anaerobic decomposition may later be hindered within the landfill mound when the pH becomes more alkaline (Barlaz and Ham, 1993). Optimum pH for methanogenic biological growth is between 6.8 to 7.4 (Barlaz, 1993). Biological decomposition of the waste is also impacted by temperature within the waste mound. Optimum growth for organisms ranged from 30° to 35° C, with a doubling of biological activity from 25° to 35° C (Watson-Craik and Jones, 1995; Barlaz, 1996).

To determine the possibility of clogging of geotextile filters for a site-specific application and changes to the leachate over time, the geotextile filter should be tested over a time period sufficient to observe the variation in leachate quality.

This leachate quality will promote clogging by the following mechanisms:

- Particulate Clogging - suspended particles in the leachate are filtered out.
- Biological Clogging – microorganisms grow in and around the filter and are "fed" by the passing leachate.
- Precipitation Clogging - precipitates from chemical (inorganic) or biochemical processes within the waste are transported by the leachate and buildup on the filter or are collected by the microbial mass.

ASTM D1987 TEST METHOD

In 1991, the American Society of Testing and Materials (ASTM), Committee D-35 on Geosynthetics, issued ASTM D 1987, "Standard Test Method for Biological Clogging of Geotextile or Soil Geotextile Filters." This method was developed to assist in the determination of the performance of candidate geotextiles with site specific leachates.

In the seven years since the test method was issued, the method has seen limited use, but is still highly regarded. It is the only D-35 flow through porous media test which has a provision for site specific fluids. The test method is conducted by mounting a geotextile filter specimen or geotextile/soil filter composite specimen in a flow column so that leachate can flow through it in either a constant or falling head condition. Flow rate is measured over time and then converted to permeability or permittivity using Darcy's equation. Between readings, the test specimen can be maintained under either nonsaturated or saturated conditions, resulting in aerobic or anaerobic conditions respectively. Several candidate geotextiles can be evaluated over time to check their serviceability for a given LCRS.

The test method is simple in its approach to determine the susceptibility of a specific geotextile or soil/geotextile filter to clogging by site specific leachate. It allows the person implementing the test leeway in the apparatus set-up location, provided the basic test procedures are followed. However, the test method does not consider the implications of other factors (i.e. temperature) which could impact biological growth on the filter. This five-year study was performed as part of an ASTM round-robin review of the test method. The results of this five-year study are detailed below.

TEST LOCATION

The test was set up at the Orange County (Florida) Sanitary Landfill located in the southeastern portion of the county. The closest major city is Orlando, which is located in the central portion of the county. Over the five-year study period, the test apparatus was set up at

two different locations at the landfill site. These locations were selected based on the ease of obtaining leachate for the test.

The first location was adjacent to the leachate storage tanks. Leachate was pumped from the nearby lined Cell 7B to two open air storage tanks. Leachate would then be loaded onto tanker trucks and hauled away for treatment. The test operator could collect the needed volume of leachate by climbing to the top of the leachate tank and dropping a five-gallon bucket into the tank would enable. This procedure for collecting a leachate sample continued for six months until the County constructed a leachate force main to pump the leachate to a nearby wastewater treatment plant and discontinued use of these leachate tanks.

After installation of the leachate force main, the test apparatus was moved to the leachate pump station at the southwest corner of Cell 7B. The leachate sample then obtained by dropping a five-gallon bucket down into the pump station. This procedure continued until the end of the study.

DESCRIPTION OF APPARATUS AND PROCEDURE

The PVC columns used for the five-year study contained only geotextile materials (Figure 1). The construction of the test apparatus was kept extremely simple. Four test columns were attached to a 0.6 meter by 1.22 meter (2 ft. x 4 ft.) board for stability. The columns and board were then attached to two wooden posts. The columns were kept in a vertical position for the falling head test.

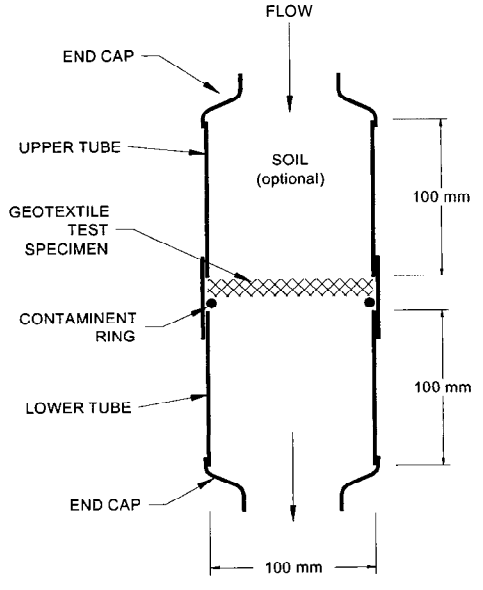

Figure 1. Flow Column which Contained Geotextile Test Specimen

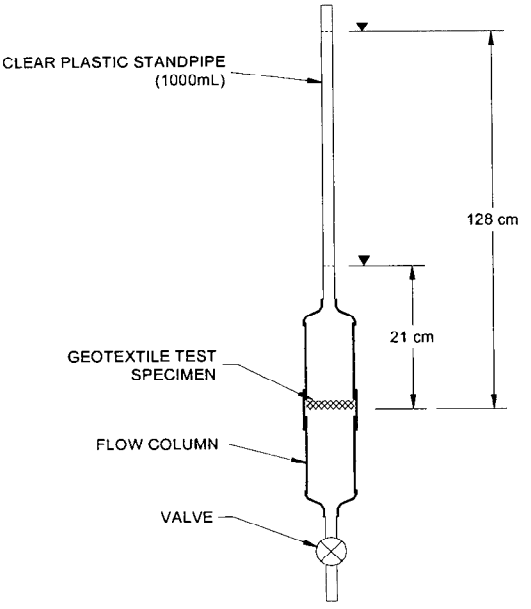

Figure 2. Flow Column with Standpipe for Variable (Falling) Head Test (1000 ml Column)

The top of the column or inlet was constructed with a female adapter that allowed a clear 34.5 mm diameter plastic standpipe to be placed on top of the column (Figure 2). The bottom of the column was constructed with a ball valve. All connections to the column were threaded connections, with Teflon tape used as a sealant. A silicon sealant was then placed on the outside of each connection. A cap was also constructed to seal the column from the ambient environment. Three clear standpipes were made of differing lengths for the volumes of 1000 ml, 500 ml and 250 ml.

The procedure consisted of first obtaining a sample of leachate. An empty bucket was then placed under the column that was to receive a leachate "feeding." The cap to the column was removed, and the standpipe was placed into the female adapter. The bottom of the standpipe had Teflon tape wrapped two to three times around it to obtain a sufficient seal between the standpipe and the adapter. The standpipe also had upper and lower markings corresponding to the known volume and height of the leachate. The column (1000 ml usually) was then filled to the top marking with leachate.

The operator opened the valve at the bottom of the column and recorded with a stopwatch the time for the leachate to drop from the top marking to the bottom marking. The operator would attempt to close the valve once the leachate level dropped below the bottom marking, thereby keeping the geotextile saturated and limiting its exposure to the air. Three feedings to each column and corresponding time recordings would occur per site visit. After the third "feeding" the standpipe was moved to the next column. The column would be filled to the top with leachate and then the cap replaced.

Any readings less than one second were considered suspect and recorded as only "less than 1 second." All readings and column volumes were recorded in a log book. Calculations for the permittivities of each column were based on the average of the three falling head readings.

Time intervals between site visits ranged from once per week to once every three months, with an overall average of once every one and one-half weeks. Several interruptions in leachate feedings did occur over the five-year study. These are discussed later in the text.

The collection of leachate from the pump station (or storage tanks) and the pouring of leachate into the standpipe did allow for some agitation or aeration of the leachate. The columns were subject to the ambient climatic conditions. The impact of the leachate aeration and landfill climatic variations shall be discussed later in the text.

LEACHATE ANALYSIS OVER A FIVE-YEAR PERIOD

The five-year study began on 2 June 1992. At this time, the Orange County Sanitary Landfill, Cell 7B, had been in operation for one and one-half years. The collected leachate emerged from waste for which the decomposition process was well underway. The leachate composition was fairly stable and therefore, not subject to the drastic biological and chemical

changes that occur after initial waste placement and the initial stages of decomposition. Review of the leachate analysis showed no indication of variation in the test parameters over the five-year study. Table 1 shows the general range of the leachate composition over the five-year period.

Table 1. Landfill Leachate Analysis

Parameter (mg/l, except where noted)	Orange County		FL Typical Leachate Range (2)	Typical Leachate Range (3)
	Mean(1)	Range(1)		
pH, field	7.32	4.3 - 8.2	5.8 - 8.6	5.3 - 8.5
Temperature (deg C)	26.00	9.6 - 31.8		
BOD	190	2 - 1,320	10.8 - 4,800	100 - 90,000
COD	1,442	12.5 - 2,960	14.9 - 10,896	150 - 100,000
Ammonia-N	688	0.07 - 1,320	1.02 - 5,020	1 - 1,500
Nitrate	0.88	0.01 - 4.96		0.1 - 50
TKN	840	42.8 - 1,718	3 - 5,620	
Sulfate	59.5	0 - 455	1 - 1,162	10 - 1,200
Total Alkalinity	4,861	452 - 9,160	19.7 - 324	300 - 11,500
TDS	5,330	136 - 9,280	142 - 20,881	
TSS	88.8	1.5 - 990	9 - 800	
Iron	4.84	0.25 - 8.47	0.5 - 77	0.4 - 2,200
Manganese	0.24	0.09 - 0.32	0.05 - 1.11	0.4 - 50

1 - Courtesy of Orange County Utilities Division
2 - Florida Landfill Leachate Report (Tedder 1992)
3 - Andreottola and Cannas, 1992

Table 2. Yearly Rainfall Data as Recorded at the Orlando International Airport.
(Courtesy of Southeast Regional Climatic Center)

Year	Rainfall (cm)	Rainfall (in.)
1992	135	53.0
1993	113	44.5
1994	172	67.8
1995	109	43.1
1996	135	53.3
1997	164	64.5

In comparison with a study of landfill leachate generated in Florida by Richard Tedder, P.E., of the Florida Department of Environmental Protection (1992), Orange County Landfill leachate is somewhat weaker than typical Florida leachate. The reason for this variation is unknown. Furthermore, Florida leachate is significantly weaker than normal leachate. This variation can be directly related to the amount of rainfall experienced by Florida landfills. Florida receives a greater amount of rain than most areas of the country. The Orange County Landfill received an estimated 1.09 meters to 1.72 meters of rain per year over the five-year study (Table 2).

The weaker than normal leachate at the Orange County Landfill suggests less of a substrate or food source with which the microbes could feed from and grow on the geotextile and less of a tendency to form inorganic and biochemical precipitates.

AMBIENT TEMPERATURE

During the five-year study, the columns were subject to the ambient temperature at the landfill. Due to the Florida climate, the columns experienced, on average, approximately 11° C (19° F) daily change in temperature. Table 3 details the mean daily temperatures and seasonal variations. Over the five-year study, the temperature changes could be more dramatic, with temperature dipping down to near or below freezing for short periods (up to 3 hours) of time.

Table 3. Mean Daily Temperature and Temperature Extremes.
(Courtesy of Southeast Regional Climatic Center)

	Degree Celsius			Degree Fahrenheit		
	Summer	Winter	Extreme	Summer	Winter	Extreme
High	33.6	21.0	36.7	92.4	69.9	98.1
Low	23.3	9.7	-3.3	74.0	49.4	26.1

Anaerobic organisms are quite capable of surviving significant elevations in temperature. Temperatures would have to exceed 40° to 45° C before the microorganisms would start dying off. It is the lower temperatures that probably impacted the biological activity taking place within the column (Watson-Craik and Jones, 1995).

A long-term temperature study of the Orange County landfill geomembrane currently in progress has shown temperature ranging from 26° C, after new waste placement to 33° C one-year later. If it can be assumed that the temperature of the geomembrane parallels that of the leachate, then the test columns were not subjected to the same temperature as that found in the Orange County Landfill. The Orange County Landfill had temperatures for optimal biological growth (Watson-Craik and Jones, 1995). The columns had less than optimal temperatures and experienced significant fluctuations in daily and yearly temperatures.

If temperature directly relates to the amount of biological activity, the geotextiles within the columns had probably less biological activity or growth than a geotextile within the Orange County landfill. The rate of biological clogging is directly related to the level of biological growth encrusting the geotextile. The impact of the variable ambient temperature is that no time relationship for the clogging of geotextiles can be correlated between the columns and the adjacent landfill.

INTERRUPTIONS IN THE TEST

Over the five-year study, several interruptions in the study occurred. These interruptions included the following:

- There was a two-month interruption due to moving the test location.
- Operator was unavailable to perform leachate feedings for periods ranging from 3 to 9 weeks. Leachate feedings occurred frequently during the initial three year period and less over the remainder of the study.
- Three and one-half years into the study, the test set-up had to be dismantled due to construction at the test site. The geotextiles remained saturated with leachate during the last feeding in this holding period of five months. This period was preceded by six months period of sporadic feedings during which the period between feedings averaged five weeks.

At no time during the study period were the geotextiles allowed to dry out.

Since a landfill will experience periods of little or no rainfall, it is assumed that a geotextile used within the landfill experiences periods of little leachate flow. These periods of low leachate flow through a geotextile would correlate to periods of biological die-off on the geotextile. These subsequent interruptions in the five-year study were not considered to have a significant impact on the results of the study, with the exception of the five-month holding period three and one-half years into the study. The five months of no leachate feeding did have a related impact and is discussed in later text.

TEST RESULTS

Figures 3, 4, and 5 show geotextile permittivity over time, with the results summarized in Table 4. The test results are detailed below according to the type of geotextiles tested and the period of testing within the five-year study.

Please note that the baseline permittivity of this study was 0.177 sec^{-1}, which is equivalent to one second for the leachate head to fall 107 cm (Figure 2). A decrease in geotextile permittivity was only calculated when the operator was able to record a time greater than one second. The geotextile's relative permeability was assessed to be 1 $x10^{-3}$ cm/sec., a value common to sand filters and typical of municipal solid waste filters.

Non-Woven Geotextiles 271 g/m^2 and 542 g/m^2

The non-woven geotextiles showed indications of clogging at approximately 154 days into the study (Figure 3). Within an 8-day period of observing a decrease in permittivity of the non-woven geotextiles, the operator recorded a decrease in permittivity from the manufacturer's reported value for the 271-g/m^2 and 542-g/m^2 geotextiles. These geotextiles saw fluctuations

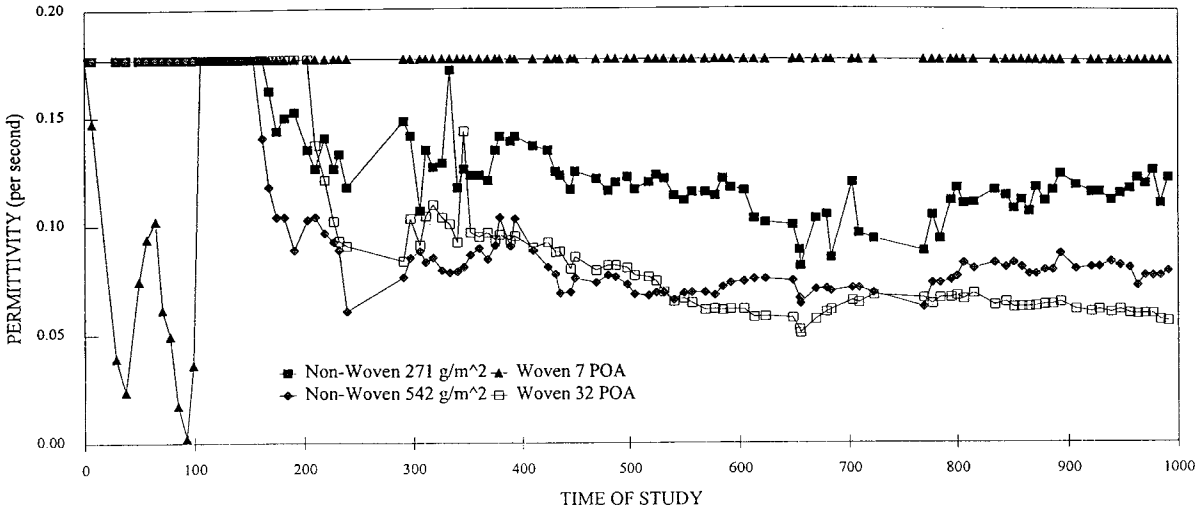

Figure 3. Field Study from Day 0 to Day 1000

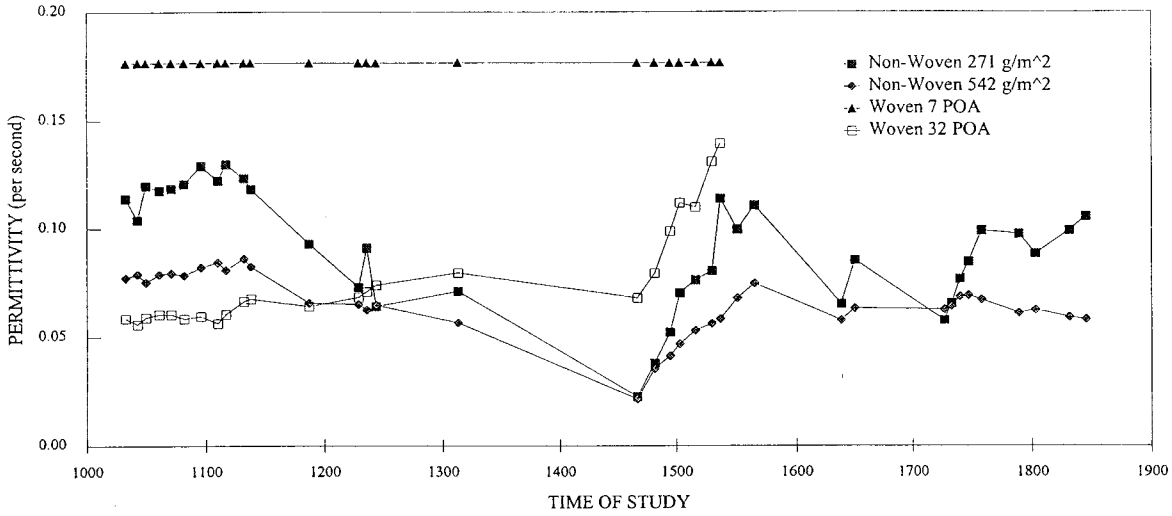

Figure 4. Field Study from Day 1000 to Day 1845

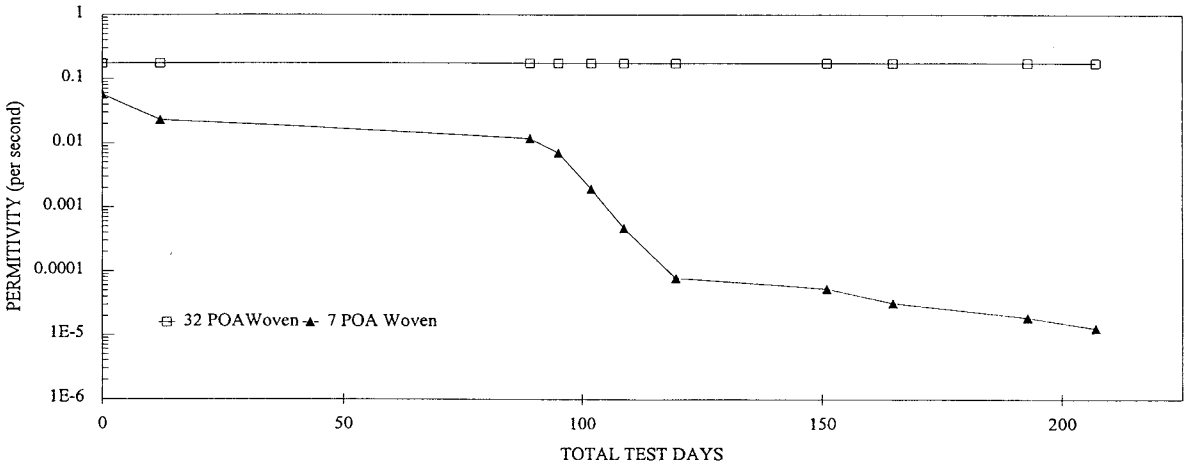

Figure 5. Second Test for Woven Geotextiles

and a gradual decrease in permittivity over the next 490 days. The permittivity then increased slightly and stabilized for 175 days (or from 1.8 to 2.3 years into the study). The permittivity of each non-woven geotextile did not drop significantly after periods of sporadic feedings, except during a period just over three years into the study. Feeding intervals were reduced to an average of once every five weeks for a six-month period (Year 3.1 to 3.6) (Figure 4). The study was then put on hold for a five-month period (Year 3.6 to 4.0). The operator recorded each geotextile's minimum permittivity the day the study continued. Their permittivities only increased slightly and quickly stabilized after the restart of the study.

As expected, the 542-g/m^2 non-woven geotextile had retained less permittivity over the study than the 271-g/m^2 geotextile. The relative permeability of both geotextiles at the end of the five-year study indicates that these geotextiles were still functional and would probably be capable of meeting design requirements for the Orange County Landfill. Before using these geotextiles in a design, however, other factors discussed in this paper should also be considered, and the results of the study should be compared with the geotextile design requirements. There was an indication that biological die-off would reduce the permittivity, but not to significant degree.

Table 4. Five Year Study Results

	Thickness (mm)	Original		Residual		Study Period (days)	Days to Achieve Reduction	Results
		ψ (sec^{-1})	k (cm/sec)	ψ (sec^{-1})	k (cm/sec)			
Non-woven, 271 g/m^2	2.44	1.5	0.37			1845		
Minimum				0.022	5.4×10^{-3}		1467	OK
Non-woven, 542 g/m^2	4.65	0.5	0.23			1845		
Minimum				0.021	7.7×10^{-3}		1467	OK
Woven, 7 POA		0.4	0.016					
1st Test - Minimum	0.41			0.002	8.2×10^{-5}	1537	93	BAD
2nd Test - Minimum	0.41			1.3×10^{-5}	5.3×10^{-7}	207	207	
Woven, 32 POA		4.8	0.34					
1st Test - Minimum	0.71			0.051	3.6×10^{-3}	1537	655	OK
2nd Test - Minimum	0.71			>0.177	1.3×10^{-2}	207	207	

ψ - Permittivity; k - Hydraulic Conductivity

Woven Geotextiles 7 POA and 32 POA

The 7 percent open area (POA) woven geotextile experienced a decrease in permittivity within one week of the start of the study or as detected during the second feeding of leachate. The geotextile experienced rapid changes in permittivity over the first 99 days of the project before estimated total recovery. The operator of the study did not record any decrease in permittivity of the 7 POA geotextile over the remaining period of the study (Figures 3 and 4).

The rapid increase in the permittivity after 99 days was questionable. After several feedings with no changes in permittivity, the operator drained the column and performed a visual

inspection of the geotextile. The operator inspected the inside of the column to see if the geotextile had broken away from the side of column, which would allow the leachate flow to by-pass the geotextile. The operator could not see to the edge of the geotextile due to the column adapter. The operator did perform a probe test by running a thin "rod" along the edge of the geotextile and column. The probe test did not reveal any separation. The operator performed several inspections (visual and probe) over the study. When the column was disassembled at the Geosynthetic Research Institute, a large gap in the underside of the edge seal was observed, confirming earlier suspicions.

The test was continued for the 7 POA geotextile until Day 1537 (4.2 years). At that time, it was determined that the 32 POA geotextile had pulled away from the side of its column.

A second test was initiated to confirm the reduction in permittivity seen at the start of the study. The initial permittivity test for the 7 POA geotextile indicated a geotextile permittivity of 0.058 sec^{-1}, or 86 percent less than the manufacturer's reported value (Table 4). The 7 POA geotextile experienced a rapid decrease of permittivity to 1.3E-05 sec^{-1} on the last day of the study (Day 207) (Figure 5). This second test result presents a large decrease in permittivity over the short test period. Figure 5 shows that rapid reduction in permittivity occurred during periods of regular feedings indicating that biological growth, and not biological die off or chemical precipitates, is probably the major cause of the clogging. The second test results supported the initial findings of the first test. Based on this study, the 7 POA woven geotextile should not be considered for use in the Orange County Landfill.

The operator recorded a decrease in permittivity from the manufacturer's reported value for 32 POA woven geotextile at Day 210 (7 months) of the study. Figures 3 and 4 show from Day 210 to 655 there was a slight downward trend in the permittivity of this geotextile, which stabilized over the remainder of the test period. Unlike the non-woven geotextiles, periods of sporadic feeding did not cause any noticeable decrease in permittivity for the 32 POA woven geotextile (Figure 4). Review of Table 4, and Figures 3 and 4, indicates that the 32 POA geotextile had less permittivity than both of the non-woven geotextiles over the same study period. Only after the five-month study hold period did the 542 g/m^2 non-woven geotextile have a permittivity less than the 32 POA woven geotextile. The 32 POA geotextile test was discontinued when the operator noticed a significant increase in permittivity and found the geotextile had broken away from the column.

The second test was started to confirm the previous results. However, the study was discontinued before a decrease in permittivity was observed. The results only indicate that clogging of the geotextile was not observed over the 207-day period of the test (Figure 5).

Although the reduction in permittivity for the 32 POA geotextile appears high, the relative permeability of the geotextile at the end of the original 4.2-year study period indicates that this geotextile was still functional and would probably be capable of meeting design requirements for the Orange County Landfill. Before using these geotextiles in a design, however, other

factors discussed in this paper should also be considered, and the results of the study should be compared with the geotextile design requirements. The reduction in permittivity was not significant and did not continue over the study period. The study results indicate that this geotextile might be acceptable for use in the Orange County Landfill, if other factors discussed in this paper are not considered. Again, before acceptance in the design, the results of the study should be compared with the geotextile design requirements.

REVIEW OF ASTM D 1987 TEST METHOD

Except for the 7 POA woven geotextile, the results of the five-year study do not correlate with what is believed to occur as a result of biological growth on geotextiles over time. Giroud (1996) and Koerner et. al. (1994) summarizing past research and field studies, stated that the permittivity of the geotextile is expected to decrease over time. Previous studies also indicated that non-woven geotextiles were more subject to biological clogging than woven geotextiles. On the contrary, this five-year study indicates that the woven geotextiles are more subject to clogging for leachate from the Orange County Landfill. This study also indicates the clogging mechanisms and resulting permittivity may somewhat stabilize or only gradually decrease over time.

A specific question remained unanswered. If leachate was sufficient to promote clogging of the 7 POA woven geotextile, what stopped the clogging from occurring on the other geotextiles? Based on these results, a further review of the ASTM D 1987 Test Method was warranted. Specifically, are there other factors that promote or hinder geotextile clogging that are not considered by the test method or not specified in the test procedures?

The previous text denotes both the weak nature of the leachate at the Orange County Landfill and the variations in the ambient temperature to which the columns were subjected. ASTM D 1987 specifically tests for clogging of geotextile filters. Weak leachate at the Orange County landfill should have less ability to promote biological growth. However, even weak leachate should promote some biological growth and cause an obvious, but somewhat slow, decrease in permittivity over a five year period. The variation in ambient temperature may have hindered biological growth, but to what extent cannot be determined. There are other factors that should be considered in attempting to relate the results of ASTM D 1987 to actual design applications.

The procedure used for this five-year study required that leachate be obtained from an open leachate tank or leachate pump station (wetwell). This leachate would be considered pre-filtered and/or "settled" leachate. Since this leachate had already flowed through drainage material and geotextile, many of the particulates would have been filtered out by the leachate collection system. The leachate was collected from the top of the liquid level in the tank or wetwell, thereby allowing any particulates to settle out of the leachate. Filtration by chemical precipitation of compounds on the biomass attached to the drainage material and geotextile within the landfill had also already occurred before sampling of the leachate. Any additional

precipitation would need to occur after the sampling of the leachate, during the feeding, and/or between feedings. This leaves biological clogging as the primary cause of decreased permittivity of the tested geotextile.

The study began approximately one and one-half years after the start of operation of the lined landfill cell and the collection of leachate. The chemistry and biology of the leachate had changed over that period. Although various phases of waste decomposition are occurring somewhere within the landfill mound, the leachate analysis indicated that the methanogenic process (accelerated methane phase) was occurring over the major portion of the landfill mound. The study did not reflect the chemical and biological history of the Orange County waste and its impact on geotextile materials within the landfill cell.

The study did not attempt to reflect the volume of leachate that must flow through each square meter of geotextile within a landfill. Low flows of leachate having low concentrations of compounds which feed the microorganisms may only have a small detrimental effect on geotextile permittivity. A higher volume of leachate flowing through the geotextile probably would have resulted in a greater rate of biological growth on the geotextile.

The falling head method for determining permittivity was selected for this study to keep the cost of the study as low as possible and for ease of set-up and operation. However, this method may have been detrimental to the study. The study procedure allowed 1000 ml of leachate to fall 1.07 meters. This caused a "flushing," or turbulent flow, through the geotextile. The greatest impact would be to the woven geotextile, which allows a rapid pass through of liquid and/or particles. Although the microorganisms have a great ability to adhere to materials even during high flow, it is possible that the rapid flow was excessive and the turbulent flow of this procedure washed some of the biomass or encrustation from the geotextile and reduced the clogging effect over time of the study. It is likely that flow within the landfill would be much less turbulent. It would have been better to slow feed the leachate through the geotextile and test for permittivity on a less frequent basis. Testing for permittivity could be increased after the clogging of the geotextile proceeded to a point where the leachate flow through the geotextile had been greatly reduced.

The test set-up and procedure allowed leachate to be poured into the top of the standpipe before each feeding. This procedure aerated the leachate before allowing it to flow into the column. Although every attempt was made to keep the geotextile within each column from being exposed to the outside air, there was probably some impact to the anaerobic microorganisms. Anaerobic organisms have an ability to recover from oxygen exposure if present in sufficient numbers. However, the apparent lack of biological clogging of the geotextiles may indicate that a sufficient population of microorganisms was not present and microbial growth/clogging was not observed. The columns were also not "air tight", and replacing the cap to each column would entrap a small amount of air in the top portion of the column. The procedures for the study did not eliminate the impact of air to the anaerobic microorganisms. The aeration of the leachate would also foster metals precipitation. However,

the leachate analysis of Table 1 showed relatively no metals present within the leachate to precipitate.

SUMMARY OF THE FIVE YEAR STUDY

The five-year study found only limited clogging in the non-woven geotextiles. No noticeable pattern of gradual decrease in permittivity was seen over the five-year study period. Only a slight decrease in permittivity was noticed after a period of sparse leachate feedings. The test results tend to support the possible use of non-woven geotextiles in Orange County Landfill designs.

The 7 POA woven geotextile experienced a rapid decrease in permittivity during the initial period of the study. At 99 days into the study, the geotextile specimen broke away from the side wall of the rigid wall perimeter. Due to this equipment malfunction, the set-up was repeated. During the second test, the 7 POA woven geotextile again experienced a rapid reduction in permittivity that would make it inappropriate for use in an Orange County Landfill design.

The 32 POA woven geotextile experienced a decrease in permittivity at 210 days into the test. Its permittivity over most of the test period was equal to or less than the non-woven geotextiles. This test result was unexpected because high POA woven geotextiles are assumed to have less surface area and to be less likely to clog over time. The state of the practice in the design of leachate collection systems recommends the use of a woven geotextile with a high POA. Due to this odd result, the set-up was repeated. During the second test the 32 POA woven geotextile showed no decrease in permittivity over a 207-day test period. The test results need to be justified and substantiated before this type of geotextile should be considered for use at the Orange County Landfill.

The ASTM D 1987 Test Method was used to determine the impact of biological clogging of various geotextiles using Orange County Landfill leachate. It is felt that this test method is a rather crude tool upon which to base leachate collection and removal system filter designs. It is felt that additional factors not clearly identified in the standard can alter the test results. Application of the test method by simplified test procedures and the interpretation of the results are at the whim of the user. A more detailed standardized test method is needed to remove various factors, which could influence the test results

RECOMMENDATIONS

Review of the five-year study results and technical literature indicated that several changes to the ASTM D1987 test procedure should be implemented to improve the results of future biological clogging tests. Recommended improvements to the test procedures are as follows:

- The use of the constant head method for leachate flow should be promoted. This would reduce the possible impact of rapid/turbulent flow through the geotextile.

- The use of the falling head method for determining permittivity should be used sparingly during the initial stages of the project or until rapid flow through the geotextile is no longer possible. Slow feedings of leachate should occur in the initial stages of the test to promote biological growth and/or clogging.
- Aeration of the leachate should be minimized during the filling of the standpipe. This may require the use of a shorter and wider diameter standpipe.
- If anaerobic biological clogging is being studied, the test set-up should be designed to limit exposure of air to the leachate. The method of capping of the column should consider removal of all entrapped air as part of the capping process.

If the user of the test method is attempting to correlate the test results to the geotextile's real time experience within the landfill, the following items are recommended:

- The leachate flow rate through the geotextile should be equal to or greater than the actual flow rate a geotextile would experience within the landfill. The flow rate through the geotextile should fluctuate in accordance with seasonal variations. The review of local monthly precipitation rates or water balance models (e.g. HELP Model) may assist in determining the appropriate flow rates.
- The test should be started during the initial operation of the landfill generating the leachate. Although this initial period of chemical and biological change is short, the geotextile within the landfill is experiencing this change.
- The geotextile used in the test should be subjected to overburden pressures, as seen by the geotextile within the landfill. This in itself may be difficult, if not impossible, to accomplish. If non-woven geotextiles are to be used in the test, the user should realize the compression of the geotextile will increase the possibility of biological clogging and reduce permittivity.
- The geotextile should be subjected to approximately the same temperature as the geotextile within the landfill to promote similar biological growth.
- Analysis of permittivity results should be based on the decrease from its original permittivity and the geotextile's relative permeability to 1×10^{-3} cm/sec. This datum is one common to sand filters and typical of municipal solid waste landfill designs.

The user of the above recommendations should realize that they will only attempt to correlate real time biological clogging of the geotextile within the column(s) to the biological clogging of the geotextile within the landfill. The geotextile within the landfill will still be subject to additional clogging mechanisms (e.g. particulate clogging). If the geotextile within the column(s) show significant reduction in permittivity, the user can reasonably assume that the geotextile within the landfill is experiencing a greater reduction of permittivity.

CONCLUSION

The usefulness of ASTM D1987 is limited in its present form. Its use is restricted to determining the decrease in permittivity of various geotextiles due to biological clogging only

and not other clogging mechanisms. This five-year study showed that the test method may not give results that relate to the current understanding or correlation between various geotextiles and their ability to biologically clog over time. The user should be aware of various factors affecting the clogging of geotextile. The user of this test method should understand the physical, chemical and biological processes occurring within a landfill before attempting to use this test. Without this knowledge and the appropriate application of this knowledge, the user of this test method may obtain unexpected results.

ACKNOWLEDGEMENTS

The authors wish to thank the Orange County Utilities Division for providing their leachate analysis results over the study period, for offering their continued support, and for allowing this biological clogging study to take place at their facility. The authors also wish to thank the Geosynthetic Institute for its support and assistance.

REFERENCES

Andreottola, G. and Cannas, P., (1992), "Chemical and Biological Characteristics of Landfill Leachate", in Landfilling of Waste: Leachate, Edited by Christensen, T.H., Cossu, R., and Stegmann, R., Elsevier Applied Science, Pg. 65-88

Barlaz, M.A., (1996) "Microbiology of Solid Waste Landfills", in Microbiology of Solid Waste, CRC Press, Palmisano, A.C. and Barlaz, M.A., Pg. 31-69

Barlaz, M.A. and Ham, R.K., (1993) "Leachate and Gas Generation", in Geotechnical Practice of Waste Disposal, Edited by Daniel, D.E., Chapman & Hall, London, Pg. 113-136

Giroud, J.P., (1996) "Granular Filters and Geotextiles Filters", Proceedings Geofilters '96, Montreal, Quebec, May 1996

Koerner, G.R., Koerner, R.M. and Martin, J.P., (1994) "Design of Landfill Leachate Collection Filters", Journal of Geotechnical Engineering, American Society of Civil Engineering, Vol. 120, No. 10, Pg. 1792-1803.

Tedder, R.B., "Comparison of Florida Landfill Leachate with Regulatory Standards and EPA Landfill Leachate", Florida Department of Environmental Regulation Document, Nov. 1992

Watson-Craik, I.A. and Jones, L.R. (1995) "Selected Approaches for the Investigation of Microbial Interactions in Landfill Sites", in Microbiology of Landfill Sites, Second Edition, Edited by Senior, E., Pg. 31-70

EFFECT OF SOIL PRESENCE ON FLOW CAPACITY OF DRAINAGE GEOCOMPOSITES UNDER HIGH NORMAL LOADS

AIGEN ZHAO, TENAX CORPORATION, USA

FILIPPO MONTANELLI, TENAX SPA, ITALY

ABSTRACT

Extensive transmissivity tests are conducted under high normal loads to investigate the effect on flow rates of soft boundaries over drainage geocomposites. Two geonet structures (tri-planar and bi-planar geonets), two types of soils (sand and clay), GCL, and a neoprene rubber are included in the tests. Long-term transmissivity tests under an in-soil environment are also performed. Under high normal loads, sand layer density is found to have an insignificant effect on the flow rate of both bi-planar and tri-planar geocomposites. The neoprene tested simulates geotextile intrusion into the geonet's core space well for the sand layer, but significantly underestimates intrusion of geotextile for clayey soil. Due to the variable nature of both neoprene and soils, site representative soils are strongly recommended for performance transmissivity tests. Under high normal loads, the reported default reduction factors for intrusion (1.5 to 2) are in agreement with the tri-planar geocomposites for sand layer; while the default reduction factors are not representative of the bi-planar geocomposite for all the boundary conditions. Long-term transmissivity tests for geocomposites and 10,000 hour long-term compressive creep tests for geonets are recommended.

INTRODUCTION

Geocomposite drain systems consist of a geonet core with a geotextile laminated to one or both sides and are designed for in-plane flow over a large surface area. Geocomposite drains are increasingly used in place of soil drains in civil and environmental applications. A geocomposite can function as a surface water removal layer in landfill final covers, a leachate collection layer over a liner system, or as a leak detection layer between two barrier layers. The most critical engineering property of a geocomposite is its in-plane flow capacity under design loads and site specific boundary conditions. The design parameter used to quantify the in-plane flow capacity is either the flow rate per unit width or hydraulic transmissivity. Transmissivity is defined as

$$\theta = k_p \cdot t = \frac{q}{i} \tag{1}$$

Where

θ = hydraulic transmissivity (m^3/sec/m)
q = flow rate per unit width (m^3/sec/m)
k_p = in-plane hydraulic conductivity (permeability) (m/sec)
i = hydraulic gradient
t = geocomposite thickness (m)

It is more appropriate to present the flow rate or transmissivity in terms of m^3/sec/m (or gal/min/ft), than m^2/sec. The latter dimension has no physical meaning. The design by function approach for geocomposite drains is described by Koerner, (1998). More specific design issues for geocomposite drains are summarized by Richardson and Zhao (1998) for steep side slopes in landfill final covers and for flat slopes of landfill barrier systems by Zhao and Richardson (1998). In the design by function approach, a drainage geocomposite must meet the following equation:

$$FS = \frac{q_{allow}}{q_{req'd}} \tag{2}$$

where FS is the overall safety factor, q_{allow} is the allowable flow rate of the geocomposite, and $q_{req'd}$ is the required flow rate. The required flow rate can be determined from a water balance model such as HELP (Schroeder, et al. 1994) or other well-documented methods. The allowable flow rate of the drainage product can be determined from

$$q_{allow} = \frac{q_{ultimate}}{RF_{in} \cdot RF_{cr} \cdot RF_{cc} \cdot RF_{bc}} = \frac{q_{ultimate}}{\prod RF} \tag{3}$$

where $q_{ultimate}$ is the ultimate flow rate (index value) measured in accordance with ASTM D4716-95. If the test setup does not simulate the actual field conditions, reduction factors shall be applied. The following default reduction factors are suggested (Koerner, 1997):

- RF_{in} = reduction factor for elastic deformation, or intrusion, of the adjacent geosynthetics into the geonet's core space, 1.5 - 2.0 for landfill primary leachate collection layer.

- RF_{cr} = reduction factor for creep deformation of the geonet and/or adjacent geosynthetics into the geonet's core space, 1.4 - 2.0 for landfill primary leachate collection layer.

- RF_{cc} = reduction factor for chemical clogging and/or precipitation of chemicals in the geonet's core space, 1.5 - 2.0 for landfill primary leachate collection layer.

- RF_{bc} = reduction factor for biological clogging in the geonet's core space, 1.5 - 2.0 for landfill primary leachate collection layer.

- $IIRF$ = product of all relevant reduction factors for the site-specific conditions.

Geotextile intrusion into geonets under low normal pressure (up to 105 kPa) was investigated by Hwu, Koerner and Sprague (1990), however, under high normal loads, rather limited data are available to verify the intrusion reduction factors. Intrusion reduction factors are a function of many variables, such as the type of geonet structure and polymer, overlying materials (sand, clay, or a GCL), normal pressure, seating time, and hydraulic gradient. This paper will focus on intrusion reduction factors under high normal loads only. Two types of geonet structures (bi-planar and tri-planar), two types of soils (sand and clay), GCL and a neoprene are included in the testing program to investigate reduction factors for geotextile intrusion into the geonet core.

Due to the tendency of polymer materials to undergo compressive creep, the flow capacity of geonet geocomposite drains under sustained compressive loads must be considered (Slocumb, Demeny and Christopher, 1986, Smith and Kraemer, 1988, Campbell and Wu, 1994, Fannin and Choy, 1995). To address long-term compressive stress on the geonet core of a geocomposite, Holtz, Christopher and Berg (1997) suggest that the design pressure on a geocomposite core be limited to either:

(a) the maximum pressure sustained on the core in a test of 10,000 hour minimum duration, or
(b) the crushing pressure of a core as defined with a quick loading test, divided by a safety factor of 5.

The long-term transmissivity test (1000 hours) and long-term compressive creep test (10,000 hours) under sustained normal loads are conducted, and the results are presented in this paper.

The transmissivity testing program is presented in the next section, followed by verification of intrusion reduction factors. The long-term transmissivity tests under in–soil environment and long-term compressive creep data are described in the next section. The paper concludes with some final remarks.

TESTING PROGRAM

Transmissivity Testing Set-Up

The in-plane flow rate (transmissivity) of a geocomposite under different boundary conditions is determined by measuring the quantity of water passing through a specimen in a specific time interval in accordance with ASTM D4716. A specimen with a loaded dimension of 305 by 355

mm is used. The flow capacity for each test is reported as a flow rate per unit width for the conditions examined. All values are corrected for water temperature. Various materials can be placed on top of the drainage geocomposite, including sand, clay, neoprene and GCL. For soil layer preparation, the sand thickness is kept constant at 25 mm. Based on the desired degree of compaction, the amount of sand required is calculated and weighed. For instance, the transmissivity tests reported here need 4.15 kg of dry sand to achieve 95% compaction, and 3.3 kg of dry sand for 75% compaction. The sand is wetted with 10% moisture. The sand layer is then compacted to the target thickness. The clay is handled with 2% moisture content to avoid "mud waves." Before performing the transmissivity tests with the GCL, the GCL is hydrated for 24 hours under 8 kPa (160 psf) pressure. The length of the neoprene was cut 2.5 mm at the two ends to avoid intrusion at the edges of the geocomposite specimen.

Testing Materials

To verify the intrusion reduction factors of different geonet structures, two types of drainage geonets are tested: a bi-planar geonet and a tri-planar geonet. Bi-planar geonets consist of two layers of ribs superimposed over each other; while tri-planar geonets are comprised of two layers of inclined ribs separated by thick vertical ribs, creating a wide flow. Figure 1 shows the profiles of the two types of geonets, with the bi-planar geonet shown on the left and the tri-planar geonet on the right.

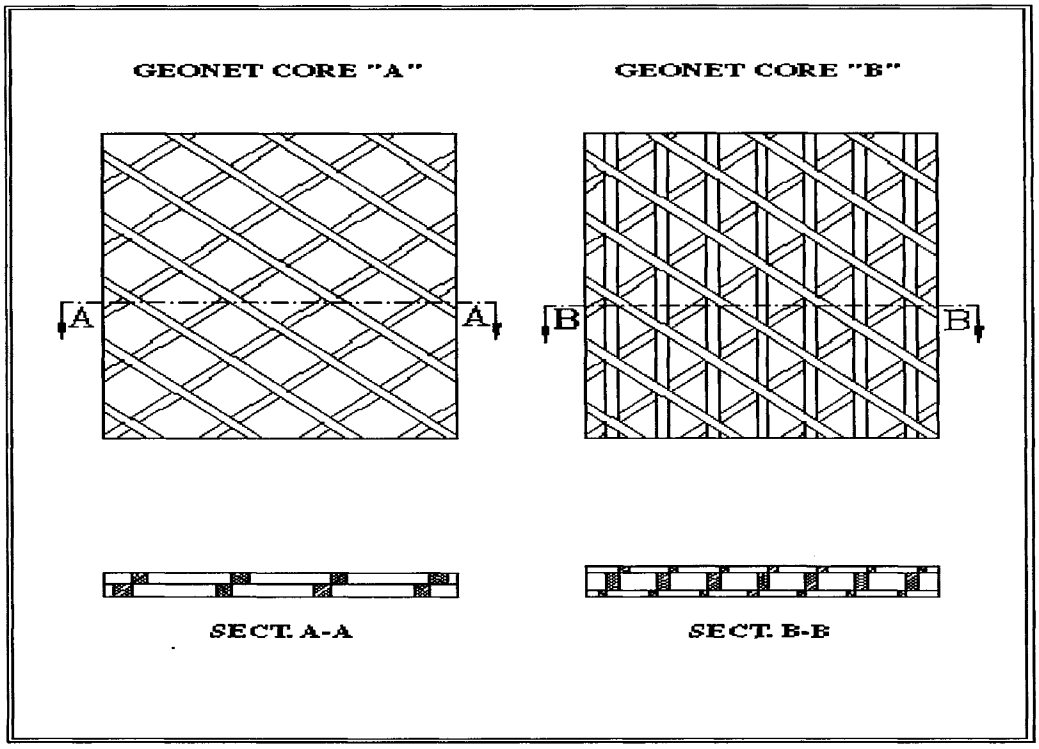

Figure 1: Profiles and cross-sections of a bi-planar and a tri-planar geonet

Geotextile-geonet-geotextile composites are used in the tests. Both bi-planar and tri-planar geonets are made of HDPE. Two layers of polypropylene non-woven geotextile are heat-bonded to the geonet by a lamination process. The geosynthetic clay liner (GCL) is made by enclosing a layer of sodium bentonite between two layers of woven geotextiles. The properties of the geosynthetic products tested are given in Table 1.

Table 1. Testing products: Bi-Planar, tri-planar geocomposites and a GCL.

Product	Thickness (mm)	Core Unit Weight (g/m^2)	Geotextile Unit Weight (g/m^2)	AOS (mm)
Bi-planar geocomposite	6	900	180	0.13
Tri-planar Geocomposite	7.6	1600	270	0.15
GCL	5.2	5000	102	-

The neoprene is placed on top of the geocomposite to investigate the possibility of simulating actual soil intrusion. The neoprene has a nominal thickness of 10 mm in accordance with EN ISO129858 test method. The properties of the neoprene are listed in Table 2.

Table 2. Properties of the neoprene used in tests

Normal pressure (kPa)	2	20	200
Thickness (mm)	9.75	9.18	3.76
Thickness Retained (%)	97.5%	91.8%	37.6%
Density (g/cm^3)			0.151
Hardness (Shore D)			2-5

Both sand and clay soils are included in the testing program. A sand layer is commonly placed over a geocomposite blanket in primary leachate collection applications as a protective/drainage layer. A compacted clay or GCL is typically used over a geocomposite in leak detection applications. The sand has a uniformity coefficient of about 2, a proctor density of

19 kN/m^3, and an optimal moisture content of 15%. The sand is called Ticino siliceous sand, since it is dredged from the Ticino River in Italy. The gradation curve of the sand is shown in Figure 2. The clay used in the tests has a plasticity index of 15, a liquid limit of 36, and a plastic limit of 21.

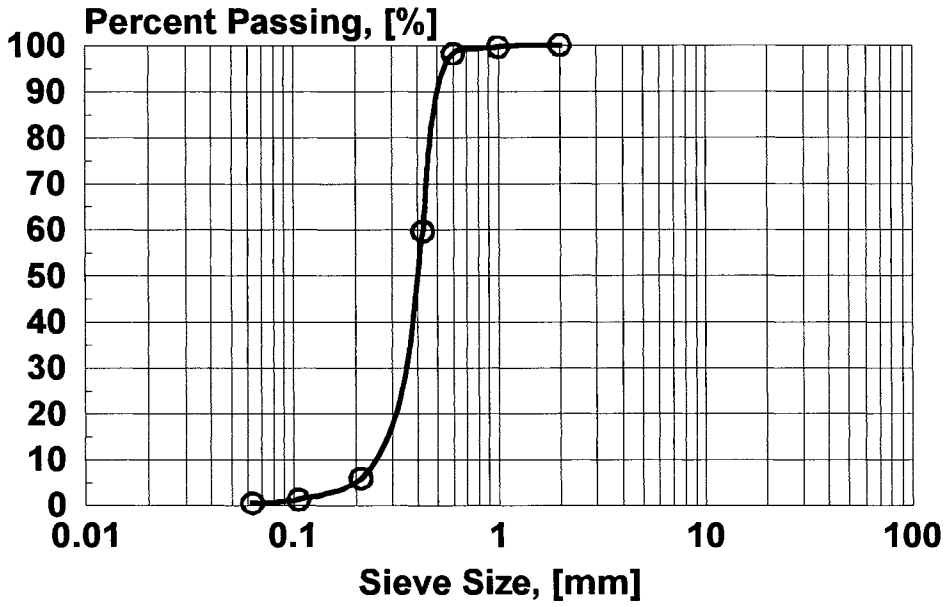

Figure 2. Grain size distribution of the sand

VERIFICATION OF REDUCTION FACTORS FOR INTRUSION

Bi-Planar Geocomposites

Transmissivity test results for the bi-planar geocomposite under different boundary conditions are listed in Table 3. The flow rate of the geocomposite tested between two steel plates is considered as the base for comparison. The retained flow rates of the bi-planar geocomposite under different testing boundary conditions are presented in Figure 3. Under 720 kPa normal load, the bi-planar geocomposite retains less than 25% of the flow rate when it is tested with either sand or clay. A significant reduction in flow rates due to geotextile intrusion into the geonet core is recorded. Under a gradient of 0.1, the retained flow rate is very low, falling below 10 percent.

The reduction factors under different testing boundaries can then be calculated and are presented in Table 4. Table 4 indicates that under a normal load of 720 kPa, the reduction factors with every overlying material tested are significantly larger than the suggested default values that ranges from 1.5 to 2. The presence of a soft material layer causes great geotextile

intrusion into the geonet flow channel. The reduction factors are also found to be heavily dependent upon hydraulic gradient. At a low gradient, reduction factors are significantly larger than those at a higher gradient. Especially for clayey soil, the reduction factor exceeds 20 at a gradient of 0.1. This is 10 times larger than the suggested default reduction factors. Neoprene is found to simulate sand behavior well, but underestimates the reduction factors in clayey soils. Neoprene above and below the bi-planar geocomposite causes the greatest geotextile intrusion, resulting a reduction factor as high as 37.5 at a gradient of 0.1. A soil layer above and below a geocomposite is not a typical application in landfill drainage systems; therefore, this testing boundary condition is not recommended.

Table 3. Flow rates (m^3/sec/m) of the bi-planar geocomposite

Test boundaries	i = 1	i = 0.5	i = 0.1
Steel plate	3.32E-04	2.05E-04	5.62E-05
Neoprene	9.71E-05	3.32E-05	4.09E-06
Neoprene above and below	3.28E-05	1.58E-05	1.50E-06
Sand 95% compaction	7.92E-05	2.69E-05	4.09E-06
Clay	7.11E-05	2.57E-05	2.73E-06

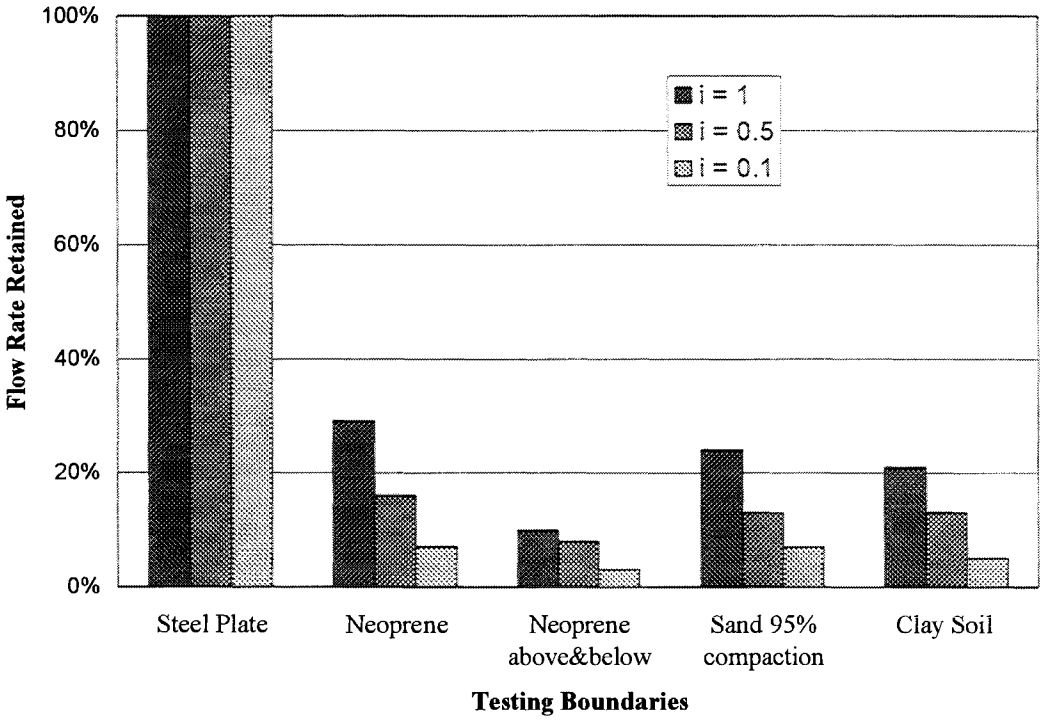

Figure 3. Retained Flow rate for the bi-planar geocomposite under different boundaries

Table 4. Reduction factors on the flow rate for the bi-planar geocomposite

Test boundaries	i = 1	i = 0.5	i = 0.1
Steel plate	1	1	1
Neoprene	3.42	6.17	13.74
Neoprene above and below	10.12	12.97	37.47
Sand 95% compaction	4.19	7.62	13.74
Clay	4.67	7.98	20.59

Tri-Planar Geocomposites

The flow rates of the tri-planar geocomposite under different boundary conditions are listed in Table 5. The same normal load (720 kPa) is applied in the transmissivity tests. The corresponding flow rate percentage compared to that tested between two steel plates is presented in Figure 4. The reduction factors under different testing boundary conditions are listed in Table 6. Under all of the testing conditions, the tri-planar geocomposite exhibits much less geotextile intrusion into the geonet's core space than the bi-planar geocomposite. This is mainly credited to the tri-planar structure. The middle flow plane contributes to the large flow rate of the tri-planar geonet; the top and bottom auxiliary planes accommodate the intrusion of geotextiles. The reduction factors of the tri-planar geocomposite with sand are in agreement with the suggested default values. The effect of soil compaction seems to be insignificant under high compressive loads. Clayey soil causes greater intrusion than sand. Neoprene simulates the geotextile intrusion for a sand layer well.

Table 5. Flow rates (m^3/sec/m) of the tri-planar geocomposite

Test boundaries	i = 1	i = 0.5	i = 0.1
Steel plate	1.27E-03	8.54E-04	3.50E-04
Neoprene	8.07E-04	5.13E-04	1.96E-04
Neoprene above and below	2.81E-04	1.28E-04	1.53E-05
Sand 95% compaction	1.00E-03	6.81E-04	2.69E-04
Sand 75% compaction	9.79E-04	6.55E-04	2.65E-04
Clay	4.92E-04	3.07E-04	9.71E-05

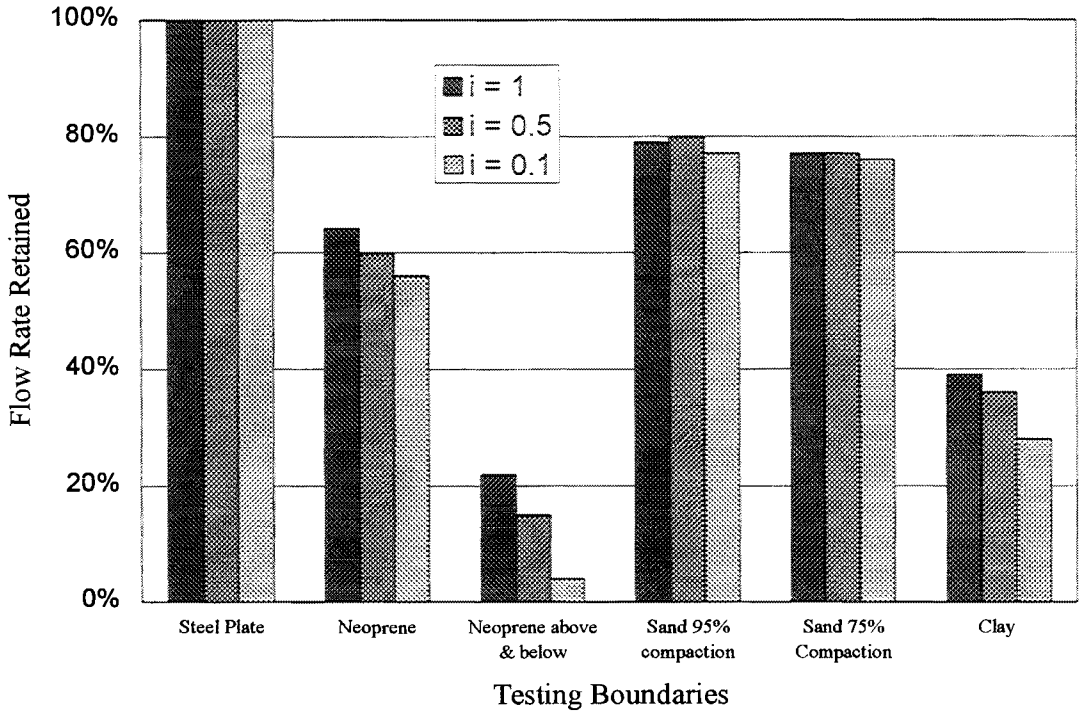

Figure 4. Retained flow rate for the tri-planar geocomposite under different boundaries

Table 6. Reduction factors on the flow rates for the tri-planar geocomposite

Test boundaries	i = 1	i = 0.5	i = 0.1
Steel plate	1	1	1
Neoprene	1.57	1.66	1.79
Neoprene above and below	4.52	6.67	22.88
Sand 95% compaction	1.27	1.25	1.3
Sand 75% compaction	1.3	1.3	1.32
Clay	2.58	2.78	3.6

Each transmissivity test listed in the above tables is conducted with a 15 minute seating time. Therefore, the results are considered as short-term data. Figure 5 presents limited data on the long-term flow rate of the tri-planar geocomposite with and without a GCL. The seating time is 100 hours, with a gradient of 1 and a normal pressure of 800 kPa. The long-term reduction factor for the tri-planar geocomposite with an overlying GCL is presented in Figure 6. Its value is about 2.

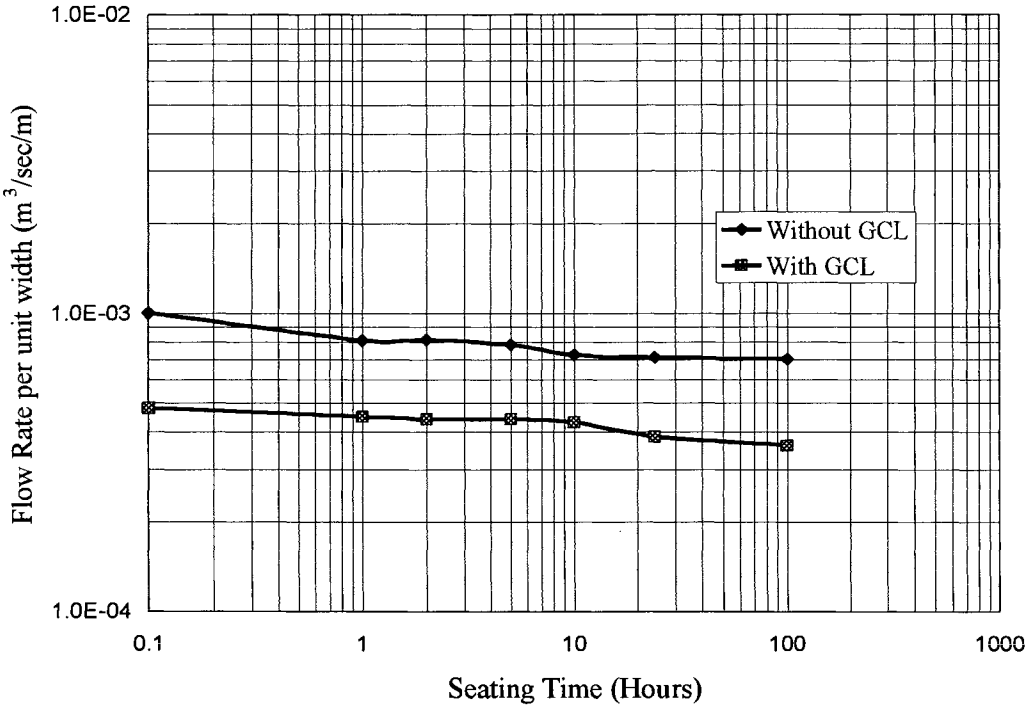

Figure 5. Flow rate for a tri-planar geocomposite with and without a GCL (After Montanelli and Rimoldi, 1995)

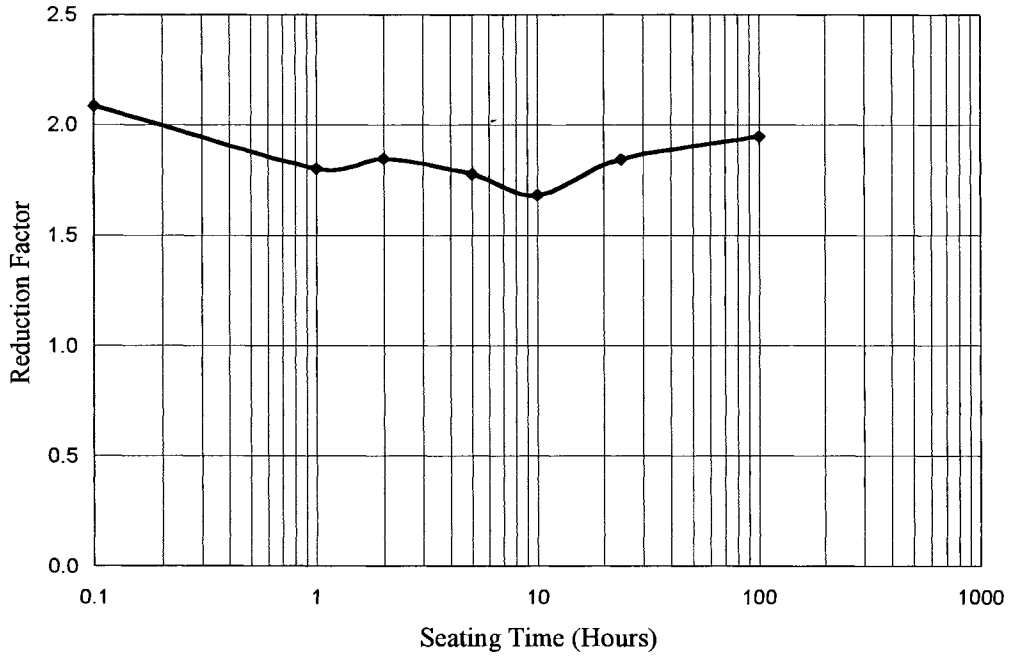

Figure 6. Long-term reduction factor of a tri-planar geocomposite with a GCL

LONG-TERM FLOW OF GEOCOMPOSITES UNDER IN-SOIL ENVIRONMENT

The long-term intrusion of the geotextile into the geonet core can be measured by transmissivity tests under sustained normal loads. Figure 7 presents the long-term flow rates for a tri-planar geocomposite up to 1000 hours. The tri-planar geocomposite retains about 65% of its flow capacity after 1000 hours. Long-term flow capacity of a geocomposite is directly related to the compressive creep behavior of the geonet. Figure 8 is a 10,000-hour compressive creep curve for the tri-planar geonet under sustained normal load of 1200 kPa. The geonet retains over 65% of its initial thickness.

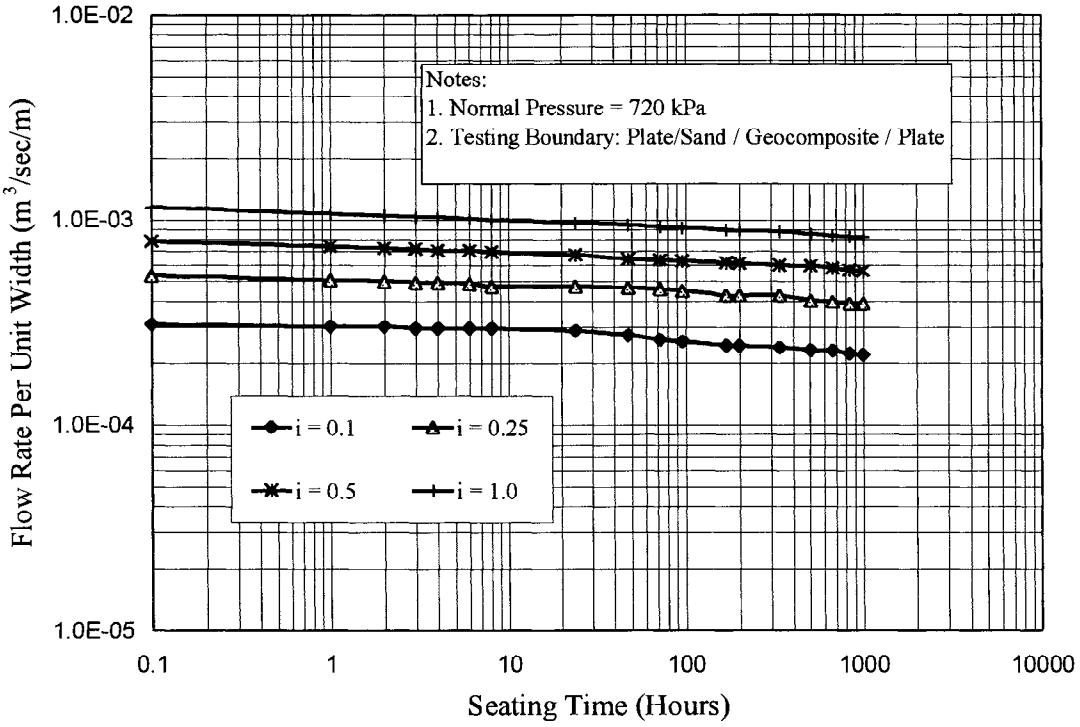

Figure 7. Long-term flow rate for a tri-planar geocomposite.

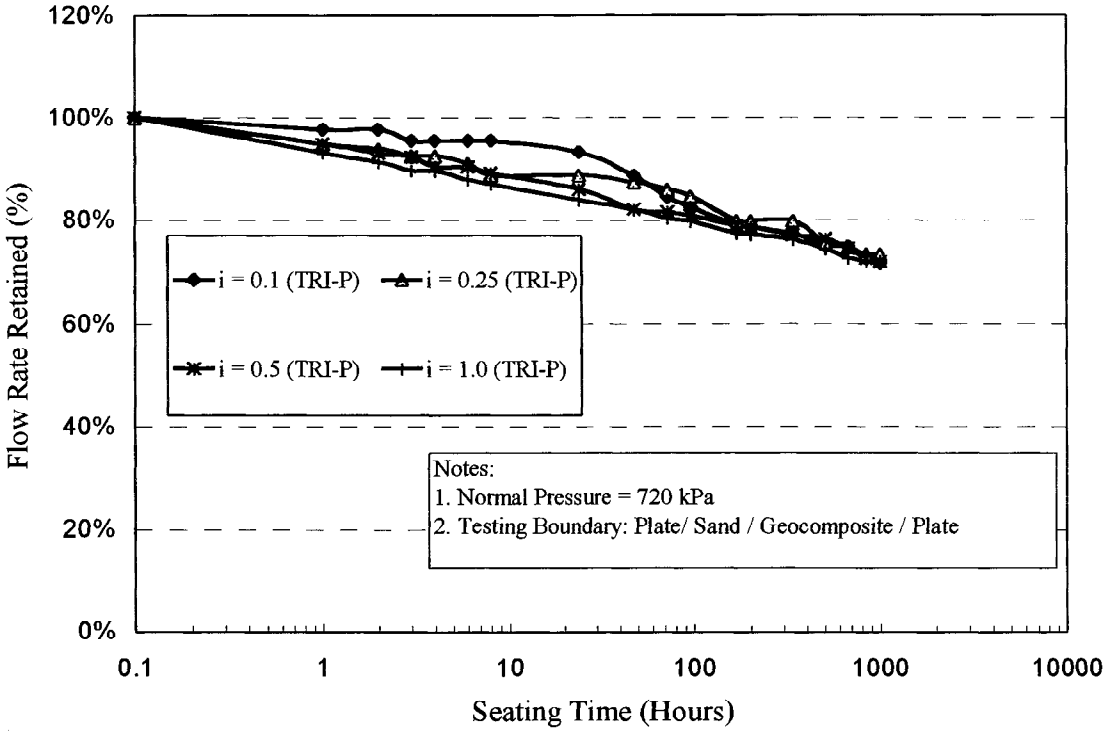

Figure 8. Long-term flow rate retained for a tri-planar geocomposite.

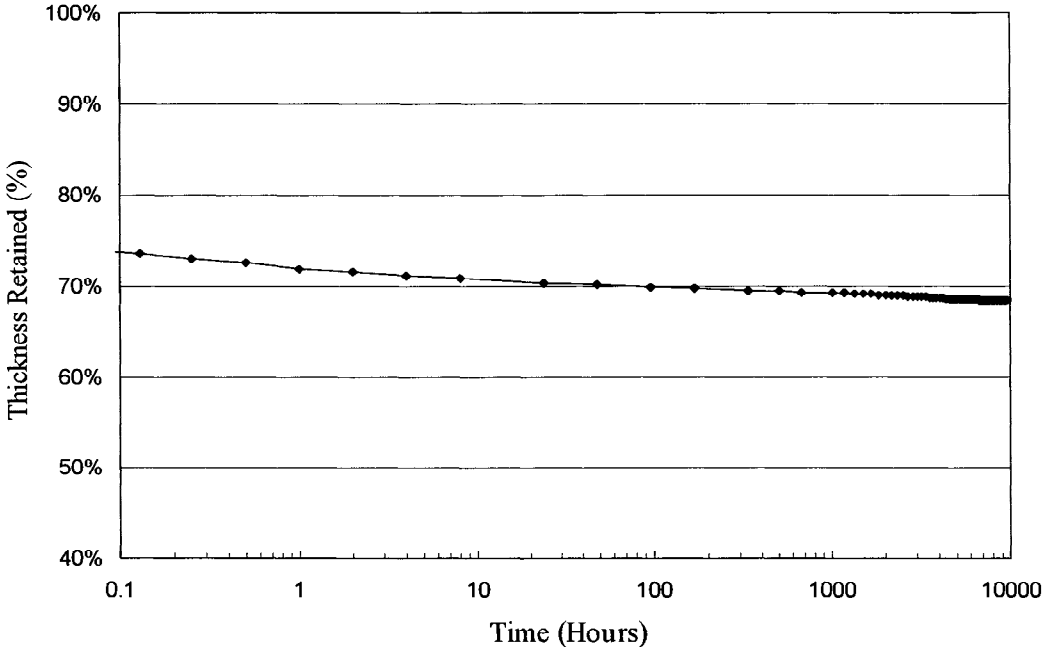

Figure 9. Long-term compressive creep curve for a tri-planar geonet (Normal pressure =1200 kPa)

CONCLUDING REMARKS

Extensive transmissivity tests are performed under high normal loads to investigate the reduction factors on flow rate due to overlying material intrusion into the geonet core. Two geonet structures (tri-planar and bi-planar geonets), two types of soils (sand and clay), GCL and a neoprene are included in the tests. Long-term transmissivity tests under in-soil environment and long-term compressive creep test up to 10,000 hours are also conducted. The following conclusions can be drawn from the experimental results presented above:

- Under high normal loads, the reduction factors for geotextile intrusion of the tri-planar geocomposite with the sand layer are found to be in agreement with the suggested default value range (1.5 to 2). The default reduction factors are not representative of the bi-planar geocomposite. The reduction factor of the bi-planar geocomposite tested due to the presence of a clayey soil layer exceeds 20.

- Sand layer compaction is found to have an insignificant effect on the flow rate of both bi-planar and tri-planar geocomposites under high normal loads.

- The neoprene tested can simulate geotextile intrusion with the sand layer for both bi-planar and tri-planar geocomposites. However, the neoprene significantly underestimates intrusion of geotextile for clayey soil. Transmissivity tests with a neoprene above and below a geocomposite greatly reduce the flow rate, with a reduction factor as high as 38 obtained. Due to variations of both neoprene and soils, the use of real soils to conduct performance transmissivity tests is strongly recommended.

- A reduction in the flow rate of geocomposites under sustained high loads occurs with respect to time. Long-term performance transmissivity tests of geocomposites and long-term compressive creep tests of geonets are recommended.

It has been noticed that variation in transmissivity test results, especially under in-soil environment, is significant. Many factors, such as different transmissivity test equipment, different types of soils and preparation procedures, seating time, etc., can contribute to this variation. Further research is needed to standardize the in-soil transmissivity testing procedure, and more comprehensive tests should be conducted to advance the understanding of the long-term behavior of various geocomposites under different conditions.

REEFERENCES

Campbell , R. and Wu, J.T.H. (1994), In-plane flow of four geosynthetics for landfill drainage, Geotechnical Testing Journal, ASTM, Vol. 17, No.1, 1994, pp. 3-16.

Fannin, R.J. and Choy, H.W. (1995), Factors influencing the long-term flow capacity of geonets, Geosynthetics'95, pp. 267-280.

Holtz, R., Christopher, B. and Berg R. (1997), Geosynthetic Engineering, BiTech Publishers Ltd, British Columbia, Canada.

Hwu, B., Koerner, R. M. and Sprague, C.J. (1990), Geotextile intrusion into geonets, Fourth International Conf. On Geotextiles, Geomembranes and Related Products, pp. 351-356.

Koerner, R. M. (1997), Designing with Geosynthetics, Fourth Edition, Prentice Hall.

Montanelli, F., and Rimoldi, P. (1995), Long-term behavior of GCL and drainage composite systems, Sardinia'95, Italy.

Richardson, G., Zhao, A. (1998) Composite drains for side slopes in landfill final covers. Geotechnical Fabrics Report, June/July, pp. 22-25, 1998.

Smith, A.D., and Kraemer, S.R. (1987). Creep of geocomposite drains, Geosynthetics'87, pp. 422-433.

Slocumb R., Demeny, D., and Christopher, B. (1986), Creep characteristics of drainage nets, Superfund'86.

Schroeder, P.R., Dozier, T.S., Zappi, P.A., McEnroe, B.M., Sjostrom, J.W. and Peyton, R.L. (1994). "The Hydrologic Evaluation of Landfill Performance (HELP) Model: Engineering Documentation for Version 3," EPA/600/R-94/168b, U.S. Environmental Protection Agency, Risk Reduction Engineering Laboratory, Cincinnati, OH.

Zhao, A. and Richardson, G. (1998) Lateral drainage systems over landfill barrier systems –flat slopes. Geotechnical Fabrics Report, August, pp. 21-23, 1998.

ARE POROSITY AND O_{95} IMPORTANT IN THE RETENTION AND PARTICULATE CLOGGING BEHAVIOR OF GEOTEXTILES?

JENNIFER L. SMITH
O'BRIEN & GERE ENGINEERS, INC., USA

SHOBHA K. BHATIA
SYRACUSE UNIVERSITY, USA

JASON RIDGWAY
O'BRIEN & GERE TECHNICAL SERVICES, INC., USA

WILLIAM HAWKINS
REEMAY INC., USA

ABSTRACT

Although the most effective means for evaluating the filtration behavior of a geotextile is to conduct a performance test, such as a long-term filtration (LTF) test or a gradient ratio (GR) test, these tests are rarely performed. As a result, designers often look toward conservative empirical clogging criteria that may or may not be appropriate for the selection of a geotextile as a filter. Empirical clogging criteria are generally based on the O_{95} and porosity of the geotextile. This study focuses on the importance of these geotextile parameters on the retention and particulate clogging potential of geotextile filters. In this study, several LTF tests were conducted on nonwoven geotextiles and polymeric meshes with similar opening sizes. By performing the tests on polymeric meshes of known opening size (and low percent open area), the effect of geotextile porosity on LTF test results can be evaluated. The extent of clogging within the geotextile and at the soil/geotextile-mesh interfaces was studied using photomicrographs of epoxied sections of the soil/geotextile-mesh systems. Based on the results of this study, it does not appear that geotextile porosity and O_{95} are important in the retention and particulate clogging behavior of geotextiles.

INTRODUCTION

Nonwoven geotextiles are commonly used in applications where their primary application is filtration. Wick drains, edge drains, earth dams, and geosynthetic fabric containers (GFCs) (Moo-Young and Ochola, 1998) are among many applications where geotextile filters are used. When geotextiles are used as filters, it is essential that the geotextile filter be properly designed. A properly designed geotextile filter will ensure good retention for erodible materials and will have adequate discharge capacity for the life of the structure.

Although the most effective means for evaluating the filtration behavior of a geotextile is to conduct a performance test, such as a long-term filtration (LTF) test or a gradient ratio (GR) test, these tests are rarely performed. Performance tests are generally considered time-consuming and expensive. As a result, designers often look toward conservative empirical filtration criteria that may or may not be appropriate for the selection of a geotextile as a filter.

Geotextile filter criteria typically include retention, permeability, and clogging requirements. It is generally assumed that the ability of a geotextile to meet these requirements is a function of the apparent opening size (O_{95}), porosity, and pore-size distribution of the geotextile, and the particle-size distribution of the surrounding soil.

The geotextile acts as a catalyst in establishing a graded soil filter behind the geotextile, in unidirectional flow conditions. The natural formation of the graded soil filter may not form if the largest pore openings in the geotextile are either too large or too small. If the largest pore openings in the geotextile are larger than the larger particles of the soil, then uncontrolled soil piping will occur. Depending on the soil gradation, either internal erosion or soil suffusion will occur. If the largest pore openings in the geotextile are much smaller than the smaller particles of soil, then the fine particles of the soil close to the geotextile will be unable to pass through the geotextile and an effective soil filter will not form. This problem may lead to blinding, blocking or clogging of the geotextile.

As described by Giroud (1996), blinding occurs when soil particles form a thin layer, or "cake", at the surface of the geotextile; blocking occurs when soil particles obstruct the geotextile filter openings; and clogging occurs when soil particles get trapped within the geotextile. Giroud (1996) theoretically quantified two of the mechanisms, blinding and clogging. It was found that more fine particles could migrate into a thick geotextile than into a thin geotextile before there was a decrease in system permeability. Blinding was found to have a more "detrimental" effect on system permeability than clogging. Giroud (1996) also noted the importance of preventing the formation of cakes of fine particles at the soil/geotextile interface, and recommended that a geotextile with openings as large as allowed by filter criteria be selected.

Significant work has been conducted on developing retention and permeability criteria for geotextiles. Summaries of existing criteria have been presented in Fischer et al. (1990) and Christopher and Fischer (1991). The focus of this paper is on clogging criteria. The primary purpose of the clogging criteria is to ensure the geotextile will adequately meet the permeability and retention criteria throughout the life of the structure. The existing clogging criteria for geotextiles are based on either: relationships between the pore openings of the geotextile and the grain size of the surrounding soil; on the porosity or percent open area of the geotextile; or on soil/geotextile performance tests. A summary of some existing geotextile clogging criteria, after Christopher and Fischer (1991), is given in Table 1.

Table 1. A summary of some existing clogging criteria (after Christopher and Fischer, 1991).

A. Critical/severe applications:	
1. Perform soil/geotextile filtration tests.	e.g. Calhoun (1972); Haliburton et al. (1982); Haliburton and Wood (1982); Giroud (1982); Carroll (1983); Christopher and Holtz (1985; 1989); Koerner (1990)
B. Less critical/non-severe applications:	
1. Perform soil/geotextile filtration tests.	
2. Minimum pore sizes for soils containing fines:	
a. $O_{95} \geq 3\ d_{15}$ for $Cu \geq 3$	Christopher and Holtz (1985; 1989)
b. $O_F \geq 4\ d_{15}$	French Committee on Geotextiles and Geomembranes (1986)
c. $O_{15} / d_{15} \geq 0.8$ to 1.2 $O_{50} / d_{50} \geq 0.2$ to 1	Fischer et al. (1990)
3. For $Cu \leq 3$, use a geotextile with maximum opening size from retention criterion.	
4. Apparent opening area:	
a. Woven geotextiles:	
Percent open area $\geq$ 4% to 6%	Calhoun (1972); Koerner (1990)
b. Nonwoven geotextiles:	
Porosity $\geq$ 30% to 40%	Christopher and Holtz (1985); Koerner (1990)

Notes:
1. $O_F = O_{90}$ obtained by wet sieving.

There are many types of clogging mechanisms, as described by Rollin and Lombard (1988). These mechanisms can be categorized as: particulate clogging, biological clogging, and chemical/biochemical clogging.

Particulate Clogging

Empirical geotextile particulate clogging criteria have been established based on comparisons between the pore openings of the geotextile, such as O_{95}, O_{90}, O_{50}, and O_{15}, and the grain sizes of the surrounding soil, such as d_{50} and d_{15}, as shown on Table 1. Although these criteria are available, it is often difficult to measure geotextile pore openings and results obtained are dependent on the technique used for their measurement (Bhatia et al., 1996). Currently, in the United States, only the O_{95} pore size is evaluated for geotextiles. There are currently no standardized techniques for measuring the pore-size distribution of a geotextile (O_{50}, O_{15}) (Bhatia et al., 1996). Similarly, information on the d_{15} of the surrounding soil is not always available to designers unless hydrometer

analyses are performed. When d_{15} information is available, the O_{95} or O_{90} required by the clogging criteria is generally smaller (for silt/clay sized particles) than the O_{95} or O_{90} required for retention of the soil.

In addition to using the largest available opening size, minimum porosity (nonwoven geotextiles) and percent open area (woven geotextiles) requirements have also been established to minimize particulate clogging potential. Porosity is defined as the ratio of void volume to total volume; whereas, percent open area is a comparison of the total open area to the total sample area. Geotextile porosity criteria were originally developed based on the principle that a geotextile should be at least as porous as an equivalent soil filter (approximately 30%). The porosity requirement was later increased to 40% (Koerner, 1990) and to the current value of 50% (FHWA, 1995). The porosity criteria were developed based on comparisons to soil and on typical properties of available materials. Limited testing was conducted to support the modifications to the porosity requirements.

In lieu of performance testing, the clogging criteria are thus evaluated by considering the opening size and permeability of the geotextile (Giroud, 1982; Christopher and Holtz, 1985). Although this approach is commonly accepted, it has been determined that the permeability and opening size of nonwoven geotextiles do not indicate clogging potential (Bhatia et al., 1990; Carroll, 1983); however, for woven geotextiles, the open area is directly related to clogging potential (Haliburton and Wood, 1982). Woven and nonwoven geotextiles with similar O_{95} values would not perform in the same manner in a filtration application, for example.

Biological Clogging

The extensive use of geotextile filters in environmental applications, such as landfill leachate collection systems, has led to the question of biological clogging of geotextile filters. Considerable work has been performed in this area (e.g., Mlynarek and Rollin, 1995; Koerner and Koerner, 1995a; 1995b; Rollin, 1996).

In biological clogging, the first mechanism is the development of a network of "biofilms". The biofilms adhere to the geotextile fibers and continue to grow. Biofilms can cause clogging of geotextiles with small openings. The second mechanism of biological clogging is the development of encrustations. Encrustations occur when bacteria alter the pH of leachates, which can lead to the dissolution of metals (decrease in pH) such as calcium and iron, or the precipitation of carbonates and sulfides from metal ions (increase in pH). When fully developed, encrustations can completely clog the interstices of a geotextile.

Recently, many researchers have investigated biological clogging and made important findings. Brune et al. (1991) concluded that both sand and nonwoven geotextile filters should not be used in environmental applications. If a geotextile filter is used, it should be a monofilament woven geotextile with a minimum O_{95} of 0.5 mm and percent open area of 30%. Koerner and Koerner

(1995a; 1995b) concluded that biological clogging occurs with both sand and geotextile filters, and if given enough time, can spread over the entire thickness of the filters. Koerner and Koerner (1995a; 1995b) also concluded that the most important factor was the opening size of the filter. Kossendey et al. (1996) concluded that microorganisms will grow at the fiber surfaces of geotextiles provided there is a sufficient supply of nutrition. The growth of microbes reduces the permeability of nonwoven geotextile filters, but does not lead to complete clogging. As long as there is no encrustation, the process is reversible. Rollin (1996) concluded that to minimize bacteria attachment, geotextiles should have a large void fraction, large pore size openings, be rigid, and have treated fiber surfaces.

Chemical and Biochemical Clogging

There are also chemical and biochemical clogging concerns for geotextile filters. Chemical clogging can result from the precipitation of salts, such as calcium carbonate, from ground water or leachate. Biochemical clogging can result when aerobic bacteria free the iron present in ground water or leachate. The iron becomes oxidized and can lead to "iron ochre" clogging.

SCOPE OF PROJECT

This study focuses on an evaluation of the importance of porosity and O_{95} on the retention and particulate clogging potential of geotextile filters. Although relationships between porosity and O_{95} retention and particulate clogging behavior have been established, these relationships have not been fully developed in order that clogging can be fully addressed by simple criteria.

Several long-term filtration (LTF) tests were conducted using both nonwoven geotextiles and polymeric meshes with similar opening sizes. The nonwoven geotextiles are relatively high porosity materials; whereas, the polymeric meshes are relatively low percent open area materials. Nonwoven geotextile porosity and woven geotextile (or in this case a polymeric mesh) percent open area are similar concepts that play similar roles (Giroud, 1996). Glass bead mixtures were used to simulate soils over the geotextiles. The objectives of the study are to:

(1) Evaluate retention and particulate clogging at the soil/geotextile-mesh interface.

(2) Compare LTF results between geotextiles (high porosity materials) and polymeric meshes (low percent open area materials) with similar opening sizes to evaluate the effect of geotextile porosity on LTF results.

MATERIALS AND TEST METHODS

Four nonwoven geotextiles from four different manufacturers were selected for this study. The geotextiles were selected based on thickness, opening size, and porosity. The geotextiles include

three needle-punched geotextiles (A1, C3, and F2) and one heat-bonded geotextile (T1). The thickness of each geotextile was measured in accordance with ASTM D1777. The filtration opening size (O_{95}) of each geotextile was evaluated using the hydrodynamic sieving method, in accordance with CAN/CGSB-148-1-10. The porosity of each geotextile was calculated, based on fiber density and thickness. Standard-size polymeric meshes with O_{95} sizes similar to the measured O_{95} values for the geotextiles were selected. The physical properties of the geotextiles and polymeric meshes selected for this study are summarized in Table 2.

Table 2. Summary of geotextile and polymeric mesh physical properties.

Material	Mass per Unit Area (g/m^2)	Thickness (mm)	Opening Size (O_{95}) (mm)	Porosity (calculated)	Percent Open Area (calculated)
Geotextile A1	203	1.90	0.123	88%	NA
Geotextile C3	136	1.56	0.154	93%	NA
Geotextile F2	200	0.75	0.108	80%	NA
Geotextile T1	133	0.51	0.128	71%	NA
Mesh #100	72	0.14	0.150	NA	11%
Mesh #120	72	0.16	0.125	NA	7%
Mesh #140	72	0.12	0.106	NA	8%

Notes:
1. Geotextile mass per unit area was provided by the manufacturer. Polymeric mesh mass per unit area, thickness, and opening size were provided by the manufacturer.
2. Porosity of the geotextiles was calculated based on a specific gravity of polypropylene equal to 0.9 and polyester equal to 1.3.
3. Percent open area of the polymeric meshes was calculated based on the thickness of the mesh provided by the manufacturer.
4. NA = not applicable.

Two glass bead mixtures ("soils") were selected for this study (MS2 and MS3). The physical properties of the "soils" selected for this study are summarized in Table 3. As shown on Table 3, the "soils" selected are similar in terms of coefficient of uniformity and curvature; however, mixture MS2 has finer particles than MS3.

The long-term filtration (LTF) test was selected to evaluate particulate clogging at the soil/geotextile-mesh interfaces. In the LTF test, a geotextile/mesh is fixed in a test cylinder and a sample of soil is placed on top of the geotextile/mesh. The flow rate through the geotextile/mesh

Table 3. Summary of glass bead mixtures ("soils") properties.

Parameter	"Soil" MS2	"Soil" MS3
d_{10} (mm)	0.018	0.033
d_{30} (mm)	0.102	0.180
d_{60} (mm)	0.250	0.450
Cu	13.9	13.6
Cc	2.3	2.2
Permeability (cm/sec)	6.0×10^{-4}	8.0×10^{-4}

Notes:
1. Particle-size was measured in accordance with ASTM D422.
2. Permeability was measured in accordance with ASTM D5084.
3. Cu = coefficient of uniformity = d_{60} / d_{10}
4. Cc = coefficient of curvature = $(d_{30})^2 / (d_{10} \times d_{60})$

is then measured over time under constant head flow conditions. By observing the relationship between flow rate and time, the compatibility of the soil/geotextile-mesh system can be evaluated. Details of the LTF test procedure are summarized in Siva and Bhatia (1993).

The flow behavior of the selected soil/geotextile-mesh systems was evaluated by measuring the cumulative flow rate through the system with time for the LTF tests. System permeability was calculated based on Darcy's law:

$$k = \frac{Q}{i\,A} \tag{1}$$

where: k = system permeability
Q = flow rate
i = hydraulic gradient (i = 5)
A= cross-sectional area.

The system permeability was then plotted versus time. In addition to calculating system permeability, the amount of soil that passed through the soil/geotextile-mesh systems for each LTF test was also measured and reported. Each LTF test was performed for a minimum of 24 hours. Since no changes in performance were observed beyond 8 hours, results are reported in this paper for an 8 hour duration only.

TEST RESULTS

Figures 1 and 2 compare the LTF performance of nonwoven, needle-punched geotextile A1, nonwoven, heat-bonded geotextile T1, and polymeric mesh #120, using two different soils (MS2 and MS3), respectively. The geotextiles and mesh have similar openings sizes, in the range of 0.123 mm to 0.128 mm. However, the porosities/percent open area of the geotextiles and mesh vary from 7% to 88%, as shown on Table 2.

The LTF results for geotextiles A1 and T1 and polymeric mesh #120 are similar in terms of system permeability, for soil MS2, as shown on Figure 1. The amount of soil passing through the soil/geotextile-mesh systems generally decreased with increasing porosity/percent open area of the geotextiles/mesh, as shown on Table 4. Although this general trend was noted, the retention behavior between the needle-punched and heat-bonded geotextiles was not significantly different. This is apparent on Figure 1, where the system permeability for two of the polymeric meshes tested required longer amounts of time to stabilize than the other systems tested, indicating that soil fines were passing through the systems. The needle-punched and heat-bonded geotextiles performed similarly. The overall system permeabilities for the MS3/geotextile-mesh system were greater than those measured using soil MS2, as shown on Figure 2. Although the overall system permeabilities were higher, the amounts of soil that passed through the MS3/geotextile-mesh systems during the tests were generally less than those for the MS2/geotextile-mesh systems.

Figures 3 and 4 compare the LTF performance of nonwoven, needle-punched geotextile F2 and polymeric mesh #140, using soils MS2 and MS3, respectively. The geotextile and mesh have similar openings sizes, in the range of 0.106 mm to 0.108 mm. The porosity/percent open area of the geotextile and mesh vary from 8% to 80%.

The LTF results for geotextile F2 and polymeric mesh #140 are similar in terms of system permeability, for soil MS2, as shown on Figure 3. The system permeabilities were similar to those for the MS2/geotextile-mesh systems shown on Figure 1. The amount of soil passing through the soil/geotextile-mesh systems also decreased with increasing porosity/percent open area, as shown on Table 4. This is also apparent on Figure 3, where the system permeability for polymeric mesh #140 required longer amounts of time to stabilize than the other systems tested, indicating that soil fines were passing through the systems. The overall system permeabilities for the MS3/geotextile-mesh system were slightly greater than those measured using soil MS2, as shown on Figure 4. Although the overall system permeabilities were only slightly higher, the amounts of soil that passed through the MS3/geotextile-mesh systems during the tests were generally greater than those for the MS2/geotextile-mesh systems. This trend was opposite to that observed for the soil/geotextile-mesh systems for geotextiles A1 and T1 and polymeric mesh #120, as shown on Table 4.

Figures 5 and 6 compare the LTF performance of nonwoven, needle-punched geotextile C3 and polymeric mesh #100, using soils MS2 and MS3, respectively. Similarly, the geotextile and mesh

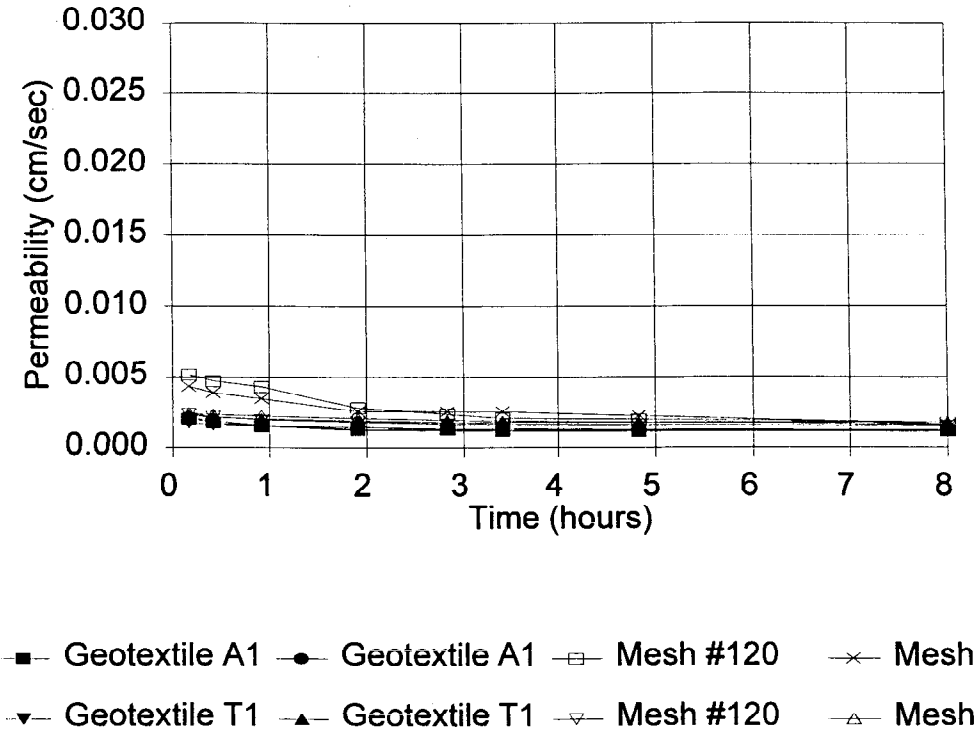

Figure 1. LTF test results for nonwoven, needle-punched geotextile A1, nonwoven, heat-bonded geotextile T1, and polymeric mesh #120, using soil MS2.

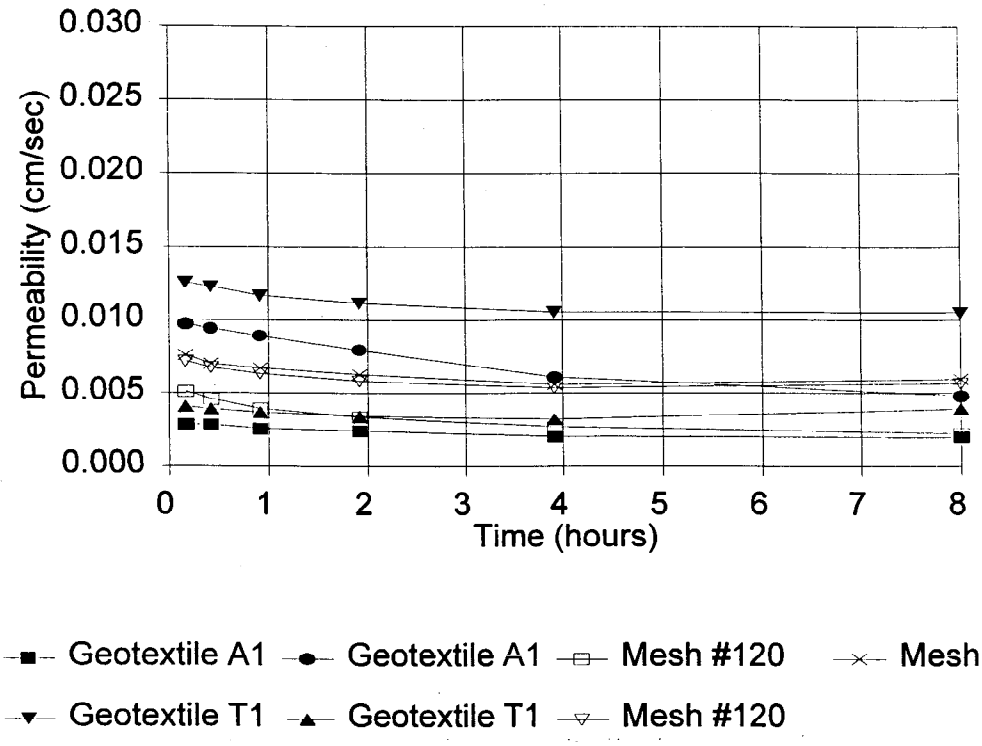

Figure 2. LTF test results for nonwoven, needle-punched geotextile A1, nonwoven, heat-bonded geotextile T1, and polymeric mesh #120, using soil MS3.

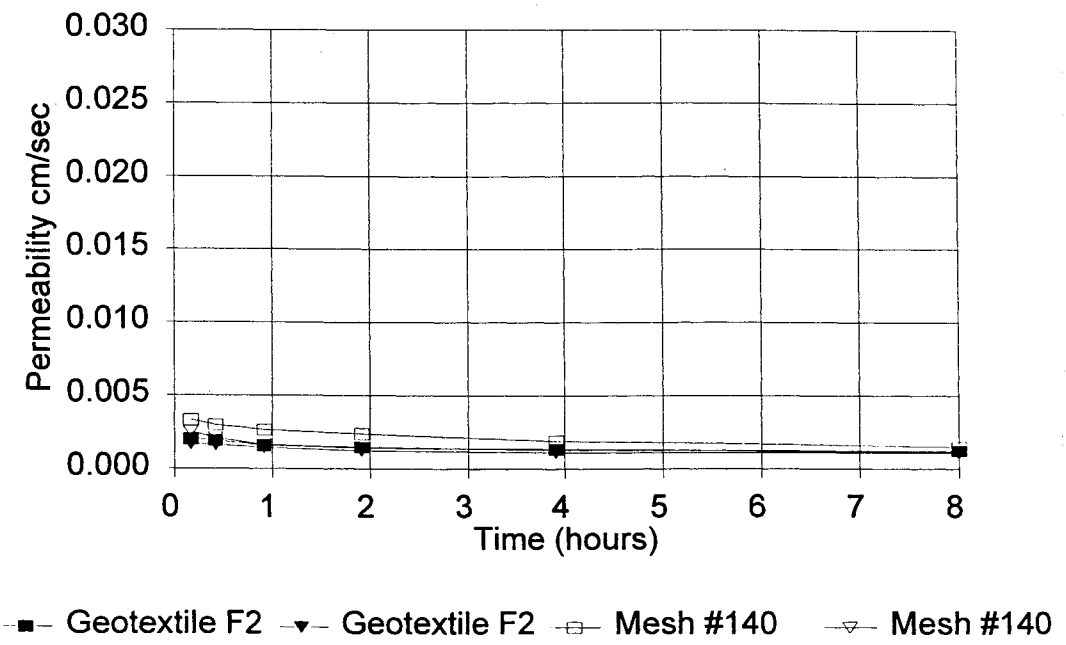

Figure 3. LTF test results for nonwoven, needle-punched geotextile F2 and polymeric mesh #140, using soil MS2.

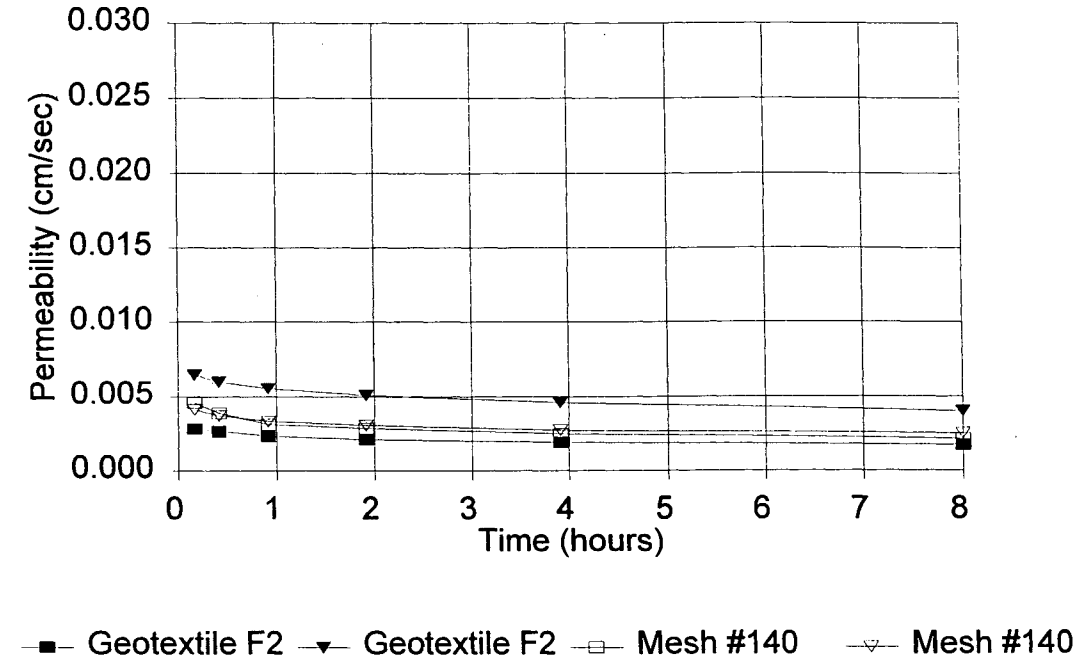

Figure 4. LTF test results for nonwoven, needle-punched geotextile F2 and polymeric mesh #140, using soil MS3.

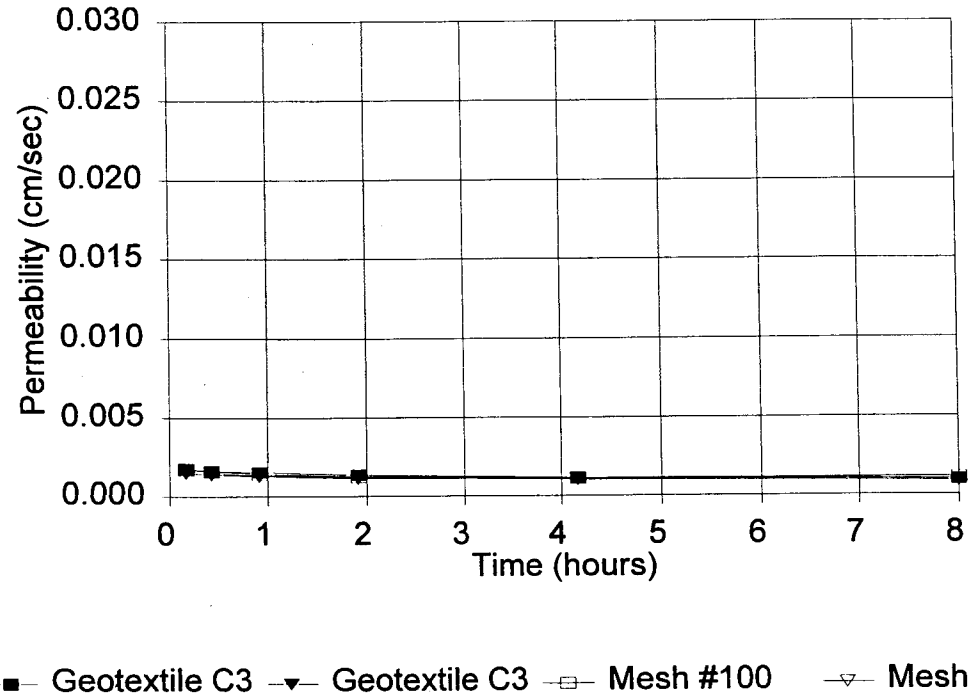

Figure 5. LTF test results for nonwoven, needle-punched geotextile C3 and polymeric mesh #100, using soil MS2.

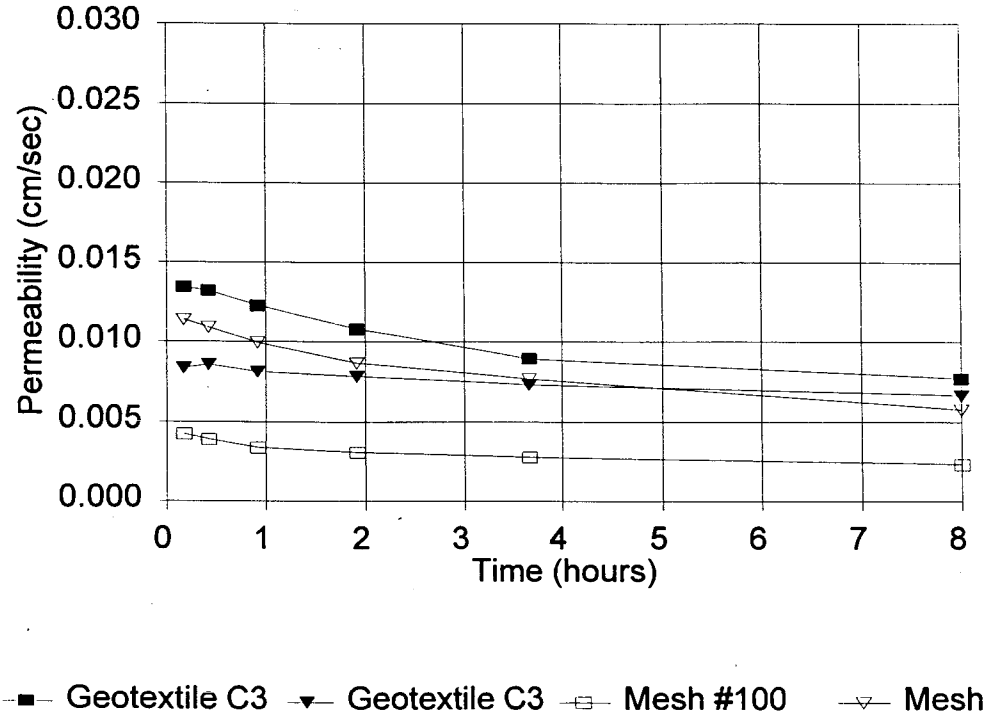

Figure 6. LTF test results for nonwoven, needle-punched geotextile C3 and polymeric mesh #100, using soil MS3.

selected have similar opening sizes (in the range of 0.150 mm and 0.154 mm), and different porosity/percent open area (in the range of 11% to 93%).

The LTF results for geotextile F2 and polymeric mesh #140 are similar in terms of system permeability, for soil MS2, as shown on Figure 5. The system permeabilities were also similar to those for the MS2/geotextile-mesh systems shown on Figures 1 and 3. The amount of soil passing through the soil/geotextile-mesh systems also decreased with increasing porosity/percent open area, as shown on Table 4. The overall system permeabilities for the MS3/geotextile-mesh system were slightly greater than those measured using soil MS2, as shown on Figure 6. Although the overall system permeabilities were higher, the amounts of soil that passed through the MS3/geotextile-mesh systems during the tests were generally greater than those for the MS2/geotextile-mesh systems. This trend was similar to that observed for the soil/geotextile-mesh systems for geotextile C3 and mesh #140, as shown on Table 4.

Table 4. Summary of the amounts of soil that passed through the soil/geotextile-mesh systems during the LTF tests.

Material	Opening Size (O_{95}) (mm)	Porosity (calculated)	Percent Open Area (calculated)	"Soil" MS2 (g/m^2)	"Soil" MS3 (g/m^2)
Geotextile A1	0.123	88%	NA	556 to 638	419 to 952
Geotextile C3	0.154	93%	NA	619 to 857	870 to 957
Geotextile F2	0.108	80%	NA	414 to 490	925 to 1065
Geotextile T1	0.128	71%	NA	725 to 1389	894 to 1294
Mesh #100	0.150	NA	11%	980 to 1052	1175 to 1552
Mesh #120	0.125	NA	7%	1711 to 1964	1002 to 1394
Mesh #140	0.106	NA	8%	1202	1629 to 1763

A comparison of the amounts of soil that passed through the MS2/geotextile-mesh systems is given in Figure 7. As shown on Figure 7, the amount of soil passing through the soil/geotextile-mesh systems generally decreased with increasing porosity/percent open area of the geotextile/mesh. Although this general trend was noted, the retention behavior between the needle-punched and heat-bonded geotextiles was not significantly different. Similar trends were observed for the MS3/geotextile-mesh systems. However, it should be noted that the maximum amounts of soil passing (or piping) through any of the systems tested were below the maximum allowable limit of 2500 g/m^2 established by Lafleur and Mlynarek (1991).

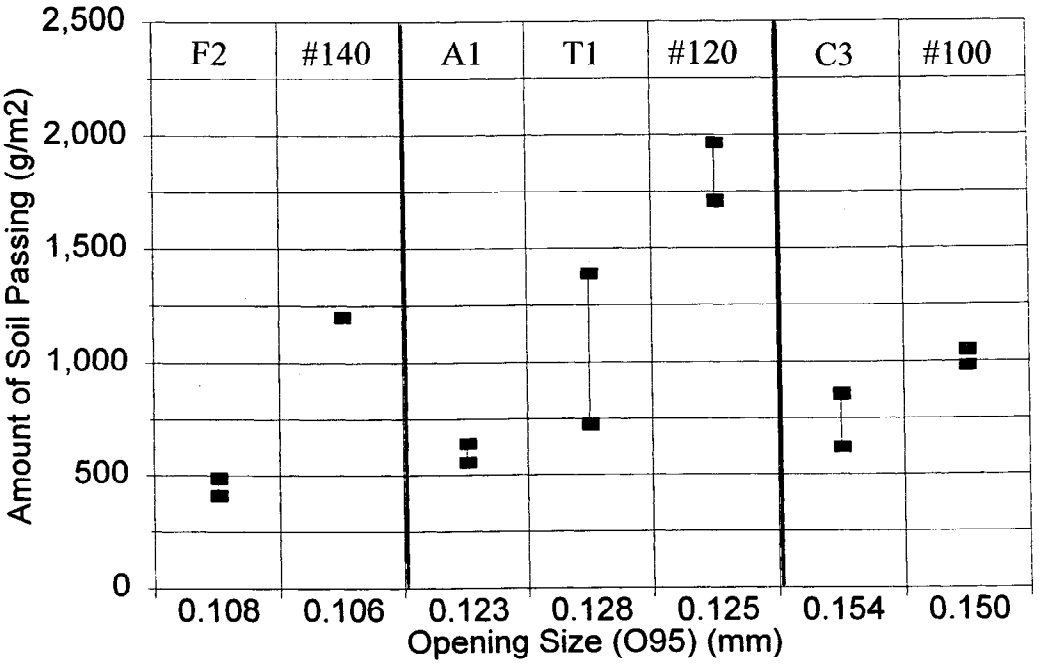

Figure 7. Comparison of the amounts of soil passing through the MS2/geotextile-mesh systems during the LTF tests versus porosity.

DISCUSSION

Sections of the soil/geotextile-mesh interfaces were epoxied and polished following completion of the LTF tests. Photomicrographs of the sections were then taken using a digital image processor. Photomicrographs comparing nonwoven, needle-punched geotextile A1, nonwoven, heat-bonded geotextile T1, and polymeric mesh #120, using two different soils (MS2 and MS3), are shown on Figures 8 and 9, respectively. The differences in soil mixtures (MS2 and MS3) can readily be seen by comparing Figures 8 and 9. The photomicrographs show the extent of particulate clogging within the filters, and the interaction between the soil particles and the filter. As discussed, similar LTF performance was also observed for the needle-punched geotextiles F2 and C3 and polymeric meshes #140 and #100, respectively. In addition, photomicrographs of the soil/geotextile-mesh interfaces were similar. Therefore, these results are not included in this discussion.

Figure 8 shows a comparison between the needle-punched geotextile A1 (porosity = 88%) (a), heat-bonded geotextile T1 (porosity = 71%) (b), and polymeric mesh #120 (percent open area = 7%) (c) for soil MS2. As shown on Figure 8 (a), a distinct bridging zone and filter cake zone were established at the interface of the soil/needle-punched geotextile interface. In addition, fine soil particles can be seen within the thickness of the needle-punched geotextile in the photomicrograph. Bridging zones were not formed at the heat-bonded geotextile (b) and polymeric mesh interfaces (c). In addition, fine soil particles were not observed within the thickness of the heat-bonded

geotextile or mesh. It is believed that the heat-bonded geotextile behaved similarly to the polymeric mesh because of their similar smooth surfaces. It is important to note that the geotextiles and polymeric mesh have similar O_{95} values (see Table 2).

Figure 9 shows a comparison between the needle-punched geotextile A1 (a), heat-bonded geotextile T1 (b), and polymeric mesh #120 (c) for soil MS3. As shown on Figure 9 (a), a distinct bridging zone and filter cake zone were also established at the interface of the soil/needle-punched geotextile interface for the MS3 soil. Filter cake zones rather than bridging zones were again observed at the heat-bonded geotextile (b) and polymeric mesh (c) interfaces.

Although the interfaces between the heat-bonded geotextile and the polymeric mesh were similar, a much larger amount of soil particles passed through the soil/mesh systems than through the soil/geotextile systems. The heat-bonded geotextiles (porosity = 68%) had a slightly larger amount of soil passing through their systems than the needle-punched geotextiles (porosity = 90%), and showed less particulate clogging within their structure. These results also indicate that nonwoven needle-punched and heat-bonded geotextiles are better able to retain soil particles than polymeric meshes of the same opening size. However, as noted above, the maximum amounts of soil passing (or piping) through any of the systems tested were below the maximum allowable limit of 2500 g/m^2 established by Lafleur and Mlynarek (1991).

These observations are consistent with Bhatia et al. (1991), Siva and Bhatia (1993), Mlynarek et al. (1995), and others. Bhatia et al. (1991) studied the retention and clogging performance of four different types of nonwoven geotextiles (continuous filament, continuous filament heat-treated, continuous filament heat-bonded, and staple fiber) with different thicknesses and porosities. LTF test results for these geotextile with a fine-grained silty soil were presented. Results presented by Bhatia et al. (1991) clearly demonstrated that geotextile thickness and porosity do not play significant roles in the particulate clogging of geotextiles. The porosity of the geotextiles ranged from 50% to 93% and had an insignificant effect on the long-term silt/geotextile system permeability. It was also apparent from their results that for the same opening size, the geotextiles of higher porosity (approximately 92%) showed a higher degree of particulate clogging (approximately 80%) and a smaller percentage of particles passing, as compared to the geotextiles of lower porosity (approximately 60%), which showed very little or no particulate clogging but higher percentages of particles passing.

Further, Siva and Bhatia (1993) studied the clogging and retention behavior of eleven nonwoven geotextiles of various manufacturing processes (porosities ranging from 60% to 90%) with six different low-plasticity silts using LTF and rapid retention testing (RRT) methods. The permeability of the geotextiles was reduced by a factor of 15 due to clogging. Other investigators, such as Saathoff (1988) and Lafleur et al. (1990), found the degree of clogging, or reduction in geotextile permeability due to clogging on the order to 2 to 70.

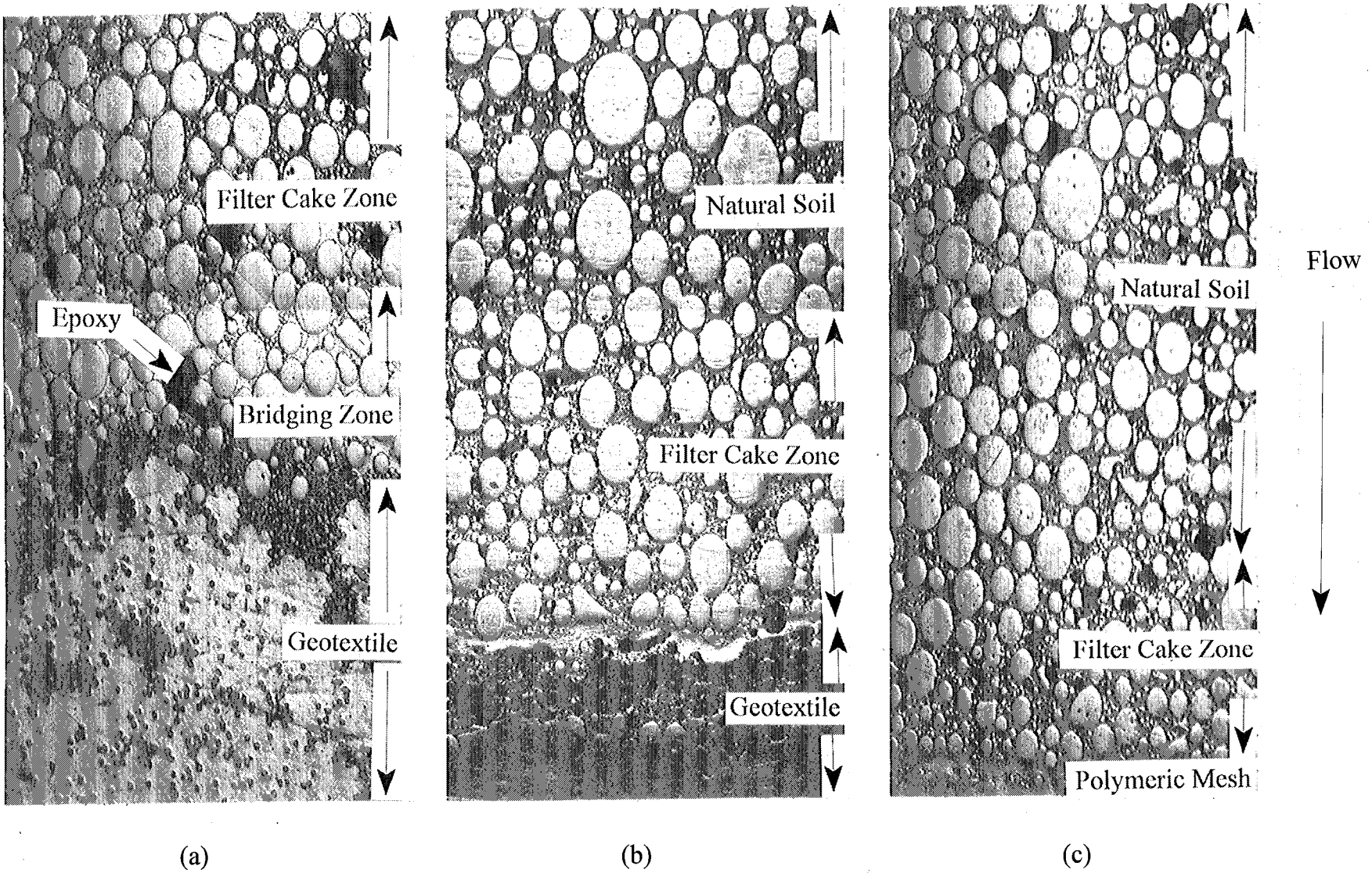

Figure 8. Photomicrographs of epoxied sections of MS2/geotextile-mesh interfaces: (a) Geotextile A1; (b) Geotextile T1; and (c) Polymeric mesh #120. (magnified 25x)

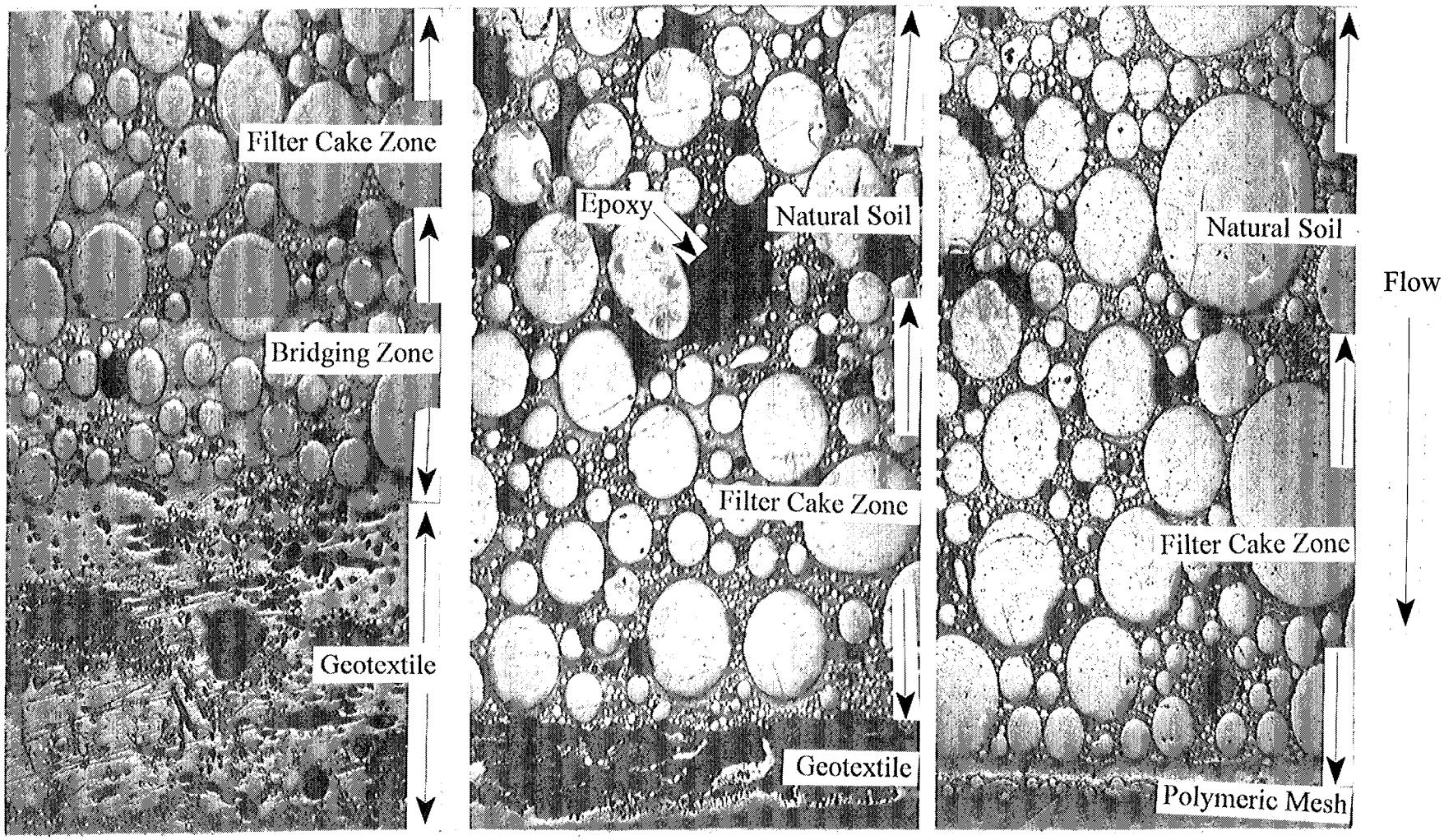

Figure 9. Photomicrographs of epoxied sections of MS3/geotextile-mesh interfaces: (a) Geotextile A1; (b) Geotextile T1; and (c) Polymeric mesh #120. (magnified 25x)

Mlynarek et al. (1995) evaluated the filtration behavior of four different heat-bonded geotextiles (porosity ranging from 49.2% to 67.9%; opening size ranging from 85 to 200 microns). The four geotextiles retained the four glass bead model soils (three unstable, one stable), while allowing water to freely pass through the geotextiles. Bridging was observed at the soil/geotextile interfaces. No significant trapping of glass bead particles within the geotextiles or washout of particles from the geotextiles was observed.

The results of this study, and others (Bhatia et al., 1991; Siva and Bhatia, 1993; Mlynarek et al., 1995) discussed above, demonstrate that there is always the possibility of a small amount of soil particles becoming trapped within a geotextile filter if there is enough porosity. This occurs as a result of the soil particles being approximately the same size as the geotextile openings. However, the reduction in geotextile permeability as a result of this phenomena - particulate clogging - is not a serious concern, as the permeability of geotextiles are generally several orders of magnitude higher than that of fine-grained soils, such as silty sands or silts.

It can be concluded that a higher porosity geotextile will retain particles within its structure, therefore a relatively small percentage of soil will pass through the geotextile structure. However, a lower porosity geotextile has limited volume/voids for particles to clog, therefore finer particles can pass through its structure, resulting in a higher percentage of soil passing. This is important for applications where retention is critical, such as for geosynthetic fabric container (GFC) applications that are used to contain contaminated sediments (Moo-Young and Ochola, 1998).

CONCLUSIONS

Based on the results of the LTF tests and an evaluation of photomicrographs of the soil/geotextile-mesh interfaces, the following conclusions were made.

- The soil retention behavior of the nonwoven needle-punched (porosity 80% to 93%) and heat-bonded (porosity 71%) geotextiles tested was not significantly different.

- Nonwoven geotextiles retain more glass bead particles than polymeric meshes of the same opening size, because of the distribution of pore sizes within their structures.

- The interface zones of the needle-punched and heat-bonded geotextiles were different. It is believed that the smooth surface of the heat-bonded geotextiles inhibited the formation of a bridging zone above the geotextiles for the conditions analyzed.

- The particulate clogging of geotextiles and the excessive fines in the filter cake zone do not appear to be related to the porosity of the geotextiles.

- It does not appear that the formation of a bridging structure is relevant to the particulate clogging potential of a geotextile.

- Based on the results of this study, it does not appear that geotextile porosity and O_{95} are important in the retention and particulate clogging behavior of geotextiles.

ACKNOWLEDGMENTS

The authors would like to acknowledge the support from the National Science Foundation and Reemay Corporation to fund this study. The authors are grateful for the assistance received from Mr. Omar R. Rodriguez in preparing the photomicrographs for this paper.

REFERENCES

Bhatia, S.K., Qureshi, S., and Kogler, R.M. (1990) "Long-Term Clogging Behavior of Nonwoven Geotextiles with Silty and Gap-Graded Sands", Geosynthetic Testing for Waste Containment Applications, ASTM STP 1081, Robert M. Koerner, editor, American Society for Testing and Materials, Philadelphia, Pennsylvania, pp. 285-298.

Bhatia, S.K., Mlynarek, J., Rollin, A.L., and Lafleur, J. (1991) "Effect of Pores Structure of Nonwoven Geotextiles on Their Clogging Behavior", Proceedings of Geosynthetics '91, Atlanta, Georgia, pp. 629-642.

Bhatia, S.K., Smith, J.L., and Christopher, B.R. (1996) "Geotextile Characterization and Pore-Size Distribution: Part III. Comparison of Methods and Application to Design", Geosynthetics International, Industrial Fabrics Association International, Volume 3, No. 3, pp. 301-328.

Brune, M., Ramke, H.G, Collins, H.J., and Hanert, H.H. (1991) "Incrustation Processes in Drainage Systems of Sanitary Landfills", Proceedings of the Third International Landfill Symposium, Sardinia, Italy, October 1991, Vol. 1, pp. 999-1035.

Calhoun, C.C. (1972) "Development of Design Criteria and Acceptance of Specifications for Plastic Filter Cloth", U.S. Army Corps of Engineers W.E.S., Vicksburg, MS Technical Report S-72-7, 83p.

Canadian Standard. "Standard Test Method for Determining the Filtration Opening Size of Geotextiles", CAN/CGSB-148-1-10.

Carroll, R.G. (1983) "Geotextile Filter Criteria", Transportation Research Record, 916, pp. 46-53.

Christopher, B.R., and Holtz, R.D. (1985), Geotextile Engineering Manual, U.S. Federal Highway Administration, Report No. FHWA-TS-86/203, 1044 p.

Christopher, B.R., and Holtz, R.D. (1989) Geotextile Construction and Design Guidelines, Prepared for Federal Highway Administration, Washington, D.C., HI-89-050, 297 pp.

Christopher, B.R. and Fischer, G.R. (1991) "Geotextile Filtration Principles, Practices and Problems", Proceedings of the GRI Seminar.

Fischer, G.R., Christopher, B.R., and Holtz, R.D. (1990) "Filter Criteria Based on Pore Size Distribution", Proceedings of the Fourth International Conference on Geotextiles, The Hague, Netherlands, Vol. 1, pp. 2899-294.

French Committee of Geotextiles and Geomembranes (1986) "Recommendations for the Use of Geotextiles in Drainage and Filtration Systems", Institute Textile de France, Boulogne-Billancourt, France.

Giroud, J.P. (1982) "Filter Criteria for Geotextiles", Proceedings of the Second International Conference on Geotextiles, Las Vegas, Nevada, U.S.A.., Vol. 1, pp. 103-108.

Giroud, J.P. (1996) "Granular Filters and Geotextile Filters", Proceedings of Geofilters '96, Montreal, Quebec, Canada, May 1996, pp. 565-680.

Haliburton, T.A., Lawmaster, J.D., and McGuffey, V.E. (1982) "Use of Engineering Fabric in Transportation Related Applications, FHWA Training Manual, Contract No. DTFH-80-C-0094.

Haliburton, T.A., and Wood, P.D. (1982) "Evaluation of the U.S. Army Corps of Engineers Gradient Ratio Test for Geotextile Performance", Proceedings of the Second International Conference on Geotextiles, Vol.. 1, Las Vegas, pp. 97-102.

Koerner, R.M., (1990) Designing with Geosynthetics, Second edition, Prentice Hall, 652 pp.

Koerner, R.M., and Koerner, G.R., (1995a) "Leachate Clogging Assessment of Geotextile (and Soil) Landfill Filters", USEPA/600/14, March 1995, 168p.

Koerner, R.M., and Koerner, G.R., (1995b) "Leachate Clogging Assessment of Geotextile and Soil Landfill Filters", Geosynthetic Research Institute Report No. 15, July 1995, 157p.

Kossendey, T.H., Gartung, E., and St. Schmidt, (1996) "Microbiological Influences on the Long-Term Performance of Geotextile Filters", Proceedings of Geofilters '96, Montreal, Quebec, Canada, May 1996, pp. 115-124.

Lafleur, J., and Mlynarek, J. (1991) "Filtration of Broadly Graded Cohesionless Soils", ASCE Journal of Geotechnical Engineering.

Lafleur, J., Mlynarek, J., and Rollin, A.L. (1990) "Clogging of Geotextiles under Pumping Loads", Fourth International Conference on Geotextiles, Geomembranes, and Related Products, The Hague, Netherlands, pp. 189-192.

Mlynarek, J., and Rollin, A.L. (1995) "Bacterial Clogging of Geotextiles - Overcoming Engineering Concerns", Proceedings of Geosynthetics '95, Vol. 1, Nashville, Tennessee, February 1995, pp. 177-188.

Mlynarek, J., Vermeersch, O.G., DeBerardino, S. (1995) "Evaluation of Filtration Design Criteria for Nonwoven Heat-Bonded Geotextiles", Proceedings of Geosynthetics '95, Vol. 1, Nashville, Tennessee, February 1995, pp. 189-202.

Moo-Young, H., and Ochola, C. (1998) "Strain Effects on the Filtration Properties of Geotextiles", Filtration and Drainage in Geotechnical/Geoenvironmental Engineering, ASCE Geotechnical Special Publication Number 78, Edited by Lakshmi N. Reddi and Mohan V.S. Bonala, pp. 123-136.

Rollin, A.L. (1996) "Bacterial Clogging of Geotextiles", Proceedings of Geofilters '96, Montreal, Quebec, Canada, May 1996, pp. 125-134.

Rollin, A.L., and Lombard, G. (1988) "Mechanisms Affecting Long-Term Filtration Behavior of Geotextiles", Geotextiles and Geomembranes, Volume 7, pp. 119-145.

Saathoff, F. (1988) "Examinations of Long-Term Filtering Behavior of Geotextiles", Durability of Geotexitles, RILEM, pp. 86-114.

Siva, U. and Bhatia, S.K. (1993) "Filtration Performance of Geotextiles with Fine-Grained Soils", Proceedings of Geosynthetics '93, Vancouver, British Columbia, pp. 483-499.

SINKHOLES BENEATH A REINFORCED EARTHFILL
A LARGE-SCALE MOTORWAY AND RAILWAY EXPERIMENT

Prof J.P. GOURC, Dr P. VILLARD, Dr H. GIRAUD
LIRIGM, UNIVERSITÉ JOSEPH FOURIER, 38041 GRENOBLE CEDEX 9, FRANCE
J.C. BLIVET, M. KHAY
CETE ROUEN, BP 245, 76121 GRAND QUEVILLY - FRANCE
B. IMBERT
SNCF - DÉPARTEMENT LIGNES NOUVELLES - 75876 PARIS - CEDEX 18, FRANCE
A. MORBOIS
SCETAUROUTE, ST QUENTIN EN YVELINES, 78286 GUYANCOURT CEDEX, FRANCE
Dr Ph. DELMAS
BIDIM GEOSYNTHETICS, BP 80, 95873 BEZONS CEDEX, FRANCE

ABSTRACT

A geosynthetic preventive reinforcement system was tested under railway line and road bedding layers in order to propose solutions to the risk of localised sinkholes related to the rise of subsurface cavities under the road or railway embankment. Full-scale experiments were conducted on an instrumented experimental site. The formation of cavities 2 and 4 metres in diameter was simulated under the fill material reinforced with geosynthetic sheets of different stiffness characteristics. Deflection, displacement and strain measurements were taken continuously on the geosynthetic sheet and within the fill material. The experimental results presented illustrate the merits of the proposed technical solution.

INTRODUCTION

In recent years, motorway and railway line construction companies have had to deal with accidents on a variety of sites where sinkholes have occurred in the fill material as a result of the presence of subsurface cavities. The cavities encountered originate either from natural phenomena related to rock dissolution by water with a high carbon dioxide content, or from human activities related to the extraction of minerals (underground gallery, tunnel, marl pit, etc.). Given the relatively small diameter (less than 4 m) of these cavities, it is often impossible to detect them during the construction works, because their small size is at the very limit of detectability by conventional survey methods, or because they are formed after the construction works (gypsum dissolution, leaching, etc.). To guard against the risks of accidents that might result from these cavities, reinforcement of the railway line and road bedding layers by underlying geosynthetic materials was considered. The aim of this reinforcement was to restrict sinkhole formation in the fill material and surface deformation to permissible values to allow traffic circulation to continue until repair work on the fill material could be implemented.

Various organisations worked in collaboration within the context of the RAFAEL research programme (Reinforcement of railway line and road bedding layers to guard against localised sinkholes) in order to implement a massive programme of full-scale tests. In all, seven

experiments on instrumented circular cavities of various diameters were conducted during track construction work for a high-speed train line (TGV Méditerranée) at the Eurre site in the Drôme department of France in May 1997: three experiments under new road carriageways and four experiments under the railway line.

Each cavity, initially filled with expanded clay beads, is gradually emptied by a suction pump, resulting in the initiation of localised collapse mechanisms. Depending on the size of the cavity tested or type of reinforcement used, the collapse phenomenon may occur immediately after emptying the cavity or only after traffic circulation tests (passage of lorries or trains).

The aims of the RAFAEL programme are twofold: first to test the efficiency of the proposed reinforcement system, and secondly to present reference tests with a view to establishing a sizing method. This experiment was also conducted in order to highlight the operating mechanisms on failure of the reinforced structure, but does not in any way correspond to the dimensional design of a structure in actual service given that the strains considered here are significantly greater than the permissible strains for a structure in normal service.

THE FULL-SCALE EXPERIMENT

Basic geometry

The experiments conducted involved cavities of 2 or 4 metres diameter, reinforced by one or two textile layers installed underneath the railway line or road at a depth of 1.5 m. Each cavity filled with expanded clay beads comprises a steel culvert for the 4 m cavities and a reinforced concrete culvert for the 2 m cavities, both 1 m in height. Suction tubes were installed in each cavity to allow the clay beads to be removed and to initiate sinkhole formation in the overlying fill material. For the road experiment, it was decided to build the motorway embankment without the top wearing course in order to be able to analyse surface phenomena more accurately (fig. 1). For the railway line experiment, a conventional TGV (high speed train) structure was installed (improved subgrade, ballast, concrete sleepers and rails) to allow the trains to circulate (fig. 2).

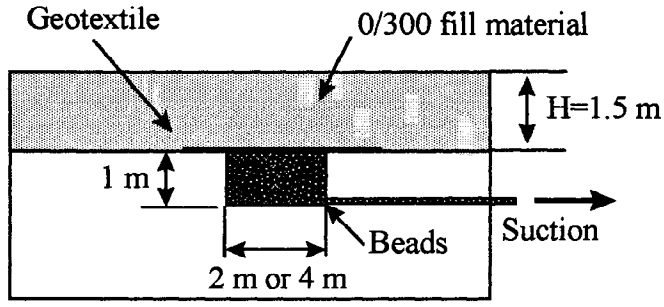

Figure 1. Geometry of the road experiment

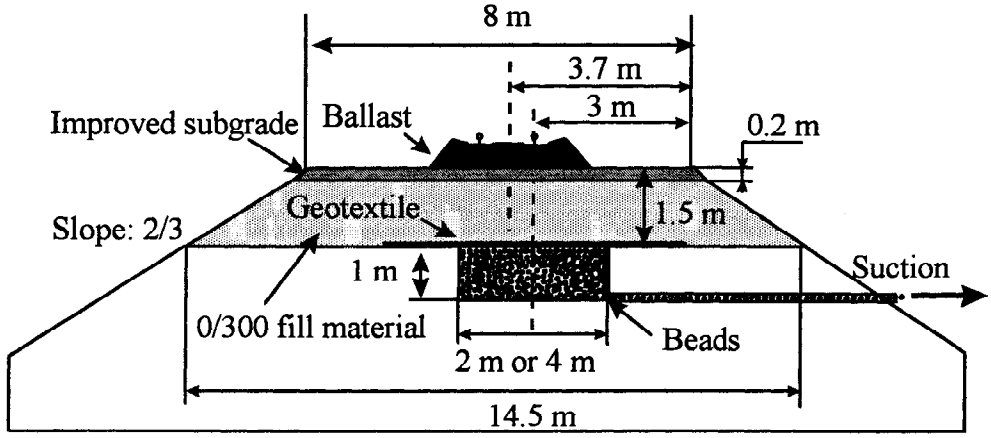

Figure 2. Geometry of the railway line experiment

Fill material

The fill material consists of 0/300 mm quarry run of density γ_d = 21,1 kN/m^3 made up of alluvial gravel-sand mixture (d_{50} = 30 mm, d_{10} = 1 mm and C_u = 50 mm). The mechanical properties of the fill material were determined by shearing tests performed on a large size (1 m x 1 m) direct shear box. The internal angle of friction ϕ and the cohesion c of the material were estimated to be 38° and 40 kPa respectively.

Geosynthetic sheets

The choice of type of geosynthetic is determined by three-dimensional modelling (Villard et al., 1998) of the membrane effect (capacity of the sheet to accommodate stress applied perpendicular to its horizontal plane by tensile bending). Depending on the cases studied, one or two geotextile sheets of different stiffness characteristics were used in order to make a comparative analysis of the results. The properties of the sheets used (stiffness J obtained at 5 % of strain and failure strength T_f) in the seven experiments (SCET1 to SCET3 for the road tests and SNCF1 to SNCF4 for the railway line tests) are given in table 1:

Table 1. Details of the experiments performed

Type of test	Cavity diameter (m)	Number of sheets	Stiffness J of the geotextile (kN/m)	Failure strength T_f of the geotextile (kN/m)
road : SCET1	2	1	1818	200
road : SCET2	4	1	1818	200
road : SCET3	4	1	3600	230
rail : SNCF1	2	1	455	50
rail : SNCF2	4	1	1818	200
rail : SNCF3	4	2	1818	200
rail : SNCF4	2	1	1818	200

Traffic acceptance tests

After emptying the cavities traffic acceptance tests were performed whenever this was possible. A lorry with a rear-axle load of 14 tonnes was used for the road experiment (with the axle comprising two double wheels with a total combined width of 1.96 m). A traction unit and SNCF traffic simulator (stabiliser) were used for the railway line experiment. The stabiliser is used in order to apply a vibrating load to the rails with adjustable frequency and intensity. Each passage of the stabiliser is equivalent to a traffic weight of 80 000 to 100 000 tonnes of goods from the ballast layer fatigue standpoint.

Instrumentation

The purpose of the instrumentation installed is to measure the strains and tensile stresses developing in the geotextile layer as well as the degree of surface and bulk settlement of the fill material. These measurements were taken continuously during the cavity emptying stage and during the traffic acceptance tests. For each cavity, four vertical displacement sensors (fig. 3 and fig. 4), anchored to the bottom of the cavity and fixed to the sheets, were used to determine the vertical bending strain of the geotextile.

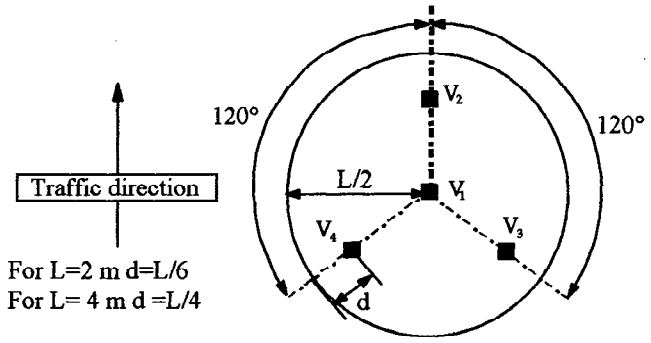

Figure 3. Installation of vertical displacement sensors

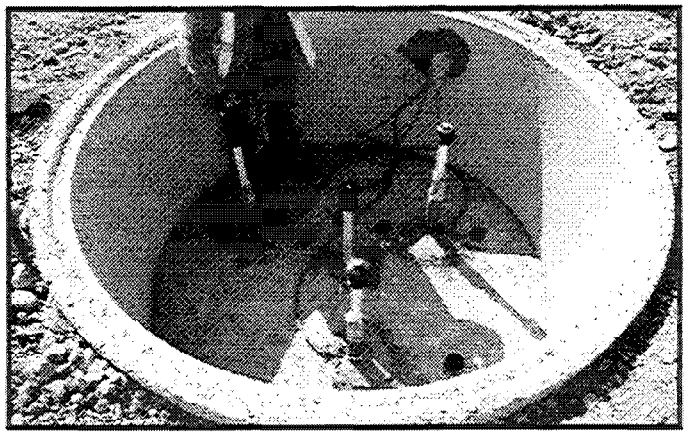

Figure 4. Overall view of the vertical displacement sensors

Five strain gauges (D_1, D_2, D_3, D_4, D_5) were installed at different points in the geotextile sheet in order to measure local strains. Five cable-type displacement sensors (C_1, C_2, C_3, C_4, C_5) were used (fig. 5 and fig. 6) to measure the extension of the sheet and to estimate the strains by differential calculation between two measurement points. With this type of instrumentation, the strains are average values obtained by the differential calculation of the displacements of two consecutive points of the sheet, whereas the strain gauges give directly the local strain values at the measurement points considered.

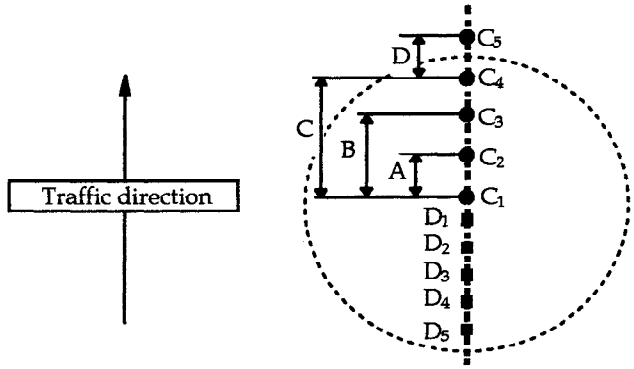

A= 0.320 m, B=0.64 m, C= 0.96 m, D= 0.30 m

Figure 5. Installation of strain gauges and cable-type displacement sensors (SCET1 : diameter L = 2m)

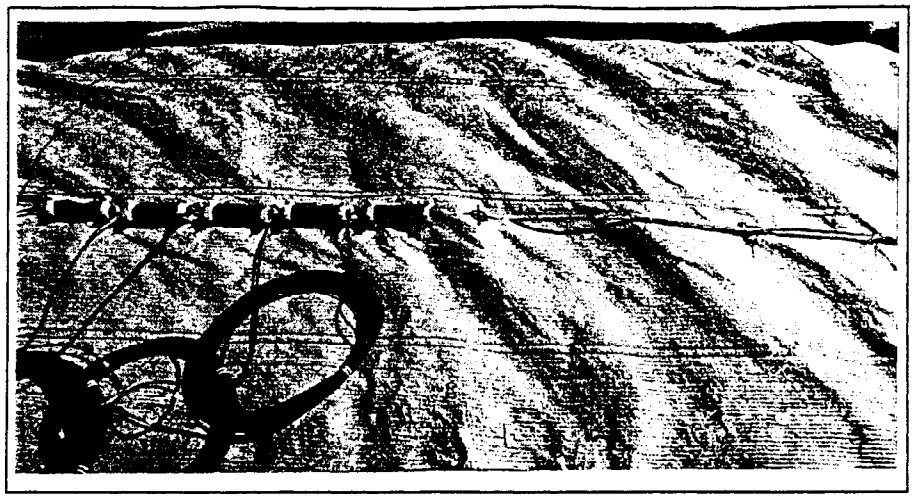

Figure 6. Overall view of the strain gauges and cable-type displacement sensors

Two horizontal inclinometer tubes were installed in the fill material in the cavity axis perpendicular to the traffic direction in order to measure vertical deflections in the body of the material. The first tube was placed 0.50 m above the sheet and the second one metre above. To limit their stiffness, the inclinometer tubes were partially sawn cross-wise every 0.50 m.

Topographical levelling measurements were carried out in the traffic circulation direction and in the transverse direction in order to measure surface deflections.

RESULTS OF ROAD EXPERIMENTS

Results of the SCET1 experiment

The SCET1 experiment (2m cavity) was performed in order to analyse the behaviour of the fill material during the cavity emptying process and during traffic circulation tests (in all, 74 lorry passes were carried out with one set of double wheels of the axle being centred on the cavity diameter). The cavity was subsequently dismantled with great care over a period of several months after the traffic acceptance tests to make a more detailed analysis of the phenomena observed.

* Cavity emptying stage

Typical results obtained from the instrumentation used during the emptying stage of the SCET1 are presented. Figures 7, 8 and 9 give respectively the vertical displacements of the sensors V_1 to V_4, the strain values deduced from the cable-type displacement sensors between measurement points C_1 to C_4, and the strains values obtained directly by the strain gauges D_1 to D_5. The topographical measurements showed that the surface layer of the fill material had not moved. However, minor displacements of the body of the fill were detected thanks to the inclinometers (0.6 mm for the lower inclinometer and 0.4 mm for the upper inclinometer).

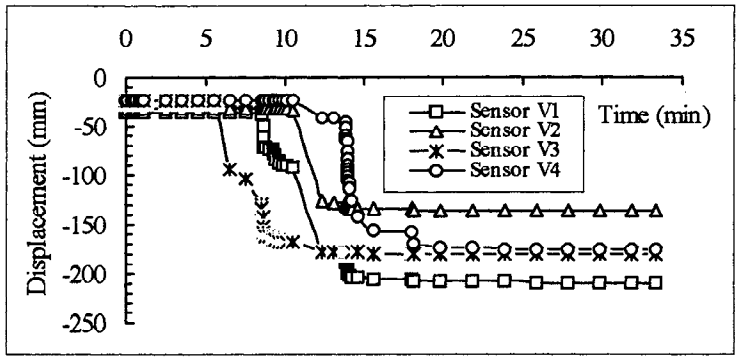

Figure 7. Vertical displacements of the geotextile sheet

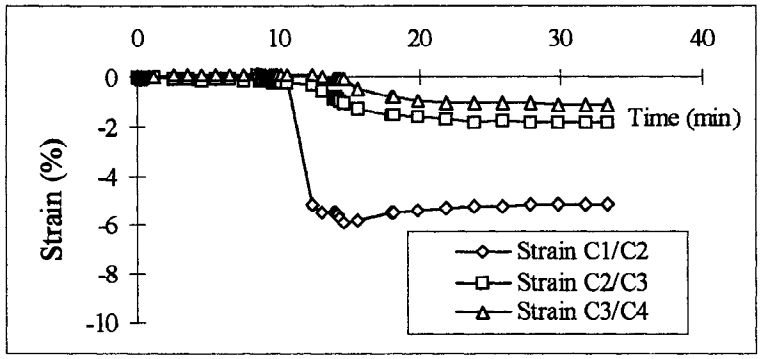

Figure 8. Sheet strain (cable-type displacement sensors)

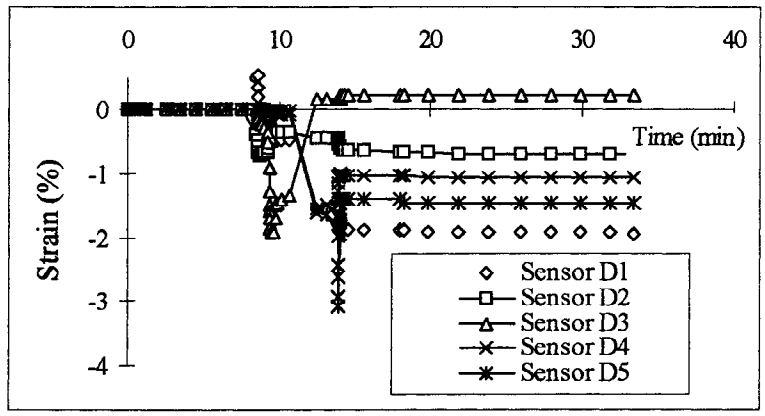

Figure 9. Sheet strain (strain gauges)

Measurements using the vertical displacement sensors (fig. 7) are taken 0.21 m from the centre of the geosynthetic sheet (sensor V_1) and from 0.14 m to 0.18 m from the edges (sensors V_2 to V_4). The strain values obtained with the cable-type displacement sensors and with the strain gauges are 2% on average with a maximum value of about 5%.

* Traffic acceptance stage

After emptying the cavity, traffic acceptance tests involving the repeated passage of a loaded lorry were undertaken without any major effect on surface displacements (w). A slight rutting effect was observed where the double wheel crossed over the cavity together with a slight settlement of the fill material. The strain values measured with the cable-type sensors or the strain gauges were more or less the same as the values found after emptying the cavity.

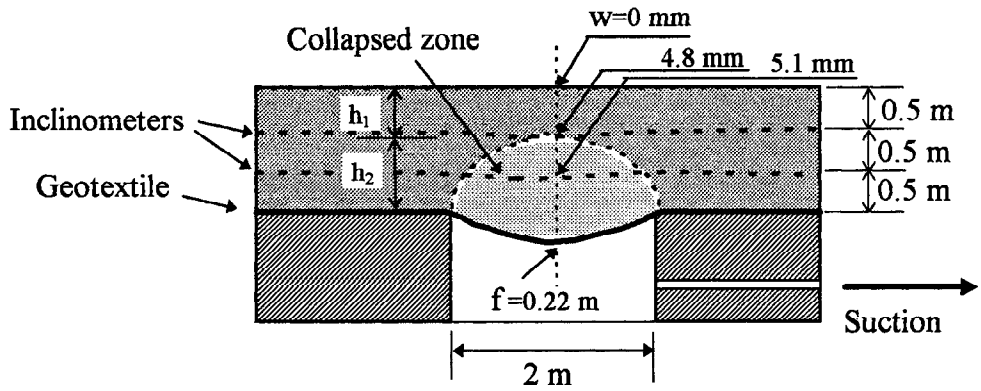

Figure 10. Geometry of the fill material after traffic acceptance tests (74 passages)

All the results obtained tend to show that a stable soil arch forms on emptying the cavity (fig. 10). Repeated passages of the lorry have only minimal repercussions on the deflection and strain measurements because most of the forces are transferred away from the cavity. The fill material and cavity were carefully dismantled in order to make a very accurate appraisal of the

shape of the arch and the extent of the sinkhole area (a collapsed soil thickness h_2 of about 1.07 m and an arch thickness at the centre of h_1=0.43 m).

The consistency of the experimental results was verified by means of simple or more complex formulations of the membrane effect (R.D. Espinoza, 1994, J.P.Giroud, 1990, Gourc et al, 1982):

- The deflection, f, in the middle of the sheet is correlated with the strain ε (assumed to be homogeneous) of the sheet by the relationship $\varepsilon = 8\,[(f/L)^2]\,/3$ (J.P. Giroud ; 1995) where L is the cavity width, thus giving a mean strain of ε =3.2 % for a deflection f of 0.22 m. The calculation is based on the safe-side assumption that the geosynthetic accommodates completely the weight of the sinkhole fill material (and the traffic load, where applicable). In a future publication, it will be shown that this is only an approximation and that the calculation can be further refined.

- The consistency between applied load and sheet strain (deflection at any point on the sheet) was verified by three-dimensional modelling of the membrane effect (P. Villard ; 1998, H. Giraud ; 1997). For a collapsed soil thickness h_2=1.07 m (γ_d= 21,1 kN/m^3) accommodated by the geotextile membrane effect and for a geotextile stiffness of J=1818 kN/m, the maximum deflection expected at the centre of the sheet by the modelling process is f = 0.224 m, to be compared with the measured value of 0.22 m.

Results of the SCET2 experiment

A sinkhole formed without warning above the 4 m diameter SCET2 cavity during the emptying process before any traffic tests. In this case, a surface subsidence w of about 0.25 m depth was observed over a 2.4 m diameter central zone, for a vertical geotextile displacement f greater than 0.60 m at the centre of the sheet. The results obtained at the end of the test are listed in table 1. In view of the fact that the majority of vertical displacement measuring sensors had already reached their travel limit, the results presented are purely indicative.

Table 1 : Results of the SCET2 experiment

SCET2 experiment	End of test
Surface deflection in the middle (w)	0.25 m
Settlement measured by upper inclinometer	> 0.15 m
Settlement measured by lower inclinometer	> 0.15 m
Sheet deflection (f)	> 0.60 m
Sheet strain (cable-type sensors)	4 to 5.5 %
Sheet strain (strain gauges)	2 to 5 %

The sinkhole was assessed by immediately removing all the material around the cavity (fig. 11), and this showed that the geotextile sheet had not failed and that a considerable number

of beads remained in the cavity, especially around the edges of the cavity. The same correlation as that made in the previous case between the measurements (deflection and strain of the geotextile as a function of sinkhole height) remain acceptable although it was somewhat difficult to perform these measurements given the problems encountered (sensors at travel limit and incomplete emptying),.

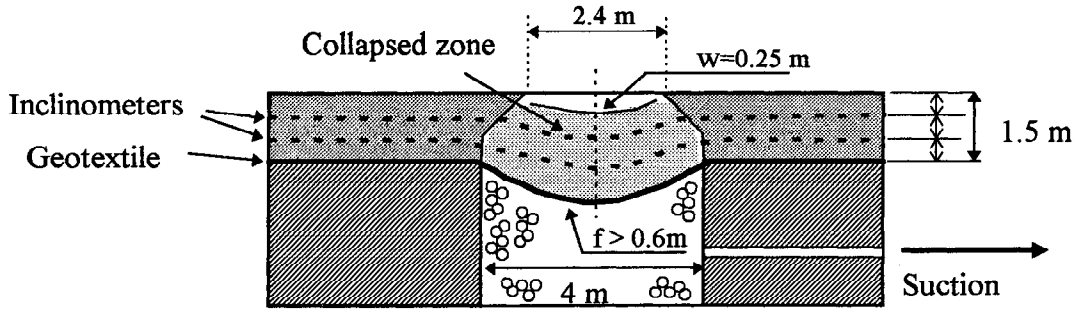

Figure 11. Fill geometry after emptying the cavity

Results of the SCET3 experiment

The SCET3 experiment was performed in order to analyse the behaviour of the fill material during the cavity emptying process and during traffic circulation tests. Compared to the cavity in the SCET2 experiment which has the same diameter of 4 m, the tested cavity is better reinforced (double stiffness of the geosynthetic support).

* Cavity emptying stage

No surface displacement (w) was detected following the emptying stage. However, measurements taken in the fill (table 2) indicate considerable vertical displacements reaching as much as 0.46 m in the middle of the sheet. The inclinometer measurements and the displacement and strain values in the sheet show that a soil thickness h_2 of about 1.35 m had collapsed. Consequently, a surface arch h_1 of fifteen or so centimetres was maintained on the surface (fig. 12).

Table 2: Results of SCET3 experiment

SCET3 Experiment	End of cavity emptying	Traffic acceptance test
Surface deflection in the middle (w)	0 m	0.25 m
Settlement measured by upper inclinometer	0.06 m	0.16 m
Settlement measured by lower inclinometer	> 0.15 m	> 0.15 m
Sheet deflection (f)	0.46 m	0.48 m
Sheet strain (cable-type sensors)	3.2 to 3.7%	2.8 to 4.7%
Sheet strain (strain gauges)	3.7 to 4.8%	3.8 to 5.3%

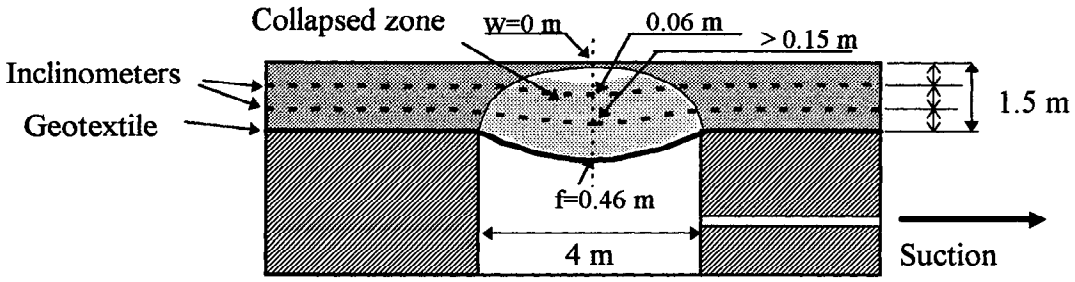

Figure 12. Geometry of the fill after emptying the cavity

* Traffic acceptance stage

Traffic acceptance tests were performed. When the 14-tonne lorry passed over the cavity for the first time (lorry axis aligned with cavity axis), a fairly significant surface collapse occurred (Figure 13). The measurements obtained (table 2 and fig. 14) revealed a maximum settlement w of 0.25 m under the left-hand pair of lorry wheels compared to only 0.05 m under the right-hand pair. Very slight increases in measured values (deflection and strain) were detected at sheet level. As the lorry passed over the cavity it caused the highly unstable surface arch to fail, a perfectly foreseeable result. The overload on the geosynthetic acting as a membrane therefore corresponds to the total thickness of the fill material (i.e., h_2= 1.5 m).

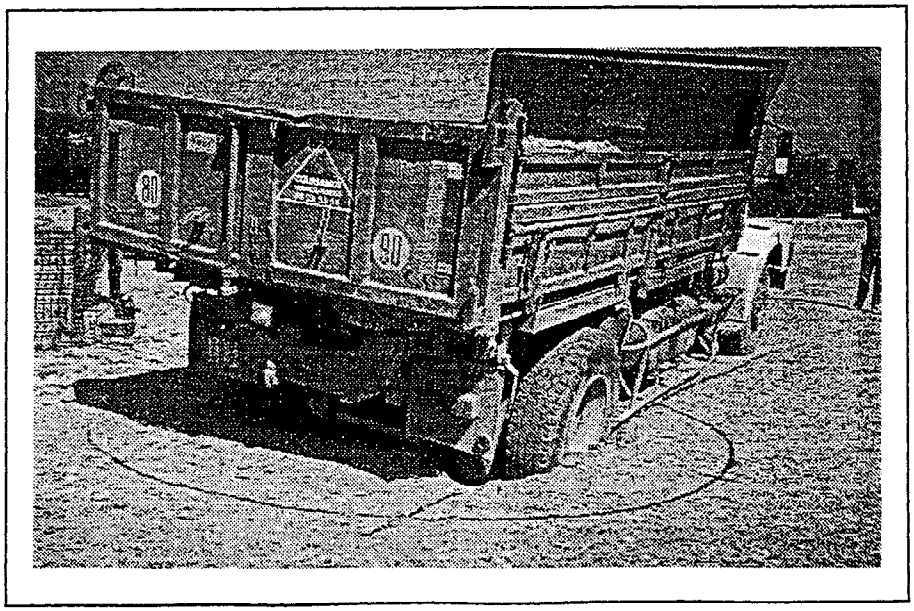

Figure 13. Subsidence of the fill surface

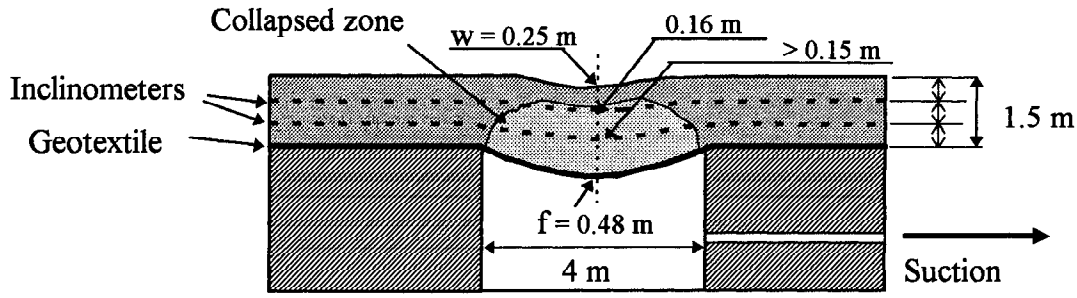

Figure 14. Geometry of the fill after collapse

The rate of accommodation of tensile stress by the sheet (T/T_f) with respect to the failure stress is estimated to be 43% taking into account the sheet strain values (maximum strain of 5.3%). Consequently, sheet failure is highly improbable and the high level of surface subsidence is the only factor impeding continuation of traffic flow. Therefore it was decided to surface fill in the sinkhole area to allow the lorry traffic to continue. Twelve lorry passages in succession were performed with the only result being additional surface rutting of 0.10 to 0.15 m. This rutting is due mainly to settlement of the uncompacted material added to fill in the sinkhole, and not to any increase in the geotextile deflection, as shown by the measurements. In addition, static tests were performed (lorry immobilised in the cavity axis). These had virtually no effect on any of the measurements taken.

Comparison of SCET2 and SCET3 cases clearly illustrates the influence of the geosynthetic material on the behaviour of the structure. For example, by comparison with the SCET2 experiment, where a complete sinkhole occurred on cavity emptying, the partial sinkholes forming for the SCET3 cavity (sinkhole height h_2 of 1.3 m) can be explained by the small strain values of the geosynthetic sheet of double stiffness. A highly unstable arch remained which, quite logically, collapsed as soon as the traffic acceptance tests started. It was also noted that it is possible to extend the operating life of the fill structure on a cavity by accepting to undertake surface repairs, with the geosynthetic acting as a membrane to accommodate at least partially the weight of the fill material and the live load.

RESULTS OF RAILWAY LINE EXPERIMENTS

Generally speaking, the results of the railway line tests are fairly similar to those of the road tests. The presence of a wearing course (improved subgrade, ballast, concrete sleepers and rails) nonetheless contributed to increasing the stiffness of the upper part of the fill and limiting surface deflections. Only the main mechanisms and the specific features of the results obtained will be described here.

Results of the SNCF1 and SNCF4 experiments

The reinforcement mechanisms observed in the 2 m diameter cavity cases are relatively similar to those obtained during the SCET1 experiment. Comparatively, the properties of the reinforcing elements used are as follows: J = 455 kN/m for the SNCF1 experiment and J = 1818 kN/m for the SCET1 and SNCF4 experiments.

The results obtained during the two experiments show that a stable arch forms in the fill material as the cavity is emptied. The sinkhole thicknesses h_2 were estimated to be 0.50 m and 0.91 m respectively for the SNCF1 and SNCF4 experiments (the lower value of h_2 for the SNCF1 case reinforced with a geotextile which had a lower value of modulus J was unexpected). However, no surface settlement w was detected during the cavity emptying stage nor during the traffic acceptance tests (repeated passage of a traction unit and traffic simulator). The displacements obtained in the geotextile sheets are consistent with the stiffness values J of the geotextiles used and with the sinkhole thickness values (respectively f = 0.26 m and 0.20 m for the SNCF1 and SNCF4 experiments). Given the high stiffness of the rolling course (rails + sleepers) which plays a force distribution role, the traffic acceptance tests have very little influence on the change in fill structure.

For comparison purposes, table 3 presents the very similar results obtained during the SCET1 and SNCF4 experiments performed under similar conditions.

Table 3: Comparison of SCET1 and SNCF4 experimental results

	Sinkhole thickness (h_2)	Geotextile deflection (f)	Surface settlement (w)
Road experiment: SCET1	1.07 m	0.22 m	0
Railway experiment: SNCF4	0.91 m	0.20 m	0

Results of SNCF2 experiment

The SNCF2 experiment involved a 4 m diameter cavity reinforced with a geotextile sheet of stiffness J = 1818 kN/m. The results obtained on emptying the cavity show that an arch forms in the fill material (sinkhole of approximate height h_2=0.91 m). No surface displacement w was detected. The geosynthetic sheet displacements exceeded the maximum measuring capacity of the sensors used (> 0.51 m). Given the bending stiffness of the rolling system (rails + sleepers), traffic acceptance tests could be completed with absolute confidence. The traffic simulator was passed over the cavity several times during which the the sinkhole rose right up to the surface. Very few differences in geotextile sheet measurements were recorded.

The results obtained on the SNCF2 experiment are worth comparing with those of the SCET2 experiment, similar from the cavity dimension and reinforcement stiffness standpoints. Comparatively, the better behaviour of the fill material in the SNCF2 experiment (which failed

during the traffic acceptance tests rather than immediately after emptying the cavity) can be explained by the presence of a stiff rolling system (ballast, rail and sleeper). However, this system did not prevent the sinkhole from forming during the traffic acceptance tests.

Results of the SNCF3 experiment

The results obtained during the SNCF3 experiment (4 m diameter cavity reinforced by two geotextiles with an overall stiffness of 3600 kN/m) should be compared with those obtained in the SCET3 experiment: two sheets of 1818 kN/m stiffness placed 50 cm apart were used in the SNCF3 experiment, while only a single sheet of 3600 kN/m stiffness was used in the SCET3 experiment.

When the SNCF3 cavity was emptied, a sinkhole of total height h_2=1.5 m was observed. The displacements of the geosynthetic sheet exceed the maximum measuring capacity of the sensors used (f > 0.51 m) whereas the surface displacement values w are of the order of 0.10 m.

Compared to the SCET3 test (h_2=1.35 m after emptying), the SNCF3 case is of interest because, for an equivalent geotextile stiffness value, it is reinforced by two geotextile sheets placed 0.5 m apart, and not by a single sheet. In this case, system operation is found to be very different thus showing the better performance of the double stiffness geotextile, despite the presence of the rolling system. Moreover, compared to the SNCF2 test (reinforced by a single sheet of stiffness J=1818 kN/m, h_2=0.91 m), here again it is found that the dual sheet system does not give such a good performance as the single sheet reinforcement. The presence of a second geotextile sheet in the body of the fill material prevents the arch from forming properly. Schematically, this can be explained by the fact that the upper geotextile sheet creates a discontinuity with the result that the behaviour becomes virtually equivalent to that of a an earfill of 1 m height.

CONCLUSIONS

The full-scale experiments carried out involved the use of considerable facilities and equipment, and showed that a solution with geosynthetic reinforcement would reduce very considerably the risks of serious accidents that might occur in the event of localised sinkholes under railway tracks. The technical solution proposed (for a 1.5 m thick earthfill embankment) would seem to be particularly well suited to small-diameter cavities (2 m) for which no significant surface displacement was recorded. For cavities of greater size (4 m), the proposed solution has proved to be of interest in as much that it provides a means of avoiding sudden, large-scale sinkholes and would also allow road and rail traffic to continue at an acceptable level subject to minor surface repairs while waiting for the proper repair works to be carried out. It is also worth noting that no case of geosynthetic tearing was observed, regardless of the experimental conditions, thus proving the merits of using such materials. This experiment, continued to failure, enabled the research group to acquire valuable experience that will be used to establish a structural design method. This will be the subject of a future publication.

The results also showed that the phenomena of sinkhole and arch formation were closely liked to the ratio between the cavity diameter and height of the fill. Other parameters are likely to play a major role in these mechanisms: characteristics of the fill material, geotextile stiffness (comparison between SCET2 and SCET3 experiments), or the presence of a sheet in the body of the fill (additional reinforcement in the case of the SCNF3 experiment). These mechanisms remain complex. Moreover, the use of an earthfill embankment with wide particle size range, bringing into play grain size effects, opens up a wide range of research possibilities.

ACKNOWLEDGEMENTS

The authors would like to thank SNCF, SCETAUROUTE and BIDIM Geosynthetics and the *Réseau des Laboratoires des Ponts et Chaussés* for their financial and technical assistance on the RAFAEL project.

REFERENCES

Espinoza, R.D., (1994), "Soil-Geotextile Interaction : Evaluation of Membrane Support", Geotextiles and geomembranes, vol.13, n°5.

Giraud, H., (1997), "Renforcement des zones d'effondrement localisé - Modélisations physique et numérique", Thèse de doctorat de l'Université Joseph Fourier de Grenoble (7 octobre 1997), pp. 79-100.

Giroud, J.P., Bonaparte, R., Beech, J.F., and Gross, B.A., (1990), "Design of soil layer-Geosynthetic systems overlying voids", Geotextiles and Geomembranes, Vol. 9, n° 1, pp. 11-50.

Giroud, J.P., (1995), "Determination of geosynthetic strain due to deflection", Geosynthetics International, Vol. 2, n° 3, pp. 635-641.

Gourc, J.P., Matichard, Y., Perrier, H., and Delmas, P., (1982), "Bearing capacity of a sand-Soft subgrade system with geotextile", Proceeding of Second Internationnal Conference on Geotextiles, Las Vegas, Aug. 1982, pp.411-416.

Villard, P., and Giraud, H., (1998), "Three-Dimensional Modeling of the Behavior of geotextile sheets as membranes", Textile Research Journal, October 1998.

EFFECTIVENESS OF GEOSYNTHETICS FOR ROADWAY CONSTRUCTION IN COLD REGIONS: RESULTS OF A MULTI-USE TEST SECTION

SCOTT A. HAYDEN, C.G.
MAINE DEPARTMENT OF TRANSPORTATION
BANGOR, MAINE

DANA N. HUMPHREY, PH.D., P.E.
UNIVERSITY OF MAINE
ORONO, MAINE

BARRY R. CHRISTOPHER, PH.D., P.E.
CONSULTANT
ROSWELL, GEORGIA

KAREN S. HENRY, PH.D.,
COLD REGIONS RESEARCH AND ENGINEERING LABORATORY
HANOVER, NEW HAMPSHIRE

CHRISTINE FETTEN
UNIVERSITY OF MAINE
ORONO, MAINE

ABSTRACT

The Maine Department of Transportation has reconstructed a 3.0 km portion of U.S. Route 1A within the towns of Frankfort and Winterport, Maine. This roadway is plagued with poor subgrade soils (A-6) and has been historically known for its poor pavement performance. The reconstruction project is providing an excellent opportunity to evaluate the effectiveness of alternative pavement sections incorporating varying geosynthetics in differing applications under northern climatic conditions. Multiple test sections encompassing the entire length of the project have been constructed using different combinations of geosynthetics including: single and multiple layers of geogrids as reinforcements with and without separation layers; high strength woven geotextile as reinforcement; woven and nonwoven geotextiles as separation/stabilization layers; and, geocomposites to provide horizontal drainage and act as a capillary barrier. A control section with no geosynthetics was also constructed. Each test section is instrumented. Along with an overview of the project, this interim paper presents the reinforcement and drainage data collected during installation and after the first year of monitoring.

INTRODUCTION

The objective of this project is to evaluate the performance of several pavement sections incorporating geosynthetics in differing applications under northern climatic conditions. The project involved reconstruction of a 3.0 km portion of U.S. Route 1A in Frankfort and Winterport, Maine. The existing pavement along this project had been plagued by cracking, rutting, and potholes. The highway required frequent maintenance to maintain a trafficable pavement surface. The conditions prompted the reconstruction project.

A subsurface investigation (Hayden, 1996) encountered moist clay soils (locally known as the Presumpscot Formation) along the entire length of the project. These soils are plastic and moist with water contents greater than 20%. Based on soil conditions and past roadway construction experiences, designers initially recommended that the subgrade soils be under cut by 150 mm and replaced with granular soil to create a stable working surface prior to placing the overlying subbase course. It was anticipated that a greater depth of undercut would be required in some areas. However, with the use of geosynthetics, the designers felt that undercutting would be unnecessary.

The majority of the project was constructed with 180 mm of asphalt and 640 mm subbase. The thickness of subbase in two areas was reduced to 580 mm. Pavement sections are being evaluated for: 1) the ability of geosynthetics to stabilize weak subgrade soils during construction; 2) the influence of the location of a geogrid in a relatively thick pavement section on pavement performance; 3) comparing the performance of a geogrid to a high modulus geotextile; and 4) the ability of a geosynthetic drainage net to remove water from the pavement section and to act as a capillary barrier. Except for item 1, the long-term pavement performance is the true measure of the effect of these experimental variables. Although evaluation will continue for many years, this interim paper presents the reinforcement and drainage data collected during installation and during the first year of monitoring.

PROJECT DESCRIPTION

The project is divided into five test sections (A-E) and a control section (Hayden et al., 1998). Each of the test sections are divided into 2 or 3 smaller subsections for a total of 12 subsections with varied geosynthetic applications in each of the subsections as shown in Figure 1. The geosynthetics and their physical properties are listed below on Tables 1 and 2.

Table 1. Geosynthetic Material (Hayden et al., 1998)

Application	Material Selected	Description
Reinforcement Geogrid	Tenax MS330	Multilayer polypropylene extruded geogrid
Reinforcement Geotextile	Mirafi 67809	Polypropylene woven
Separation/Stabilization Geotextile	Mirafi 180N	Polypropylene staple filament needle punched nonwoven
Geocomposite Drainage Net	Tenax Tendrain 100-2	Tri-planer geonet

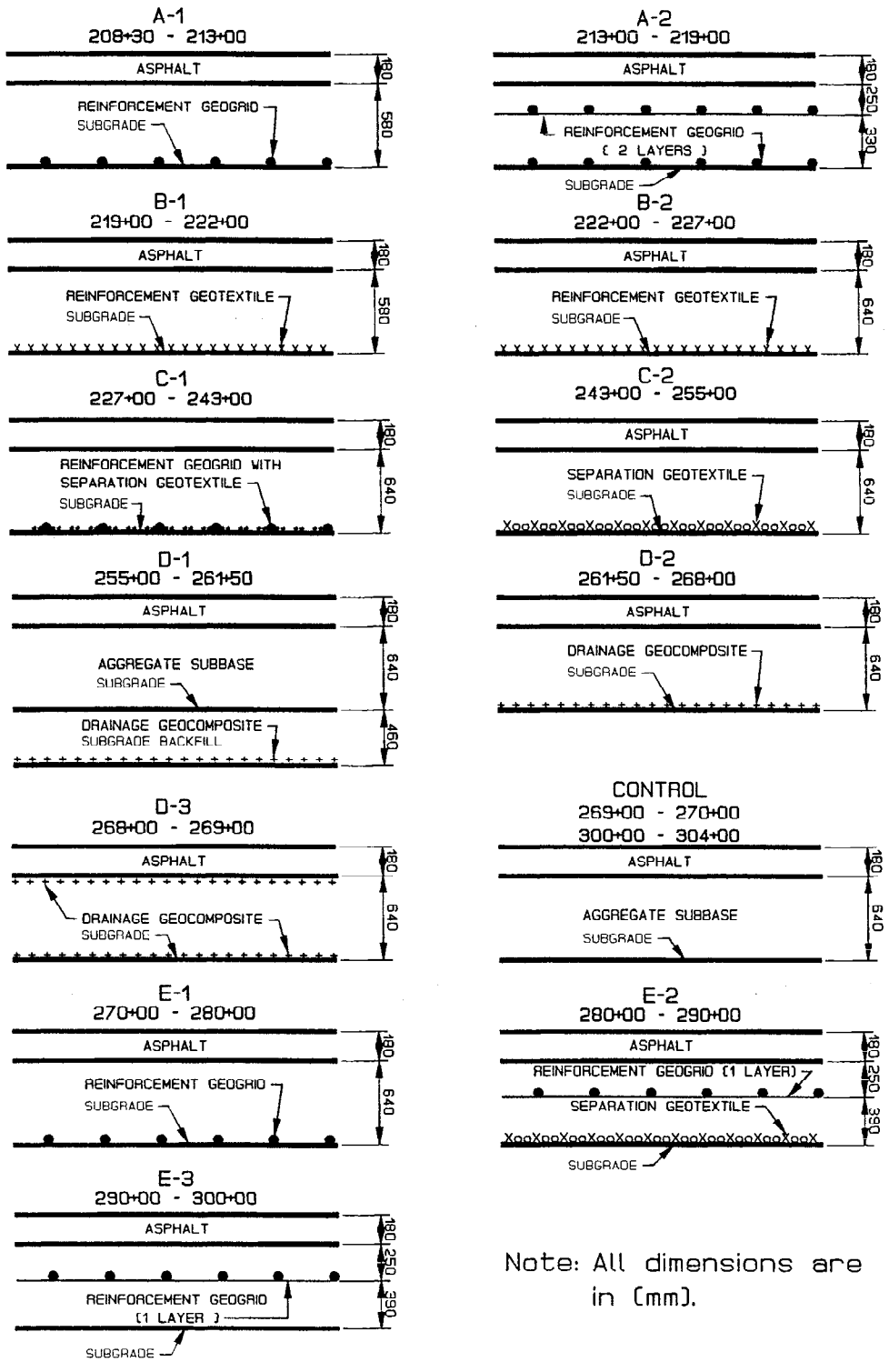

Figure 1. Test Section Schematics (Hayden et al., 1998)

Table 2. Geosynthetic Property Requirements

Application	Geosynthetic Properties	Test Method	Minimum Permissible Value
Reinforcement Geogrid	Tensile Modulus @ 5% strain (MD)	ASTM D4595	175 kN/m
	Tensile Modulus @ 5% strain (XD)	ASTM D4595	350 kN/m
	Ultimate Tensile Strength (MD & XD)	ASTM D4595	175 kN/m
	Percent Open Area		50%
Reinforcement Geotextile	Mullen Burst Strength	ASTM D3786	3000 kPa
	Puncture Strength	ASTM 4833	490 N
	Trapezoid Tear Strength	ASTM 4533	330 N
	Apparent Opening Size	CW-02215	0.30mm max.
	Permittivity	ASTM D4491	0.02/sec^{-1}
Separation/ Stabilization Geotextile	Grab Tensile/Elongation	ASTM D4632	910 N / 50%
	Mullen Burst Strength	ASTM D3786	2800 kPa
	Puncture Strength	ASTM 4833	580 N
	Trapezoid Tear Strength	ASTM D4533	350 N
	Apparent Opening Size	ASTM D4751	80 mm max.
Drainage Geonet	GEONET CORE		
	Tensile Strength MD	ASTM D4595	14 kN/m
	Compressive Behavior (% Retained thickness)	ASTM D1621	
	@ 2400 kPa (short term)		50 %
	@ 1200 kPa (5,000hrs)		60 %
	Resign Density	ASTM D1505	0.940 g/cm^3
	Resign Melt Index	ASTM D1238	1.0 g/10 min.
	Thickness	ASTM D5199	7.6 mm
	GEOTEXTILE		
	Apparent Opening Size	ASTM D4751	0.125 mm
	Permittivity	ASTM D4491	1.26 sec^{-1}
	Permeability	ASTM D4491	0.3 cm/sec
	Grab Tensile Strength	ASTM D4632	1000 N
	GEOCOMPOSITE		
	Ply Adhesion	ASTM D413	14.6 N/m

Construction began May 1997 and extended into November 1997. The construction began at the north end of the project and proceeded backwards with respect to stationing. Thus test section E was constructed first whereas test section A was constructed last. Climatic conditions during construction were unusual as Maine experienced the second driest summer since records have been taken. Even though extremely favorable climatic conditions existed soil problems were still encountered. The control section, which was built with no geosynthetics and no stabilization lift, failed during construction (June, 1997). Subsequently, the clay soils in this area were undercut 600 mm and replaced with gravel. A 820 mm pavement section was then constructed over the undercut. In addition to this soil problem in the control section, over 50 undesirable soil locations were identified during construction in test section

areas. The contractor requested that these areas be undercut. However, since these locations were in areas where geosynthetics were to be utilized, the request for undercutting was denied. Subsequently, construction equipment and traffic were able to operate along these areas in the test sections without incident.

GEOGRID INSTRUMENTATION

Tensile forces in the geogrid were measured with custom-built, full bridge load cells. This was the only viable option for the three-layer geogrid used on this project, especially since the geogrid ribs were too narrow to mount a strain gage directly on the ribs. The load cells were mounted in place of selected ribs of the geogrid. Each end of the load cells were clamped to the geogrid by two strips of aluminum bar that were bolted and epoxied to adjacent ribs as shown in Figure 2. The load cells were designed to have the same stiffness as the geogrid ribs that they replaced so that they would have minimum impact on the load-deformation behavior of the geogrid. Most of the load cells were mounted perpendicular to the centerline of the road, however a few load cells were mounted parallel to the centerline to measure any tensioning of the geogrid in the longitudinal direction. Wide strip tensile tests were conducted on geogrid samples containing a load cell to develop a relationship between the load cell reading and the force carried by the geogrid. Tests were performed on five samples with gages mounted perpendicular to the roll direction and five mounted parallel to the roll direction to ensure that a reasonable calibration was obtained.

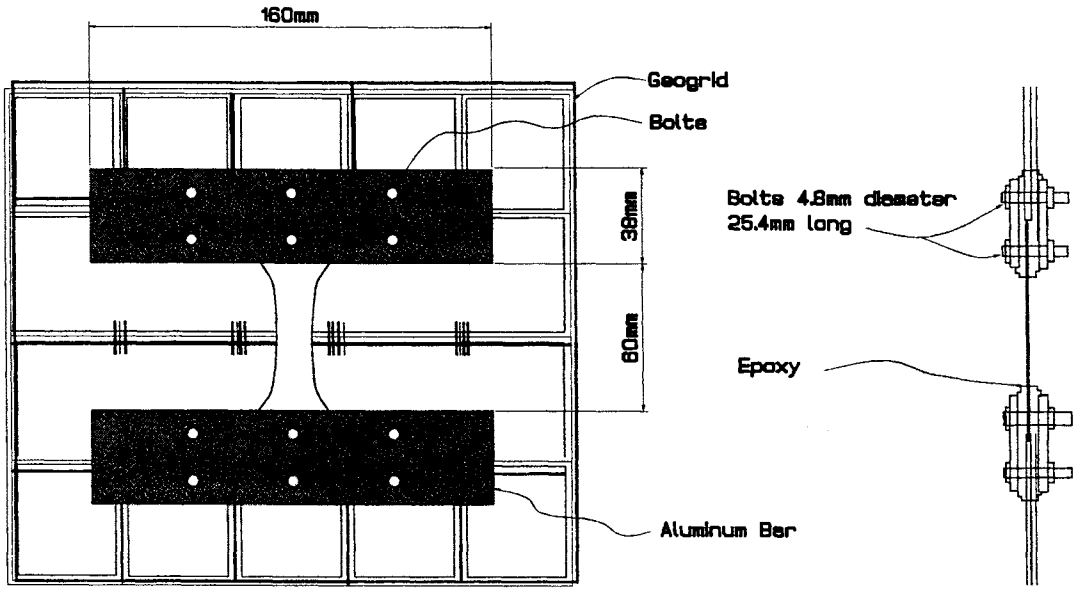

Figure 2. Schematic of Load Cell Attached to Geogrid

Load cells were installed on the geogrid at several stations in subsections A-1, A-2, and E-3. At each station, six load cells were installed perpendicular to the centerline and one was installed parallel to the centerline. In section A-2 there are two layers of geogrid and both are instrumented as described above. Unfortunately, 43% of all load cells failed during installation, most likely due to impact from the overlying coarse (up to 150 mm diameter) aggregate or severe bending of the geogrid. The latter occurred due to a wave of geogrid that developed ahead of aggregate spreading, which lifted the geogrid

up to 150 mm off the underlying soil. Additional gages failed after installation, most likely due to water intrusion or malfunction of the electrical circuits. The magnitude of gage loss is not excessive as compared to other studies. Fortunately a sufficient number of load cells to characterize the stress-strain response of the geosynthetics continue to function

The force per unit width in the geogrid measured by load cells mounted perpendicular to the centerline are shown on Figures 3 and 4. Five out of the eight load cells showed a force per unit width between about 0.75 and 1.0 kN/m. This is about 5% of the ultimate tensile strength of the geogrid. One gage (Sta.210+38, Gage LC9) measured a higher force per unit width of about 1.75 kN/m while another gage (Sta. 290+50, Gage LC10) measured a lower force per unit width of about 0.5 kN/m. Thus, the force per unit width in the geogrid was only a small faction of the material's ultimate tensile strength. Moreover, the force per unit width developed during initial placement of the overlying aggregate. There has been little change in force since installation. The effect of a relatively small tensile force per unit width in the geogrid on pavement performance must still be evaluated.

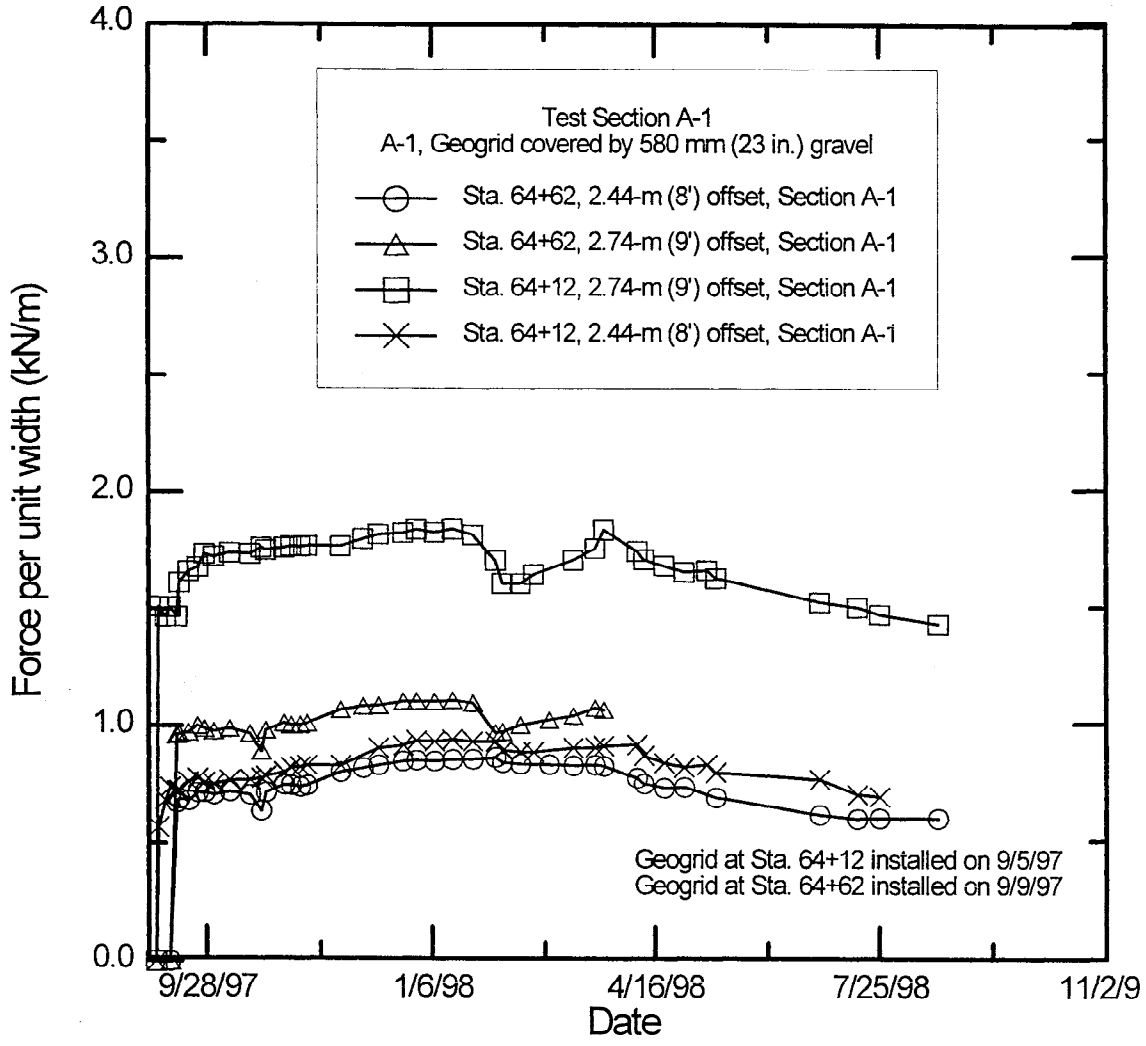

Figure 3. Geogrid Force Per Unit Width, Test Section A-1

Gage LC14 at Sta. 290+50 (Figure 4) exhibited unexpected behavior. The scatter of the data suggests that this gage is not always working properly, yet the data also suggests that the geogrid at this location was in compression. A possible explanation is that the wave of geogrid that typically advanced ahead of aggregate placement, as described above, could have been trapped beneath the aggregate at this location. This raises the possibility that the geogrid may have developed very localized areas of compression.

The gages mounted parallel to the centerline showed forces per unit width ranging from about 1.0 to 3.0 kN/m. As with the gages parallel to the centerline, the majority of the force developed during initial placement of the overlying aggregate. Complete results are given in Fetten (1998).

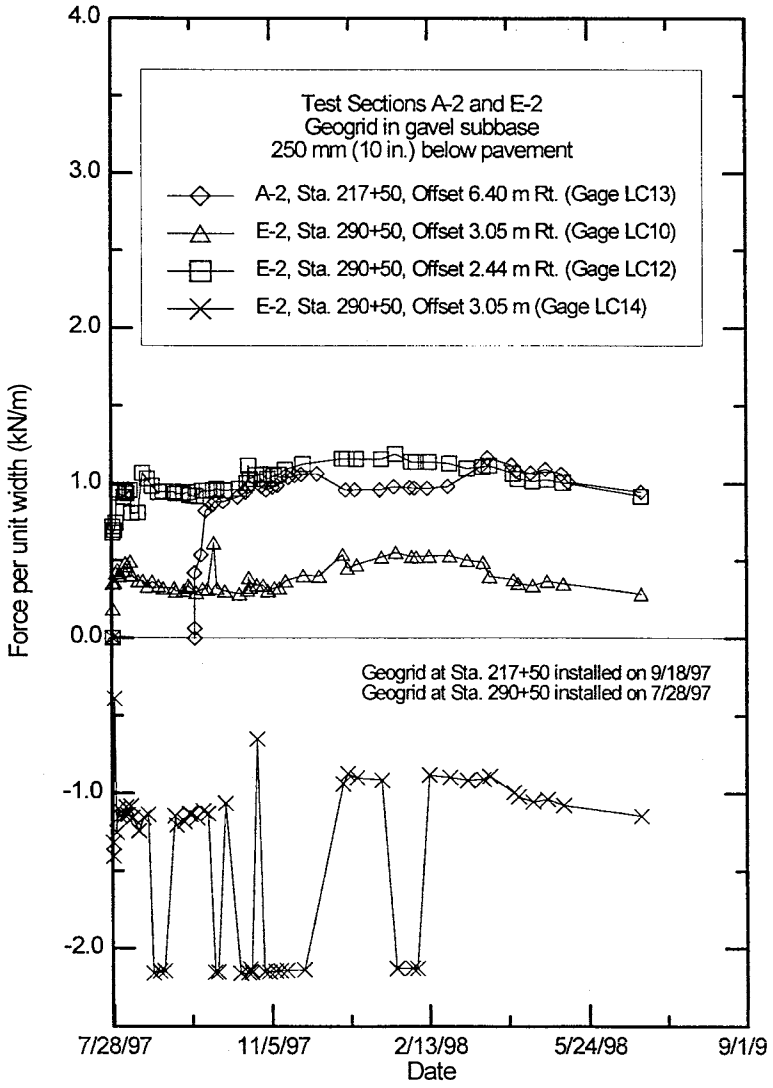

Figure 4. Geogrid Force Per Unit Width, Test Section A-2 and E-3

GEOTEXTILE INSTRUMENTATION

The reinforcement geotextile in subsections B-1 and B-2 were instrumented with strain gages to measure the strain in the geotextile. The strain gages were Texas Measurements model YL-60 with presoldered lead wires. To attach the strain gages to the geotextile, the surface was thoroughly cleaned with soapy water, and then Texas Measurements surface preparation agent B was applied. A cyanoacrylate CN adhesive was then applied to the gage and the gage was attached to the geotextile. The gage was protected by either pieces of nitrile rubber and neoprene with silicone caulking to seal the perimeter or just using silicone caulking to form a protective cover over the gage. The methods were equally effective. Gages were placed in pairs on both sides of the geotextile to eliminate the effects of bending. In each subsection, six pairs of gages were mounted perpendicular to the centerline and one pair was mounted parallel to the centerline. They were located beneath the outside wheel path of the northbound lane. In general, these gages have proved to be very reliable and only a few gages have failed to operate properly.

Wide strip tensile tests were conducted on strain gauged specimens of geotextile to develop a relationship between the strain gage reading and the force carried by the geotextile. Tests were performed on five samples with strain gages mounted perpendicular to the roll direction and five mounted parallel to the roll direction to ensure that a reasonable calibration was obtained. In general, these gages have proved to be very reliable and only a few gages have failed to operate properly.

The results for the gages mounted perpendicular to the centerline are shown in Figures 5 and 6. The results shown are the average of the reading from pairs of gages mounted on the top and bottom of the geotextile. Taking the average eliminates the effects of bending. The force per unit width in November, 1997 (about two months after completion of construction) ranged from about zero to 2 kN/m in eleven out of the twelve gages, however one gage (Figure 5) had a force per unit width of about 6 kN/m. Gages that were located less than 1 m apart had different forces indicating the force was influenced by local conditions such as the degree of wrinkling of the geotextile at the time of placement, the strength of the underlying subgrade, and the degree of tensioning that occurred due to rutting by construction vehicles. As with the geogrid, most of the force developed due to placement of the overlying aggregate. However, most gages showed a continued increase in force for the first few weeks after installation and an additional increase in force during March and April of 1998. Overall the forces are only a small fraction of the tensile strength of the geotextile (see Table 2). The effect of such a small force on long-term pavement performance must still be evaluated.

The long-term force should really be termed "apparent force" since the force in the geotextile was determined indirectly using the strain gages mounted on the geotextile. This opens the door to factors that could have changed the strain gage reading but not the force in the geotextile. It is possible that the gages were affected by temperature, however, stable readings during penetration of the freezing front in December, 1997, and January, 1998, suggest that this is not the case. The geotextile could also undergo creep, which is strain of the geotextile under constant force. This would cause an increase in strain, but the force could remain constant or even decrease. However, creep appears to be an unlikely cause since the force in the geotextile was only a small fraction of its ultimate strength and creep becomes significant only at higher stress levels (Shrestha and Bell, 1982). Thus, it appears that the geotextile did experience an increase in force during the spring melt and that the increase was permanent at some of the

gage locations although other possible causes cannot be completely discounted. Additional results are presented in Fetten (1998).

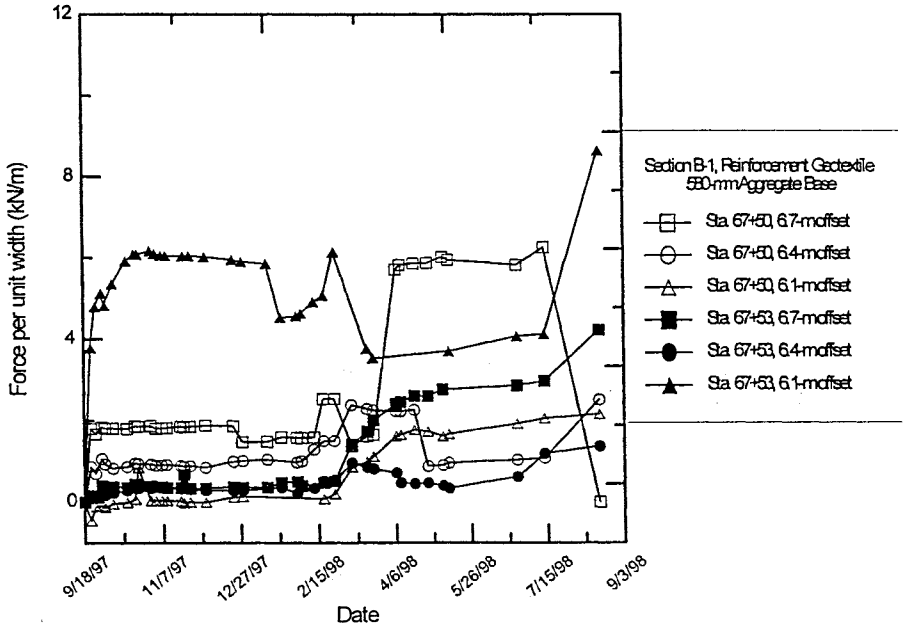

Figure 5. Force Per Unit Width in Geotextile in Test Section B-1

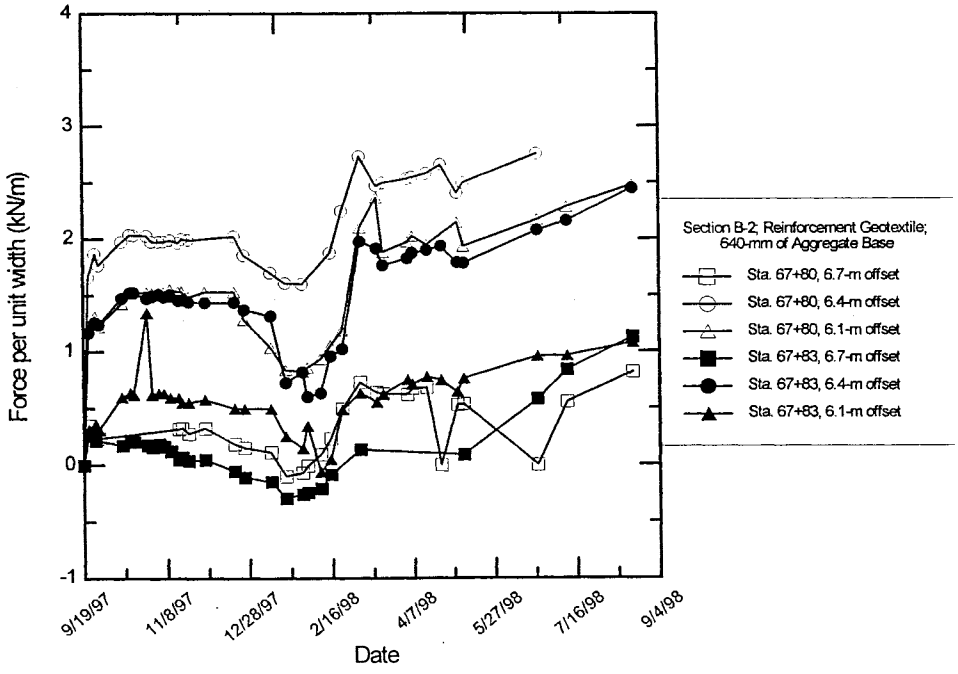

Figure 6. Force Per Unit Width in Geotextile in Test Section B-2

FALLING WEIGHT DEFLECTOMETER RESULTS

Pavement performance was measured with a falling weight deflectometer (FWD) prior to reconstruction and in April, 1998, soon after the end of the Spring thaw. Prior to reconstruction, the project had 127 to 254 mm of pavement. At the time of the April, 1998, measurements there was 146 mm of pavement. The FWD results were processed with the Darwin Pavement Design and Analysis System. The results of the back calculated structural number (SN) are shown in Figure 7. The sections labeled F-1 and F-2 are the control sections. It is seen that the highest SN in April, 1998, was obtained in the control sections. These results are not surprising considering these sections were constructed with an additional 600 mm of subbase aggregate due to poor subgrade conditions. The next highest structural number was obtained in section D-1 and was essentially the same as measured in the control section. In this section, the subgrade was undercut by 460 mm to allow placement of the drainage geocomposite. The subgrade was brought back to grade by compacted fill that was a mixture of clay, sand, and gravel. This mixture had a lower water content than the native subgrade soils. It is likely that this drier mixture was stiffer than the in-place subgrade soils. However, it is also possible that consolidation induced by drainage had a stiffening effect on the soil. The SN in the remaining sections varied between 4.9 and 6.4. The difference between sections was due, at least in part, to factors other than the geosynthetics. For example subsection A-1, which had 580 mm of subbase over one layer of geogrid, had a structural number of 5.5 while subsection E-1, which has 640 mm of subbase over one layer of geogrid, had a structural number of 6.5.

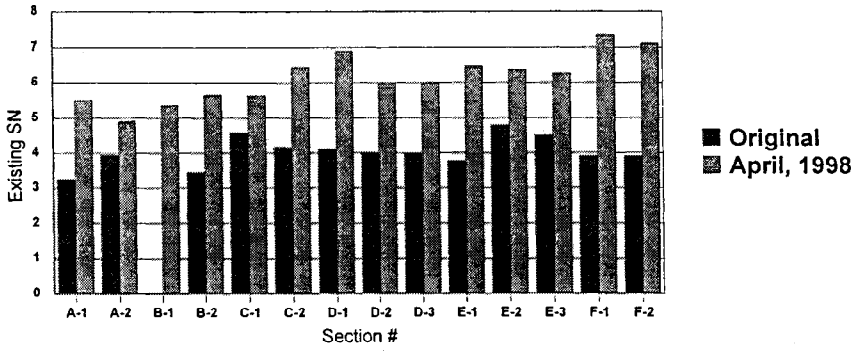

Figure 7. Original and April Structural Numbers

DRAINAGE INSTRUMENTATION

The drainage test sections consist of three individual drainage sections D-1, D-2, and D-3 as described by Hayden et al. (1998). A high compressive modulii, high flow rate, geocomposite drainage net was placed at 460 mm below subgrade, at subgrade, and directly beneath the pavement in the respective test sections. In each of the drainage test sections an internal drainage collection system was installed on both sides of the road directly beneath the shoulder break to collect water captured in the geocomposite drainage net (Figure 8). The drainage collection system was outletted at eight separate locations labeled outlet A-H. Monitoring stations were constructed at six outlet locations A-F (Table 3).

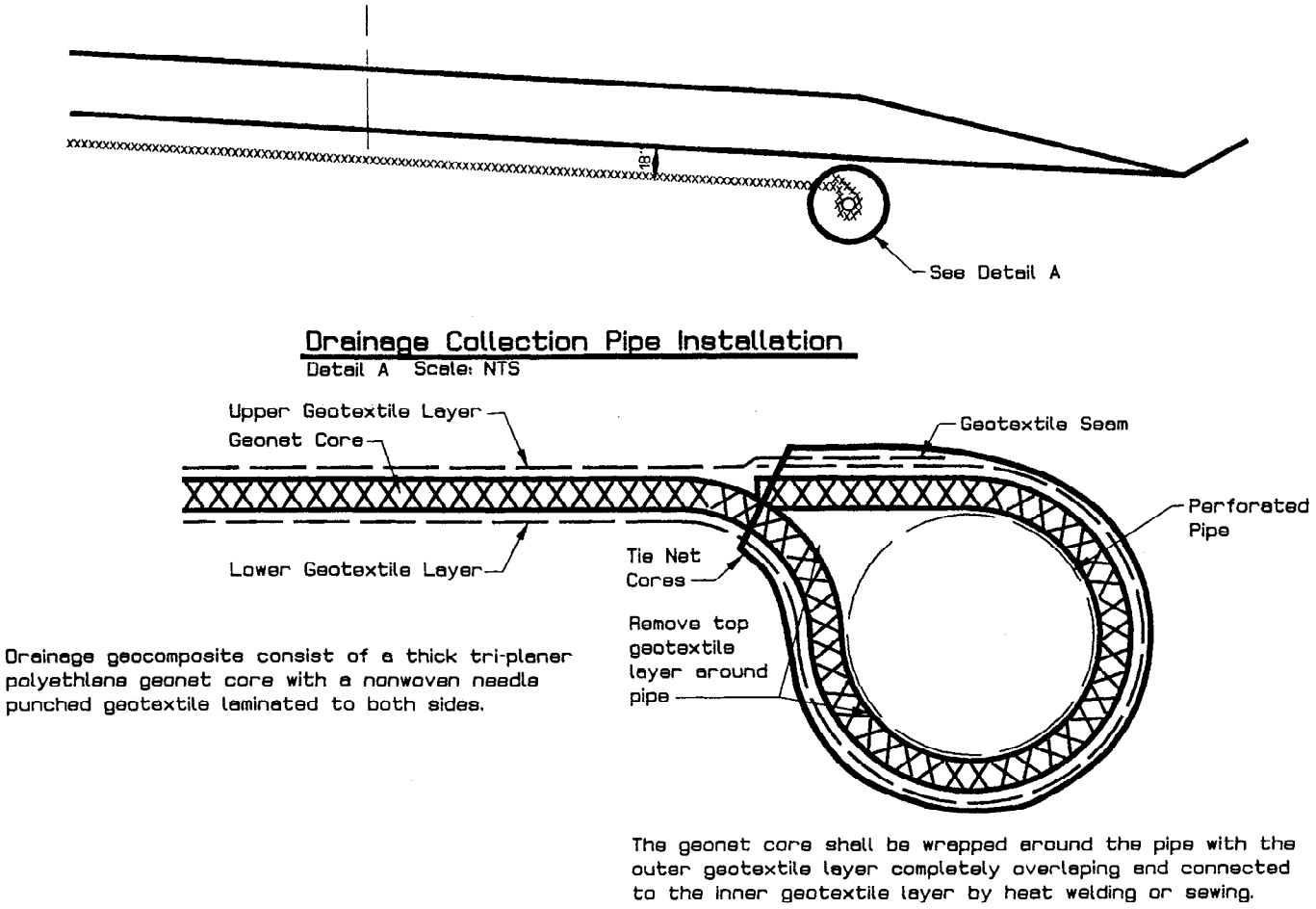

Figure 8. Drainage Collection System Schematic

At each of the monitored locations the outlet pipe is connected to a tilt bucket (Figure 9) housed in a protective wooden structure. A micro switch is positioned on the tilt buckets and is actuated every other time the tilt bucket dumps. The micro switch is, in turn, connected to a traffic counter which records the number of dump cycles of each tilt bucket. Data is collected continually 24 hours a day. The traffic counter software then provides daily or monthly reports, which presents the total number of dump cycles per hour, per day. This information is then downloaded over phone lines from the traffic counter on project to the Maine Department of Transportation offices.

Data collection began in March 1998 for outlets B through F. Data collection at outlet A did not begin until late June. Discharge volumes (L/m) from monitored outlets per length drained section are listed in Table 4. The six-month volume (L/m) totals for each outlet indicates that outlet C recorded the highest volume per length drained section and outlet F recorded the least flow. The greatest monthly flow recorded at each of the monitored locations was encountered during the month of March. Discharge volumes per length drained were considerably less for the months of April through August. The volume (L/m) of discharge in the month of March accounted for 63% of the total six-month discharge volume.

Discharge during the months of April through August accounted for less than 10% of the total for each of the months monitored except for the month of July which accounted for 20% of the total.

Table 3. Monitored Outlet Locations and Details

Monitored Outlet Locations	Test Section Designation	Drainage Pipe Location	Geocomposite Location
Outlet A 261+40 right	D-1	255+00 - 260+00 right 152 m drained section	Geocomposite is located (460 mm) below subgrade and is placed along the low side of a super elevated turn.
Outlet B 261+40 left	D-1	260+00 - 261+50 left 46 m drained section	Geocomposite located (460 mm) below subgrade in a standard section.
Outlet C 261+40 right	D-1	260+00 - 261+50 right 46 m drained section	Geocomposite located (460 mm) below subgrade in a standard section.
Outlet D 268+00 left	D-2	261+50 - 268+00 left 200 m drained section	Geocomposite is located at subgrade along the low side of a super elevated turn in areas.
Outlet E 268+00 left	D-3	268+00 - 269+00 30 m drained section	Geocomposite is located at subgrade in a standard section.
Outlet F 268+00 left	D-3	268+00 - 269+00 30 m drained section	Geocomposite is located directly beneath the pavement in a standard section.

Table 4. Discharge Volumes from Monitored Outlets Per Length of Drained Section (L/m)

	Outlet A D-1	**Outlet B** D-1	**Outlet C** D-1	**Outlet D** D-2	**Outlet E** D-3	**Outlet F** D-3	**Monthly Totals**
March	-	77	1094	118	0	0	1289 (63%)
April	-	0	0	91	0	0	91 (4%)
May	-	0	0	94	0	0	94 (5%)
June	0	4	63	73	6	0	146 (7%)
July	2	0	339	56	0	0	397 (20%)
August	0	0	7	0	0	0	7 (1%)
Totals	2	81	1503	432	6	0	2024 (100%)

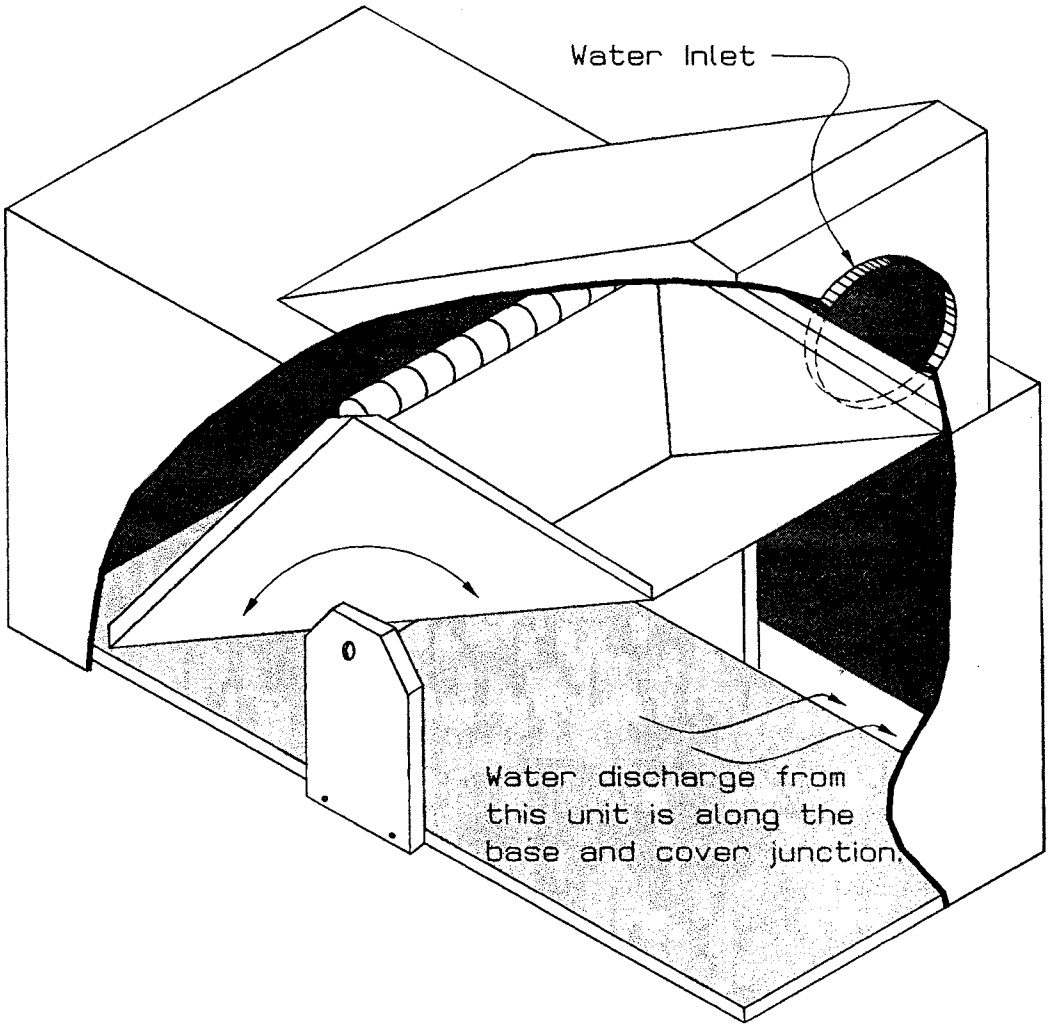

Figure 9. Tilt Bucket Schematic (Revised from Wisconsin DOT, 1996)

Heavy flow activity during the month of March corresponds strongly with the thawing of ice lenses as verified by thermocouple readings and frost heave elevation surveys. Outlet C recorded the greatest discharge of the six monitored outlets. Water discharged (L/m) from Outlet C is collected from a 45 m run of drainage geocomposite located 460 mm below subgrade. Outlet D recorded the second greatest discharge (L/m) during March. This outlet drains a 200 m length of road with the drainage geocomposite placed directly at subgrade.

Discharge during the months of April through August corresponds strongly with precipitation events and water table levels. Over 400 mm of rain fell on the project area during these 5 months. Tilt bucket activity would begin shortly after each rain event and ended the same day or the next day after the rain ceased. As the water table lowered through summer, the time between rainfall and tilt bucket activity increased. Outlet C and Outlet D recorded the greatest discharge (L/m) during April through August with 55% and 42 % respectively. Water discharged from Outlet C is collected from a 45 m run of

drainage geocomposite located 460 mm below subgrade. Water discharged from Outlet D is collected from a 200 m run of drainage geocomposite located directly at subgrade.

Outlets E and F recorded very little water discharge. Outlet E only recorded a six-month discharge volume of 6 liters per meter of section drained. Outlet F recorded even less with only a trace of water. Outlets E and F drain a 30 m length section constructed on a fill area. Outlet E collects water from the geocomposite placed at subgrade whereas Outlet F collects water from the geocomposite placed directly beneath the asphalt pavement.

A graph of the total monthly discharge volumes per length of drained section and rainfall is shown below (Figure 10.)

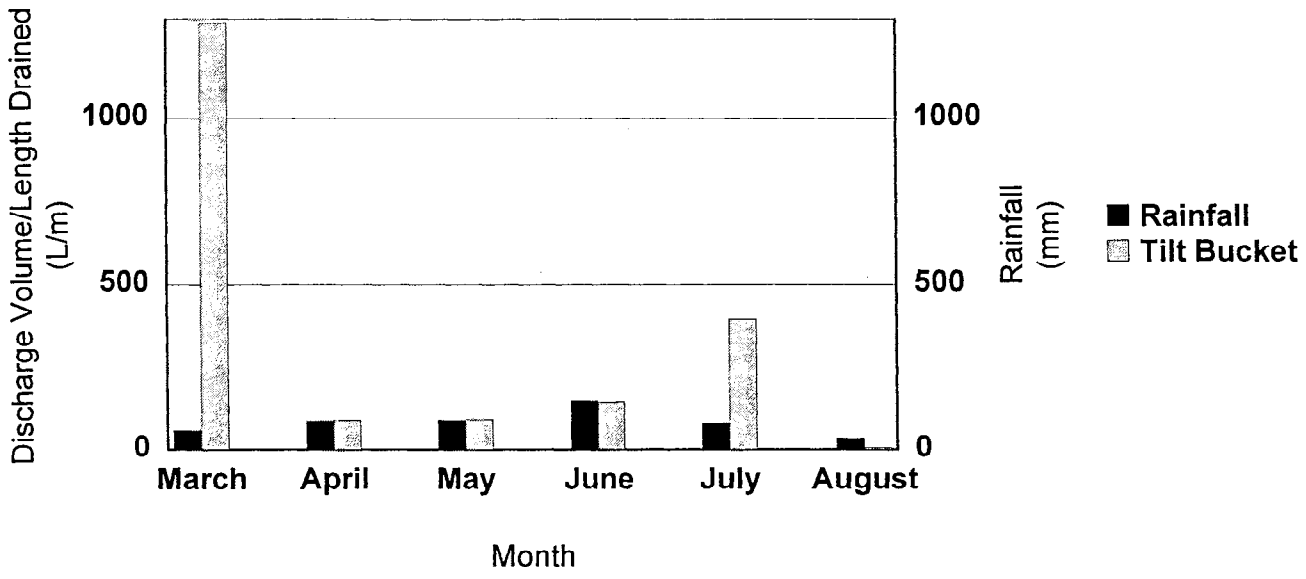

Figure 10. Total Monthly Discharge Volumes Per Length Drained Section

Based upon tilt bucket limitations, the volumes recorded at each of the six monitored outlet locations could be considerably lower than the actual volumes reported. The tilt buckets were not able to dump when subjected to flow rates greater than approximately 7 L/min. Flow rates as high of 57 L/min were measured manually during site visits. In addition, tilt buckets experienced difficulties in accurately measuring flow rates less than 0.25 L/min due to surface tension. Site visits revealed that water being discharged at these low flow rates failed to drop vertically into the collection bin but rather clung to the sides and traveled down the inner walls and exited the tilt bucket without ever entering the collection bin.

FROST HEAVE MITIGATION

A capillary barrier can potentially reduce frost heave by preventing (or greatly reducing) water flow between the water table and the freezing front in freezing soils when it is placed above the water table and below the depth of freezing. Test section D-1 was constructed to study the influence of a geocomposite, functioning as a capillary barrier, with respect to frost heave mitigation. Subgrade was undercut 460 mm and the geocomposite was placed. The undercut material consisted of a mixture of native clay soils and old base course material. The geocomposite was then covered with the material originating from the undercut (Hayden et al, 1998). Thermocouples were installed within the drainage sections to monitor frost penetration. The instrumentation was also complemented with a periodic survey of frost heave conducted between the months of December and April. In addition, samples of the soil underlying and overlying the geocomposite were collected during construction by Dr. Karen Henry and Ms. Rosa Affleck of the U.S. Army Cold Regions Research and Engineering Laboratory (CRREL) as part of a CRREL laboratory study (Henry and Affleck, 1998) to determine the frost susceptibility of the sampled soils and the influence of a geocomposite, functioning as a capillary barrier, on frost heave of that soil.

The analysis of the 1997-1998 fall, winter, and spring field data had not been fully analyzed at the time of this writing thus no conclusions based upon site instrumentation can be given. However, research related to this project (Henry, in press) and CRREL laboratory results (Henry and Affleck, 1998) using samples collected from the project and the same geocomposite product indicates that the geocomposite eliminated frost heave in the soil samples compacted to simulate field conditions and frozen at typical freezing conditions.

CONCLUSIONS

Data obtained from the sections with geogrid reinforcement indicated that the forces in the geogrid were only a small fraction of the material's ultimate tensile strength and these forces developed primarily during the initial placement of the overlying aggregate. The location of the geogrid in the pavement section had an insignificant effect on the resulting force. Likewise, data from the sections with geotextile reinforcement show that the forces were small compared to the material's ultimate strength and that most of the forces developed during initial placement of the overlying aggregate. The measured forces in the geotextile varied over small distances suggesting that the forces were influenced by local conditions such as initial wrinkling of the geotextile, strength of the subgrade, and the degree of tensioning that occurred due to rutting by construction vehicles. The falling weight deflectometer (FWD) results were inconclusive in evaluating the effect of the geosynthetics. The effect on pavement performance of using geogrids and geotextiles with relatively small tensile force in thick pavement sections must still be evaluated.

Data from drainage monitoring outlets indicate that a geocomposite drainage net placed at subgrade or below subgrade is successful in rapidly removing water from beneath the roadway. The placement of such a drainage layer is especially useful for removing the most damaging waters present during the spring thaw. Spring discharge rates of 81700 L/day were encountered. A measured improvement in stiffness for the section in which the drain was placed in the subgrade may have been the result of this drainage as well as greater compaction of the soil placed over the geocomposite. Drainage during

summer months was best realized where the drainage net is placed within cut sections in areas where the water table is relatively shallow.

In terms of performance, the use of geosynthetics facilitated construction in areas where the subgrade was weak with out the necessity of additional undercuts. Construction equipment and traffic was able to operate on sensitive clay type soils during construction without incident even though a stabilization lift was eliminated from the design. Where geosynthetics were not used (i.e., in the control sections), an additional 600 mm of stabilization aggregate was required. Currently all sections appear to be providing adequate performance, however, only with long term monitoring will we be able to determine which of the schemes are the most effective.

ACKNOWLEDGMENTS

This project involved the expertise from many other people besides the authors. In great appreciation we would like to thank and recognize Ms. Rosa Affleck of CRREL, Dr. Aigen Zhao of Tenax Corporation, Mr. Phil Dunn of MDOT, Mr. Steve Hall of MDOT, Mr. Steve Colson of MDOT, and Mr. Terry White of MDOT for their technical support and financial resources.

REFERENCES

Fetten, C.P. (1998), "Instrumentation and Performance of Geosynthetics Beneath Flexible Pavements in Winterport and Frankfort, Maine," M.S. Thesis, Dept. of Civil and Environmental Engineering, University of Maine, Orono, ME., 138 p.

Hayden, S.A., Christopher, B.R., Humphrey, D.N., Fetten, C.P., and Dunn, P.A., Jr. (1998) "Instrumentation of Reinforcement, Separation and Drainage Geosynthetic Test Sections used in the reconstruction of a Highway in Maine" Proc., 9th International Conference on Cold Regions Engineering, Duluth, MN., September 1998, pp. 420-433.

Hayden, S.A. (1996) "A Subsurface Investiagation for a 1.9 Mile Portion of Route 1A in the Towns of Frankfort and Winterport," unpublished report, State of Maine Department of Transportation, Report No. 96-11, Bangor, ME., 40 p.

Henry, K.S. (in press) "The use of geosynthetics to mitigate frost heave in soils," Ph. D. Dissertation, Civil Engineering Department, University of Washington, Seattle, WA.,333 p.

Henry, K.S., and Afflect, R. (1998) Freezing Tests on Lean Clay with Tenax Tri-Planar Geocomposite as Capillary Barrier, Contract Report to Tenax, Inc., from U.S. Army Cold Regions Research and Engineering Laboratory, Hanover, NH., 13 p.

Shrestha, S.C., and Bell, J.R. (1982), "Creep Behavior of Geotextiles Under Sustained Loads," Proceedings of the Second International Conference on Geotextiles, Las Vegas, NV, Vol. III, p. 769-774 and discussion Vol. IV, pp. 120-122.

IN-GROUND TEST FOR GEOSYNTHETIC REINFORCED FLEXIBLE PAVED ROADS

ANDREA CANCELLI,
UNIVERSITY OF MILAN, ITALY
FILIPPO MONTANELLI,
TENAX SPA, ITALY

ABSTRACT

The traffic of vehicles on the surface of roads yield deformations in the pavement structure that are a function of both the traveling loads and the mechanical characteristics of the pavement itself. These deformations are either reversible (elastic deflections) or permanent (plastic ruts). With the cyclic application of traffic load, these deformations degrade the pavements and irregularities, ruts, longitudinal asphalt cracks, alligator cracks appear on the surface.

The structural strength of flexible pavement is related to its constitutive elements: the asphalt layer, the granular base, the in-situ subgrade soil and the geosynthetic reinforcement. Geosynthetics are, nowadays, commonly used in flexible road base reinforcement by inserting them typically at the interface between the aggregate base course and the subgrade.

The aim of this in-ground test is to quantify and evaluate the structural contribution of geosynthetic reinforcement to pavement systems and to develop a sound design algorithm based upon actual empirical testing of geogrid reinforced road sections.

INTRODUCTION

This paper deals with the analysis of the results of a full scale pavement test conducted on several reinforced and unreinforced paved sections where the following variables were investigated: subgrade strength, gravel base thickness, geosynthetic type, number of Equivalent Axle Loads (EAL). This is a continuation of previously published papers on the ability of geosynthetics to successfully improve the pavement life and reduce the creation of ruts (Montanelli et. al., 1997 and Cancelli et al. 1996). Similar existing studies were performed on unreinforced and reinforced sections and a comprehensive discussion of the results is given by Perkins and Ismeik (1997).

The design method for flexible pavement systems is based upon either the theoretical or the empirical approaches: i.e.: limiting shear failure method, limiting deflection method, empirical regression method. The testing results presented in the paper are valuable data for the safe application of both analytical and practical design approach.

TEST DESCRIPTION

To verify the reinforcement capability of the geosynthetics for base reinforcement, a 210 m long road section 4 m wide was carefully constructed using laboratory procedures to obtain reliable and reproducible data for in-situ measurements and comparisons between reinforced and unreinforced sections. The road section is similar to an oval ring, having rectilinear sections of 36 m and 20 m of length with 90° curves of 17 m radius as shown in figure 1. The outer edges of the curves were slightly raised giving a "parabolica" effect to facilitate the vehicle turning without deceleration.

Underneath the cross sections of the rectilinear portions of the road, a 4 m wide 1.2 m deep trench was excavated and lined with an impermeable plastic membrane to maintain the fill soil moisture. The in-situ CBR values of the soil in the excavated sections were estimated at around 10%.

Subsequently the excavated trenches were filled in the lower half with saturated silty clay soil. The subgrade soil was installed in a thickness of at least 0.7 m having a CBR of about 1%, 3% and 8% as shown in figure 2. The subgrade soil has a fines content (#200 sieve) of 60% having the following Attemberg limits: L.L. = 31% and I.P. =11%.

The CBR value of the subgrade clay was controlled by varying the moisture content in the clay itself. Preliminary laboratory CBR tests were conducted to determine the theoretical appropriate water content and subsequently the CBR was verified in-situ. The CBR laboratory tests, conducted in agreement with ASTM D-1883:87, were performed without the typically required 24 hours minimum saturation time, thus the obtained and reported values of CBR shall be considered as upper boundary values. The in-situ CBR values were verified by using a standard penetration probe and the obtained results correlated to the laboratory tests.

Above the 0.70 m thick clay layer, several reinforcement layers were installed. The dimensions of the reinforcing layers were 2.2 m by 4.6 m to allow 0.2 m overlap along the road centerline and 0.3 m overlap across the road section between adjacent reinforcement layers. Up to 56 different sections were installed including reinforced and unreinforced sections (control sections), having different subgrade strengths and base thickness'. The test layout of the 56 sections is shown in figure 1.

A few sections were monitored by installing eight electrical strain gages on the geogrid

reinforcements across the section width. The scope was to monitor the level of applied stresses during the wheels load passes and during the life of the pavement section; i.e.: installation, front and rear wheel load passes, cycle number, and at-rest condition (Figure 2).

Above the geosynthetic layers, the remaining portion of the road section was filled with well graded and compacted gravel excavated from a local quarry. The thickness of the aggregate layer ranged between 0.30 m and 0.50 m depending upon cross section type. The in-situ CBR of the installed gravel layer was estimated to be equal to 30% for analytical purposes. No higher density could be reached without overstressing the unreinforced sections.

Similar geosynthetic reinforced sections were positioned closely to each other and to the control section to enhance the validity of the comparison. This technique allows for greater precision in determining absolute and relative reinforcement effects since all the properties of the soils are similar as a result of the sections being filled at the same time using the same soil type and handling procedures.

A 75 mm thick layer of asphaltic concrete was placed on all the road sections. The asphalt layer was prepared in agreement with the Italian highway specification but with higher bitumen content to enhance asphalt ductility and thus road profile measurements.

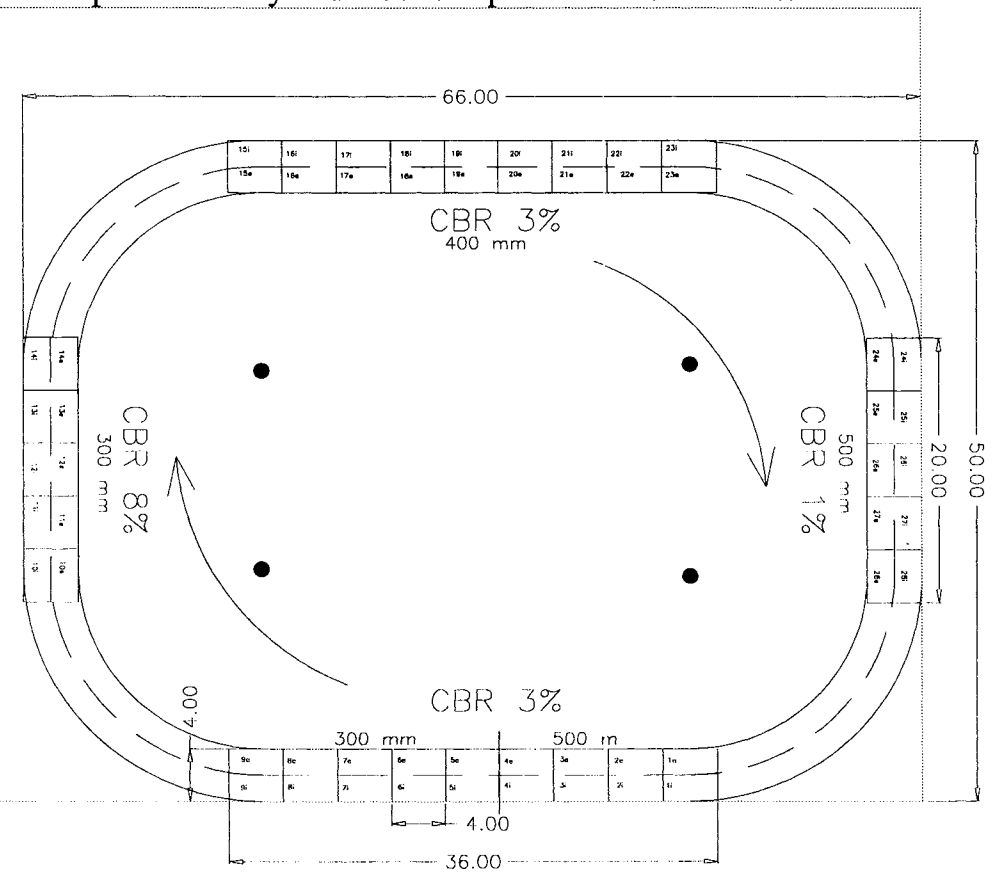

Figure 1: Plan view of the full scale in ground test road (m)

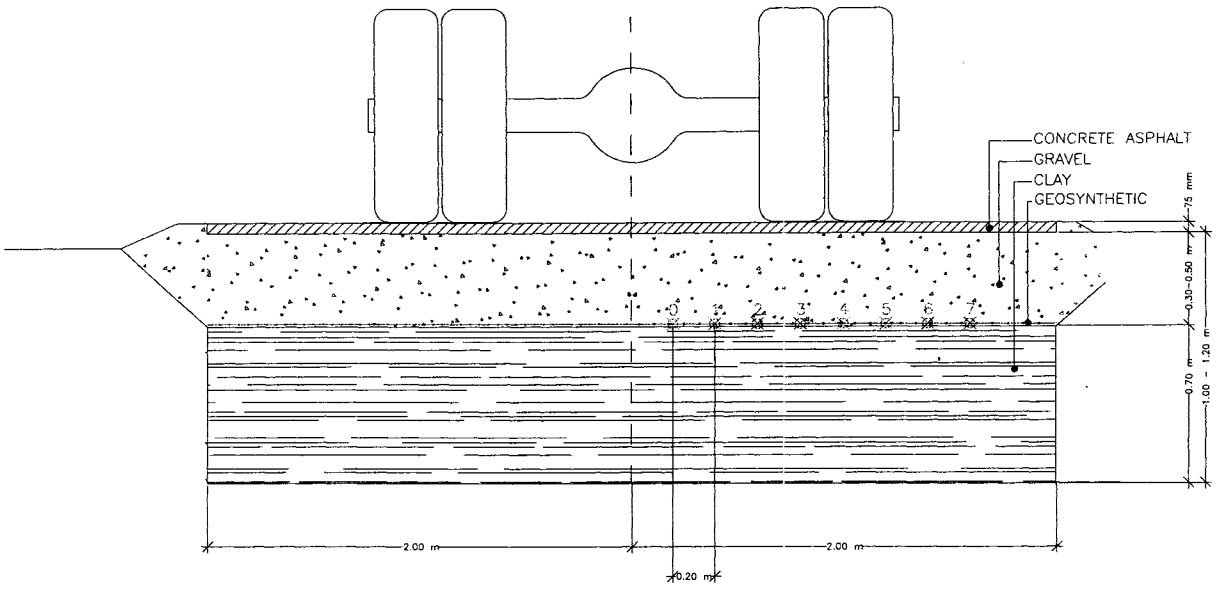

Figure 2: Cross section of the full scale in ground test road and strain gage layout

Up to 160,000 Equivalent Axle Loads were applied by a vehicle running along the length of the road in clockwise direction only. The vehicle followed a well defined path given by the centerlines painted along the asphalt layer. Thus, the wheels always traveled along the same path, so that the axle wheel loads are channalised along the testing section. At the time this report was prepared, only the data up to 80,000 EAL were fully analyzed and reported. Some of the data have not yet been fully analyzed. These data are related to the last 80,000 EAL, the strain gages response and the load plate tests conducted on the unpaved sections before starting the loading cycles These data will be reported in future publications.

The vehicle used in the tests is a standard truck having a double wheel rear axle and a single wheel front axle. The rear and the front axle are loaded with 90 kN and 45 kN respectively, thus each wheel carries an equivalent load of 22.5 kN. The truck is loaded with concrete deadweights. All the tires are inflated at a pressure of 800 kPa. The vehicle tires are 10R20 type with 16 plies radial structure and are U.S. D.O.T. approved. A schematic detail of the vehicle is given in figures 3 and 4.

The truck travels at a constant speed of 20 km/h, thus a full loop is performed in about 60 second. This speed is lower than the standard average truck speed, but high enough to be comparable. This speed has the advantage of generating higher vertical loads without the trade-off of not generating enough energy and horizontal dynamic loads as per pseudo-static speed of 10 km/h or less. Based upon published theoretical and empirical data (BS 7533:92), we can define the following criteria for the definition of the 80 kN Equivalent Axle Load for each vehicle lap:

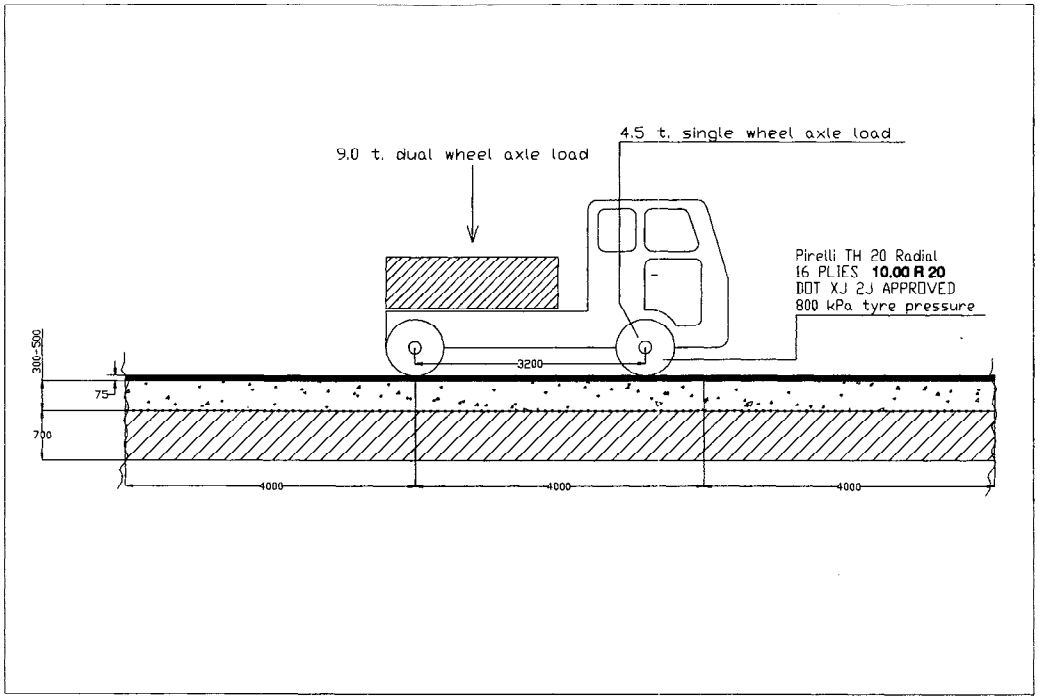

Figure 3: Side view of the truck vehicle and longitudinal cross section

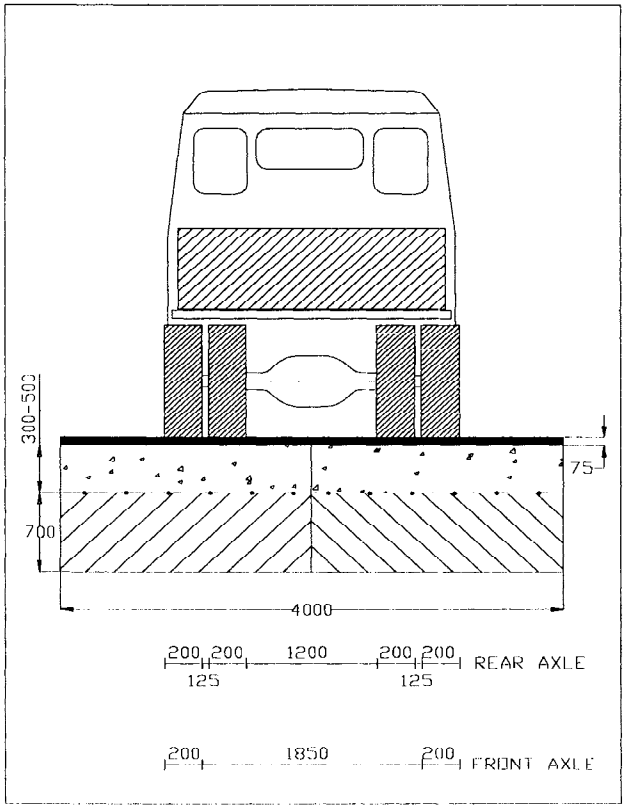

Figure 4: Rear view of the truck vehicle and cross section

- The rear double wheel axle load of 90 kN is equivalent to 1.61 EAL of 80 kN (18,000 lb.) due to the fourth power law applied to the load ratio: (90/80)4 = (factor of 1.61);
- The front single wheel axle load of 45 kN is equivalent, for road sections having a structural number SN between 2.5 and 4.0, to a double wheel axle load of 90 kN (factor of 1.61);
- Each axle passes, being channalised along a single track and not distributed across the full width of the road is equivalent to 3 passes (factor of 3) (Figure 5, 6 and 7);
- Thus, for each vehicle cycle, the EAL load factor is: (1.61 + 1.61) x 3 = 9.66. For simplicity, we will use a factor of 10 in the following discussions.

Some of the geosynthetics tested are listed in table 1 together with their reported properties. The products tested can be classified among the following categories:

a) single layer biaxially oriented polypropylene geogrids manufactured by extrusion process;
b) multi-layers biaxially oriented polypropylene geogrids manufactured by extrusion process;
c) woven polyester geogrids;
d) slit film woven fabrics;
e) composite structures; i.e.: extruded geogrid and nonwoven geotextiles, woven and nonwoven geotextiles.

Table 1: Product codes and nominal properties

Product Code	Category - N. Layers	MD x TD Tensile Strength, kN/m	MD x TD Tensile Strength @ 2% ε, kN/m	MD x TD Junction Strength, kN/m	MD x TD Aperture Size, mm
GGML2	b - 2	13.5 X 20.5	4.1 X 6.0	12.2 X 18.5	21 X 25
GGML3	b - 3	20.0 X 30.7	6.1 X 9.0	18.0 X 27.7	14 X 17
GGML5	b - 5	22.0 X 35.0	6.0 X 10.0	19.8 X 31.5	12 X 12
GGR1	a - 1	12.1 X 20.5	4.0 X 5.8	10.9 X 18.4	25 X 33
GGR2	a - 1	17.0 X 31.5	5.4 X 8.7	15.3 X 28.3	25 X 33
WGTX	d - 1	30.0 X 30.0	4.0 X 5.0	---	---

DATA COLLECTION AND ANALYSIS

The rut depths were measured as a function of the numbers of cycles, aggregate thickness, sub-grade shear strength and geosynthetic type. The data were collected to determine the ability of the reinforcements to distribute the load over a wider sub-grade surface area, to minimize differential settlement and thus to extend the pavement life.

The rut depths were measured by means of a specially designed rectilinear beam, having a 2 m span, over which an electronic micrometer having an accuracy of ±0.01 mm was installed. The beam was placed across the road section to be measured and properly positioned horizontally by

means of a waterlevel having an accuracy of ±0.02 mm/m; thus an overall accuracy of ±0.05 mm across the beam width for the overall device was reached (figure 8).

The test sections were marked with a solid yellow line along the centerline and along the measurement cross-sections placed in the middle of each section. The transversal borderlines of each section were marked with dotted yellow lines (figure 9). The measurement cross-section lines were marked with a Fisher type nail at the intersections with the centerline.

The head of the nails were used during each measurement either for shooting the elevation measurements by means of a telescopic unit and for zeroing the micrometer prior to taking the measurements. The rut measurements across the cross-sections were taken every 0.10 m starting from the nail head.

The rut depths were measured at 0, 30, 50, 100, 300, 500, 1000, 2000, 4000, 8000 cycles on most of the sections, together with the elevation quotes. In the following analysis, the maximum rut depths for each cross-section is defined as the difference of the maximum uplift and downlift values for the specific cycle of measures (figure 11). This criterion is given by the fact that, for the quality of the road surface, both the truck and the driver are sensible to the difference between the uplift and the downlift rut and not to the downlift values only.

Post traffic photos on most of the sections were taken to record and qualitatively compare the performance behavior. The asphalt layer was inspected to determine the longitudinal and transverse cracks or the formation of alligator cracks.

Some measurements and tests were performed prior to the actual experimental portion of the full scale test. The soil and asphalt were classified in respect to the type, gradation and moisture content, and CBR tests were performed both in the laboratory and in-situ. In situ the layer thickness and density were inspected. On the geosynthetics, the following tests were performed: tensile properties, unit weight, mesh size and other typical QC tests. Load plate tests were conducted on the unpaved sections for the determination of the E_{v2} moduli performed in agreement with SNV 670317a with 300 mm plate. In addition up to 8 strain gages were glued on the geogrid layers for the determination of actual in-situ geogrid stress (Figure 2).

SCOPE OF THE TEST ANALYSIS

The results of the reinforced sections are compared with the corresponding unreinforced section to show the advantages of geosynthetics in increasing the road service life, reducing the rut depth and savings in aggregate. The tests are analyzed to show the following results:

- comparisons between reinforced and unreinforced sections;
- comparisons between reinforced sections at several gravel thickness';
- comparisons between reinforced sections at different CBRs;
- qualitative comparison between geosynthetics.

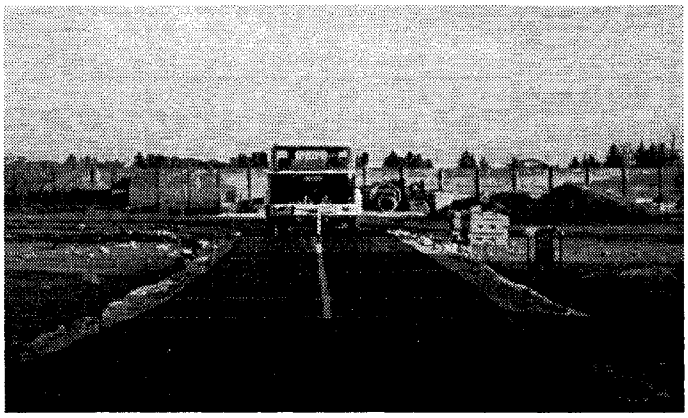

Figure 5: Full scale in-ground testing of geosynthetic reinforced flexible pavements

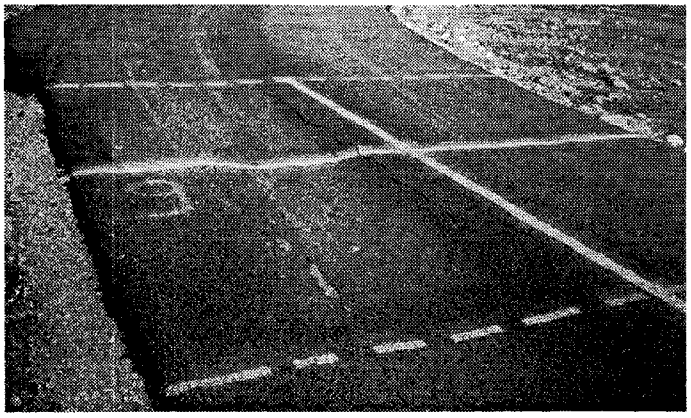

Figure 6: Control section (9e) with CBR = 3 and T = 300 mm after 1000 EAL

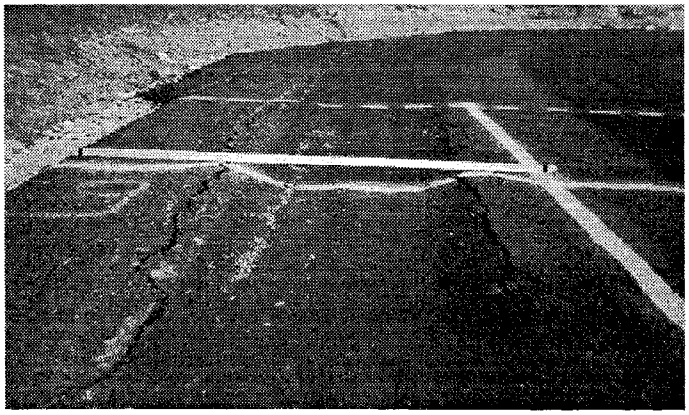

Figure 7: Control section (9e) with CBR = 3 and T = 300 mm after 3000 EAL

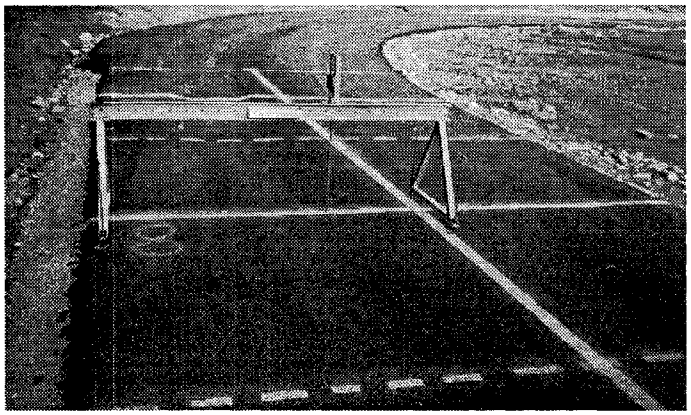

Figure 8: GGML2 and GGR1 section with CBR = 3 and T = 300 mm after 1000 EAL. The measurement beam. is shown.

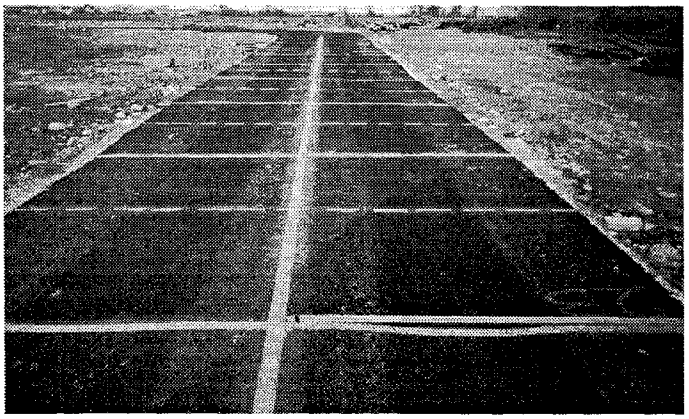

Figure 9: Control and reinforced sections with CBR=3 and T=400mm after 3000 EAL

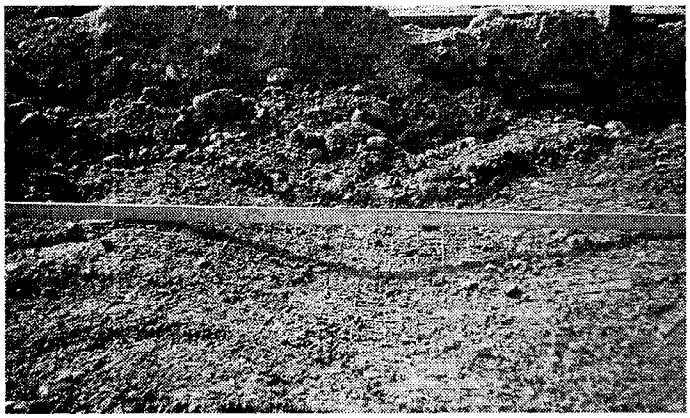

Figure 10: GGML2 Section with CBR=3 and T=300 mm recovered after 80000 EAL.

Rut geometry for reinforced and unreinforced sections was analyzed to determine differences in depth and shape of the reinforced sections, thus interpreting the functions played by the geosynthetic such as reinforcement, separation and membrane effect.

Suggested design charts, function of the geosynthetic type, sub-base soil shear strength, number of cycles, aggregate thickness and allowed rut depth can be prepared to allow engineers to design successful paved roads. These charts quantify the performance increase by the use of a reinforcement layer by comparing the test results at a given rut depth for either unreinforced and reinforced sections.

ANALYSIS OF THE TEST RESULTS

The section built with CBR equal to 3% and 400 mm base thickness, was built first. It was noticed while saturating the clay on-site that more water than the one required in laboratory was needed to obtain the target CBR. Since most of these sections were already built, to avoid an uneven distribution of the moisture content in the clay, the section with 400 mm gravel did not reach the target CBR equal to 3% but a final value of 5%.

The reinforcement effects of the geosynthetics used was immediately evident from the beginning when the unreinforced sections n. 28e and 28i, originally designed with 500 mm of aggregate base thickness and 700 mm of clay with CBR equal to 1 %, had to be excavated prior the placement of the asphalt course. The achieved strength of the unreinforced sections was not enough to support the weight of the paving vehicle. By physically loading the top of the base course layer, it was possible to create heavy deformations, pumping of the water up to the surface crust and aggregate cracking. The E_{v1} soil modulus, measured with a 300 mm diameter plate in agreement with SN 670312a, was as low as 300 kPa, while similar reinforced sections were up to 3 times stronger. The recorded settlement at 250 kPa applied pressure was 17 mm.

Based upon the above observations, it was decided to excavate the first 1.0 m depth from the unreinforced sections n. 28e and 28i and to replace it with a new aggregate base layer of 1.0 m to reach the existing elevation. The new layout for cross-section 28i and 28e was 0.2 m of clay , 1.0 m of gravel base and 75 mm of asphalt. Consequently, paving of all the area having CBR equal to 1.0% was performed.

The control section 9e, (unreinforced) with CBR equal to 3% and 0.3 m base thickness, reached more than 25 mm maximum rut depth in 50 cycles. After 500 cycles, the maximum rut depth was 142 mm, thus it was decided to excavate it, to re-grade the existing base by importing additional gravel and to re-pave the whole section with 75 mm asphalt (Fig. 6 and 7).

The enclosed charts (Fig. 11 to 31) and table 2 show the benefits of reinforced vs. unreinforced sections for the geosynthetics listed in table 1. In the below charts, it is possible to see: how the rut geometry proceeds with the repetition of loading cycles; the dimension of the rut

areas and by comparison a quantitative and qualitative behavior between sections. In table 2 are reported the maximum cycle rut depth for each section and measurement cycle.

Table 2: Product codes, cross section layout and maximum rut depth

				80 kN EAL number								
Test	Product	CBR	Base	0	500	1000	3000	5000	10000	20000	40000	80000
n.	Code	%	mm	Maximum rut depth, mm								
24e	GGML5	1	500	0.0	---	1.8	1.9	2.4	2.7	4.4	6.8	10.6
25e	GGR2	1	500	0.0	---	3.9	4.1	5.0	6.3	8.1	10.5	16.0
25i	GGML3	1	500	0.0	---	2.3	2.6	3.2	5.0	6.2	8.5	11.6
27e	GGR1	1	500	0.0	---	9.9	11.3	11.4	15.7	16.8	19.8	24.9
27i	GGML2	1	500	0.0	---	10.2	12.8	13.2	15.4	16.5	18.2	21.0
28e	Control	1	1000	0.0	---	5.1	5.4	5.8	7.2	8.1	9.7	12.4
5i	GGML5	3	300	0.0	---	8.2	9.8	11.7	12.2	13.1	14.9	16.7
8e	GGR1	3	300	0.0	---	9.5	11.8	12.5	14.9	17.2	18.4	19.6
8i	GGML2	3	300	0.0	---	6.7	8.1	8.8	10.2	11.3	12.6	14.3
9e	Control	3	300	0.0	26.5	44.4	90.5	142	---	---	---	---
15e	GGML5	3	400	0.0	---	1.3	1.3	1.4	2.4	2.7	3.0	3.3
20e	WGTX	3	400	0.0	---	4.5	5.3	5.8	6.2	6.9	7.9	10.0
21e	GGR2	3	400	0.0	---	1.9	2.0	2.4	2.6	3.3	4.0	5.4
21i	GGML3	3	400	0.0	---	1.2	1.6	2.0	2.3	2.8	3.7	5.4
22e	GGR1	3	400	0.0	---	1.6	2.6	2.9	4.0	3.8	5.3	6.6
22i	GGML2	3	400	0.0	---	2.3	3.1	3.3	4.2	4.8	5.5	6.8
23i	Control	3	400	0.0	13.8	15.7	18.3	19.4	20.3	21.5	23.2	25.0
1e	Control	3	500	0.0	7.2	7.9	8.1	10.4	12.6	12.6	13.7	15.0
1i	GGML5	3	500	0.0	---	4.3	4.6	5.5	7.2	8.8	10.3	11.3
2e	GGR1	3	500	0.0	---	5.6	7.0	8.3	10.4	10.9	11.6	12.7
2i	GGML2	3	500	0.0	---	4.0	4.7	5.4	6.1	8.0	8.9	11.3
11i	Control	8	300	0.0	2.1	2.9	3.7	3.4	4.5	4.7	6.3	7.6
12e	GGR1	8	300	0.0	---	1.6	2.7	2.8	3.4	3.9	5.4	7.3
12i	GGML2	8	300	0.0	---	2.0	2.6	3.2	4.3	5.1	5.8	6.8

CONCLUSIONS

The results obtained from this experimental research work supports the following conclusions as shown in figures 32 to 36. In these figures the data collected in table 2 are graphically presented for sections having identical base thickness and CBR.

- At a given maximum rut depth, a geogrid reinforced gravel base is equivalent to a much thicker unreinforced base. By comparing fig. 33 and 35, reinforced sections with 300 mm base behave similarly to unreinforced sections with 500 mm gravel base thickness;
- The GGML2 multi-layer geogrid, with a mesh opening suitable for the dimensions of the aggregate and subgrade soil, provides good results in reinforcing the road structure. The reinforcing capacity of the multi-layer geogrids can be mobilized at lower deformation than the typical heavier single layer geogrid. No intrusion of soil particles from the fill soil was recorded when the tests sections were excavated (figure 10);
- Multi-layers geogrids provide the best base reinforcement results for subbase soils having CBRs equal to 3% or lower as shown in Figure 32 and 33;
- No major differences were found between different single layer integral geogrids. The higher tensile modulus geogrids have shown better contribution at CBRs 3% or lower as comparing the results shown in Figure 32, 34 and 35 with the tensile properties reported in table 1;
- The percent reduction of rutting, between reinforced and unreinforced sections, increases with reducing the subgrade CBR, for all geosynthetics (figure 32 and 36);
- The Traffic Improvement Factor (Montanelli et al. 1997) for road service life increases for deep allowed ruts, lower CBR values and lower pavement structural number. A traffic improvement factor of 10 for a rut depth of 5 and 10 mm can be used for most of the soil conditions and appropriate geogrid type;
- The structural layer coefficient of the aggregate, when calculated in agreement with Cancelli et. al. (1996), can be increased by a geogrid layer, having a layer coefficient ratio ranging from 1.5 to 2.0.
- High strength woven geotextiles provide good separation functions but limited reinforcement action. A rut depth of 5 mm is reached within 2000 EAL while with geogrids up to 80000 EAL. Thus the relative Traffic Improvement Ratio of geogrids is up to 40 times greater than woven geotextiles.
- Geogrids placed at the subbase/aggregate interface are effective for increasing the service life of a paved road. The geogrid layers are able to mobilize stresses within the reinforced sections, preventing local shear failure and deformations. The geogrid strains, measured by means of the strain gages attached to the geogrid ribs, show minimum amount of stress been developed when the wheel loads are applied (Figure 2 and 37). This indicates that the failure mode appears mainly for fatigue mechanism when appropriate reinforcement is used;
- The elastic geogrid strains, for a biaxial geogrid having a tensile modulus of 350 kN/m, measured under the front and rear wheel loads are greater under the wheel vertical and greatly reduce when moving out from the vertical line. The magnitude of these elastic strains are less than 0.2% for most of the sections monitored (Figure 37) being larger for low CBRs and for lower aggregate base thickness'.

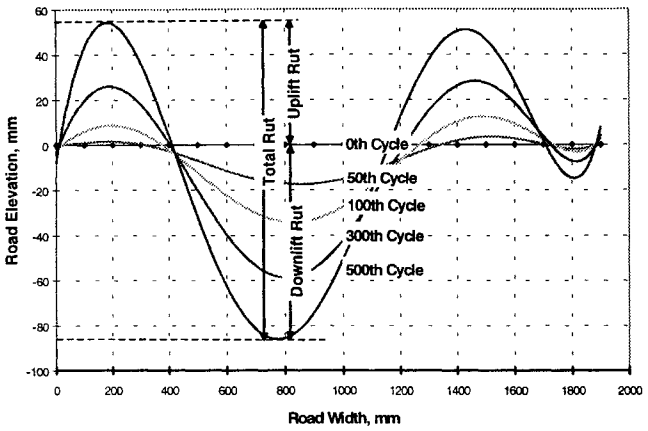

Figure 11: Cross-sectional profile of the test sections, showing the maximum (total) rut depth and downlift and uplift rut.

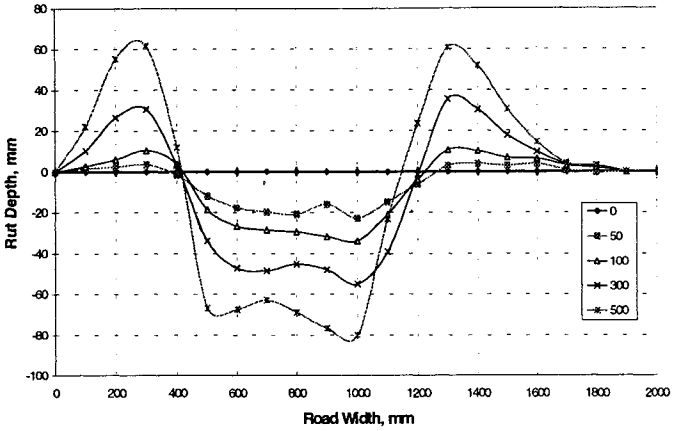

Figure 12: Rut depth profile, Control section, CBR = 3, T = 300 mm

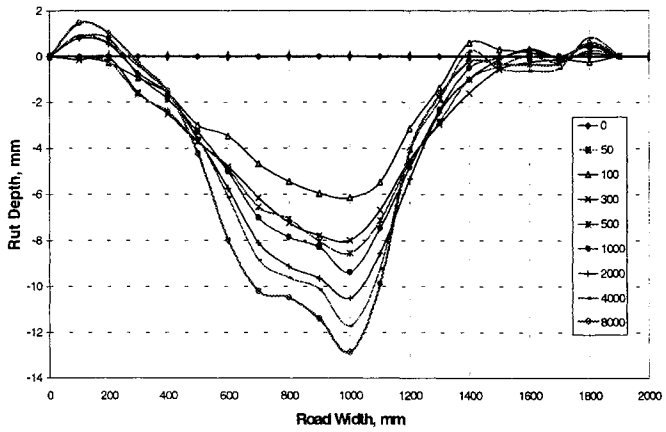

Figure 13: Rut depth profile, GGML2 section, CBR = 3, T = 300 mm

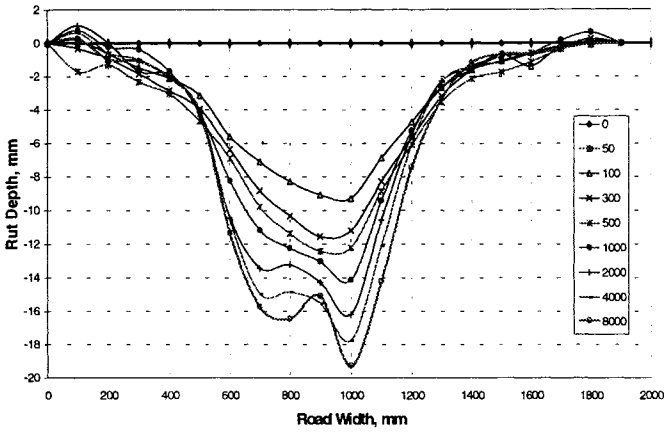

Figure 14: Rut depth profile, GGR1 section, CBR = 3, T = 300 mm

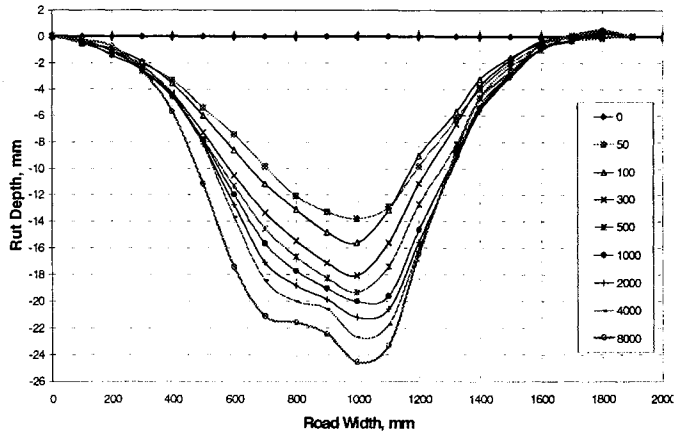

Figure 15: Rut depth profile, Control section, CBR = 3, T = 400 mm

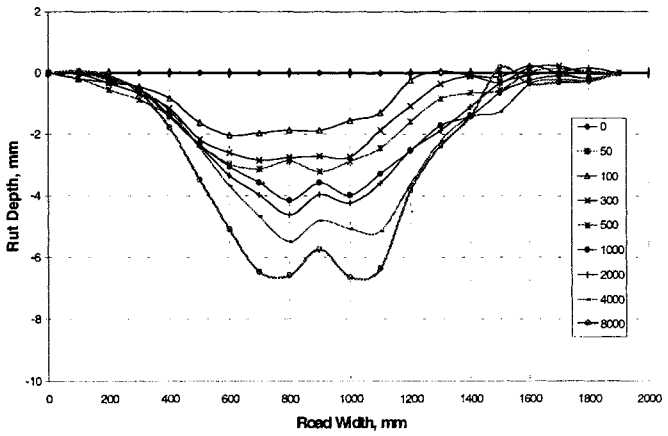

Figure 16: Rut depth profile, GGML2 section, CBR = 3, T = 400 mm

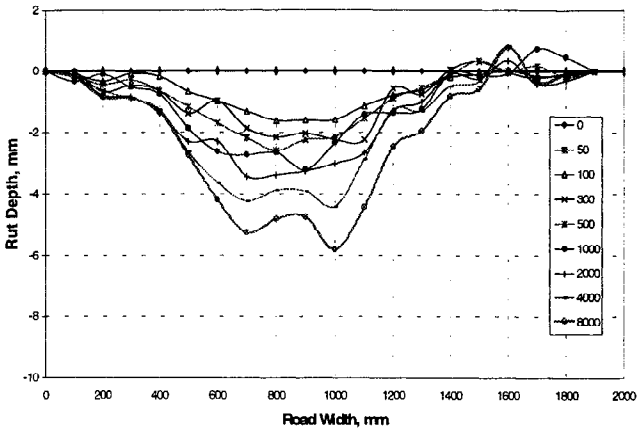

Figure 17: Rut depth profile, GGR1 section, CBR = 3, T = 400 mm

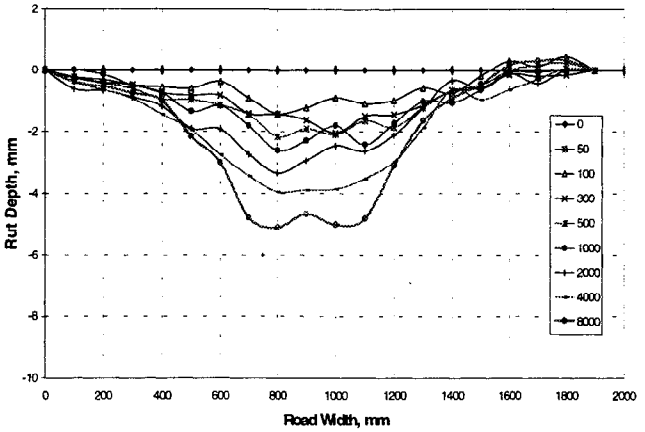

Figure 18: Rut depth profile, GGR2 section, CBR = 3, T = 400 mm

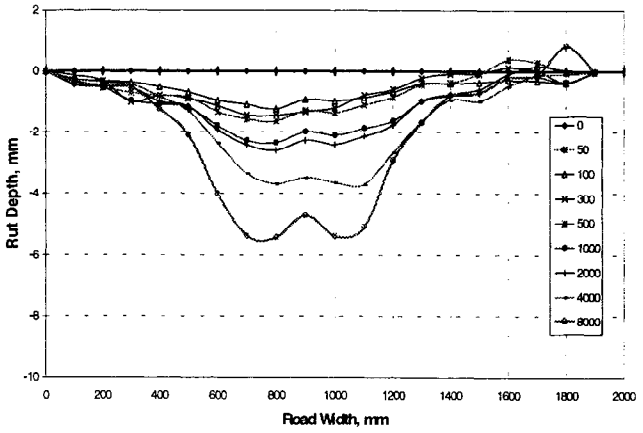

Figure 19: Rut depth profile, GGML3 section, CBR = 3, T = 400 mm

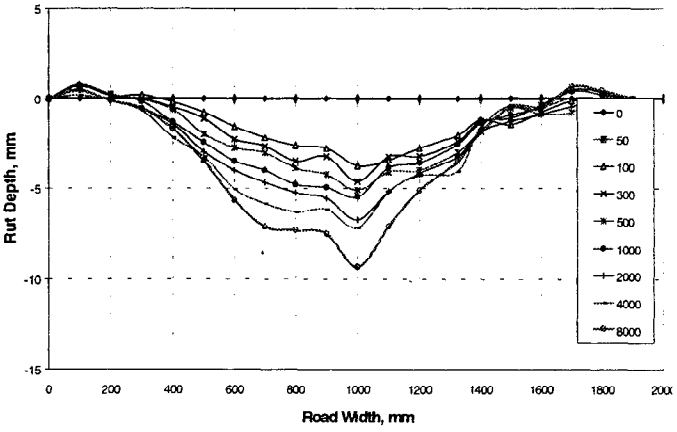

Figure 20: Rut depth profile, WGTX section, CBR = 3, T = 400 mm

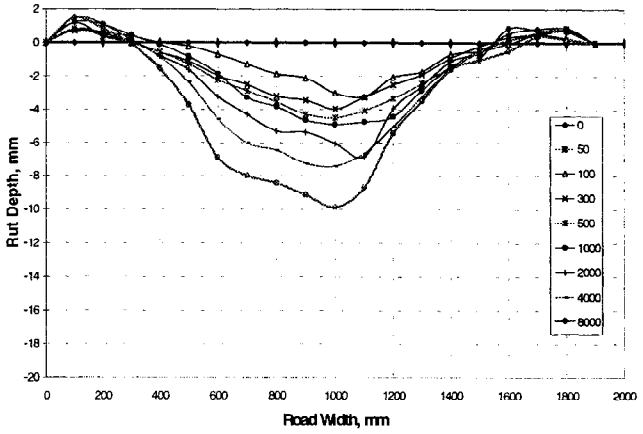

Figure 21: Rut depth profile, GGML2 section, CBR = 3, T = 500 mm

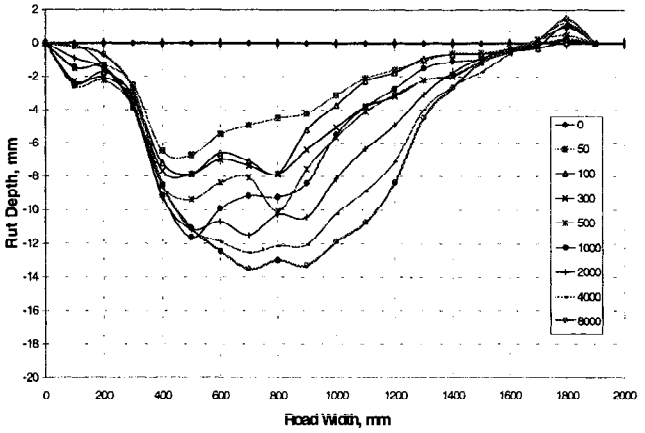

Figure 22: Rut depth profile, Control section, CBR = 3, T = 500 mm

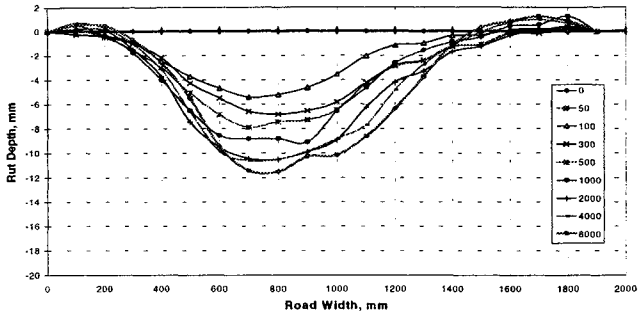

Figure 23: Rut depth profile, GGR1 section, CBR = 3, T = 500 mm

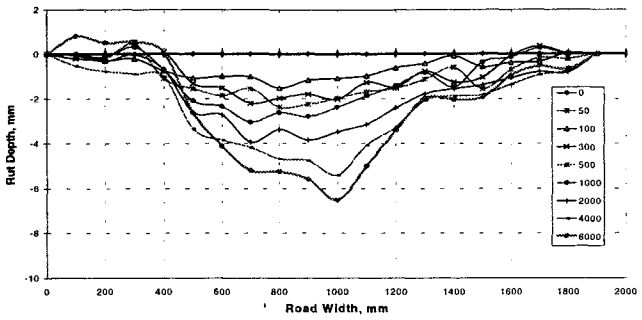

Figure 24: Rut depth profile, GGR1 section, CBR = 8, T = 300 mm

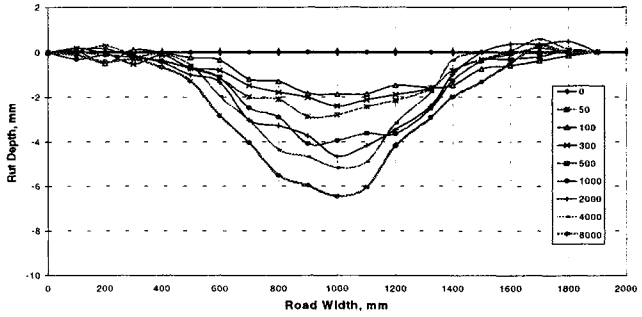

Figure 25: Rut depth profile, GGML2 section, CBR = 8, T = 300 mm

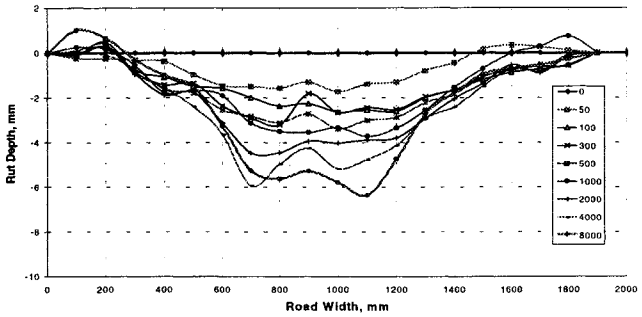

Figure 26: Rut depth profile, Control section, CBR = 8, T = 300 mm

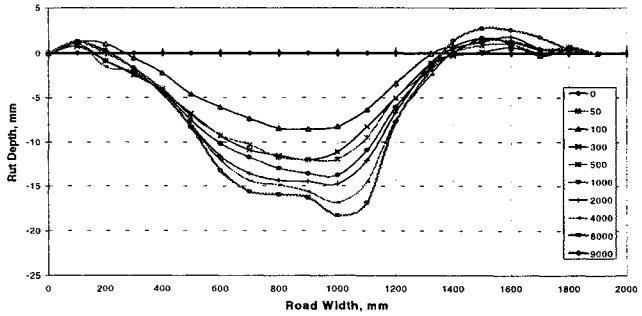

Figure 27: Rut depth profile, GGML2 section, CBR = 1, T = 500 mm

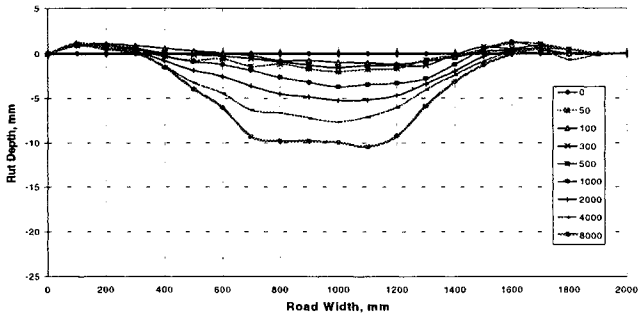

Figure 28: Rut depth profile, GGML3 section, CBR = 1, T = 500 mm

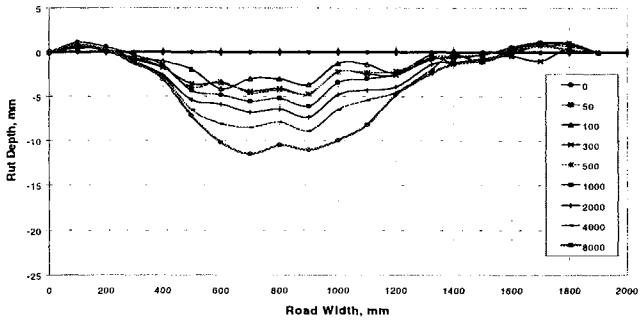

Figure 29: Rut depth profile, Control section, CBR = 1, T = 1000 mm

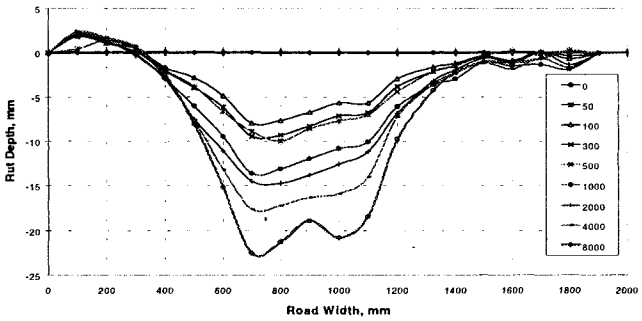

Figure 30: Rut depth profile, GGR1 section, CBR = 1, T = 500 mm

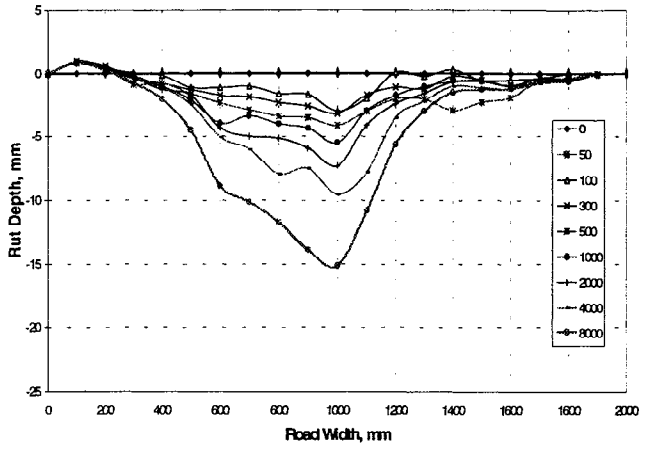

Figure 31: Rut depth profile, GGR2 section, CBR = 1, T = 500 mm

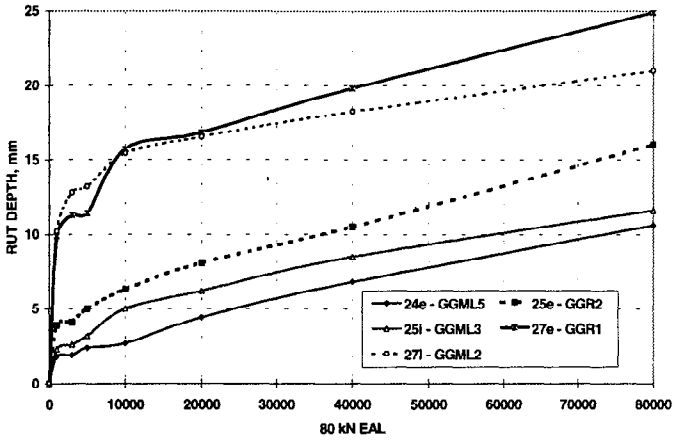

Figure 32: Maximum rut depth vs. EAL number at CBR=1 and T=500 mm.

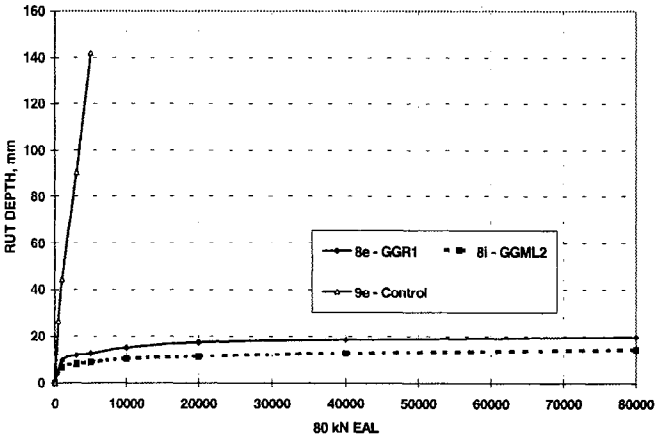

Figure 33: Maximum rut depth vs. EAL number at CBR = 3 and T=300

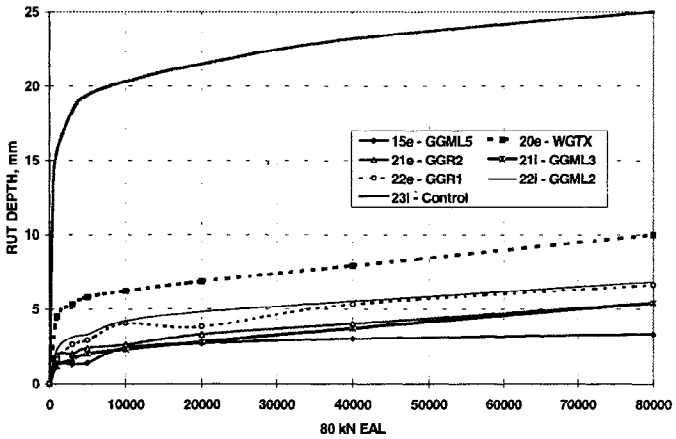

Figure 34: Maximum rut depth vs. EAL number at CBR=3 and T=400 mm.

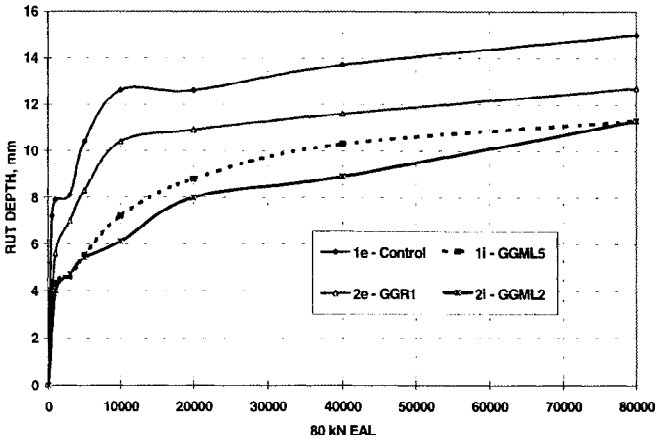

Figure 35: Maximum rut depth vs. EAL number at CBR=3 and T=500 mm.

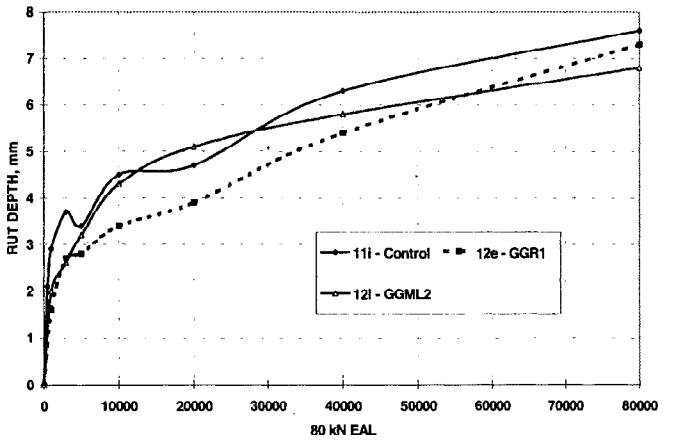

Figure 36: Maximum rut depth vs. EAL number at CBR = 8 and T= 300 mm.

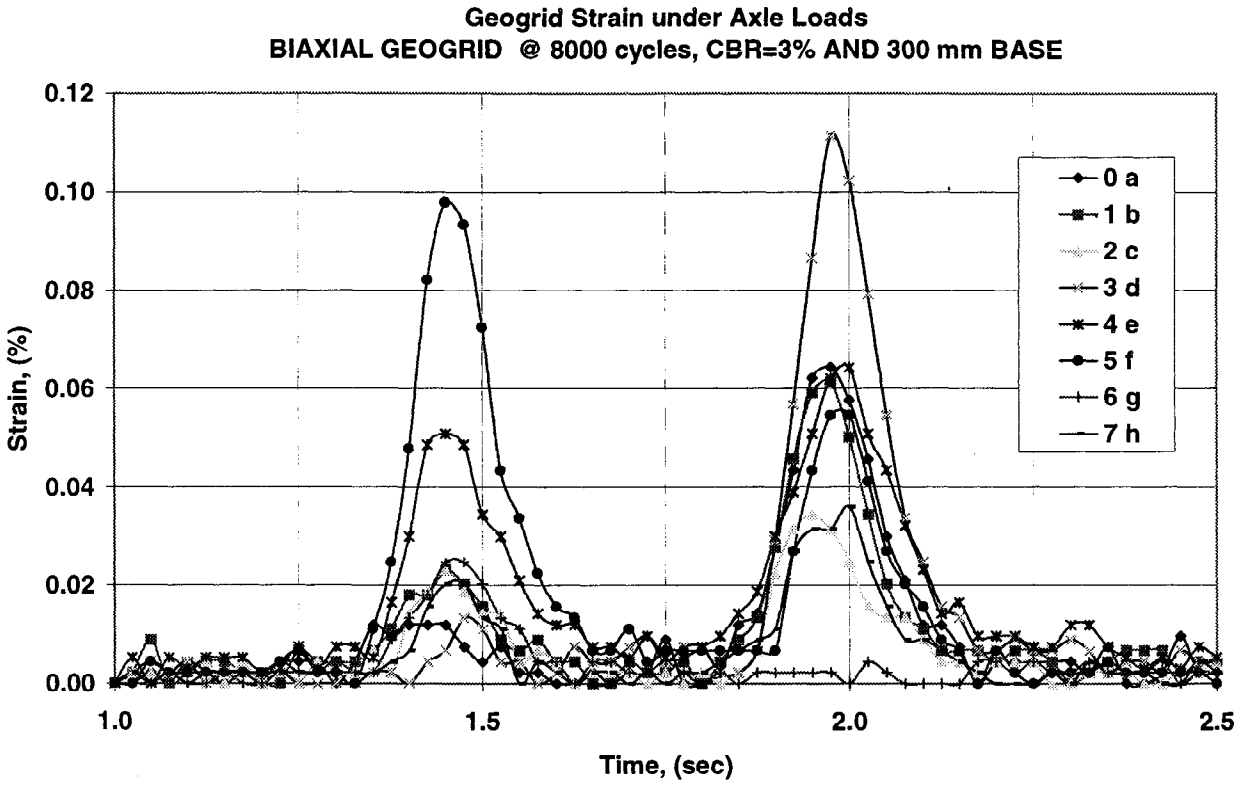

Figure 37: Geogrid rib tensile strain at 8000 cycles measured under the front (left) and rear (right) wheel passage.

REFERENCES

ASTM D1883:87, 1987, "Standard Test Method for CBR (California Bearing Ratio) of Laboratory- Compacted Soils" Annual Book of ASTM Standards.

BS 7533:1992, 1992, "Guide for structural design of pavements constructed with clay of concrete block pavers" British Standards Institution.

Cancelli, A., Montanelli, F., Rimoldi, P., and Zhao, A., 1996, "Full scale laboratory Testing on geosynthetics reinforced paved roads" Proceedings of the International Symposium on Earth Reinforcement, pp. 573-578.

Montanelli, F., Zhao, A., and Rimoldi, P., 1997, "Geosynthetics-reinforced pavement system: testing and design" Proceeding of Geosynthetics '97, pp. 619-632.

Perkins, S.W., and Ismeik, M., 1997, "A synthesis and evaluation of geosynthetic-reinforced base layers in flexible pavements: part I", Geosynthetics International, pp. 549-604.

SNV 67031a, 1981, "Essai de charge avec plaques M_E" Association Suisse de Normalisation.

FACTORS IN PAVING FABRIC FAILURES

Thomas L. Baker, P.E.
Amoco Fabrics and Fibers Company

Mark L. Marienfeld, P.E.
Amoco Fabrics and Fibers Company

ABSTRACT

This paper examines the findings of sixty-five investigations into the unsatisfactory performance of pavements containing paving fabric interlayer systems. The investigations were performed over a period of more than 15 years on projects scattered across the United States. Based on the results of the failure investigations, a variety of factors are examined for their impact on the performance of the paving fabric system. Paving fabric installation reports are also evaluated to give additional insights into the causes of failures and areas for careful monitoring during installation. Based on the results of the investigations several common characteristics can be observed. The most significant factor found to affect the performance of the system is the amount and uniformity of asphalt tack coat used in installation. Based on the findings of the complaint investigations examined, conclusions are made and recommendations are given on issues requiring attention both during installation and for future research.

INTRODUCTION

This paper reviews the records from evaluations of 65 cases where a paving fabric did not perform up to expectations. These records have been compiled from records of the former Phillips Fibers Corp. and Amoco Fabrics and Fibers Co. going back to 1982. To first put the scope of this study into perspective it should be pointed out that paving fabric system failures are relatively rare. In the peak year covered by this paper, 1982, there were 10 paving fabric complaint evaluations performed nationwide. In that same year there were over 250 documented paving fabric installations in California alone and that is thought to represent a fraction of the projects installed there. Based on known volumes of paving fabric production, the total of 65 complaints is thought to represent on the order of 0.1% of the total number of paving fabric projects installed during the period covered.

To gain additional insight into possible root causes of some of the complaints, available installation records of the former Phillips Fibers Corp. from California in 1982 are used. During 1982 there were over 250 paving fabric installations in California for which documentation was found. California and the

year 1982 were chosen for a variety of reasons. First, by 1982 paving fabric use in California had progressed from an experimental status to accepted practice. At the same time, the technology was still new enough that it was felt that most of the installations were still being installed by the former Phillips Fibers Corp., and records were available.

As with any geosynthetic system, there is a wide variety of factors that can affect the performance of a paving fabric system. In the case of paving fabric installation, these factors may include tack coat application and uniformity, type of tack coat used, surface condition and preparation, overlay considerations and climatic or geographic considerations. The goal of this evaluation is to identify recurring factors present in poorly performing projects in the hope that identification of common elements in these failures can improve the overall performance of future paving fabric system installations.

When properly installed, the paving fabric system enhances the life of an overlay by reducing the recurrence of reflective cracking and reducing water movement through the pavement surface into the base and subgrade. The paving fabric system consists of two elements, the paving fabric itself and a layer of asphalt cement tack coat. The asphalt tack coat, saturating the fabric, forms a low permeability layer and bonds the system to the existing pavement and overlay. The fabric stabilizes and holds the tack coat in place and dissipates movements from underlying pavement, thus minimizing the transfer of cracking to the overlay. The performance of the paving fabric system is mutually dependent on the performance of the fabric and the asphalt tack coat.

Installation of the paving fabric system generally follows the same pattern wherever it is used. First the surface is prepared by removing loose material and sealing cracks as necessary. An asphalt cement tack coat is then applied to the existing pavement surface. Typically, paving fabric manufacturers recommend a tack coat application of about 1.13 liters per square meter (0.25 gallons per square yard). This anticipates the fabric absorbing about 0.90 liters per square meter (0.20 gallons per square yard) and 0.23 liters per square meter (0.05 gallons per square yard) to bond the system together with the existing pavement and the overlay. After spraying the tack coat the paving fabric is rolled onto the sprayed surface. Finally, an asphalt cement concrete overlay is placed over the fabric. The heat of the overlay and pressure applied by compaction of the overlay draw the tack coat into the paving fabric and complete the process.

PROJECT PROFILE

As mentioned previously, the records of 65 investigations performed since 1982 are evaluated in this study. The projects investigated are scattered across the United States and part of Canada as shown in Figure 1. The poorly performing projects include a cross section of public and private facilities. For the purpose of this paper, the projects are broken down into: (1) city and county roads and streets, (2) parking lots both light and heavy duty, (3) airport runways and taxiways, (4) state highway projects, (5) playgrounds and tennis courts, (6) other and (7) unknown with reference to the failure investigations. A comparison, by type of project, of the relative frequency of complaints investigated to the documented installations in California in 1982 is shown in Figure 2. The relative distribution of all projects installed in California in 1982 and the types of projects from the complaints investigated in the period from 1982 through 1997 are relatively close. In general, city and county roads were the most frequent source of

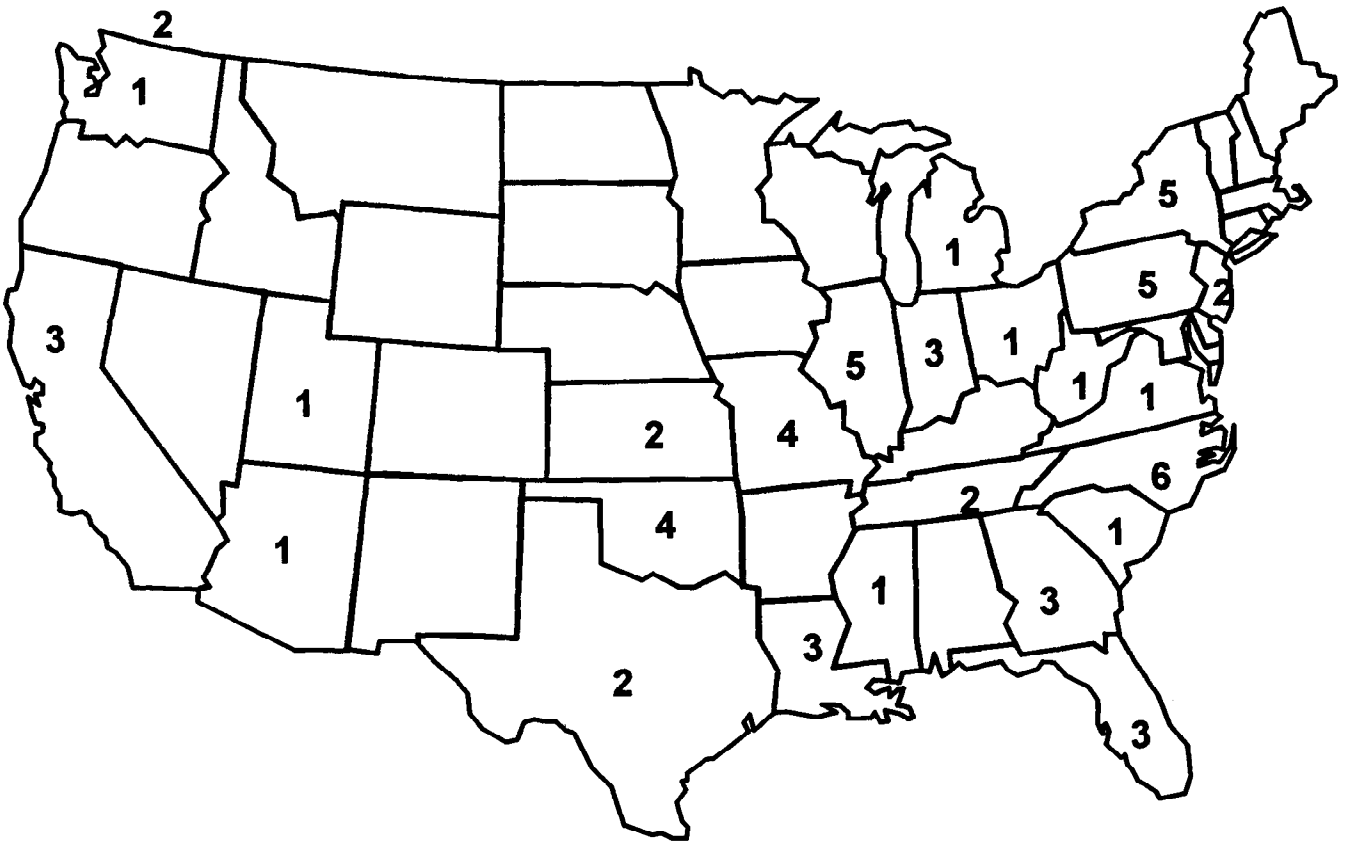

Figure 1 - Locations and numbers of complaints investigated.

complaints as well as the most frequent type of installation. Parking lots are the second leading type of installation as well as source of complaints.

The paving fabric used in the complaints investigated and the 1982 project sample was a polypropylene, staple fiber, needle-punched nonwoven with unit weights in the 120 to 135 grams per square meter (3.5 to 4 ounces per square yard) range. This is the most common type of paving fabric used in the United States.

Seven of the complaints, about 11%, are recorded as having a Portland cement concrete original pavement. The remaining pavements are either asphalt cement concrete or unknown. A relatively large number do not indicate the type of original pavement. In all of the complaints the overlay was an asphalt cement concrete. The overlays in the complaints investigated averaged 1.32 inches thick with about eight of the complaints having an average overlay thickness less than on inch. The 1982 sampling of projects indicates about 4% of the original pavements as Portland cement concrete. An asphalt concrete overlay was used in all but five of the documented projects from 1982. These five other projects used chip seal surfaces. The average thickness documented in the installation reports was 1.72 inches with about 6% having overlay thicknesses of one inch or less.

The nature of the complaints can be generalized as early cracking, shoving and delamination. Cracking is frequently subjective and open to interpretation. Typically, it is the result of the overlay

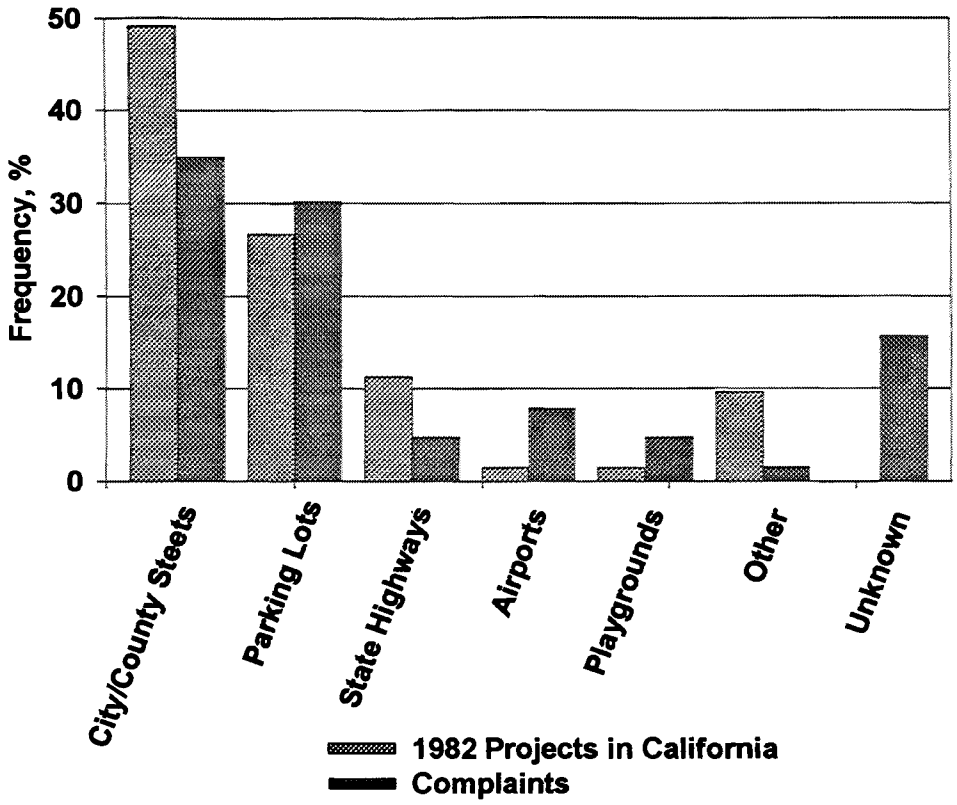

Figure 2 - Generalized distribution of complaints by project type compared to the distribution of documented projects in California in 1982.

developing reflective or fatigue cracks earlier than anticipated. In some cases, these complaints may be the result of overly optimistic expectations or promotion rather than actual performance. Complaints of early cracking may be expressed several years after the installation. The more serious complaints included delamination and shoving of the overlay. These two types of complaints may be closely related. Shoving is generally expressed as rutting or mounding of the asphalt in the overlay. An example of shoving is shown in Figure 3. Delamination is the complete loss of bond between the overlay and existing pavement with a resulting torn dislocation in the surface of the overlay. An example of delamination is shown in Figure 4. Shoving and delamination are generally reported 8 to 16 months after installation but have been observed as quickly as one month after installation. Of the 65 complaints investigated, 11 involved delamination and 6 shoving of the overlay.

CAUSES OF FAILURES

Complaints were generally investigated by field observation and testing of cores of the pavements including the paving fabric. The evaluations of the cores included measurement of the overlay and original pavement thicknesses, evaluation of the overlay asphalt content and aggregate gradation, and

Figure 3 - Shoving of overlay on a city street in New York.

extraction of the tack coat from the paving fabric. The extraction of the tack coat from the paving fabric involved repeatedly washing the fabric in solvent until the asphalt was removed. From these tests and observations, the amount of tack coat in the fabric was calculated and observations about the probable cause of problems made. Two overlay related factors not investigated, and conspicuous by their absence, are the degree of overlay compaction and pavement and overlay temperature at the time of placement. Unfortunately, construction details on which to evaluate these factors are rarely available.

The causes of paving fabric system failures identified in our investigations included amount of tack coat in the fabric, overlay related issues and other construction related factors. The frequencies of occurrence of the various factors in the projects investigated for this study are shown in Figure 5. Where more than one cause was identified, each was used equally in calculating the percentages shown in Figure 5. By far the single most prominent factor involved in the problems investigated was too little tack coat. The lack of sufficient tack coat in the paving fabric was identified as contributing to problems in almost 75% of the cases investigated. The second leading factor identified were overlay related issues including both too thin an overlay and a poor overlay asphalt concrete mixture. These were involved in a relatively minor 20% of the cases evaluated.

It is interesting to note that none of the investigations reported a heavy tack coat rate as a cause of distress. It is known that too heavy of an asphalt tack coat can lead to reduced bonding of the overlay and/or asphalt bleeding through the overlay. This may imply that owners did not generally consider these as problems or that in typical practice it may not occur. Since only 5 of the 65 projects investigated had average tack absorption rates of 0.90 liters per square meter (0.20 gallons per square yard) or greater, we suspect that excessive tack coat application does not often occur.

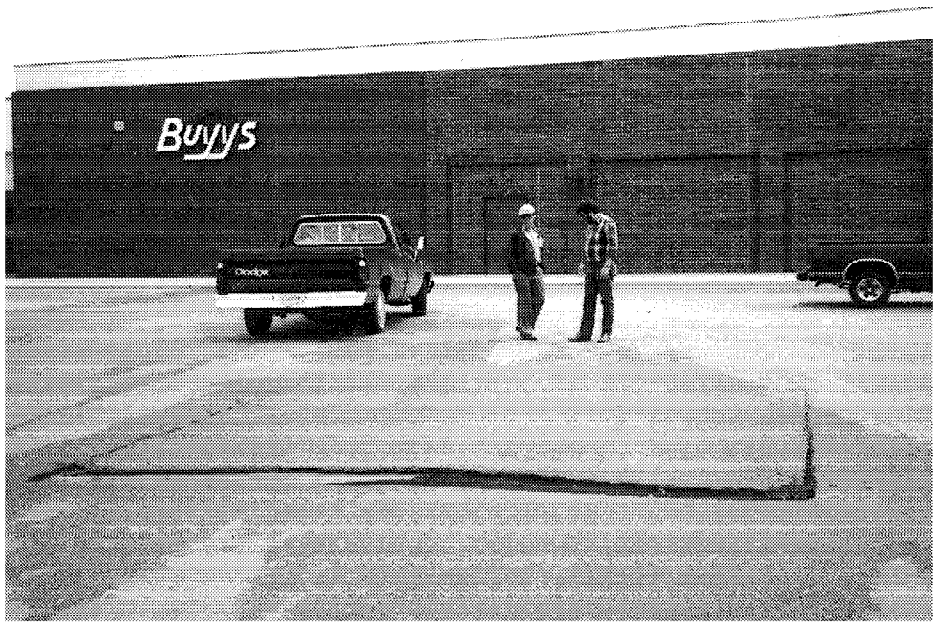

Figure 4 - Delamination of overlay in a parking lot in Indiana

TACK COAT

Amount of Tack Coat. The amount of tack coat present in the paving fabric was identified as the leading cause of failures in paving fabric installations. Too little tack coat was either a primary or secondary factor in about 75% of the failures investigated. It is not uncommon to pull apart pavement cores from failures and find there is no visible asphalt in the paving fabric. At the least, this substantially reduces the waterproofing benefit of the paving fabric. In extreme conditions, the fabric will not bond properly to the existing pavement or overlay. The damage resulting from this can include, shoving or occasionally complete delamination of the overlay. The damage shown in the photographs in Figures 3 and 4 are the result of too little asphalt tack coat in the fabric.

Most manufacturers of paving fabric recommend a tack coat application rate of about 1.13 liters per square meter (0.25 gallons per square yard) for 120 to 135 gram per square meter (3.5 to 4 ounces per square yard) paving fabric. This allows 0.23 liters per square meter (0.05 gallons per square yard) to bond the fabric to the existing pavement and new overlay and 0.90 liters per square meter (0.20 gallons per square yard) to saturate the paving fabric. The ability of the paving fabric to absorb asphalt tack is determined from the standardized asphalt retention test, ASTM D 6140, in which a paving fabric sample is soaked in liquid asphalt to determine how much will be absorbed by the fabric. Other investigations (Baker 1997, Marienfeld 1998) have shown that at least 0.77 liters per square meter (0.17 gallons per square yard) is needed in the fabric to provide an effective moisture barrier beneath the overlay. A minimum fabric asphalt absorption of 0.77 liters per square meter (0.17 gallons per square yard) implies a field application rate of about 1.0 liters per square meter (0.22 gallons per square yard). It should be noted that at application rates over about 1.27 liters per square meter (0.28 gallons per square yard)

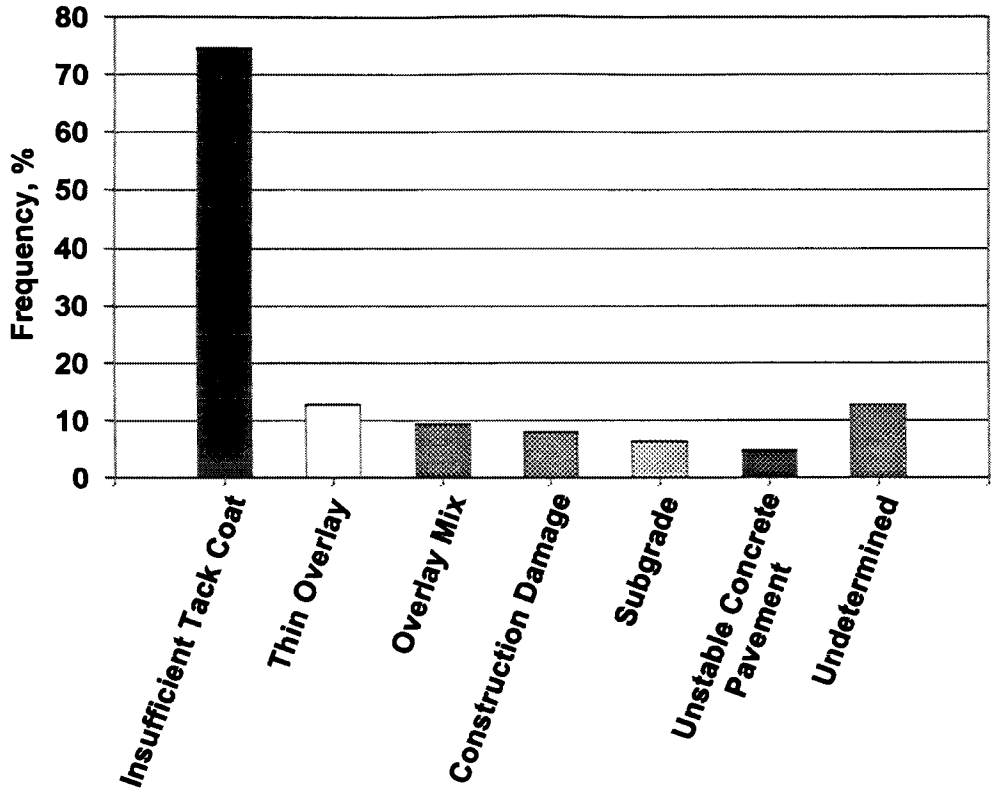

Figure 5 - Causes of complaints investigated. Where more than one potential problem was identified, both were used in the frequency calculation, thus the total is greater than 100%.

pick-up of the paving fabric by truck tires can occur on hot days. Thus, the optimum application rate for full benefit of the paving fabric system is between 1.0 and 1.27 liters per square meter (0.22 and 0.28 gallons per square yard).

A review of the actual results of the of the core test results is informative. Figure 6 shows the results of the tack coat extractions from the paving fabric in the cores. This includes 237 cores from the 65 jobs mentioned previously. The results in this figure include core test results from all projects investigated without regard to the cause of unsatisfactory performance. The results are somewhat deceptive in that even poorly installed jobs occasionally have thick spots in the tack coat that were encountered in the cores. From these results it can be observed that the tack coat quantity in the paving fabric is frequently marginal at best. It appears that fully 76% of the cores had a low tack coat amount in the fabric, less than 0.77 liters per square meter (0.17 gallons per square yard). In fact, 42% of the paving fabric in the cores had less than 0.45 liters per square meter (0.10 gallons per square yard) of tack coat.

A narrower review of the cases in which delamination was reported is informative. There were 11 cases where delamination was reported. In eight of these cases the average amount of tack coat in the fabric was 0.45 liters per square meter (0.10 gallons per square yard) or less with one project having an

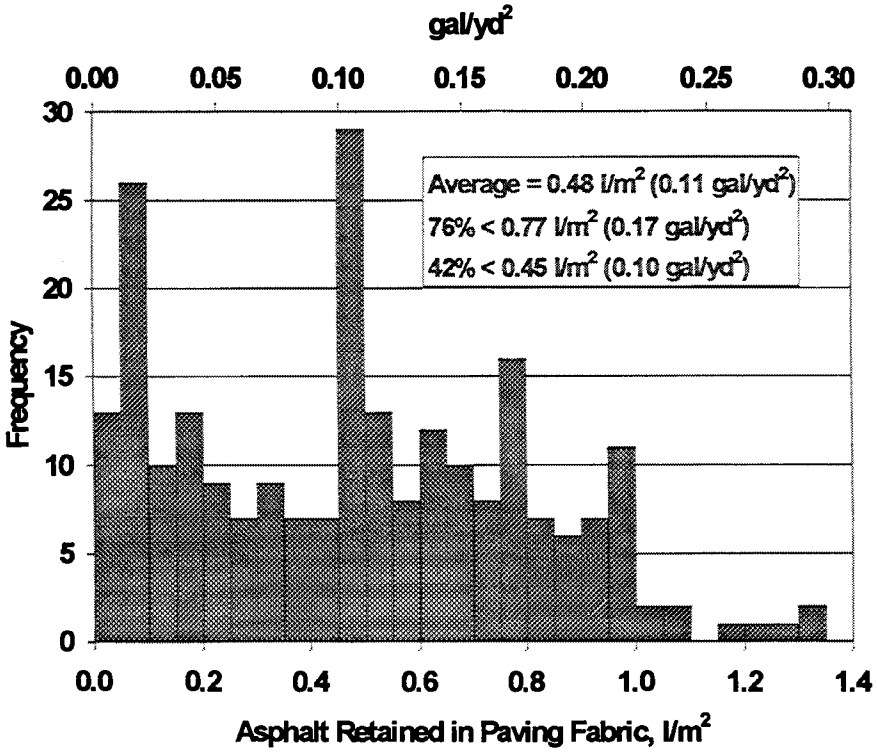

Figure 6 - Tack coat extracted from paving fabric contained in cores from complaints investigated.

average of only 0.05 liters per square meter (0.01 gallons per square yard) in the fabric. The highest project average measured in any of the cases reporting delamination was 0.59 liters per square meter (0.13 gallons per square yard). This strongly implies that severe failure can be expected wherever the tack coat in the fabric is less than about 0.45 liters per square meter (0.10 gallons per square yard). At higher rates the project may not manifest the more severe forms of distress but still will not provide the full waterproofing and reflective cracking relief benefits. The very low amounts of tack coat frequently observed in cases of delamination may suggest that the installations were made using only the nominal 0.23 liters per square meter (0.05 gallons per square yard) tack application typically used when placing an overlay on an existing pavement without a paving fabric.

In addition to low application amounts, there appears to be another set of conditions that could result in a low amount of tack in cores of paving fabric. Inadequate rolling or too low of an overlay temperature may create conditions in which the tack may not be taken up by the fabric. In fact, the rapid heat loss of thin overlays is part of the reason that overlays less than an inch thick are not recommended when using paving fabric, unless special procedures are followed. Anecdotal evidence, however, suggests that these potential causes are not generally encountered in highway construction but may be more of a concern in smaller projects such as parking lot or tennis court overlays.

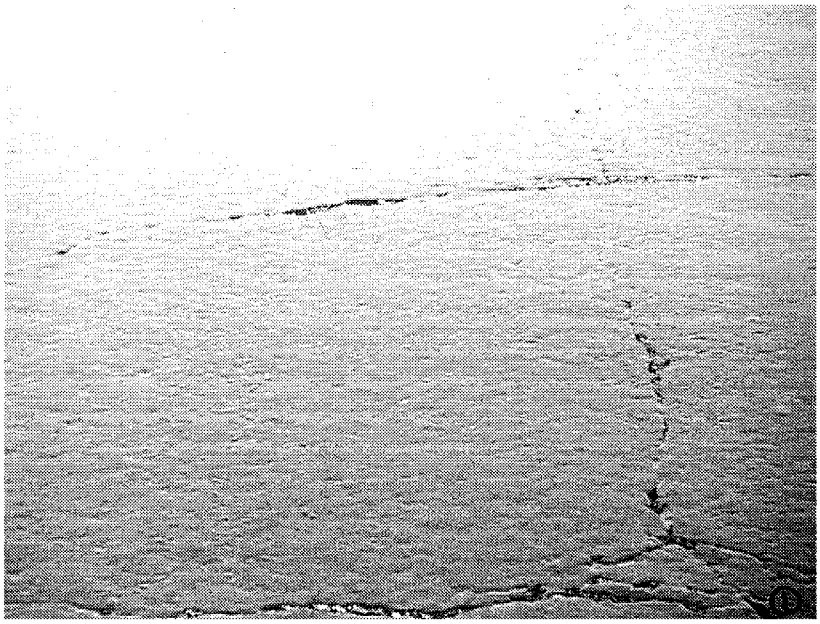

Figure 7 - Dry spots left in tack coat due to inadequately filled cracks.

Tack Coat Variability. As mentioned earlier, lack of uniformity in the tack coat application can also be observed in the projects evaluated. Of the projects identified with a low amount of tack coat, about 35% had locations with higher amounts present. The widest spread across any project was 0.09 to 0.95 liters per square meter (0.02 to 0.21 gallons per square yard). Variations are often encountered when an attempt was made to core both good and bad areas of a project for comparison purposes. These locally high concentrations may be due to continued spraying of the tack while the truck is stopped or similar circumstances. These local irregularities may be the cause of seemingly unexplainable poor paving fabric system performance in spots on some projects.

Type of Tack Coat. Typically, manufacturers of paving fabric recommend uncut paving grade asphalt cement for tack coats with paving fabric. Occasionally, for the sake of convenience or for lack of understanding, asphalt emulsions are used instead. The sample of installation reports reviewed suggested that emulsions may be used in slightly less than 10% of total projects, most notably in relatively small projects such as parking lots, playgrounds and tennis courts. A review of the failure investigations covered by this report sheds some light on concerns associated with use of asphalt emulsions with paving fabric. Asphalt emulsions generally contain at least 30% water. This presents some special considerations in the installation of paving fabric and has contributed to several problems. The first and principal concern is that to get an application rate of 1.13 liters per square meter (0.25 gallons per square yard) about one-and-a-half times that much emulsion must be applied. This results in a very large amount of liquid and the perception is that it is too much, which in turn results in a tendency to use too little tack with emulsions. If the application rate is the same as used for asphalt cement at a standard 1.13 liters per square meter (0.25 gallons per square yard), the actual amount of residual asphalt left after evaporation of

the water is only about 0.77 liters per square meter (0.17 gallons per square yard). If a surface demand of about 0.23 liters per square meter (0.05 gallons per square yard) is assumed, this only leaves about 0.54 liters per square meter (0.12 gallons per square yard) to saturate the fabric. This is far short of the amount shown to provide the full paving fabric benefit. This concern is supported by the findings from failure investigations. In the six cases in which emulsions were known to have been used all were found to be low in tack quantity in the paving fabric with a job average range of 0.23 to 0.63 liters per square meter (0.05 to 0.14 gallons per square yard). Further, emulsions were used in three of the 11 reported cases of delamination. Based on tack coat application rates, given in the sample of installation reports, most of the projects which use an emulsion may have applied too little tack coat.

In the failure investigations in which an emulsion was used, the amount of tack present in the fabric was widely variable across the job, with some areas having as much as six times the tack coat found in other areas of the same job. This highlights the next concern when using emulsions. They tend to be very fluid and will readily run if placed on a sloping pavement or into low spots on relatively level surfaces. This creates the wide variability observed in some of the projects. This was noted on several of the installation reports reviewed. The installation reports from 1982 in California also suggest a couple of other potential concerns when using emulsions. It takes up to roughly four hours for the water to evaporate off from emulsions. In about a quarter of the projects in which emulsions were used with paving fabric the water had not completely evaporated off when the paving fabric or the overlay were placed. Finally, one installation report contained a comment that the weather was so cold that the emulsion froze when sprayed onto the pavement surface.

OVERLAY CONSIDERATIONS

The second leading cause of unsatisfactory paving fabric system performance observed were combined concerns with the overlay. These were identified as either primary or secondary causes in 13 of the 65 projects. As mentioned earlier, it was not possible to investigate overlay compaction and placement temperature and their potential involvement in any of the complaints studied. There are two factors in the overlay placement that have been observed in the complaint investigations performed, too thin an overlay and an unstable overlay asphalt concrete mix. The first is the overlay thickness. Installation of the paving fabric system depends on the heat of the overlay to sufficiently soften the tack such that the pressure applied during compaction will force the softened tack into the fabric. This is also obviously dependent on the temperature of the existing pavement, the temperature of the overlay and the ambient temperature. It has been observed over the years that where the overlay thickness is less than about 25 mm (1 inch) it will not retain the heat long enough to adequately soften the asphalt tack coat such that it will be uniformly absorbed by the paving fabric. In the failures evaluated, overlay thicknesses less than 25 mm (1 inch) were measured on the cores obtained from 12 projects, about 19% of the total. As would be predicted, low tack coat was measured in 9 of the 10 projects in which asphalt extraction was performed where a thin overlay was observed. In these cases the low amount of tack in the fabric was the immediate cause of the failure and the relatively thin overlay a likely root cause of the problem. A review of the sample of installation reports suggests that thin overlays may have occurred in less than 6% of projects overall.

The other problem associated with the overlay was an unstable asphalt concrete mix. This was reported in 10 of the failures investigated. It frequently appeared as a secondary factor with a low tack

Figure 8 - This broken pavement was left in place under the paving fabric.

coat amount in the paving fabric. Although not directly supported by the data, there may be a link here with shoving complaints. Part of the action of paving fabric in the system is slightly reducing the bond between the overlay and the existing pavement. It may be possible that where the overlay bond is reduced below some critical point by a low amount of tack coat, that a border line stable overlay mix may be allowed to shove on the surface of the paving fabric and result in shoving. At this point this is somewhat speculative and beyond the reasonable scope of this paper, but it bears some consideration.

EXISTING PAVEMENT CONSIDERATIONS

Within the framework of the existing pavement condition are lumped a variety of both pavement and subgrade conditions. For the most part, the work performed in evaluating project cores was not able to distinguish between problems with the existing pavement or the subgrade. Therefore, cracks in the base pavement of cores could have been attributable to either subgrade or pavement condition. Cracking can be a sign of unsound pavement which should not be covered with paving fabric according to manufacturers. Where cracks are not filled to the top, the asphalt tack coat tends to run down into the cracks and leave a dry spot in the paving fabric (Marienfeld 1997). This allows a spot where water can penetrate through the system. An example of this condition is shown in Figure 7. Unfilled cracks were observed in the pre-existing pavement portion of cores from nine, 14%, of the complaints. A review of the sample of installation reports suggests that adequate surface preparation may be a largely ignored detail of paving fabric system installation. In about 20% of the installation reports, notes were made about inadequate crack filling or lack of other surface preparation. The number goes up to about 40% of the parking lot installations and even higher for playgrounds. In some cases, the lack of surface

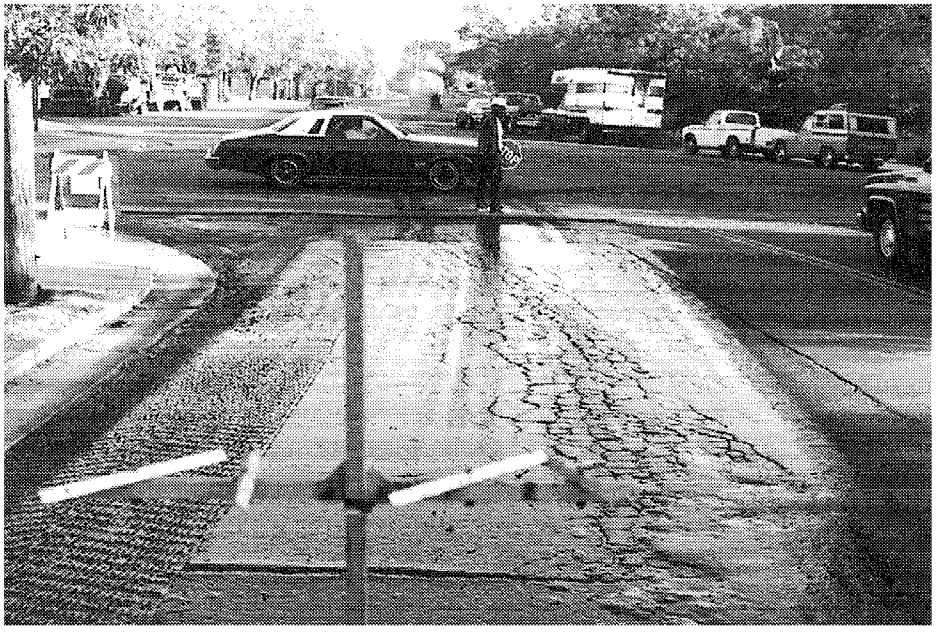

Figure 9 - Area of unstable base material left under the paving fabric

preparation left some very unsound conditions in place when the paving fabric was placed as shown in Figures 8 and 9. Where conditions like these occur, the paving fabric is unlikely to substantially improve the performance of the overlay and blaming the paving fabric for the poor performance is unwarranted. It still happens, however. One file has notes to the contractor regarding inadequate surface preparation and notes back from the contractor accepting the consequences. Even so, when the project developed problems later, the customer came back to the paving fabric manufacturer. In light of the these findings it may be possible that inadequate surface preparation is the principal factor in many the cases where other definite causes were not identified for the failure. The high occurrence in the installation reports coupled with encountering cracks in cores, even with limited drilling, supports this speculation.

Some discussion should also be given to the occurrence of unstable Portland cement concrete (PCC). This was observed in three of the cases investigated. This is about half of the projects investigated which contained PCC pavements. Work by the California DOT (Predoehl 1990) has indicated that early reflective cracking can be anticipated where movement of existing PCC is greater than about 0.1 mm (0.004 inches). This is relatively little movement. Where PCC pavements will be overlaid, the best strategy may be to use a crack and seat or other method to first stabilize the existing pavement and then place an asphalt concrete leveling course (Hannon 1987). Based on the comments in the installation reports, the general practice appears to be to use a leveling course beneath the paving fabric without otherwise stabilizing the existing PCC pavement. This practice may, in many cases, be insufficient.

GEOGRAPHIC CONSIDERATIONS

The combined 10 complaints from New York and Pennsylvania may indicate that climate in these areas is more demanding of the paving fabric system than elsewhere in the United States. On the other hand, good installations are known in northern areas (Bernard 1996). In fact Wisconsin, with similar climatic conditions and relatively high paving fabric usage, has no reported complaints. It appears that although the northern climate as represented by New York and Pennsylvania place additional demands on the paving fabric system these demands may be overcome by details of installation technique. The end results may be that the harsher climate just is not as tolerant of problem installations as milder climates. Several people experienced in paving fabric installation in these areas were interviewed to determine any potential reasons why the two areas of cold weather have differing levels of paving fabric performance. Possible causes noted included the fact that the short construction season in the northern states finds contractors trying to extend their construction season into colder than recommended conditions. These colder conditions can amplify the effects of marginal construction practices noted previously.

CONCLUSIONS

As reported in many previous studies, proper installation of paving fabric is critical to successful performance. Almost every reported and investigated failure of the system could be traced to improper installation procedures. Among the principal causes identified in this review the following issues stand out:

- The single leading cause of failure of overlays containing paving fabric is too little tack coat applied during installation.
- Serious delamination of the overlay from the existing pavement is generally associated with fabric tack coat absorption rates less than 0.45 liters per square meter (0.10 gallons per square yard).
- Although not initially resulting in a catastrophic failure, too little tack coat will also not allow the pavement waterproofing capability of the paving fabric system and long term benefits will not be realized.
- Use of asphalt emulsion frequently leads to a low tack coat application rate and has other limitations that are often overlooked.
- Inadequate surface preparation, including removal of loose material and crack filling are often overlooked.
- The climate in northern areas may place an additional stress on poor installation practices.

The projects reviewed are thought to represent less than about 0.1% of the paving fabric projects installed. This implies that where manufacturer guidelines are followed, there is no cause for concern. Increased knowledge of how the system should be installed and in some cases increased field inspection can easily eliminate the small percentage of paving fabric projects which experience performance problems.

REFERENCES

Baker, T.L. "The Most Overlooked Factor in Paving Fabric Installation", Geotechnical Fabrics Report, Volume 16, Number 3, April, 1998.

Bernard, F. and J.H. Dobrosielski, "Canadian Climate Tests Paving Fabric's Performance", Geotechnical Fabrics Report, Volume 14, Number 3, April, 1996.

Hannon, J. and J. Miner, "AC Overlay Strategies for PCCP Pavement Using Asphalt Saturated Textiles", Geosynthetic '87 Conference, February, 1987.

Marienfeld, M.L. and S.K. Guram, "Overview of Field Installation Procedures for Paving Fabrics", Proceedings of the 11th GRI Conference, Geosynthetics Research Institute, Drexel University, December, 1997.

Marienfeld, M.L. and T.L. Baker, "Paving Fabric Interlayer System as a Pavement Moisture Barrier", 77th Annual TRB Meeting, January, 1998.

Predoehl, N.H., "Evaluation of Paving Fabric Test Installations in California", CALTRANS, February, 1990.

GEOSYNTHETIC REINFORCED ASPHALT OVERLAY FAILURE ASSESSMENT

C. Joel Sprague
Sprague & Sprague Consulting Engineers, Greenville, SC, USA

Martin Andrews
Geotech Associates, Trinidad and Tobago

Richard Emerson
c/o Wilbur Smith Associates, Columbia, SC

ABSTRACT

The authors were involved in assessing the likely causes of premature pavement failure along the still-under-construction sections of the East Bank Demerara Highway in Georgetown, Guyana. The objectives of the assessment were to analyze the failures and, based on visual inspections, limited testing and measurements, and data obtained from contracting and consulting staff, determine the likely causes of the failures.

Two types of failures were the focus of this investigation.

1.) The slippage of the wearing course within 24 hours of placement in some limited areas where asphalt reinforcing grid and paving fabric were used; and
2.) The apparent premature reflection of cracks in the underlying old pavement into the new pavement surface in areas with and without grid and/or paving fabric.

These failure conditions were investigated with respect to generally accepted design and construction techniques related to conventional and reinforced asphalt overlays.

This paper reviews the findings of the investigation and highlights the likely causes of the failures while pointing out critical aspects of a successful paving fabric or grid installation. Additionally, a theoretical analysis of asphalt reinforcement is presented which correlates well with the observed results of this project.

OVERVIEW AND OBJECTIVES

The project contractor NH International, Ltd. (NHI) and the Ministry of Public Works represented by Wilbur Smith Associates, Inc. (WSA) contracted for an independent assessment of the likely causes of premature pavement failure along the still-under-construction sections of the East Bank Demerara Highway. The objectives of the assessment were to analyze the failures and, based on visual inspections, limited testing and measurements, and data obtained from contracting and consulting staff, determine the likely causes of the failures. Two types of failures were the focus of this investigation.

1.) The slippage of the wearing course within 24 hours of placement in some limited areas (estimated at less than 20% of total) where asphalt reinforcing grid and paving fabric were used; and
2.) The apparent premature reflection of cracks in the underlying old pavement into the new pavement surface in areas with and without grid and/or paving fabric.

The investigation was conducted on September 6 and 7, 1997. The investigation was not intended to be a comprehensive review of associated pavement design, but rather to focus on the correct and consistent use of generally accepted construction procedures and adherence to project specifications.

GENERALLY ACCEPTED PRINCIPLES

Asphalt Overlay

Commonly, existing paved roads are overlain with an asphalt overlay when the existing surface becomes too cracked, rutted, or pot-holed to provide acceptable comfort and safety to the driving public. The overlay is designed to achieve a desired service life given projected traffic and assumed or measured existing pavement conditions. The overlay achieving its design life, therefore, is contingent upon the accuracy of both the traffic forecasting and the assessment of properties/thicknesses associated with the existing pavement structure and subgrade. Unfortunately, for most roads, traffic and pavement conditions vary substantially along the roadway making it unlikely that a single overlay thickness will be appropriate for the entire road. In lieu of varying asphalt thicknesses, interlayer materials are commonly incorporated into overlay construction, especially over areas with extensive cracking, to enhance reflective cracking resistance and to provide a moisture barrier to prevent infiltration of water into the underlying road structure.

Interlayers.

An interlayer may have modest strength such as a paving fabric and absorb stresses or have high strength and absorb strains such as reinforcement grid. According to Lytton (1989), cracks may be retarded or arrested by geotextiles or geogrids if the proper material properties are selected and good construction techniques are used. Lytton also provides equations, based on extensive testing, that enable the designer of a geotextile or geogrid reinforced asphalt overlay to design an appropriate overlay thickness and corresponding reinforcement fabric width and strength and tack coat application rate to, ". . . if properly constructed, turn a reflection crack into a horizontal plane beneath the reinforcing layer and thus delay the reflection cracking indefinitely." Lytton outlines some key principles associated with reinforced asphalt design and construction:

- The required thickness of the overlay increases as the width and frequency of cracks in the old pavement increase.
- The required thickness of overlay decreases as the stiffness of an interlayer increases and as the ratio of stiffness of an interlayer to the overlay increases.
- The required amount of tack coat between the old pavement, the new pavement, and an interlayer to assure the preferred mechanism of reinforcement should be slightly over optimum (i.e. the amount of residual asphalt required to saturate the reinforcement and satisfy the asphalt "hunger" of the adjacent pavement surfaces).
- Excessive variance in tack coat viscosity (too fluid or too firm) and thickness (too thick or too thin) can have negative effects on the stability of the reinforced asphalt overlay.

INTERVIEWS

Mr. Richard Emerson, Resident Engineer, of WSA and Mr. Eamon Regan, Project Superintendent, with NHI were interviewed to develop background knowledge of the project. Following are the comments received from the interview.

Paving Procedures

1.) Generally the project involved widening the original road from two 2.74 m (9 ft) lanes to two 3.35 m (11 ft) lanes with paved shoulders and overlaying the entire widened surface. The widening project was approximately 26 km (16 miles) long.

2.) Widening was accomplished by excavating a trench on either side of and adjacent to the existing pavement. The trench measured approximately 1.25 to 1.83 m (4 to 6 ft) wide and 76 cm (30 in) deep. The bottom of the trench was typically comprised of insitu clay soils which were too weak to compact.

3.) The trench was backfilled with 46 cm (18 in) of white sand compacted to 95% standard Proctor followed by 30 cm (12 in) of a sand/clay blend compacted to achieve a minimum soaked CBR of 25 and unit weight of 18 kN/m^3 (115 lb/ft^3). Both soils met the project specifications for gradation and blending.

4.) A prime coat of emulsified asphalt and a 5 cm (2 in) thick asphaltic concrete widening strip was then placed above the trench fill to bring the surface even with the existing pavement surface.

5.) After blowing off the road surface, leveling course (laid in 1 or more passes) was placed over the existing road surface and the adjacent widening strip to create a smooth surface with the appropriate crown. The leveling course thickness ranged from 1.6 cm (5/8 in) to as much as 15 cm (6 in). A tack coat of RS-1 asphalt emulsion, as specified, was sprayed on the existing road surface and trench fill prior to placement of the leveling course. The tack coat application rate was visually estimated at 0.45 l/m^2 (0.10 gal/yd^2) to achieve 0.23 l/m^2 (0.05 gal/yd^2) residual asphalt.

6.) After compaction of the leveling course by a pneumatic tired roller, the surface of the leveling course received an application of RS-1 emulsified asphalt tack coat at the rate of 0.45 l/m^2 (0.10 gal/yd^2) to achieve a residual asphalt cement application of 0.23 l/m^2 (0.05 gal/yd^2). In areas where paving fabric or reinforcement grid were to be applied, an additional 2.3 l/m^2 (0.5 gal/yd^2) of emulsion was spray-applied using a hand-held wand. The tack coat application rate was visually estimated. No measurements of tack coat quantities were made. Judgement on time-to-break was based on the tack coat color changing from brown to black.

7.) In areas where paving fabric and/or reinforcing grid were to be used, the fabric or grid were cut into pieces approximately 15 m (50 ft) in length and placed by hand on the road surface after waiting approximately 20 to 30 minutes for the tack coat to cure (i.e. for the water to evaporate). Any apparent wrinkles were brushed out of the fabric using brooms. Foot prints were apparent when walking on the fabric/grid indicating tack coat was being taken up. A thin layer 0.6 cm (0.25 in) of loose asphalt concrete was dispersed by shovel on the fabric/grid to prevent the fabric/grid from sticking to the tires of the paving machine as it passed over. Paving fabric was generally used in areas of excess alligator cracking and grid was used and centered over the joint between the existing and widened pavement. Paving fabric and grid were used between stations 200+00 and 400+00.

8.) Asphaltic concrete wearing course was then spread after waiting approximately 20 to 30 minutes for the tack coat to cure (i.e. for the water to evaporate). The asphalt was laid at a thickness of

approximately 5 cm (2 in) loose and compacted to achieve a specified minimum thickness of 3.8 cm (1.5 in). The temperature and loose thickness of asphalt was regularly measured. Newly paved areas were typically coned-off for 4 to 5 hours prior to being opened to traffic.

Notable Observations

9.) The existing pavement structure included approximately 5 cm (2 in) of asphaltic concrete or sand asphalt wearing course over 10 to 30 cm (4 to 12 in) of a sand/clay blend, broken bricks, or gravel. All underlain by 9 to 12 m (30 to 40 ft) of soft clay.

10.) Some areas were paved at night. Primarily between stations 213+00 and 236+00.

11.) A water pipeline was installed in a trench adjacent to the west side of the newly rehabilitated roadway shortly after completion of paving. Pipeline backfill was apparently not compacted.

12.) Heaviest traffic loading is in the northbound lane and often happens at night as a result of loaded trucks traveling at high speeds heading toward Georgetown ports.

Description of Failures

13.) Two types of failures were in need of explanation:
Failure #1. Slippage immediately (within 12 to 24 hours) after overlay completion.
Failure #2. Reflective cracking, primarily parallel to the underlying reinforcing grid.

14.) Of the 26 km of road widening with paving fabrics and reinforcing grids, it was estimated that less than 20 percent of the road length experienced unexpected paving failures.

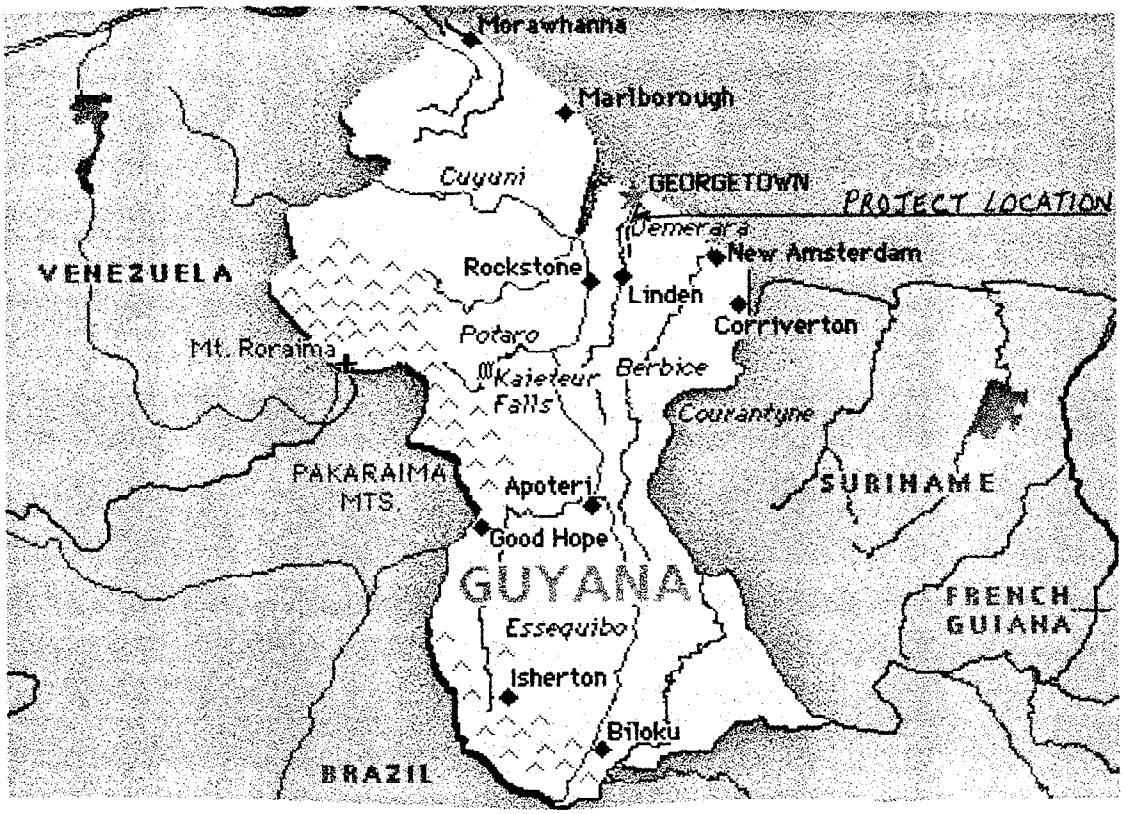

Figure 1. Project Location

FIELD AND LABORATORY INVESTIGATION

A field investigation was performed, including the drilling of pavement cores to evaluate the consistency of construction procedures as described above. The pavement cores were measured to document the thicknesses of the various pavement layers and to obtain fabric/grid samples at strategic points in the northbound lane. The fabric/grid samples were taken into the laboratory and weighed. The difference in weight as compared to control samples was calculated and converted to a volumetric measure of the asphalt cement absorbed by the interlayer material. Table 1 summarizes the findings of the field investigation. The paving fabric used on the project was a 3.8 m wide polypropylene nonwoven referred to as PETROMAT and the reinforcing grid was a 1 m wide composite consisting of a woven, coated polyester grid bonded to a polyester nonwoven, referred to as BITUTEX. Conformance testing of the fabric and grid was not performed to document their properties.

Table 1. Findings of Field Investigation

Station & Distance in from Edge of Widening	Observation	Core #	Overlay Thickness cm (in.)	Interlayer	Leveling Course Thickness cm (in)	Original Pavement Thickness cm (in.)	Interlayer Asphalt Content l/m^2 (gal/yd^2)
350+00 @ 46 cm (18 in)	Good area / no cracking	1	5 (2)	Grid/fabric composite	5 + 6.4 (2 + 2½)	5 (2) sand asphalt	1.18 (0.26)
349+85 @ 46 cm (18 in)	Good area / slight longitudinal cracking	2	5 (2)	Grid/fabric composite	5 + 6.4 (2 + 2½)	5 (2) sand asphalt	1.49 (0.33)
341+05 @ 200 cm (78 in)	Overlay & interlayer slipped & removed	3	Removed	Removed	12.7 (5)	Not retrievable	-
340+57 @ 200 cm (78 in)	Adjacent to slipped area	4	1.9 (¾)	Grid/fabric composite	Uncompacted, not retrieved	Not retrieved	0.63 (0.14)
340+59 @ 200 cm (78 in)	Adjacent to slipped area	5	1.9 (¾)	Grid/fabric composite	3.8 (1½), very rich, broke up	Not retrieved	0.59 (0.13)
302+82 @ 132 cm (52 in)	Slippage cracks on surface but pavement still intact	6	3.18 (1¼)	Paving fabric	3.18 (1¼)	5 (2) sand asphalt	Not retrievable
302+82 @ 200 cm (78 in)	Slippage cracks on surface but pavement still intact	7	3.8 (1½)	Grid/fabric composite	3.8 + 3.18 (1½ + 1¼)	5 (2) sand asphalt	1.27 (0.28)
300+65 @ 200 cm (78 in)	Adjacent to slipped area / overlay slipped on top of interlayer	8	3.18 (1¼)	Grid/fabric composite	3.8 (1½)	Broke up, unretrievable	1.49 (0.33)
300+65 @ 137 cm (54 in)	Adjacent to slipped area / overlay slipped on top of interlayer	9	3.18 (1¼)	Paving fabric	6.35 (2½)	5.72 (2¼) sand asphalt	0.95 (0.21)
** 278+00 @ 200 cm (78 in)	In recently patched strip where slipped material was removed	10	3.18 (1¼)	Grid/fabric composite	6.35 (2½)	Sand asphalt broke up	1.72 (0.38)
*300+55 @ 152 cm (60 in)	Paving fabric adhered to the road. Overlay slipped off.	-	-	Paving fabric	-	-	0.45 (0.10)

* Paving fabric had been driven on and had holes in it. Apparently some of material and asphalt cement worn away.

** Core taken from area patched by Ministry after slipped material had been removed. Tack coat was uncut asphalt cement hand applied.

OBSERVATIONS

Field and Laboratory Investigation

A review of the data and observations resulting from the field investigations revealed that the existing road structure and the new construction were more variable than desired. At the locations sampled, especially those associated with the short-term failure condition, it was apparent that contributing factors included inadequate overlay thickness and tack coat. Additionally, insufficient compaction of or excessive asphalt cement content in the leveling course along with lack of support from the existing road structure may have contributed to the immediate (overnight) nature of the failure. Still, comparison of cores 8 and 9 demonstrate that slippage can occur even when the overlay is much closer to the specified 3.81 cm (1½ in) thickness and the tack coat quantities are close to or above those required. The difference with the failure sections associated with cores 8 and 9 is that slippage came above rather than below the interlayer. This appeared to demonstrate that the quantity of tack coat applied to the underlying surface and subsequently absorbed by the interlayer does affect the horizontal stability of the reinforced overlay. Still, the field evidence by itself was not sufficient to conclude the cause of slippage. (The interviews provided important additional information.)

Evidence relating to premature cracking was even less clear, but there was a clear pattern of longitudinal cracks occurring in the new overlay above the outside edges of the grid reinforcement. This appeared to indicate that the grid/fabric composite was indeed performing its job of interrupting the vertical reflection of the joint between the existing pavement and the widening and turning the associated strain sideways. But the crack reappeared at the edge of the grid indicating that the reinforcing strip was probably not wide enough to fully dissipate the strain caused by the joint. Additionally, it appeared that one wheel path of the normal northbound traffic naturally falls near the joint made by the widened section causing repeated shearing of the joint and, therefore, great likelihood of reflective cracking. Unfortunately, continued longitudinal cracking can be expected from the on-going shearing of the joint and will be worsened significantly if the widened section is able to settle or move laterally out as a result of limited bearing support or confinement.

Interviews

Some questionable practices were revealed during the interviews with the representatives of NHI and WSA which may have contributed to the failure conditions under review. These practices included:

- No routine measurement of tack coat application was used to verify tack coat quantities. The time allowed (20 - 30 minutes) for the tack coat to cure or "break" may have been sufficient for normal light applications (< 0.45 l/m^2 (0.1 gal/yd^2)), but were grossly inadequate for the heavier rates associated with tacking of the paving fabric or grid (> 1.13 l/m^2 (0.25 gal/yd^2)) which may require 2 hours or more.
- Some of the construction requiring higher application rates was done at night, further extending the time needed to allow the emulsion to cure.
- Apparently, insufficient funding was available to permit reconstruction of those areas experiencing wide-spread base failure. It is well recognized that overlaying an existing pavement that has experienced base failure is, at best, a temporary solution that will experience similar failure patterns prematurely.

CORRELATION TO DESIGN OF ASPHALT REINFORCEMENT

The field and laboratory data combined with the interviews provided valuable insight into the possible causes of failure as noted in the previous section. Still, it is valuable to know if these failures (and more wide-spread successes) could have been anticipated. To this end, a review of asphalt reinforcement design and an associated sensitivity analysis follows.

Remedial Measures and Mechanisms

Remedial measures most commonly used to address deteriorating road surfaces can be separated into two classes according to Rigo (1993):

1. Modification of the overlay characteristics; and
2. Placement of a membrane interlayer between the old structure and the new overlay.

Clearly, on the Demerara Highway project the second approach was taken. The use of an interlayer can create one or more of the following mechanisms as (a.) stress relief, (b.) reinforcement, and (c.) reduction of water infiltration. The reinforcement mechanism associated with the paving grid is the focus of the design approach used herein.

Potential Failure Modes

Lytton (1989) outlines three distinct failure modes associated with stress relief and reinforcement.

Mode 1 - Stress Relief. In this mode of failure, the reflection crack propagates rapidly upward from an old crack to the stress-relieving interlayer. The crack stalls at the interlayer for a while, and then propagates from the top of the interlayer upward to the surface. In this mode, the interlayer, commonly an asphalt-saturated fabric or asphalt rubber interlayer with low stiffness, stores the large associated strains at low stress levels. This leads to retarding or "stalling" of, but not preventing, crack propagation.

Mode 2 - Stress Relief. In this mode the crack propagates upward from the bottom of the overlay and temporatily terminates at the stress relieving interlayer. Another crack then begins at the top of the overlay and propagates downward to the interlayer. This mode occurs when the interlayer is placed within the overlay such as when a leveling course is used.

Mode 3 - Reinforcement. In a reinforcement failure, the crack propagates upward to the reinforcing interlayer. The crack then makes a right angle turn and moves along the interface between the reinforcement and underlying material and propagates laterally until insufficient energy is left to move any further. Interestingly, Lytton (1989) has noted that for the reinforcement mode to develop, debonding must occur between the lower layer and the reinforcement. This mode also requires the fabric or grid be sufficiently thick and that its stiffness to be greater than the surrounding material.

Reinforcing Interlayers & Associated Stiffnesses

High-strength and high-stiffness polymer and glass grids and fabrics are being used on an ever increasing basis

for either strip or full-width overlay applications of flexible pavements. The grid or fabric system is intended to reinforce the resulting overlayed pavement. According to Barksdale (1991), the grid's ability to reinforce is largely dependent on its stiffness, assuming that a slack-free installation is accomplished. The stiffness of the grid/fabric is defined as the tensile force applied per unit width of material divided by the resulting displacement. The strength characteristic perpendicular to the cracks to be overlayed is used in design. On this project that is the cross machine direction (XMD). The approximate XMD tensile strength characteristics of the paving grid used on the Demerara Highway project are shown in Table 2.

TABLE 2. Reinforcing Grid XMD Product Properties

Reinforce-ment	Ultimate XMD Strength, kN/m	Ultimate XMD Elongation, %	5 % XMD Tensile Strength kN/m	XMD Stiffness @ 5% kN/m	2 % XMD Tensile Strength kN/m	XMD Stiffness @ 2% kN/m
Grid	47	16	11	220	9	450

CONVERSION: kN/m x 5.71 = lb/in

Design Model

Lytton (1989) provided an equation for determining the required overlay thickness for a given reinforcing grid or fabric interlayer. The equation requires the designer to determine, or assume, numerous variables associated with the reinforcement as well as the asphalt pavement. To achieve debonding, which is critical to developing the Mode 3 mechanism, an AC-10 or AC-20 tack coat applied at more than 0.68 l/m^2 (0.15 gal/yd^2) above optimum is appropriate.

The grid tensile properties, along with other assumed material properties, were used in a theoretical assessment aimed at determining if the failures and successes of the asphalt reinforcement on the Demerara Highway project could have been anticipated. Equation 1 from Lytton (1989) was used for the assessment.

Equation 1: $d_o = \{k_o \Delta / [(f_{to}) (1+np) \beta \sinh(\beta w/2)]\} \{\cosh(\beta w/2)-1\}$

Table 3 shows the range of material property inputs that may apply based on Hoff (1979), Rigo (1993), and Vanelstraete, et al (1997). Selected results of the sensitivity analysis are shown in Table 4.

An important input is the crack movement that must be "reinforced". Hoff (1979) provides a coefficient of thermal expansion of 1.4 x 10^{-5}/°F for asphaltic concrete. Based on this, for a 2.74 m (9 ft) lane width and a 22°C (40°F) change in temperature, the expected crack movement would be approximately 0.0015 m (0.06 in). This value of crack opening movement was used in the analysis.

Table 3. Design Inputs

Abbreviation	Description	0°C	20°C	40°C
d_o	Overlay thickness	Calc.	Calc.	Calc.
f_{to}	Overlay tensile strength, Mpa	5	2	0.5
E_o	Overlay elastic stiffness modulus (thermal), MPa	2000	200	20
k_o	Tack coat shear stiffness, MPa/m	2000	1000	200
E_i	Interlayer stiffness modulus, Mpa	5000	5000	5000
n	Elastic stiffness ratio, reinforcement:overlay	Calc.	Calc.	Calc.
A_i	X-sectional area of reinforcement, m^2/m	.0001	.0001	.0001
p	X-sectional area ratio, reinforcement:overlay	Calc.	Calc.	Calc.
β	SQRT (k_o / $E_u d_u$)	Calc.	Calc.	Calc.
E_u	Elastic stiffness of underlayer – Cracked	1250	500	125
E_u	Elastic stiffness of underlayer – Minimal Cracking	7500	3000	200
Δ	Crack opening, m	.0005-.0015	.0005-.0015	.0005-.0015
d_u	Thickness of underlayer, m	.05	.05	.05
W	Reinforcement width, m	1.0	1.0	1.0

Note: When $d_{oCalc.} > d_{oActual}$, fracture failure occurs. When $d_{oCalc.} < d_{oActual}$, debonding occurs.

Table 4. Input and results of reinforced overlay assessment

Temp. °C	k_o N/m^2	Δ m	f_{to} N/m^2	N	p	E_u N/m^2	d_u m	W m	d_o, m (in.)	Savings w/ Reinf. m (in.)
20	$1x10^9$	0.0015	2000000	0	0	$5x10^8$	0.05	1.0	0.109 (4.29)	-
40	$1x10^8$	0.0015	500000	0	0	$1.25x10^8$	0.05	1.0	0.094 (3.71)	-
20	$1x10^9$	0.0015	2000000	25	0.0025	$5x10^8$	0.05	1.0	0.103 (4.04)	0.006 (0.24)
40	$1x10^8$	0.0015	500000	250	0.0025	$1.25x10^8$	0.05	1.0	0.058 (2.28)	0.036 (1.42)
20	$1x10^9$	0.001	2000000	0	0	$5x10^8$	0.05	1.0	0.073 (2.87)	-
40	$1x10^8$	0.001	500000	0	0	$1.25x10^8$	0.05	1.0	0.063 (2.47)	-
20	$1x10^9$	0.001	2000000	25	0.0025	$5x10^8$	0.05	1.0	0.068 (2.67)	0.005 (0.20)
40	$1x10^8$	0.001	500000	250	0.0025	$1.25x10^8$	0.05	1.0	0.039 (1.52)	0.024 (0.94)

A review of Table 4 reveals that as the project temperature increases, the asphalt properties significantly diminish (as might be expected) but the reinforcement properties do not. Thus, at higher project temperatures the reinforcement has greater impact on performance. Additionally, it should be noted that smaller crack movement requires less overlay thickness and benefits somewhat less from reinforcement.

As noted in Table 1, overlay thickness ranged from under 0.025 m (1.0 in) to 0.05 m (2.0 in). Therefore, since the actual overlay thickness was generally less than the required thickness as shown in Table 4, fracture failure of the overlay (at the end of the reinforcement) would be expected wherever the overlay was somewhat thin. This seems to mirror the field observations which found areas where the crack between the road and the widened extension reflected through, not directly above the crack, but at the end of the grid.

CONCLUSIONS

A comprehensive investigation has been made of the failed pavement sections along the East Bank Demerara Highway, including interviews, field evaluations, and laboratory measurements. Both short-term and potential long-term failure conditions were examined. The short-term (overnight) failures involved slippage of some sections underlain by paving fabric and reinforcing grid. This slippage was primarily attributable to unsatisfactory tack coat application (including inadequate application rate and insufficient cure time) and, perhaps, inadequate overlay thickness. Where total slippage occurred, the actual residual tack coat application rate was as low as 0.59 l/m^2 (0.13 gal/yd^2). Manufacturers clearly recommend residual tack coat in excess of 1.13 l/m^2 (0.25 gal/yd^2). Additionally, the cure time was no more than 30 minutes, while manufacturers' recommendations require complete curing which would be expected to take up to 2 or 3 hours for an asphalt emulsion in a humid environment or during night-time construction. It should be noted that a very straight-forward procedure for determining tack coat application rates in the field is described in ASTM D 2995 Standard Practice for Determining Application Rate of Bituminous Distributors.

The potential long-term failure condition associated with premature longitudinal cracking was primarily a result of the joint between the existing road structure and the widening. The location of this joint, directly below the wheel path made shear induced reflective cracking inevitable, though the use of asphalt reinforcing grid has effectively absorbed some of the strain of the crack and shifted the location of the reflected crack. Similarly, reflective cracking associated with the alligator cracking in the old pavement surface has apparently been reduced in areas where paving fabric was properly installed, but cracks will eventually return since reconstruction was not possible.

Overall, except for the areas which exhibited immediate failure and some isolated areas of reflected longitudinal and alligator cracking associated with insufficient underlying support, the pavement investigated (between stations 200+00 and 400+00) appears to be stable. In light of the variability of the original road structure it is not possible to project an expected life for the rehabilitated road.

Interestingly, the attempt to correlate the field observations to design theory proved potentially beneficial. Clearly, there are complex interrelationships among the reinforcement and asphalt properties. The design analysis showed that for the assumed asphalt properties for this project and climate, the asphalt reinforcement should prove beneficial. This appears to correlate well with the observed performance of the portion of the project which was well constructed.

AKNOWLEDGEMENTS

The authors appreciate the support of Mr. Louis Austin of the Ministry of Public Works and Communications, Wilbur Smith Associates, and N.H. International Limited.

REFERENCES

Barksdale, R.D., *Fabrics in Asphalt Overlays and Pavement Maintenance*, NCHRP Synthesis 171, Transportation Research Board, National Research Council, Washington, D.C., 1991, pp. 8-9 & 25-26.

Hoff, G.C. (1979), Chemical, Polymer and fiber Additives for Low Maintenance Highways, Noyer Data Corporation, Park Ridge, NJ, pp. 8-36.

Lytton, R.L. (I 989), "Use of Geotextiles for Reinforcement and Strain Relief in Asphalt Concrete", Geotextiles and Geomembranes, Vol. 8, pp. 217-237.

Rigo, J.M., General Introduction, Main Conclusions of the 1989 Conference on Reflective Cracking in Pavements, and Future Prospects, *Reflective Cracking in Pavements - State of the Art and Design Recommendations, Proceedings of the Second Int'l RILEM Conference*, Liege, Belgium, E & FN SPON, 1993, pp. 3-20.

Vanelstraete, A., deBondt, A.H., and Courard, L. (1997), "Characterization of Overlay Systems", Prevention of Reflective Cracking in Pavements, RILEM Report 18, pp. 61-83.